Realising Complex Quantum States of Matter via Symmetries and Heating

Joseph Tindall

Wolfson College

University of Oxford

A thesis submitted for the degree of

Doctor of Philosophy

Hilary 2021

Acknowledgements

Nothing of import is ever achieved alone. This thesis is no exception and it would be amiss not to give credit to the people who have, both directly and indirectly, helped shape it and my time as a PhD student.

First, and foremost, my thanks goes to my supervisor Professor Dieter Hans Jaksch, without whom this work could not exist. His guidance and knowledge helped spark and shape a number of the ideas present in this thesis. Moreover, the freedom he gave me as a PhD student, combined with his high academic standards, has allowed me to grow as a researcher and produce the best possible work I can.

A number of people both inside and outside of the Jaksch group are also responsible for initiating and shaping the work contained here. To Berislav Buča, Carlos Sánchez Muñoz, Frank Schlawin, Jonathan Coulthard, Michael Sentef and Stephen Clark: I am ever grateful for your help, knowledge and guidance as mentors and colleagues. I am also thankful to the other members of the Jaksch group who have made my time in the Clarendon as a PhD student so enjoyable and stimulating.

Of course, this thesis is not just the product of my time doing academic research. Without my family and friends I would not be where I am today and I would not have had the motivation to produce the work detailed here. So to my parents Denise and Simon, my sisters Anna and Helen and to my friends - both in and outside of Oxford - thank you.

Lastly, but by no means least, my gratitude goes to my partner Hannie. Your companionship and continuous belief in me these last few years have been wonderful.

Abstract

Identifying mechanisms which can guide many-body quantum systems into regimes where properties such as entanglement and long-range coherence are manifest is a fundamental goal for those working in the field of strongly correlated systems. With this comes the potential to realise and exploit states of matter such as superconductors and superfluids, where quantum behaviour is observable at the macroscopic level.

In this thesis we study how symmetries and heating can, counterintuively, be used to realise phases of matter with such desirable properties. We prove how heating a many-body system whilst preserving certain symmetries — such as those of the special unitary group — result in the formation of maximum entropy states which are confined to a subspace of the total Hilbert space and are capable of possessing finite, completely uniform off-diagonal correlations. This mechanism is termed heating-induced order and is independent of any microscopic details.

We use the Hubbard model as a central example where this mechanism can be observed. Heating is introduced to the system via periodic driving or local dissipation and we study the various ordered steady states which emerge in this setup. We discuss the applicability of this mechanism to the thermodynamic limit and its relevance to recent solid-state experiments observing photo-induced superconductivity in irradiated compounds.

We then show how, in an open quantum system, the satisfaction of a set of simple symmetry-based conditions guarantees an absence of stationarity and the formation of coherent oscillations in the long-time limit. We prove how this result subsumes and goes beyond the established notion of a Decoherence Free Subspace. When these conditions are satisfied in the presence of heating-induced order we observe the formation of an entangled, correlated state undergoing identical limit cycles at all positions in space. This leads us to formulate a novel process for quantum synchronisation which is based on the combination of these symmetry-based conditions and the mechanism of heating-induced order.

Contents

List of Figures

Introduction

Background

It is a long-standing conjecture that, in a very distant future, our universe will reach thermodynamic equilibrium characterised by a cessation of motion and an absence of any physical phenomena [1, 2, 3]. Known as the 'Heat Death of the Universe', this seemingly irreversible fate is underpinned by the natural tendency of isolated systems, under the mutual interactions of their constituents, to move towards a state of uniform temperature and maximum entropy [4].

Our everyday experience, on the other hand, contrasts with this idea and abounds with a variety of co-operative, feature-rich phenomena. From the orbital motion of the planets to the flocking of animals, from the chaotic movement of traffic to the flow of charge through a transistor the world around us is driven by complex behaviour at all length scales. Even if these are transient processes in the evolution of the universe, our understanding and modelling of them is, and has been, fundamental to our technological and economical development.

At the quantum level a similar story is developing. Following the inception of the laws of quantum mechanics in the early 20th century, significant research was devoted to understanding how they were compatible with the foundational theories of thermodynamics and statistical mechanics established in the centuries prior [5, 6]. This was, in part, achieved by the work of John von Neumann who, alongside introducing the density matrix and a corresponding notion of entropy, established the Quantum Ergodic Theorem (QET) - connecting the time-averaged behaviour of a wavefunction to the microcanonical average over the Hilbert Space [7, 8, 9]. These developments marked the start of the field of quantum statistical mechanics [10, 11].

Despite this, criticisms were made of the QET suggesting that it is 'vacuous' and more a statement on the mathematical structure of the Hilbert space as opposed to anything physical [9, 12]. As a result many considered the question of how, given the linear and time-reversible nature of the Schrödinger equation, isolated quantum

systems can relax to a state which resembles thermal equilibrium to be unanswered. An alternative answer to this problem was provided by Deutsch and Srednicki [13, 14] at the end of the century in the form of the Eigenstate Thermalisation Hypothesis (ETH). The ETH details how this relaxation can occur via thermalisation at the level of the eigenstates of the observables in question and has been verified for a number of setups [15, 16, 17, 18]. The applicability of this hypothesis, however, is dependent on the observable at hand and it is generally considered to only be valid for local, few-body observables. Moreover, even if an observable does possess these properties the ETH does not necessarily apply: for example, in both single-particle and many-body systems the presence of a static, disordered potential landscape prevents relaxation on any reasonable timescale [19, 20, 21, 22].

The ETH makes statements on *isolated* quantum systems — as opposed to those coupled to an environment or driven by a coherent, temporal source. In general, the interaction between a many-body quantum system and a vast environment or an energetic source should quickly drive it to an equilibrium state where quantum effects such as coherence and entanglement are suppressed. There are a growing number of setups, however, where this is not the case. For example, recent experiments have demonstrated the induction of high-temperature superconducting states via irradiation of solid-state materials with intense THz laser pulses [23, 24, 25]. Moreover, in the context of open systems, various proposals exist for dissipative quantum computing where decoherence from an environment can actually protect, or enhance, quantum information protocols [26, 27, 28].

Understanding the underlying mechanisms which guide systems away from their anticipated equilibrium states, as well as addressing the generality of the ETH, are problems at the forefront of research in quantum physics. This prominence is, in part, the result of a recent revolution in theoretical and experimental quantum physics, where significant progress has been made in both the numerical simulation and explicit realisation of highly controllable quantum systems — which can serve as testbeds for tackling these kind of problems.

On the experimental front this revolution is a direct result of continued advances in creating highly controllable, coherent lasers and magnetic fields. These precise tools have resulted in a variety of techniques that can be be used to cool and manipulate the states of individual atoms. Many Nobel prizes have been awarded for these techniques and their application (1997, 2001, 2005, 2012, 2018) — the development of various optical and magnetic cooling process [29, 30, 31, 32] and the ensuing realisation of Bose-Einstein condensates by the cooling and trapping of dilute atomic gases

[33, 34] being notable examples. These seminal achievements have ushered in the start of the 21st century as an unprecedented era of experimental quantum physics, with researchers becoming increasingly adept at probing and controlling a variety of systems — from the single qubit to quantum gases and solid state materials.

In parallel with this, theoretical research on these kinds of systems has grown rapidly. The introduction of the Density Matrix Renormalisation Group as a numerical technique in 1992 [35, 36, 37], alongside the continued growth in computing power, has rendered a variety of quantum setups computationally tractable and created a significant conjunction between experimental and theoretical research. At this conjunction a common goal prevails: to harness and understand the properties of these quantum systems, with a view to the realisation of states of matter such as room temperature superconductors [38, 39] and devices such as fully programmable, fault-tolerant, quantum computers [40, 41, 42].

Identifying and understanding the mechanisms by which quantum systems — whether isolated, driven or dissipative — can avoid their anticipated relaxation and be guided into long-lived, exploitable, coherent phases is a fundamental step in achieving this goal. Through this, proposals for realising these desirable states of matter, and technologies which utilise them, can be formulated and subsequently implemented.

Thesis Contributions

It is within this narrative that this thesis fits, making several key contributions towards it. For our first contribution we identify how the symmetry structure of certain quantum systems means that heating can, instead of being deleterious towards quantum effects, be used as a resource to guide the system toward maximum entropy steady states with coherent off-diagonal long-range order — the intrinsically quantum property underpinning exotic phenomena such as superconductivity and superfluidity. We term this remarkable effect heating-induced order.

We use the Hubbard model, a paradigmatic model for correlated electrons in solid-state materials, as a key example of where this behaviour can be observed. Heating is introduced to the system via periodic driving or local dissipation and we analytically and numerically construct the various ordered and unordered steady states which emerge in this setup. These states are classified based on the symmetries which the heating mechanism respects and whether the underlying lattice is bi-partite or not. These results leads us to discuss experiments where this setup could be realised and such ordered states observed.

Along these lines, we consider the driven Hubbard model on a frustrated quasi-1D triangular lattice and show that the irregular geometry of the lattice leads to a novel pathway by which the mechanism of heating-induced order can occur in the charge sector, despite the underlying lattice not being bi-partite. This driven triangular lattice constitutes a simple model for a recent experiment where the organic compound $\kappa - (\mathrm{BEDT} - \mathrm{TTF})_2\mathrm{Cu}[\mathrm{N}(\mathrm{CN})_2]\mathrm{Br}$ was irradiated with infrared light [43]. Dynamical superconductivity was observed in this compound following this irradiation and the mechanism of heating-induced order may therefore be connected to these experimental results.

For the second major contribution of this thesis we show how, in a generic open quantum system, symmetry-based dissipation can, counterintuitively, cause the system to avoid its anticipated relaxation to a stationary equilibrium state and instead undergo coherent, persistent oscillations in the long-time limit. We achieve this by formulating a series of simple mathematical conditions for the existence of a special type of symmetry operator — the strong dynamical symmetry (SDS) operator — which guarantees that the governing Liouvillian possesses purely imaginary eigenvalues. These conditions make no statements about the microscopic details of the system and environment and we show how they subsume and go beyond the established notion of a Decoherence Free Subspace.

We then demonstrate how the two major results of this thesis — these SDS conditions and the mechanism of heating-induced order — form the foundation for a novel process by which perfect synchronisation can occur in a quantum system. This synchronisation mechanism does not rely on taking the quantum limit of a classical oscillator or identifying a specific parameter regime in a single delicately controlled system and is thus markedly different to previous work. We prove how the corresponding imaginary eigenmodes, whose excitement leads to the coherent oscillations and synchronisation of the system, are robust to symmetry breaking perturbations. Finally, we identify several physical models where this robust symmetry-induced synchronisation can be observed, performing extensive numerical and analytical calculations to this effect. The combination of the heating and the SU(2) nature of the SDS operator in these setups means the observed synchronisation is underpinned by long-range correlations and entanglement, making it truly quantum in nature.

Thesis Structure

The structure of this thesis is as follows:

In chapter 1 we introduce the theory necessary for treating both driven and open quantum systems, which forms the backbone of many of the results in this thesis. In the context of driven systems we introduce the Floquet formalism which addresses the time evolution of a closed system subject to a periodic driving field. In the open case we describe and derive the various master equations which are used to approximate the dynamics of a system interacting with an external environment. Finally, we introduce the various mathematical and computational tools which are applied extensively in this thesis and can be used to directly analyse and simulate driven and dissipative systems.

In chapter 2 we introduce the first results of this thesis. We start by describing the role of symmetries in both open and closed many-body quantum systems. This knowledge allows us to show how the steady states of a quantum system subject to continuous heating, which could originate from periodic driving or via the interaction with an external environment, can be written in terms of the eigenstates of the operator representations of the system's symmetries. As a consequence the properties of these maximum entropy steady states are strongly dependent on the type of symmetries the system possesses under heating. We compare two cases: a U(1) symmetric system and an SU(2) symmetric system. In the former the steady states are always featureless outside of a fixed single observable whilst in the latter we are able to prove that they will generally (i.e. for the majority of initial states) host off-diagonal long-range order. We discuss how this result applies more broadly, with systems which possess symmetries such as SU(N) and SO(N) also capable of hosting ordered, off-diagonal steady states when heating is applied which respects these symmetries. We term this mechanism of inducing ordered steady states via the heating of a system in the presence of such symmetries 'heating-induced order'.

In chapter 3 we then focus on the Hubbard model as an example of a physical system where this phenomenon can be observed. When defined over a bi-partite lattice, the Hamiltonian possesses a dual SU(2) symmetry structure and we simultaneously diagonalise the operator representation of these symmetries. This result allows us to analytically construct the steady states of the system under continuous heating. As a consequence of the mechanism of heating-induced order, these states possess long-range order in the SU(2) channels which are preserved and we study how the magnitude of this order scales with factors such as system size, lattice geometry and

filling. These results lead to the exciting possibility of inducing states which host either superconducting order, spin-wave order or even both simultaneously and we discuss how this could be achieved in an experimental setting.

In this vein, in chapter 4, we connect this mechanism of heating-induced order in the Hubbard model to a recent experiment observing photo-induced superconductivity in the molecular compound $\kappa - (\mathrm{BEDT} - \mathrm{TTF})_2\mathrm{Cu}[\mathrm{N}(\mathrm{CN})_2]\mathrm{Br}$. We present a simplistic model of the experimental setup based on a periodically driven quasi-1D triangular Hubbard model and show how the mechanism of heating-induced order occurs due to a unique and unexpected interplay between the driving and the lattice geometry. This interplay leads to the transient formation of an off-diagonal charge ordered state which may explain the superconducting observations in this experiment. More generally, we discuss how these results provide an understanding of how geometry can affect the response of strongly correlated systems under driving.

In chapter 5 we move on to focus on the phenomenon of non-stationarity in quantum systems, first describing typical mechanisms by which these systems can relax to an equilibrium state. We then introduce a set of symmetry-based conditions which, when satisfied, guarantee that an open quantum system will avoid this anticipated relaxation and undergo persistent, coherent oscillations in the long-time limit. We show how these conditions subsume and go beyond the well-established concept of a Decoherence Free Subspace: the resulting dynamics involving an interplay between both coherence and dissipation. We take the dissipative Hubbard model in the presence of a homogeneous magnetic field as a realistic setup which can satisfy the aforementioned conditions and numerically observe the resulting oscillatory non-stationary behaviour, with the sites of the open system undergoing identical, coherent oscillations in the long-time limit.

The constituents of such a system undergoing phase-locked, coherent oscillations is a hallmark feature of quantum synchronisation. This leads us to show how, in chapter 6, our conditions for non-stationarity — alongside the mechanism of heating-induced order — can be used to achieve perfect synchronisation in a generic open quantum system. Using perturbation theory, we demonstrate how this synchronisation is, to first order, unaffected by symmetry breaking perturbations. We present results from two paradigmatic examples where this robust synchronisation can be observed: the charge-dephased Hubbard model and a chain of qutrits. We show how, in each example, the induced synchronisation is underpinned by both long-range correlations and entanglement.

Finally, in the conclusion, we summarize the results of this thesis and discuss the many interesting avenues of future research it opens up - a number of which are actively being investigated.

Publications

A number of the results contained here have been published in papers involving the author of this thesis. The following are those for which JT was lead author:

- J. Tindall, B. Buča, J. R. Coulthard and D. Jaksch, Heating-Induced Long-Range η-Pairing in the Hubbard Model, *Physical Review Letters* **123**, 030603 (2019).

- J. Tindall, C. Sánchez Muñoz, B. Buča and D. Jaksch, Quantum synchronisation enabled by dynamical symmetries and dissipation, *New Journal of Physics* **22**, 013026 (2020).

- J. Tindall, F. Schlawin, M. Buzzi, D. Nicoletti, J. R. Coulthard, H. Gao, A. Cavalleri, M. A. Sentef and D. Jaksch, Dynamical order and superconductivity in a frustrated many-body system, *Physical Review Letters* **125**, 173001 (2020).

- J. Tindall, F. Schlawin, M. Sentef and D. Jaksch, Analytical Solution for the Steady States of the Driven Hubbard model, *Physical Review B* **103**, 035146 (2021).

For each of these papers JT wrote the manuscript, ran the numerical calculations and contributed substantially to discussions on the ideas presented. The remaining papers, in which JT was co-author, are listed below and specific contributions are detailed for each one:

- B. Buča, J. Tindall, and D. Jaksch, Non-stationary coherent quantum many-body dynamics through dissipation, *Nature Communications* **10**, 1730 (2019). *JT performed the numerical calculations, helped edit the manuscript and contributed substantially to discussions on the ideas presented in the paper.*

- M. Buzzi, D. Nicoletti, M. Fechner, N. Tancogne-Dejean, M. A. Sentef, A. Georges, M. Dressel, A. Henderson, T. Siegrist, J. A. Schlueter, K. Miyagawa, K. Kanoda, M.-S. Nam, A. Ardavan, J. R. Coulthard, J. Tindall, F. Schlawin, D. Jaksch, A. Cavalleri, Photo-molecular high temperature superconductivity, *Physical Review X* **10**, 031028 (2020).

JT ran the Matrix-Product-State calculations and made substantial contributions to the theoretical side of the manuscript.

Computational Resources

A number of computational resources were used in the development of this thesis and the aforementioned papers. Matrix Product State calculations for finding the ground state of a many-body quantum system and dynamically evolving it out of equilibrium were performed using both the Tensor Network Theory library [44] and Tenpy [45] — C and Python based libraries respectively for simulating large, low-dimensional, correlated quantum systems. For smaller systems, where exact diagonalisation routines were possible, calculations were performed with either self-written algorithms or QuTip — an open source Python-based toolbox for simulating open and closed quantum systems [46].

In terms of hardware, low intensity calculations were run on a custom-built workstation with a 3.6GHz i9-9900k processor, Nvidia Geforce RTX 3070 GPU and 32GB of RAM. Larger calculations were submitted to the University of Oxford Advanced Research Computing (ARC) facility Arcus-b — a high performance multi-core, multi-node computing cluster.

Funding

This PhD project has been funded by the Engineering and Physical Sciences Research Council (EPSRC) and the generous financial support of Dr Simon Harrison.

References

[1] W. Thomson, "On a universal tendency in nature to the dissipation of mechanical energy," *Proc. R. Soc. Edinb. A*, pp. 139–142, 1857.

[2] S. Frautschi, "Entropy in an expanding universe," *Science*, vol. 217, pp. 593–599, 1982.

[3] F. C. Adams and G. Laughlin, "A dying universe: The long-term fate and evolution of astrophysical objects," *Rev. Mod. Phys.*, vol. 69, pp. 337–372, 1997.

[4] E. Guggenheim, *Thermodynamics: an Advanced Treatment for Chemists and Physicists*. North-Holland Publishing Co., Amsterdam, 1985.

[5] S. Carnot, *Réflexions sur la puissance motrice du feu et sur les machines propres à développer cette puissance* (*Reflections on the motive power of fire*). Bachelier Libraire, Paris, 1824.

[6] J. Gibbs, *Elementary Principles in Statistical Mechanics*. Dover Books on Advanced Science, C. Scribner's Sons, New York, 1902.

[7] J. V. Neumann, "Beweis des ergodensatzes und des H-theorems in der neuen mechanik (Proof of the ergodic theorem and the H-theorem in quantum mechanics)," *Z. Physic*, vol. 57, pp. 30–70, 1929.

[8] J. V. Neumann, "Proof of the quasi-ergodic hypothesis," *Proc. Natl. Acad. Sci.*, vol. 18, pp. 70–82, 1932.

[9] P. Bocchieri and A. Loinger, "Ergodic foundation of quantum statistical mechanics," *Phys. Rev.*, vol. 114, pp. 948–951, 1959.

[10] J. V. Neumann and R. Beyer, *Mathematical Foundations of Quantum Mechanics*. Goldstine Printed Materials, Princeton University Press, Princeton, 1955.

[11] W. Schieve and L. Horwitz, *Quantum Statistical Mechanics*. Cambridge University Press, Cambridge, 2009.

[12] I. E. Farquhar and P. T. Landsberg, "On the quantum-statistical ergodic and H-theorems," *Proc. R. Soc. A*, vol. 239, p. 134–144, 1957.

[13] J. M. Deutsch, "Quantum statistical mechanics in a closed system," *Phys. Rev. A*, vol. 43, pp. 2046–2049, 1991.

[14] M. Srednicki, "Chaos and quantum thermalization," *Phys. Rev. E*, vol. 50, pp. 888–901, 1994.

[15] M. Rigol, V. Dunjko, and M. Olshanii, "Thermalization and its mechanism for generic isolated quantum systems," *Nature*, vol. 452, pp. 888–901, 2008.

[16] H. Kim, T. N. Ikeda, and D. A. Huse, "Testing whether all eigenstates obey the eigenstate thermalization hypothesis," *Phys. Rev. E*, vol. 90, p. 052105, 2014.

[17] V. Alba, "Eigenstate thermalization hypothesis and integrability in quantum spin chains," *Phys. Rev. B*, vol. 91, p. 155123, 2015.

[18] R. Steinigeweg, A. Khodja, H. Niemeyer, C. Gogolin, and J. Gemmer, "Pushing the limits of the eigenstate thermalization hypothesis towards mesoscopic quantum systems," *Phys. Rev. Lett.*, vol. 112, p. 130403, 2014.

[19] P. W. Anderson, "Absence of diffusion in certain random lattices," *Phys. Rev.*, vol. 109, pp. 1492–1505, 1958.

[20] R. Nandkishore and D. A. Huse, "Many-body localization and thermalization in quantum statistical mechanics," *Annu. Rev. Condens. Matter Phys.*, vol. 6, pp. 15–38, 2015.

[21] X. Li, S. Ganeshan, J. H. Pixley, and S. Das Sarma, "Many-body localization and quantum nonergodicity in a model with a single-particle mobility edge," *Phys. Rev. Lett.*, vol. 115, p. 186601, 2015.

[22] S. Gopalakrishnan and S. Parameswaran, "Dynamics and transport at the threshold

of many-body localization," *Phys. Rep.*, vol. 862, pp. 1–62, 2020.
[23] W. Hu, S. Kaiser, D. Nicoletti, C. R. Hunt, I. Gierz, M. C. Hoffmann, M. Le Tacon, T. Loew, B. Keimer, and A. Cavalleri, "Optically enhanced coherent transport in $YBa_2Cu_3O_{6.5}$ by ultrafast redistribution of interlayer coupling," *Nat. Mat.*, vol. 13, pp. 705–711, 2014.
[24] M. Mitrano, A. Cantaluppi, D. Nicoletti, S. Kaiser, A. Perucchi, S. Lupi, P. Di Pietro, D. Pontiroli, M. Riccò, S. R. Clark, D. Jaksch, and A. Cavalleri, "Possible light-induced superconductivity in K_3C_{60} at high temperature," *Nature*, vol. 530, pp. 461–464, 2016.
[25] A. Cavalleri, "Photo-induced superconductivity," *Contemp. Phys.*, vol. 59, pp. 31–46, 2018.
[26] D. A. Lidar, I. L. Chuang, and K. B. Whaley, "Decoherence-free subspaces for quantum computation," *Phys. Rev. Lett.*, vol. 81, pp. 2594–2597, 1998.
[27] A. Beige, D. Braun, B. Tregenna, and P. L. Knight, "Quantum computing using dissipation to remain in a decoherence-free subspace," *Phys. Rev. Lett.*, vol. 85, pp. 1762–1765, 2000.
[28] F. Verstraete, M. M. Wolf, and C. J. Ignacio, "Quantum computation and quantum-state engineering driven by dissipation," *Nat. Phys.*, vol. 5, pp. 633–636, 2009.
[29] W. D. Phillips and H. J. Metcalf, "Cooling and trapping atoms," *Sci. Am.*, vol. 256, pp. 50–56, 1987.
[30] C. N. Cohen-Tannoudji and W. D. Phillips, "New mechanisms for laser cooling," *Phys. Today*, vol. 43, pp. 33–40, 1990.
[31] S. Chu, "Laser Trapping of Neutral Particles," *Sci. Am.*, vol. 266, pp. 70–76, 1992.
[32] D. E. Pritchard, "Cooling neutral atoms in a magnetic trap for precision spectroscopy," *Phys. Rev. Lett.*, vol. 51, pp. 1336–1339, Oct 1983.
[33] M. H. Anderson, J. R. Ensher, M. R. Matthews, C. E. Wieman, and E. A. Cornell, "Observation of Bose-Einstein condensation in a dilute atomic vapor," *Science*, vol. 269, pp. 198–201, 1995.
[34] K. B. Davis, M. O. Mewes, M. R. Andrews, N. J. van Druten, D. S. Durfee, D. M. Kurn, and W. Ketterle, "Bose-Einstein condensation in a gas of sodium atoms," *Phys. Rev. Lett.*, vol. 75, pp. 3969–3973, 1995.
[35] S. R. White, "Density matrix formulation for quantum renormalization groups," *Phys. Rev. Lett.*, vol. 69, pp. 2863–2866, 1992.
[36] F. Verstraete, V. Murg, and J. Cirac, "Matrix product states, projected entangled pair states, and variational renormalization group methods for quantum spin systems," *Adv. Phys.*, vol. 57, pp. 143–224, 2008.
[37] R. Orús, "A practical introduction to tensor networks: Matrix product states and projected entangled pair states," *Ann. Phys.*, vol. 349, pp. 117–158, 2014.
[38] M. Somayazulu, M. Ahart, A. K. Mishra, Z. M. Geballe, M. Baldini, Y. Meng, V. V. Struzhkin, and R. J. Hemley, "Evidence for superconductivity above 260 K in lanthanum superhydride at megabar pressures," *Phys. Rev. Lett.*, vol. 122, p. 027001, 2019.
[39] E. Zurek, "Pushing towards room-temperature superconductivity," *American Physical Society Viewpoint*, 2019.
[40] F. Arute *et al.*, "Quantum supremacy using a programmable superconducting processor," *Nature*, vol. 574, pp. 505–510, 2019.
[41] W. D. Oliver, "Quantum computing takes flight," *Nature News and Views*, 2019.
[42] D. M. Lucas, C. J. S. Donald, J. P. Home, M. J. McDonnell, A. Ramos, D. N. Stacey,

J.-P. Stacey, A. M. Steane, and S. C. Webster, "Oxford ion-trap quantum computing project," *Phil. Trans. R. Soc. A*, pp. 1401–1408, 2003.

[43] M. Buzzi, D. Nicoletti, M. Fechner, N. Tancogne-Dejean, M. A. Sentef, A. Georges, T. Biesner, E. Uykur, M. Dressel, A. Henderson, T. Siegrist, J. A. Schlueter, K. Miyagawa, K. Kanoda, M.-S. Nam, A. Ardavan, J. Coulthard, J. Tindall, F. Schlawin, D. Jaksch, and A. Cavalleri, "Photomolecular high-temperature superconductivity," *Phys. Rev. X*, vol. 10, p. 031028, 2020.

[44] S. Al-Assam, S. R. Clark, and D. Jaksch, "The tensor network theory library," *J. Stat. Mech.: Theory Exp.*, p. 093102, 2017.

[45] J. Hauschild and F. Pollmann, "Efficient numerical simulations with tensor networks: Tensor Network Python (TeNPy)," *SciPost Phys. Lect. Notes*, p. 5, 2018.

[46] R. Johansson, P. Nation, and F. Nori, "Qutip 2: A python framework for the dynamics of open quantum systems," *Comput. Phys. Commun.*, vol. 184, pp. 1234–1240, 2013.

Chapter 1

Theory: Driven and Dissipative Quantum Systems

In this chapter a theoretical description of driven and dissipative quantum systems is introduced, which will be necessary for setting the context of this thesis. We begin in section 2.1 with coherently driven systems, motivating this field and detailing methods for treating the inclusion of time-dependent terms in a Hamiltonian. In section 2.2 we move on to the theory of dissipative quantum systems, introducing the field and deriving notable master equations for describing the evolution of a system coupled to an environment. We then focus specifically on the Gorini–Kossakowski–Sudarshan–Lindblad (GSKL) equation, which we derive for the case of weak coupling to an environment. We detail the mathematical properties of this equation and its relevance as a general quantum map for a Markovian open system. We numerically solve the equation for the simple, instructive example of a harmonic oscillator immersed in a finite temperature bath. We also introduce the concept of a Decoherence Free Subspace in the context of both the GSKL equation and open systems in general. In the last section of this chapter, Matrix Product State and quantum trajectory routines for the efficient simulation of driven and dissipative quantum systems are introduced. These computational methods will be used extensively in the rest of the thesis.

1.1 Driven Quantum Systems

Motivation

It is well known that driving can drastically change the behaviour and properties of physical systems. Examples in classical systems include the Kapitza pendulum, where vibrations in the suspension point of a pendulum can stabilize the inverted

position [1], and suspension bridges, where winds can create structural instabilities with potentially disastrous consequences [2].

Unsurprisingly, the transformative power of driving has also been recognised in the context of quantum systems. Similar advances in technology to those which led to the realisation of ultracold atomic lattices mean that quantum systems can be controlled, and have their properties altered, with coherent, periodic laser pulses [3, 4].

Treating Driven Quantum Systems

In this thesis, we will be treating various quantum systems under the influence of coherent, periodic driving. This driving typically modifies the Hamiltonian, making it periodic and time-dependent, i.e. $H \to H(t) = H(t + \mathrm{T})$ where T is the driving period and t is time. The form of the Schrödinger equation remains the same as in the time-independent case (from here on we will always set $\hbar = 1$)

$$\mathrm{i}\frac{d\,|\psi(t)\rangle}{dt} = H(t)\,|\psi(t)\rangle\,, \tag{1.1}$$

where $|\psi(t)\rangle$ is the state of the system at time t. Despite this, the solution is more intricate than the direct exponentiation $|\psi(t)\rangle = \exp\big(-iHt\big)\,|\psi(0)\rangle$ which solves the time-independent case. Specifically, due to the time-dependence in H, we have to build up the solution over a finite time-interval via an infinite product of the time-independent solution over infinitesimally small intervals

$$|\psi(t)\rangle = \lim_{N\to\infty} \exp\big(-\mathrm{i}H(t)\delta t\big)\exp\big(-\mathrm{i}H(t-\delta t)\delta t\big)\ldots\exp\big(-\mathrm{i}H(0)\delta t\big)\,|\psi(0)\rangle\,, \tag{1.2}$$

where $\delta t = \lim_{N\to\infty} t/N$. This is more formally written as an 'ordered exponential'

$$|\psi(t)\rangle = U(t,0)\,|\psi(0)\rangle = \mathbb{T}\exp\left(-\mathrm{i}\int_0^t H(t')dt'\right)|\psi(0)\rangle\,, \tag{1.3}$$

where $U(t,0)$ is the unitary propagator from time 0 to time t and $\mathbb{T}$ is an operator which time-orders the exponential[1] and is necessary because the Hamiltonian does not, in general, commute with itself at different times.

The most straightforward way to numerically implement the formal solution in Eq. (1.3) is in the manner of Eq. (1.2) but with a finite N. The value of N needs to be made sufficiently large in order to avoid incurring significant errors from ignoring the time-ordering operator over a given interval δt. For additional accuracy, one can use

[1] This operator orders any product of operators such that their time-ordered arguments increase from left to right: i.e. $\mathbb{T}O(t_2)O(t_1)O(t_3) = O(t_3)O(t_2)O(t_1)$ if $t_3 > t_2 > t_1$.

the integrated Hamiltonian over a given time interval $t' \to t' + \delta t$ in the exponential instead of just $H(t')$.

From an analytical perspective the time-ordering and integration in Eq. (1.3) make interpreting the effect of the Hamiltonian on the system difficult. Here it is useful to apply Floquet theory, a ubiquitous mathematical tool for treating periodic linear differential equations [5] which is often used to analyse the evolution induced by time-periodic Hamiltonians [6, 7, 8, 9].

Floquet theory allows us to introduce an effective, time-independent Floquet Hamiltonian H_{F} which defines the time evolution of the system over a stroboscopic period, i.e.

$$U(\mathrm{T}, 0) = \exp(-\mathrm{i}H_{\mathrm{F}}\mathrm{T}) = \mathbb{T}\exp\left(-\mathrm{i}\int_0^{\mathrm{T}} H(t')dt'\right). \tag{1.4}$$

This effective Hamiltonian can be constructed through a Floquet-Magnus expansion which corresponds to writing the Floquet Hamiltonian as an infinite series

$$H_{\mathrm{F}} = \sum_{n=0}^{\infty} \mathrm{T}^n \Omega_n, \tag{1.5}$$

and using a recursive procedure to relate the series terms Ω_n to the original Hamiltonian $H(t)$ [10, 11]. The first few terms in the series read

$$\begin{aligned} \Omega_0 &= \frac{1}{\mathrm{T}}\int_0^{\mathrm{T}} H(t')dt', \\ \Omega_1 &= \frac{1}{2\mathrm{i}\mathrm{T}^2}\int_0^{\mathrm{T}}\int_0^{t'} [H(t'), H(t'')]dt''dt', \end{aligned} \tag{1.6}$$

and subsequent terms are generated by further nested integrals and commutators [11]. The propagator in Eq. (1.4) only gives us access to the state of the system at 'stroboscopic' instances of time $t = n\mathrm{T}$ $n \in \mathbb{Z}$ and thus is not a 'proper' propagator in the sense it does not provide a full solution to the system's dynamics and cannot be used to observe any micromotion (dynamics on timescales shorter than T). In order to access such timescales a 'kick' operator can be defined in terms of the Floquet Hamiltonian and the more general propagator $U(t, 0)$ [12], which does give access to the system's micromotion.

This kick operator is, however, more complicated than the Floquet Hamiltonian and so the dynamics of the system are often analysed from a 'coarse-grained' perspective using just H_F. Construction of this Floquet Hamiltonian usually involves a truncation of Eq. (1.5) up to some $n = m$ and is more accurate for larger driving frequencies and when the desired evolution time is relatively short. This truncation

often shares qualitatively similar properties to the full series expansion and thus can offer useful information on the response of the system to the driven Hamiltonian [6, 13]. In general, however, the full series does not converge and thus it is difficult to identify an appropriate truncation that can be made, especially when considering the dynamics on longer time-scales [14, 15].

This general lack of convergence of the summation in Eq. (1.5) is intimately tied to the notion of ergodicity in many-body quantum systems. Even if the Hamiltonian contains only short-range operators, the higher order terms in the Floquet-Magnus expansion contain products of multiple copies of these operators and thus repeated application of the Floquet propagator is capable of exciting a multitude of eigenstates of the Hamiltonian. This typically[2] leads to the time-evolution of the driven system covering the whole of phase space and the formation of a featureless infinite temperature state in the long-time limit, a mechanism termed Floquet heating [14].

Engineering driven quantum systems is thus often a case of setting up Floquet Hamiltonians which establish dynamical order on some transient timescale, whilst mitigating the effects of heating within this prethermal regime. In the subsequent chapters, we will take a very different approach to this by imposing certain symmetries on quantum systems whilst they undergo Floquet heating. The resulting maximum entropy states[3] which form in the relevant symmetry subspace in the long-time limit are capable of hosting desirable long-range correlations and thus are the target of the periodic driving — as opposed to some transient, prethermal state.

In the next section of this chapter we move onto a description of quantum systems coupled to an environment; which can also have a dramatic influence on the system's dynamics and is capable of inducing the formation of such correlated maximum entropy states.

1.2 Dissipative Quantum Systems

Motivation

The state of an isolated system, whether driven or undriven, is described by a pure wavefunction $|\psi(t)\rangle$ which is a complex valued vector defined over the Hilbert space $\mathcal{H}$.

[2] Many-body localised systems and integrable systems are known exceptions to this [16, 17, 18, 19] — at least in the sense they avoid Floquet heating on any reasonable timescale.

[3] As we will further clarify in the following chapter, in this thesis we define a maximum entropy state as the identity matrix over all available basis states in the relevant symmetry subspace. For pure states, we are referring to the state which mimics such an identity matrix at the level of few-body observables.

The time dynamics is described by the Schrödinger equation which has the solution in Eq. (1.3), where the time-ordering and integration are redundant if the Hamiltonian is time-independent.

If, instead, we now consider a composite Hilbert space which is formed from two subspaces or systems $\mathcal{H} = \mathcal{H}_A \otimes \mathcal{H}_B$ — how can we describe the state of, say, system A only? This is the question which led von Neumann to introduce the density matrix, a statistical ensemble of pure states [20]. If the state of the system in the total Hilbert space is $|\psi(t)\rangle$, then the state of system A is a 'reduced' density matrix found by tracing out the degrees of freedom of B, i.e. $\rho_A(t) = \mathrm{Tr}_B\big(|\psi(t)\rangle\langle\psi(t)|\big)$ where we have taken the partial trace over the basis vectors which span $\mathcal{H}_B$. Additionally, the time dynamics in A can be found by taking the partial trace of the von Neumann equation

$$\frac{\partial \rho_A(t)}{\partial t} = -\mathrm{i}\ \mathrm{Tr}_B\big[H, |\psi(t)\rangle\langle\psi(t)|\big]. \tag{1.7}$$

Equation 1.7 is a *quantum mechanical master equation* as it describes the full dynamics of both the diagonal and off-diagonal elements of the density matrix. It has the formal solution

$$\rho_A(t) = \Lambda_t\big[\rho_A(0)\big] = \mathrm{Tr}_B\Big(U(t)\,|\psi(t)\rangle\langle\psi(t)|\,U(t)^\dagger\Big), \tag{1.8}$$

where $\Lambda_t\big[\,\cdot\,\big]$ is the map which propagates the density matrix forward in time and $U(t) = \exp(-\mathrm{i}Ht)$.

This is more than just an exercise in reduced density matrices and partial traces. Equations (1.7) and (1.8) are at the heart of the concept of open quantum systems, accurately describing the time-dependence of a system A we wish to probe which is in contact with a second system B — often described as the 'environment'.

The problem of a quantum system coupled to an environment is easily stated and encapsulated in Eq. (1.8). Despite this, its solution is not so straightforward. Firstly, being able to write down a full Hamiltonian describing the action of both the system and the environment is not often possible. Whilst the system of interest may be precisely defined, the environment is usually much larger — containing a vast number of interacting degrees of freedom (d.o.f) which are complicated to model, let alone take the partial trace over. Furthermore, even if the map Λ_t which time-evolves the system's density matrix can be written down, applying it to propagate the system forward in time is a difficult task in itself — the non-unitary nature of the map, as well as the exponentially growing size of the Hilbert space if it is a many-body system are significant obstacles.

No quantum system, however, is truly isolated and one of the first examples where an open quantum system treatment found use was in the field of quantum optics [21] which stemmed from the development of the laser in the early 1960s. Methods were required to accurately describe the competition between the coherent and incoherent dissipative mechanisms at work in the lasing process [22]. In addition, out of the field of quantum optics have sprung various research areas ranging from ultracold atomic systems [23, 24] to ion-trap quantum computers [25]. In these areas, a rigorous understanding and modelling of the effect of decoherence and dissipation is crucial to developing robust, coherent quantum setups and technologies.

It is for these reasons, and the general complexity of the problem, that the extent of research into describing and modelling open quantum systems is vast. Many different approaches have been taken — from rigorous mathematical work to more empirically based treatments specific to the problem at hand. An exhaustive description would extend beyond the length of this thesis and so here we focus on some of the most notable results which are pertinent to our work.

Treating Open Quantum Systems

The following derivations are partially based on the methodology described in Refs. [21, 22, 26, 27, 28].

The Nakajima–Zwanzig Equation - Possibly the most general treatment of an open quantum system comes from the Nakajima–Zwanzig equation (NZE) which was developed, independently, by Sadao Nakajima and Robert Zwanzig during the late 1950s [29, 30]. Nakajima and Zwanzig sought steady state solutions for the state of a system (S) which is coupled to an environment (E). The Hilbert space is $\mathcal{H} = \mathcal{H}_S \otimes \mathcal{H}_E$ and the total dynamics is governed by the Quantum Liouville equation

$$\frac{\partial \rho(t)}{\partial t} = -\mathrm{i}[H_S + H_E + \alpha H_{\mathrm{int}}, \rho(t)], \tag{1.9}$$

where $\rho(t)$ is the density matrix of the system + environment[4] at time t and H_S, H_E and H_{int} are, respectively, the Hamiltonians governing the system, environment and the system-environment interaction. The dimensionless parameter α quantifies the strength of the system-environment coupling.

To make things simpler we move into the interaction picture, where all operators, including the density matrix, are denoted with a prime and can be related to their

[4]The full state of the system + environment is taken here to be a density matrix $\rho(t)$ as opposed to a pure state $|\psi(t)\rangle$ in order to be as general as possible.

counterparts in the Schrödinger picture via $A'(t) = \exp(\mathrm{i}(H_S + H_E)t)A\exp(-\mathrm{i}(H_S + H_E)t)$. In this picture the equation of motion for the density matrix reads

$$\frac{\partial\rho'(t)}{\partial t} = -\mathrm{i}\alpha[H'_{\mathrm{int}}(t), \rho'(t)] = \alpha\mathcal{L}(t)\rho'(t), \tag{1.10}$$

where $\mathcal{L}(t)$ is defined as $\mathcal{L}(t)\bullet = -\mathrm{i}[H'_{\mathrm{int}}(t), \bullet]$ and encodes the time-dynamics of the system.

The key methodology in deriving the NZE is to introduce a projection operator $\mathcal{P}^2 = \mathcal{P}$ which projects the density matrix onto a 'relevant' part of the total Hilbert space, i.e. $\rho'_R = \mathcal{P}\rho'$ [26]. This projector is defined explicitly with $\rho'_R = \mathcal{P}\rho' = \mathrm{Tr}_E(\rho') \otimes \rho_E$, i.e. it takes the reduced density matrix of the system and couples it to some fixed state of the environment ρ_E. This projection means we can focus on deriving an equation which explicitly describes the dynamics of $\rho'_R(t)$ — as opposed to the dynamics of the density matrix in the total Hilbert space. Naturally this projection also introduces $\mathcal{Q} = 1 - \mathcal{P}$ and $\rho'_I = \mathcal{Q}\rho'$, the projector and density matrix for the 'irrelevant' part of the Hilbert space.

We proceed by applying these projectors to Eq. (1.10)

$$\frac{\partial}{\partial t}\begin{pmatrix}\rho'_R(t)\\ \rho'_I(t)\end{pmatrix} = \alpha\begin{pmatrix}\mathcal{P}\\ \mathcal{Q}\end{pmatrix}\cdot\begin{pmatrix}\mathcal{L}(t)\rho'_R(t) + \mathcal{L}(t)\rho'_I(t)\\ \mathcal{L}(t)\rho'_R(t) + \mathcal{L}(t)\rho'_I(t)\end{pmatrix}, \tag{1.11}$$

giving us the equations of motion for the density matrix in both the relevant and irrelevant part. Next, we integrate the equation for ρ'_I

$$\rho'_I(t) = \mathcal{G}(t,0)\rho'_I(t=0) + \alpha\int_0^t \mathcal{G}(t,s)\mathcal{Q}\mathcal{L}(s)\rho'_R(s)ds, \tag{1.12}$$

where $\mathcal{G}(t,s) = \mathbb{T}\exp(\alpha\int_s^t \mathcal{Q}\mathcal{L}(s')ds')$ is a time-ordered propagator, and substitute the expression for $\rho'_I(t)$ into the equation of motion for $\rho'_R(t)$ to get

$$\frac{\partial\rho'_R(t)}{\partial t} = \alpha\mathcal{P}\mathcal{L}(t)\rho'_R(t) + \alpha\mathcal{P}\mathcal{L}(t)\mathcal{G}(t,0)\rho'_I(0) + \alpha^2\int_0^t \mathcal{K}(t,s)\rho'_R(s)ds, \tag{1.13}$$

where $\mathcal{K}(t,s) = \mathcal{P}\mathcal{L}(t)\mathcal{G}(t,s)\mathcal{Q}\mathcal{L}(s)\mathcal{P}$ is the memory kernel.

Equation (1.13) can be simplified if we make several assumptions. The first assumption is that the system and the environment are uncorrelated at time $t = 0$: $\rho(0) = \rho_S(0) \otimes \rho_E(0)$. Physically, this can be interpreted as the system and environment not coming into contact with each other until the 'origin' time $t = 0$. Following this assumption, we can then choose $\rho_E(0)$ to be consistent with ρ_E, the fixed state of the environment which $\mathcal{P}$ projects onto, then we have $\mathcal{P}\rho(0) = \rho(0)$ and so $\rho'_I(0) = Q\rho'(0) = 0$ (obviously $\rho'(0) = \rho(0)$). The second assumption is

more technical and corresponds to assuming that the odd moments of the interaction Hamiltonian with respect to the bath vanish, i.e.

$$\mathrm{Tr}_B\left(\left(\prod_{i=1}^{2n+1} H_{\mathrm{int}}(t_i)\right)\rho_E\right) = 0, \tag{1.14}$$

from which we can show that $\mathcal{P}\left(\prod_{i=1}^{2n+1}\mathcal{L}(t_i)\right)\mathcal{P} = 0$.

Whilst this second assumption is not always used in deriving the NZE equation, it simplifies the final equation and will be useful further on. Moreover, this assumption is often found to be valid. For example, in a thermal environment composed of harmonic oscillators, then H_e will be quadratic in the creation and annihilation operators, whilst the system-bath coupling is likely to be linear [31] — leading to odd moments of $\mathcal{L}$ vanishing upon taking the trace over the environment. Taking this assumption, along with our assumption about the initial state, it follows that Eq. (1.13) reduces to

$$\frac{\partial \rho_R'(t)}{\partial t} = \alpha^2 \int_0^t \mathcal{K}(t,s)\rho_R'(s)ds, \tag{1.15}$$

which is the Nakajima–Zwanzig equation. This is an exact equation for the dynamics of the relevant part of the system, given our two assumptions.

Whilst the NZE is elegantly expressed in Eq. (1.15), it is very difficult to solve as it is non-local in time, with the current state of the system being dependent on its full history which is written within the memory kernel $\mathcal{K}(t,s)$. As a consequence, applications and solutions of the NZE are sparse, typically limited to systems with a small number of degrees of freedom and coupled to baths of fairly simple structure — a predominant example being one or two qubits coupled to bosonic baths [32, 33, 34, 35].

Nonetheless, these examples are often instructive on the validity of the variety of approximations made in order to simplify the NZE into a more soluble equation which can be used to treat a larger variety of open quantum systems. In the following we systematically introduce these approximations, deriving increasingly soluble master equations for the dynamics of an open quantum system.

Before we proceed with the derivation it is important to introduce the various timescales involved in our open system problem. The first, τ_R, is the timescale of the dynamics of the total system + environment and describes the time in which the density matrix of the system will vary appreciably when coupled to the environment — this is the timescale we are interested in and wish to witness the system's dynamics over. There are two further timescales τ_E and τ_S which are, respectively, the timescale on which the system effects the environment and the timescale on which the system

relaxes when left under the sole influence of its own Hamiltonians H_s. We will see that the relative magnitudes of τ_R, τ_E and τ_S will play a key role in the subsequent approximations.

Born Approximation - One of the first approximations we can make is to take the interaction term αH_{int} to be small relative to the energy scales (i.e. the differences in eigenvalues) of both H_S and H_E. This weak-coupling approximation motivates us, by expanding $\mathcal{G}(t,s)$ in powers of α, to truncate Eq. (1.15) up to a certain order in the interaction parameter α. The simplest truncation we can do is to second order in α, i.e letting $\mathcal{G}(t,s) = 1 + \mathcal{O}(\alpha)$ so that

$$\frac{\partial \rho'_R(t)}{\partial t} = \alpha^2 \int_0^t \mathcal{P}\mathcal{L}(t)\mathcal{Q}\mathcal{L}(s)\mathcal{P}\rho'_R(s)ds + \mathcal{O}(\alpha^3). \tag{1.16}$$

This truncation, along with our earlier odd-moment assumption $\mathcal{P}\mathcal{L}(t)\mathcal{P} = 0$, effectively means that states in the irrelevant part of the Hilbert space are unaffected by the interaction Hamiltonian. As a result, if the initial state of the environment $\rho_E(0) = \rho_E$ is in equilibrium with respect to the Hamiltonian H_{E} then it will be stationary in time.

It is worth mentioning that we are only considering the environment to be unaffected by the interaction Hamiltonian when viewed over the timescale of interest τ_R. The system is able to affect environment on the timescale τ_E and induce correlations but if they are weakly coupled and the environment is sufficiently large compared to the system then $\tau_E \ll \tau_R$ and these excitations will quickly decay away on the scale of τ_R. The weak-coupling approximation we have made is thus intrinsically related to the assumption that the timescales τ_R and τ_E are well separated, with $\tau_E \ll \tau_R$.

Returning to Eq. (1.16), we can simplify it by using $\mathcal{Q} = 1 - \mathcal{P}$, applying the odd-moment assumption and ignoring the term of order α^3 to get

$$\frac{\partial \rho'_R(t)}{\partial t} = \alpha^2 \int_0^t \mathcal{P}\mathcal{L}(t)\mathcal{L}(s)\mathcal{P}\rho'_R(s)ds. \tag{1.17}$$

Now we revert from the projection operator picture and re-introduce $\mathcal{L}(t)\bullet = -\mathrm{i}[H'_{\text{int}}(t), \bullet]$ and the projection $\mathcal{P}\rho'(t) = \text{Tr}_E(\rho'(t)) \otimes \rho'_E = \rho'_S(t) \otimes \rho'_E$ which is the tensor product of the reduced density matrix of the system at time t and the initial state of the environment. With this re-introduction, and by tracing over the environment afterwards, we get

$$\frac{\partial}{\partial t}\rho'_S(t) = -\alpha^2 \int_0^t \text{Tr}_E\Big([H'_{\text{int}}(t), [H'_{\text{int}}(s), \rho'_S(s) \otimes \rho'_E]]\Big)ds. \tag{1.18}$$

which is the *Born* approximation to the NZE. We note that this equation can also be arrived at by directly integrating Eq. (1.10) and re-substituting it back into the equation — making the assumption that, due to the weak coupling between the system and the environment, they remain uncorrelated $\rho'(t) = \rho'_S(t) \otimes \rho'_E$ for all times, with the state of the environment approximately unchanged in time [26] and having no back-action on the system when viewed over the timescale of interest τ_R.

Time Locality and the Markov Approximation - Equation (1.18) is still an integro-differential equation which is non-local in time, i.e. the dynamics of the system still depend on the integration of the full history of the system. In order to render the equation manageable we want it to be time-local. We can achieve this by letting $\rho'_S(s) \to \rho'_S(t)$, which is the first step in the Markov approximation, and arriving at

$$\frac{\partial}{\partial t}\rho'_S(t) = -\alpha^2 \int_0^t \mathrm{Tr}_E\big([H'_{\mathrm{int}}(t), [H'_{\mathrm{int}}(s), \rho'_S(t) \otimes \rho'_E]]\big) ds. \tag{1.19}$$

This equation is now time-local, although it is still dependent on the initial preparation of the system and the bath. In order to rectify this we perform the second step in the Markov approximation which involves the substitution $s \to t - s$ and taking the upper limit on the integral $t \to \infty$, giving us the Redfield Equation [36]

$$\frac{\partial}{\partial t}\rho'_S(t) = -\alpha^2 \int_0^\infty \mathrm{Tr}_E\big([H'_{\mathrm{int}}(t), [H'_{\mathrm{int}}(t-s), \rho'_S(t) \otimes \rho'_E]]\big) ds. \tag{1.20}$$

The Markov approximation, which consisted of the replacement $\rho'_S(s) \to \rho'_S(t)$ and letting the upper limit on the integral in Eq. (1.19) go to infinity, is justified under the earlier assumption that the time-scale of the open system's dynamics τ_R is orders of magnitude larger than the time τ_E on which any correlation functions within the environment decay. As a result the environment has a short-term memory and Eq. (1.20) has coarse-grained out the time-scale on which the bath's correlation functions decay. The Redfield equation is Markovian: the state of the system at time $t + dt$ is dependent solely on the previous state of the system at time t.

The Redfield equation was first derived by A. G. Redfield in the context of Nuclear Magnetic Resonance spectroscopy [36], providing an equation of motion for the dynamics of a system of nuclear spins coupled weakly to a crystal lattice and under the influence of an external magnetic field. It has since found application in a number of problems, most successfully decribing electron transfer in biological and chemical reaction processes [37, 38, 39, 40].

Nonetheless, the equation is still difficult to solve, even numerically, as it describes the evolution of the system over both the timescale τ_S on which the system would

relax under its own Hamiltonian and the timescale τ_R on which the state of the system varies due to its coupling with the environment. We will now see how the rotating wave approximation can be used to separate out these time-scales.

Further Simplifications and the Rotating Wave Approximation - We proceed in an attempt to render Eq. (1.20) into a more tractable form. Firstly, without loss of generality, we will absorb α into the system-bath interaction and write it in the form $H_{\text{int}} = \sum_\mu A_\mu \otimes B_\mu$ where A_μ and B_μ are Hermitian operators acting on the system and environment respectively. The A_μ operators can be expressed in terms of eigenoperators of the system Hamiltonian H_S by introducing

$$A_\mu(\omega) = \sum_{E-E'=\omega} \mathcal{P}_E A_\mu \mathcal{P}_{E'} \qquad \mathcal{P}_E = |E\rangle\langle E|, \tag{1.21}$$

where $|E\rangle$ is the eigenvector of H_S with energy E. From this it is clear that $A_\mu(\omega)$ is a valid eigenoperator, i.e. $[H_s, A_\mu(\omega)] = -\omega A_\mu(\omega)$, which satisfies

$$e^{\mathrm{i}H_S t} A_\mu(\omega) e^{\mathrm{i}H_S t} = e^{-i\omega t} A_\mu(\omega). \tag{1.22}$$

By introducing the adjoint $A_\mu^\dagger(\omega)$ we also observe the relations $[H_S, A_\mu^\dagger(\omega) A_{\mu'}(\omega)] = 0$ and $A_\mu^\dagger(-\omega) = A_\mu(\omega)$, alongside the completeness condition $\sum_\omega A_\mu(\omega) = \sum_\omega A_\mu^\dagger(\omega) = A_\mu$.

The interaction term can now be written as $H_{\text{int}} = \sum_{\mu,\omega} A_\mu(\omega) \otimes B_\mu$, which we rotate into the interaction picture via $H'_{\text{int}} = \sum_{\mu,\omega} e^{-i\omega t} A_\mu(\omega) \otimes B'_\mu$. Substituting this into our master equation in Eq. (1.20) and expanding the commutators we get

$$\frac{\partial}{\partial t}\rho'_S(t) = \sum_{\omega,\omega'} \sum_{\mu,\mu'} e^{\mathrm{i}(\omega-\omega')t} \Gamma_{\mu\mu'}(\omega) \left(A_{\mu'}(\omega) \rho'_S(t) A_\mu^\dagger(\omega') - A_\mu^\dagger(\omega') A_{\mu'}(\omega) \rho'_S(t) \right) + \text{h.c.} \tag{1.23}$$

where

$$\Gamma_{\mu\mu'}(\omega) = \int_0^\infty e^{\mathrm{i}\omega s} \mathrm{Tr}_E(B_\mu'^\dagger(t) B'_{\mu'}(t-s)\rho_E) ds, \tag{1.24}$$

are the environment correlation functions. As ρ_E is a stationary state of the environment $[H_E, \rho_E] = 0$ we find that these correlations functions are time-translationally invariant and we can write $\mathrm{Tr}_B(B_\mu'^\dagger(t) B_{\mu'}(t-s)\rho_E) = \mathrm{Tr}_B(B_\mu'^\dagger(s) B_{\mu'}(0)\rho_E)$, removing the dependence on t.

We now introduce the rotating wave approximation, also commonly referred to as the secular approximation. Our earlier approximations were motivated by assuming the time-scale on which the correlation functions within the environment decay[5] is much smaller than the time-scale of the total system + environment dynamics.

[5]We note that the bath's correlations will only truly decay if it is infinitely large, involving a continuum of frequencies and avoiding the quantum analogue of the Poincaré recurrence theorem [41].

Now τ_S, the typical time-scale of the internal evolution of the system, can be directly related to the average value of $1/|(\omega-\omega')|$. The rotating wave approximation involves assuming this time-scale is much smaller in comparison with the relaxation time τ_R of the system when it is under the action of both its own Hamiltonian and the influence of the environment. As a result, the term $e^{\mathrm{i}(\omega-\omega')t}$ will oscillate rapidly over the course of the time-scale τ_R, averaging to zero. Consequently we can neglect the cross terms in Eq. (1.23) to find

$$\frac{\partial}{\partial t}\rho'_S(t) = \sum_{\omega}\sum_{\mu,\mu'}\Gamma_{\mu,\mu'}(\omega)\Big(A_{\mu'}(\omega)\rho'_S(t)A^\dagger_\mu(\omega) - A^\dagger_\mu(\omega)A_{\mu'}(\omega)\rho'_S(t)\Big) + \text{H.c.} \quad (1.25)$$

Deconstructing $\Gamma_{\mu,\mu'}(\omega)$ as

$$\begin{aligned}\Gamma_{\mu,\mu'}(\omega) &= \frac{1}{2}\gamma_{\mu,\mu'}(\omega) + \mathrm{i}S_{\mu,\mu'}(\omega),\\ \gamma_{\mu,\mu'} &= \Gamma_{\mu,\mu'}(\omega) + \Gamma^*_{\mu',\mu}(\omega),\\ S_{\mu,\mu'}(\omega) &= \frac{1}{2\mathrm{i}}\big(\Gamma_{\mu,\mu'}(\omega) - \Gamma^*_{\mu',\mu}(\omega)\big),\end{aligned} \quad (1.26)$$

we finally arrive at the interaction picture master equation

$$\frac{\partial}{\partial t}\rho'_S(t) = -\mathrm{i}[H_{LS}, \rho'_S(t)] + \mathcal{D}(\rho'_S(t)), \quad (1.27)$$

where we have defined the 'Lamb Shift' Hamiltonian which renormalizes the energy levels of the system [28]

$$H_{\mathrm{LS}} = \sum_{\omega}\sum_{\mu\mu'} S_{\mu,\mu'}(\omega)A_\mu(\omega)^\dagger A_{\mu'}(\omega), \quad (1.28)$$

and we also have

$$\mathcal{D}(\rho'_S(t)) = \sum_{\omega}\sum_{\mu,\mu'}\gamma_{\mu,\mu'}(\omega)\Big(A_{\mu'}(\omega)\rho'_S A^\dagger_\mu(\omega) - \frac{1}{2}\{A^\dagger_\mu(\omega)A_{\mu'}(\omega), \rho'_S(t)\}\Big). \quad (1.29)$$

We can return to the Schrödinger picture by performing the substitution: $\rho'_S(t) = \exp(-\mathrm{i}(H_S + H_E)t)\rho_S(t)\exp(\mathrm{i}(H_S + H_E)t)$ and taking advantage of the relation in Eq. (1.22) which tells us $\mathcal{D}(\rho'_S(t)) = \exp(-\mathrm{i}(H_S + H_E)t)\mathcal{D}(\rho_S(t))\exp(\mathrm{i}(H_S + H_E)t)$. Equation (1.27) in the Schrödinger picture then reads

$$\frac{\partial}{\partial t}\rho_S(t) = -\mathrm{i}[H_{LS} + H_S, \rho_S(t)] + \mathcal{D}(\rho_S(t)). \quad (1.30)$$

The GSKL Equation - The dissipator term in this equation can be re-written by performing a diagonalisation of the matrix $\gamma(\omega)$ formed from the coefficients $\gamma_{\mu,\mu'}(\omega)$. We have that

$$\gamma_{\mu,\mu'}(\omega) = \int_{-\infty}^{\infty} e^{\mathrm{i}\omega s}\mathrm{Tr}_E\big(B^\dagger_\mu(s)B_{\mu'}(0)\rho_E\big)ds, \quad (1.31)$$

which follows from combining Eqs. (1.26) and (1.24), along with the time-translational invariance of the environment correlations $\mathrm{Tr}_E\big(B^\dagger_\mu(t)B_{\mu'}(t-s)\rho_E\big)$. This invariance also means they are of the positive type [42] and so, from Bochner's theorem [43], the Fourier transform is as well, leading to the matrix $\gamma(\omega)$ being positive semidefinite. Hence we can diagonalise $\gamma(\omega)$ via the unitary transform $v(\omega)$

$$v^\dagger(\omega)\gamma(\omega)v(\omega) = \begin{pmatrix} \gamma'_1(\omega) & 0 & 0 & 0 \\ 0 & \gamma'_2(\omega) & \cdots & 0 \\ \vdots & \vdots & \ddots & \vdots \\ 0 & 0 & \cdots & \gamma'_N(\omega) \end{pmatrix}. \tag{1.32}$$

We can also use this transformation to introduce a new operator basis $L_j(\omega) = \sum_\mu v_{\mu,j}A_\mu(\omega)$. It then follows that Eq. (1.30) is equivalent to

$$\frac{\partial}{\partial t}\rho_S(t) = -\mathrm{i}[H_{LS}+H_S,\rho_S(t)] + \sum_{i,\omega}\gamma'_i(\omega)\big(L_i(\omega)\rho_S(t)L_i^\dagger(\omega) - \frac{1}{2}\{L_i^\dagger(\omega)L_i(\omega),\rho_S(t)\}\big). \tag{1.33}$$

Equation (1.33) is in the form of the Gorini–Kossakowski–Sudarshan–Lindblad equation, which in this thesis we refer to as the GSKL equation. This celebrated master equation can be more generally written as

$$\frac{\partial}{\partial t}\rho(t) = \mathcal{L}\rho = -\mathrm{i}[H,\rho] + \sum_j \gamma_j\big(L_j\rho L_j^\dagger - \frac{1}{2}\{L_j^\dagger L_j,\rho(t)\}\big), \tag{1.34}$$

and describes the dynamics of the density matrix of a system, ρ, under the coherent evolution of the Lamb-shifted Hamiltonian H and that of jump operators L_j describing the interaction between the system and an environment. We have also introduced $\mathcal{L}$ which is often referred to as the Liouvillian superoperator; it is not the same Liouvillian as in Eq. (1.10) and acts solely on the Banach space (the bounded space of linear operators) of the system, as opposed to the Banach space of the system and environment. We note that the Lamb shift H_{LS} is often ignored in applications of the GSKL equation in literature [44, 45].

The GSKL equation is frequently used when studying open quantum systems. Despite the number of approximations used to reach it, it has found validity in many problems and is much more tractable than its counterparts we derived along the way. In the following we will explore the properties of the GSKL equation, as well as introducing several physical examples of open systems which can be described and solved using this equation.

The GSKL Equation

The GSKL equation in Eq. (1.34) has the solution

$$\rho(t) = \Lambda_t \rho(0) = e^{\mathcal{L}t}\rho, \tag{1.35}$$

where the map Λ_t encodes the time evolution of the system. It can be shown that this map satisfies several physical properties that we would expect of our Markovian master equation

$$\begin{aligned}
&\bullet\ \mathrm{Tr}(\Lambda_t \rho(s)) = \mathrm{Tr}(\rho(s)) \quad \forall \rho - \text{Trace Preservation},\\
&\bullet\ \Lambda_t \rho(s) \geq 0 \quad \forall \rho(s) \geq 0 - \text{Positivity Preservation},\\
&\bullet\ \Lambda_t \Lambda_s = \Lambda_{t+s} - \text{Semigroup Property},\\
&\bullet\ \lim_{t\to 0} \Lambda_t \rho(s) = \rho(s) - \text{Continuity}.
\end{aligned} \tag{1.36}$$

Properties 1 and 2 dictate that the positivity and trace of any density matrix is preserved under Λ_t, ensuring that any valid density matrix remains a valid density matrix. Property 3 is known as the semigroup property and reflects the Markovian nature of the equation — the time-evolution of the system is only dependent upon its current state and not its past. Finally, the fourth property states that the map is continuous and well-behaved in the limit $t \to 0$.

Complete Positivity - It can actually be shown that Λ_t has a stronger property than positivity, known as complete positivity [46, 47]. Specifically, we can show

$$\Big(\Lambda_t \otimes 1_{n\times n}\Big)\sigma \geq 0 \tag{1.37}$$

where n is an arbitrary positive integer and $1_{n\times n}$ is the $n \times n$ identity matrix. Meanwhile, σ is a positive density matrix living over the composite space formed from the tensor product of the Banach spaces, $\mathcal{B}(\mathcal{H})$ and $\mathcal{B}(\mathcal{H}')$, in which Λ_t and $1_{n\times n}$ exist.

Equation (1.37) is a stronger property than positivity as it is possible to find maps which preserve positivity but are not completely positive. This difference is intrinsically quantum and occurs due to the existence of density matrices which are entangled with another system which the map does not act on. The transpose operation $A \to A^T$ is a map which is positive but not completely positive. Complete positivity, as opposed to just positivity, is a condition which we require from any physical map — ensuring that even if the system it acts on is entangled with another system positivity is preserved.

Whilst complete positivity and the properties of Eq. (1.36) can be directly proven for the GSKL equation it is also instructive to take the opposite approach and ask the

question: what is the most general form of a quantum map which satisfies these properties? The answer to this question can actually be proven to be the GSKL equation [47, 48], i.e. it is the most general completely positive, trace preserving Markovian quantum map. This proof is the axiomatic approach to deriving the GSKL equation and has helped consolidate it as a fundamental equation in the field of open quantum systems[6]. Other, more general, descriptions of open systems are not able to integrate out the environment so completely whilst remaining physical.

Thermo-field Doubling and The Liouvillian Superoperator - The Liouvillian $\mathcal{L}$ in Eq. (1.34) encodes the time-dynamics of the GSKL equation. The most direct way to treat this equation numerically is to perform a 'thermo-field doubling' or 'vectorization'. This involves taking the Banach space for the system $\mathcal{B}(\mathcal{H}_S)$ and vectorizing all of its elements, i.e.

$$\forall A = |x\rangle\langle y| \in \mathcal{B}(\mathcal{H}_\mathcal{S}), \quad |x\rangle\langle y| \to |x\rangle \otimes |y\rangle = ||A\rangle\rangle\,. \tag{1.38}$$

We denote these vectorized operators with a double ket $||\bullet\rangle\rangle$ and note that the inner product $\langle\langle A||\, B\rangle\rangle$ is equivalent to the Hilbert Schmidt norm $\mathrm{Tr}(A^\dagger B)$.

From this, we can now introduce the superoperator space which is the space of operators acting on this vectorized space, formally equivalent to $\mathcal{B}(\mathcal{B}(\mathcal{H}_S))$. We can then rewrite the matrix product AB as a matrix-vector product, with one of the matrices being vectorized and the other being elevated to the superoperator space. Specifically, left and right multiplication of a target matrix A becomes equivalent to

$$AB \to (1 \otimes B^T)\,||A\rangle\rangle\,, \qquad BA \to (B \otimes 1)\,||A\rangle\rangle\,, \tag{1.39}$$

where 1 is the identity matrix with the same dimensions as A and B (all matrices written here are square).

We can apply these tools to the GSKL equation, vectorizing the density matrix $\rho \to ||\rho\rangle\rangle$ and elevating the remaining operators to the superoperator space

$$\frac{\partial}{\partial t}\,||\rho\rangle\rangle = \mathcal{L}\,||\rho\rangle\rangle = \left(-\mathrm{i}(H\otimes 1 - 1\otimes H^T) + \sum_j \gamma_j\left(L_j\otimes L_j^* - \frac{1}{2}(L_j^\dagger L_j\otimes 1 + 1\otimes L_j^T L_j^*)\right)\right)||\rho\rangle\rangle\,. \tag{1.40}$$

This is now a matrix-vector version of the GSKL equation, where the Liouvillian $\mathcal{L}$ is an $n^2 \times n^2$ matrix or superoperator, with n the dimension of the Hilbert space of the system $\mathcal{H}_S$. The formal solution to Eq. (1.40) then reads

$$||\rho(t)\rangle\rangle = e^{\mathcal{L}t}\,||\rho(0)\rangle\rangle\,, \tag{1.41}$$

[6]Whilst arguably much more elegant, in the axiomatic approach the physical meaning of the jump operators is less clear than when following the microscopic approach that we have taken here.

and expectation values, i.e. $\mathrm{Tr}(O\rho(t))$, can be taken by either 'un-vectorizing' $||\rho(t)\rangle\rangle$ and taking the trace or vectorizing O and taking the inner product. Solving the GSKL equation is now simply a case of building the superoperator from the Hamiltonian H and jump operators L_j, exponentiating it and applying it to the vectorized density matrix.

Clearly, if we can diagonalise the superoperator matrix[7] $\mathcal{L}$ we have everything we need to know to find the time-dynamics of the system. From this diagonalisation we have

$$\mathcal{L} = \sum_{i=1}^{n^2} \lambda_i \, ||i_R\rangle\rangle \, \langle\langle i_L|| \,, \tag{1.42}$$

where $||i_R\rangle\rangle$ and $\langle|i_L\rangle|$ are the right and left eigenvectors of $\mathcal{L}$, with λ_i the corresponding eigenvalue. We note that, unlike for unitary quantum evolution, we do not generally have $||i_R\rangle\rangle = (\langle\langle i_L||)^\dagger$. Following this diagonalisation, Eq. (1.41) then reads

$$||\rho(t)\rangle\rangle = \sum_i c_i e^{\lambda_i t} \, ||i_R\rangle\rangle \,, \qquad c_i = \langle\langle i_L|| \, \rho(0)\rangle\rangle. \tag{1.43}$$

The spectrum of eigenvalues $\{\lambda_i\}$ reveals crucial information about the time dynamics of the system. These eigenvalues have several significant properties

$$\begin{aligned} &x \in \{\lambda_i\}, \exists y \in \{\lambda_i\} = x^* - \text{Conjugate Symmetry}, \\ &\forall x \ \in \ \{\lambda_i\}, \ \mathrm{Re}(x) \leq 0, \\ &\exists x \ \in \{\lambda_i\}, \ x = 0 - \text{Steady State}. \end{aligned} \tag{1.44}$$

The first property is a result of the conjugate symmetry of the GSKL equation $(\mathcal{L}\rho)^\dagger = \mathcal{L}\rho^\dagger$ which ensures that all eigenvalues of the Liouvillian come in conjugate pairs. The second, which states that all eigenvalues have a non-positive real part is a consequence of the semigroup property of the Liouvillian [26, 27]. Finally, the third implies the existence of at least one steady state $\mathcal{L}\rho_{ss} = 0$, which is a consequence of the complete positivity of $\mathcal{L}$ [27].

In Fig. 1.1 we illustrate these properties by plotting the spectrum of a Liouvillian built from random matrices. The conjugate symmetry is reflected in the symmetry of the plot around the x-axis, whilst the anticipated steady state is clearly observed at the origin. All the eigenvalues also have real part ≤ 0.

This negativity of the real part of the eigenvalues has significant implications for the time dynamics of the system. In Eq. (1.43) the exponentiation of the eigenvalues

[7] We note that this is not always the case. It can, however, always be brought into block-diagonal Jordan Form [49].

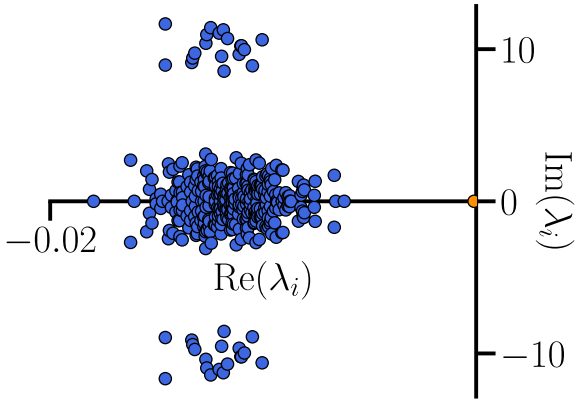

Figure 1.1: Spectrum of Eigenvalues of the Liouvillian superoperator of the GSKL equation, given in Eq. (1.34). The underlying Hilbert space has dimension $n = 20$ with the Hamiltonian a random Hermitian matrix and the 2 jump operators each drawn at random from the complex Ginibre ensemble (i.e. they are $n \times n$ matrices with elements all drawn independently and at random from a Gaussian distribution with 0 mean and variance $1/n$ [50]). We have set $\gamma_j = 1,\ \forall j$.

will lead to any eigenvectors for which $\mathrm{Re}(\lambda_i) < 0$ decaying away. As a result any memory of the overlap between the initial state and these modes will be lost and so the dynamics of the GSKL equation is irreversible. Moreover, the system will be attracted to the fixed points where $\mathrm{Re}(\lambda_i) = 0$, and hence,

$$\lim_{t\to\infty} ||\rho(t)\rangle\rangle = \sum_{i\in X} c_i e^{\mathrm{iIm}(\lambda_i)t}\, ||i_R\rangle\rangle\,, \tag{1.45}$$

where X is the reduced subset of eigenmodes for which $\mathrm{Re}(\lambda_i) = 0$.

It is worth stating that if the dissipative part of the GSKL equation disappears, i.e. $\gamma_j = 0\ \forall j$, then it reduces to the von-Neumann equation and the Liouvillian becomes skew-hermitian with all eigenvalues satisfying $\mathrm{Re}(\lambda_i) = 0$. Here, there is no decay, the left and right eigenvectors coincide $\langle\langle i_L|| = (||i_R\rangle\rangle)^\dagger$, and the dynamics is completely unitary $\forall t$.

Example: Harmonic Oscillator in a Finite Temperature Bath

In order to illustrate some of these concepts we will take a simple, physical example of the GSKL equation — a harmonic oscillator in contact with a finite-temperature bath [51] — and simulate it by explicitly building and diagonalising the Liouvillian superoperator. The GSKL equation in this example reads

$$\frac{\partial}{\partial t}\rho(t) = \mathcal{L}\rho(t) = -\mathrm{i}[\omega n, \rho(t)] + \gamma(\bar{n}+1)D[a] + \gamma\bar{n}D[a^\dagger], \tag{1.46}$$

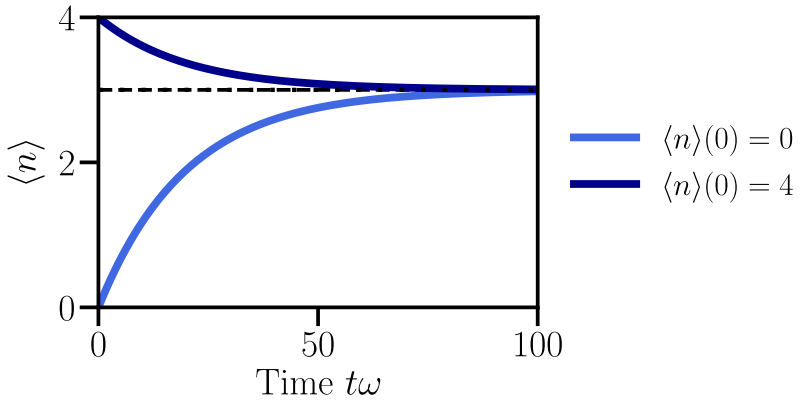

Figure 1.2: Number of quanta $\langle n \rangle$ vs time for a single harmonic oscillator coupled to a finite-temperature bath described in Eq. (1.46). We choose the initial states $|\psi(0)\rangle = |0\rangle$ and $|\psi(0)\rangle = |4\rangle$ — where $|n\rangle$ is the state with n quanta and we also fix a maximum number of quanta $N_{\max} = 50$. The temperature of the bath is $k_B T = \omega/(\ln(4) - \ln(3))$, which corresponds to $\bar{n} = 3$, and we set $\gamma = \omega$. The dotted line is the number of quanta in the steady $\rho_{ss} \propto \exp(\beta\omega n)$.

where $a^\dagger$ and its adjoint are the bosonic creation and annihilation operators for a single mode, $n = a^\dagger a$ is the number operator, ω is the frequency of the harmonic oscillator and $\bar{n} = (\exp(\beta\omega) - 1)^{-1}$ with $\beta = 1/k_B T$ the inverse temperature of the bath. We have also defined the dissipator

$$D[O] = O\rho(t)O^\dagger - \frac{1}{2}\{O^\dagger O, \rho(t)\}, \tag{1.47}$$

for brevity. The terms $D[a]$ and $D[a^\dagger]$ describe the transfer of quanta in the oscillator to and from the bath and $\bar{n}$ is the average number of quanta in the bath, which is in equilibrium at temperature T. Equation (1.46) can be derived microscopically, assuming the bath-oscillator coupling is both linear and weak, via the methods described earlier [51, 52].

We now solve for the dynamics of the system by building the Liouvillian superoperator, exponentiating it, and applying the resulting propagator to the initial state just as in Eq. (1.41). For numerical reasons, we fix a maximum number of levels to our oscillator N. By observing that increasing N does not change our results, we can be sure that they reflect the dynamics of a harmonic oscillator in the limit $N \to \infty$.

In Fig. 1.2 we plot the dynamics of the occupancy $\langle n \rangle$ of the harmonic oscillator versus time. The system relaxes to a steady state with the same occupancy as the bath, which is the sole fixed point of the map $\exp(\mathcal{L}t)$ as it is the only eigenvalue of $\mathcal{L}$ where $\mathrm{Re}(\lambda_i) \not< 0$. Depending on the initial number of quanta this relaxation corresponds to a net loss or gain of particles. We can in fact prove that the form of

the steady state is $\rho_{ss} \propto \exp(\beta\omega n)$ which is a thermal state at the same temperature as the bath with $\langle n \rangle = \bar{n}$. Given *any* state at $t = 0$ the system will relax towards this thermal distribution. All information contained within this initial state, including any coherences and entanglement, will irreversibly decay away during the dynamics via the eigenmodes of the superoperator where $\mathrm{Re}(\lambda_i) < 0$.

Alongside being able to write down a simple form for the steady state, Eq. (1.46) actually admits an analytical solution for all times [53]. Being able to derive an analytical expression for the full time-dynamics of a system governed by the GSKL equation is typically infeasible. In this instance, the simple structure of the open system at hand has made this possible. In the next section we will discuss methods available for treating more complex instances of the GSKL equation, as well as the driven quantum systems which we introduced in section 2.1. Prior to this, we will use some of the tools we have introduced here to discuss a notable example of open systems which, unlike the harmonic oscillator, do not relax to a fixed steady state.

Decoherence Free Subspaces

In our simulation of a harmonic oscillator in contact with a finite-temperature bath we observed its relaxation to a thermal state with the same temperature as the bath. This is typical of a generic open quantum system[8], with the environment causing the system to decohere and relax to a stationary equilibrium ensemble.

This is not, however, always the case and there are exceptions to this rule. One such exception, which we will be comparing with one of the major results of this thesis, is that of the Decoherence Free Subspace (DFS) [56, 57, 58, 59]. A DFS is a region of the Hilbert space of a system $\mathcal{H}_S$ which is protected from the environment and undergoes coherent unitary evolution.

This can be introduced mathematically by considering an open quantum system with the full Hamiltonian of the system and environment as

$$H = H_{\mathrm{S}} \otimes 1_{\mathrm{E}} + 1_{\mathrm{S}} \otimes H_{\mathrm{E}} + \sum_i A_i \otimes B_i, \tag{1.48}$$

where H_{S} and H_{E} are the Hamiltonians of the system and environment, which exist in their respective Hilbert spaces $\mathcal{H}_{\mathrm{S}}$ and $\mathcal{H}_{\mathrm{E}}$. The final summation in Eq. (1.48) runs over a series of Hermitian operators which describe the interaction between the system and environment.

[8] By generic we mean one which is not integrable [54] or in, say, a many-body localised phase [55].

A DFS of the system — which is a subspace of the Hilbert space, $\mathcal{H}'_{\mathrm{S}} \subset \mathcal{H}_{\mathrm{S}}$ spanned by the set of basis states $\{|\phi\rangle\}$ — can then be identified if the following statements are true

- $A_i |\phi\rangle = a_i |\phi\rangle\,, \qquad a_i \in \mathbb{R}\ \forall i, \phi$
- The system Hamiltonian H_{S} does not map states out of the subspace $\mathcal{H}'_{\mathrm{S}}$, i.e. $H_{\mathrm{S}} |\phi\rangle$ is also within $\mathcal{H}'_{\mathrm{S}}$ and so H_{S} is block-diagonalisable.
- The system and environment are not be entangled at the origin time $t = 0$, preventing the environment from being able to map states out of $\mathcal{H}'_{\mathrm{S}}$.

Under these conditions it follows that the projection of the total Hamiltonian in the Hilbert space $\mathcal{H}'_{\mathrm{S}} \otimes \mathcal{H}_{\mathrm{E}}$ is

$$H' = H'_{\mathrm{S}} \otimes 1_{\mathrm{E}} + 1'_{\mathrm{S}} \otimes \left(H_{\mathrm{E}} + \sum_i a_i B_i \right), \tag{1.49}$$

where H'_{S} is the projection of H_{S} onto the DFS and $1'_{\mathrm{S}}$ is the identity matrix over the DFS. It is clear from this equation that this subspace and the environment are completely separated, making any dynamics within it completely unitary, although there is some back-action on the bath.

If our open system is describable via the GSKL equation in Eq. (1.34) then the first condition can be translated to the existence of a subspace of the Hilbert space where $L_j |\phi\rangle = c_j |\phi\rangle \ \forall j$, i.e. all the basis states which span $\mathcal{H}'_{\mathrm{S}}$ are degenerate eigenvectors of the jump operators. The second condition is immediately satisfied as it was assumed in the derivation of the equation and the third condition remains the same.

We now provide a simple example of a DFS within the GSKL picture. Consider a pair of qubits, each with two possible states $|\uparrow\rangle$ and $|\downarrow\rangle$, in the presence of a magnetic field and collective loss, i.e.

$$\frac{\partial \rho(t)}{\partial t} = -\mathrm{i}\omega[S^z, \rho(t)] + S^- \rho(t) S^+ - \frac{1}{2}\{S^+ S^-, \rho(t)\}, \tag{1.50}$$

where $S^z = \sum_{i=1,2} \sigma_i^z$ and $S^- = \sum_{i=1,2} \sigma_i^-$ and the subscript indexes the qubit on which the Pauli matrix acts. We can then immediately show that the space spanned by the basis states $\{|\uparrow\downarrow\rangle - |\downarrow\uparrow\rangle\,, |\downarrow\downarrow\rangle\}$ satisfies the conditions for a DFS as they are annihilated by S^- and they are also eigenvectors of S^z.

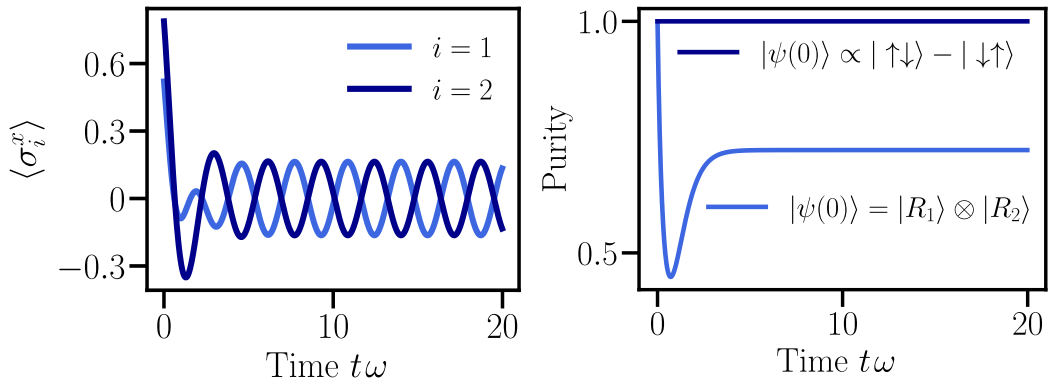

Figure 1.3: Dynamics of two qubits described by the master equation in Eq. (1.50). Left) Time dynamics of the x-magnetisation for the initial state $|\psi(0)\rangle = |R_1\rangle \otimes |R_2\rangle$ where R_i is a random, normalized, state for qubit i. Right) Time dynamics of the purity $\mathrm{Tr}(\rho^2)$ of the density matrix for two different initial states.

In Fig. 1.3 we plot the dynamics of this system using the superoperator method. We see that, for each qubit, the magnetisation in the x-direction oscillates continuously in time — indicating an absence of equilibration. These oscillations correspond to a continuous phase relationship between the off-diagonal matrix elements $(|\uparrow\downarrow\rangle - |\downarrow\uparrow\rangle)\langle\downarrow\downarrow|$ and $|\downarrow\downarrow\rangle(\langle\uparrow\downarrow| - \langle\downarrow\uparrow|)$. The anti-symmetry of these matrix elements guarantees that the oscillations of the two qubits will also be anti-symmetric, which we observe in Fig. 1.3.

In Fig. 1.3 we also plot the purity of the density matrix as a function of time. For an initial state which lives completely in the DFS of the system we see that the system remains in a pure state due to the unitary nature of the dynamics. For a more general random initial state we see that the dynamics lead to a mixed density matrix with the corresponding decoherence introduced by the loss operator. Interestingly, compared to the previous example of a finite temperature Harmonic Oscillator, the long-time dynamics of the system is dependent on the initial state. This is because in this example the presence of a DFS means there are multiple steady states and even a pair of eigenmodes with $\mathrm{Re}(\lambda_i) = 0$ but $\mathrm{Im}(\lambda_i) \neq 0$. The overlap of the initial state with these modes corresponds to information which will be preserved and not decay away during the dynamics whilst all other information will be lost.

The example we have presented here is not limited to just having two non-interacting qubits. It is straightforward to show that the eigenvectors of the Casimir operator $S^2 = S^+S^- + S^-S^+ + (S^z)^2$ which are annihilated by S^- form a DFS for any number of qubits governed by the master equation in Eq. (1.50). Additionally,

this DFS will still exist when introducing certain types of interactions between the qubits, such as a homogeneous $x - x$ interaction.

The notion of a DFS was recognized as having important ramifications for the fields of quantum computing and information processing [60, 61]. In realising a robust, fault-tolerant quantum processor one of the biggest challenges is overcoming the errors induced by the decoherence and dissipation from the ever-present environment [62, 63]. Decoherence Free Subspaces provide a way of mitigating these effects and coherently storing and manipulating information in quantum registers.

Furthermore, whilst it is difficult to write down the specific system-environment interaction in many experimental quantum setups, the engineering of a DFS can act to reduce the effects on the system of some unwanted external influences. A number of experimental protocols have realized DFSs in this manner [64, 65]. For example, a single qubit was encoded as the DFS of a pair of trapped Beryllium ions [66] and shown to store information for an order of magnitude longer when in this setup compared to on its own.

1.3 Methods for Simulating Driven and Dissipative Quantum Systems

The Exponential Size of Many-Body Quantum Systems

In the open system examples in the previous section the dimension of the corresponding Banach spaces were relatively small (specifically 16 for the pair of qubits and 2601 for the Harmonic oscillator) and so an exact representation of the density matrix — and the governing superoperator — was possible. If we have an interacting many-body system — for example multiple coupled harmonic oscillators or a chain of qubits — then things become significantly more challenging. For a system composed of L d-level quantum 'spaces' or subsystems, such that the Hilbert space is $\mathcal{H} = \otimes_{i=1}^{L} \mathcal{H}_i$ with $\dim(\mathcal{H}_i) = d \ \forall i$, then the Hilbert and Banach space dimensions are d^L and d^{2L} respectively.

This exponential growth is sometimes referred to as the 'curse of dimensionality' and is a significant obstacle to the simulation of both closed and open quantum systems. For example, a chain of 18 qubits would require a memory of around 4 Megabytes for storing the wavefunction and 1 Terrabyte for the density matrix[9]. Meanwhile, a chain of 36 qubits would require a memory of just over 1 Terabyte for

[9] Assuming a full construction and storage of the wavefunction/density matrix where each complex number takes up 16 bytes of memory.

the wavefunction and 75 Zetabytes for the density matrix — around the total amount of data stored on Earth[10].

These memory requirements mean that exact numerical calculations on many-body systems are limited. Whilst exploiting symmetries present in the system can help alleviate some of these memory costs, the aforementioned exponential growth will still severely restrict the system sizes that can be treated. The dynamics of these systems is, however, often of significant interest. As a result, a number of methods have been developed in order to more efficiently simulate them and in this section we will introduce several of these, which are used extensively in this thesis.

The Monte Carlo Wavefunction Approach to the GSKL Equation

The first of these methods is known as the quantum trajectory or the Monte Carlo wavefunction approach to the GSKL equation [67, 68, 69]. As is typical of Monte Carlo methods, we aim to derive a stochastic version of our equation of motion which can be ensemble averaged to give the true dynamics of the system. We start by recasting the GSKL equation as

$$\frac{\partial}{\partial t}\rho(t) = \mathcal{L}\rho = -\mathrm{i}\big(H_{\mathrm{eff}}\rho - \rho H_{\mathrm{eff}}^{\dagger}\big) + \sum_j \gamma_j L_j \rho L_j^{\dagger}, \tag{1.51}$$

where $H_{\mathrm{eff}} = H - \frac{\mathrm{i}}{2}\sum_j L_j^{\dagger}L_j$ is an effective, non-Hermitian, Hamiltonian for the system. We then take the state of the system at time $t = 0$ to be $|\psi(0)\rangle$. If the initial state is mixed instead of pure, then $|\psi(0)\rangle$ should be appropriately sampled from $\rho(0)$. We then stochastically evolve $|\psi(0)\rangle$ in time via a series of N time steps, of size Δt, to reach $|\psi(t)\rangle$ at time $t = N\Delta t$. In order to perform a single step at some time t' we perform the following procedure

- Apply $\exp(-\mathrm{i}H_{\mathrm{eff}}dt)$ to $|\psi(t')\rangle$ to get $|\tilde{\psi}(t'+\Delta t)\rangle = \exp(-\mathrm{i}H_{\mathrm{eff}}\Delta t)\,|\psi(t')\rangle$.
- Compute the norm $\mathcal{N} = \langle\tilde{\psi}(t'+\Delta t)|\tilde{\psi}(t'+dt)\rangle$.
- Draw a random number R between 0 and 1. If $R < \mathcal{N}$ then the state at time $t'+\Delta t$ is $|\psi(t'+\Delta t)\rangle = (1/\sqrt{\mathcal{N}})\,|\tilde{\psi}(t'+\Delta t)\rangle$. Return to the start of the procedure and repeat until the desired time t is reached.

[10] At the time of writing (August 2020).

- If $R > \mathcal{N}$ then calculate the set of probabilities $\{p_j\}$ with $p_j = \langle\psi(t')|L_j^\dagger L_j|\psi(t')\rangle$. Draw another random number between 0 and 1, renormalize the distribution of p_j such that $\sum p_j = 1$ and use the new random number to select one of these j, which we label n. The likelihood of selection should reflect the corresponding probability p_n.

- Calculate the state at time $t' + \Delta t$ via $|\psi(t' + \Delta t)\rangle \propto L_n |\psi(t')\rangle$ and normalize it. Return to the start of the procedure and repeat until the desired time t is reached.

A single evolution of $|\psi(0)\rangle$ until time t is known as a trajectory and, due to the fixed value of Δt, the described algorithm is only accurate to first order[11] in Δt. By performing N separate trajectories and averaging them we form an approximation to the dynamics of $\rho(t)$ under Equation (1.51). Specifically we have

$$\rho(t) \approx (1/N) \sum_{k=1}^{N} |\psi(t)\rangle_k \langle\psi(t)|_k \,, \tag{1.52}$$

where the subscript k runs over the N independent trajectories we have calculated. In the limit $(N, \Delta t) \to (\infty, 0)$ we recover the exact dyanmics of $\rho(t)$ [67].

Single-time expectation values $\langle A\rangle$ can be calculated at a time t by statistically averaging over the expectation value $\langle A_k\rangle$ of each trajectory at that time. As the trajectories are independent the statistical error is just giving by the standard error of the mean, i.e. $\Delta(\langle A\rangle) = \frac{\sigma}{\sqrt{N}}$ where σ is the standard deviation of the samples $\langle A_1\rangle, ..., \langle A_N\rangle$. The number of trajectories required to ensure that $\Delta(\langle A\rangle) \ll \langle A\rangle$ and give a reasonable approximation to the dynamics of $\rho(t)$ will depend on the problem at hand as well as the exact accuracy desired. In this thesis we will adopt the first order trajectory procedure described above and use values of $N \approx 500$ — we find that the corresponding uncertainty is then sufficiently small for our purposes.

Whether it is advantageous to use this trajectories approach over the direct superoperator method described in the previous section is dependent on the specifics of the problem being considered. The Monte Carlo approach has several advantages. Firstly, it only requires construction of pure states and operators (which are typically sparse) acting on those states — there is no need to build memory-expensive superoperators or density matrices. Secondly, if one is only interested in single-time

[11] Higher order approximations are achieved by allowing jumps to occur at varying points in time — as opposed to just integer multiples of Δt.

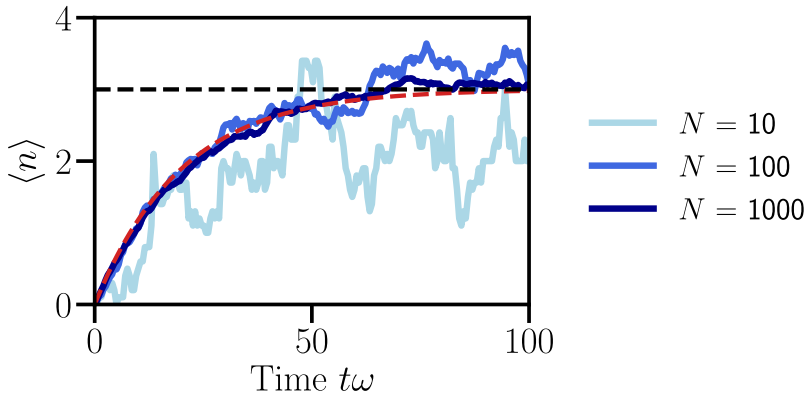

Figure 1.4: Trajectories approach simulating the number of quanta $\langle n \rangle$ vs time for a single harmonic oscillator coupled to a finite-temperature bath described in Eq. (1.46) — N is the number of trajectories used in the simulation. We choose the initial state $|\psi(0)\rangle = |0\rangle$ - where $|n\rangle$ is the oscillator mode with n quanta, we also fix a maximum number of quanta $N_{\max} = 50$. The temperature of the bath is $k_B T = \omega/(\ln(4) - \ln(3))$, which corresponds to $\bar{n} = 3$, and we also set $\gamma = \omega$. The dotted black line is the number of quanta in the steady $\rho_{ss} \propto \exp(\beta\omega n)$. The red dotted line corresponds to the numerical solution calculated using a superoperator approach and exact diagonalisation. The relative error $\frac{\Delta(\langle n \rangle)}{\langle n \rangle}$ on $\langle n \rangle$, where $\Delta(\langle n \rangle)$ is the standard error on the mean, was calculated at each point in time and for each value of N. For $N = 10, 100$ and 1000 the relative error (averaged over all times) was $0.40, 0.12$ and 0.04 respectively.

expectation values[12] only one pure state needs to be stored in memory at a given time. This also means the trajectories can be trivially parallelised with no required cross-communication between parallel instances; statistical averaging of expectation values can be done at the end of the simulation.

If we return to our example of the open dynamics of a chain of 18 qubits we can see that a Monte Carlo approach is sensible as any modern day computer easily meet the memory requirements for storing the wavefunction in a trajectories calculation whilst the 1 Terrabyte requirement for the density matrix would make the superoperator method beyond the reach of most personal computers.

We have applied this Monte Carlo method to the example of a harmonic oscillator in a finite temperature bath, which we treated via the superoperator method in the previous section. Figure 1.4 demonstrates how the Monte Carlo result improves with increasing number of trajectories N, converging towards the solution calculated in the superoperator approach.

[12]Two-time correlators and non-linear functions of the density matrix, such as the von–Neumann entanglement entropy, require manipulation of multiple trajectories at once.

Matrix Product State Methods

Whilst the quantum trajectories approach allows us to do avoid the expensive memory cost of the superoperator picture, the size of the many-body system we can treat is still limited by the exponential growth of the Hilbert space dimension. Here we introduce the Matrix Product State (MPS) formalism which, for certain many-body systems, provides a method to efficiently represent states and operators and avoid this exponential growth. We will provide a concise summary of the main points of this method. For further details we refer the reader to a number of much more exhaustive works written on this subject [70, 71, 72, 73].

In a seminal paper in 1992, Steven R. White demonstrated a numerical algorithm, known as the Density Matrix Renormalization Group (DMRG) algorithm for efficiently calculating the ground state, and its properties, for chains consisting of hundreds of interacting $s = 1/2$ or $s = 1$ quantum spins [74]. Given the impossible memory costs of simulating these systems directly, and the generality of White's method to other chains with short-range interactions, this work was a major breakthrough in the simulation of 1D quantum systems. Just over a decade later, G. Vidal provided an efficient algorithm for calculating the time dynamics of 1D chains where the growth in entanglement is limited, known as the Time Evolving Block Decimation (TEBD) method [75].

It was around the time that Vidal's work on TEBD was published that it was realised the MPS formalism is an ideal way to unify and describe the DMRG and TEBD algorithms. We can introduce this formalism through the MPS representation of the wavefunction $|\psi\rangle$ of a 1D many-body system. This wavefunction for an open boundary chain of L sites, or subsystems, each with d quantum levels, reads

$$|\psi\rangle = \sum_{\sigma_1,\sigma_2,...,\sigma_L=1}^{d} C_{\sigma_1,\sigma_2,...,\sigma_L} |\sigma_1, \sigma_2, ..., \sigma_L\rangle , \tag{1.53}$$

where the quantum numbers $\sigma_1, \sigma_2, ..., \sigma_L$ each run from 1 to d and are used to index the d^L different basis states of the system. The coefficients $C_{\sigma_1,\sigma_2,...,\sigma_L}$ form a tensor with L indices and d^L total elements. The heart of the MPS formalism is a representation of this exponentially large tensor via a series of smaller tensors, i.e.

$$C_{\sigma_1,\sigma_2,...,\sigma_L} = A_{\sigma_1} A_{\sigma_2} A_{\sigma_3} ... A_{\sigma_L}, \tag{1.54}$$

where the A_{σ_i} are a series of L rank-3 tensors, one for each site i. These tensors each have three indices. The physical index σ_i is 'exposed' and has dimension d whilst

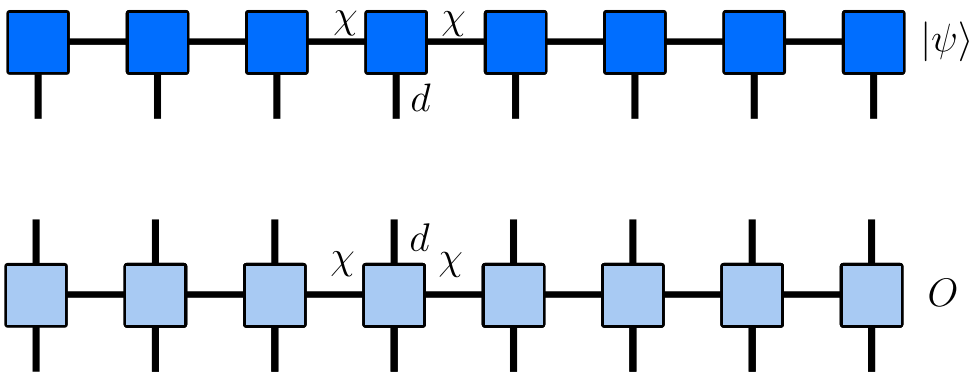

Figure 1.5: Top) Matrix Product State representation of the wavefunction $|\psi\rangle$ for a quantum chain. The squares correspond to rank-3 tensors with a 'downwards' leg of dimension d and left and right legs of dimensions χ, which are connected with neighbouring tensors. Bottom) Matrix Product Operator representation of an operator O acting on a quantum chain, the squares correspond to rank-4 tensors with 'downwards' and 'upwards' legs of dimension d and left and right legs of dimensions χ, which are connected with neighbouring tensors.

the bond indices are 'hidden' as they are contracted with neighbouring tensors via matrix multiplication. For the tensors in the bulk of the chain both bond indices have dimension χ, whilst the two tensors A_{σ_1} and A_{σ_L} have one bond index of dimension χ and the other is of dimension 1 — ensuring that the matrix product in Eq. (1.54) collapses to a scalar. For a periodic chain all the tensors have two bond indices of dimension χ and the trace is taken over the matrix product to ensure it collapses to a scalar. The series of tensors for an open boundary chain is pictured in Fig. 1.5, with the square blocks indicating the rank 3 tensors on each site.

This tensor decomposition written in Eq. (1.54) and pictured in Fig. 1.5 forms the MPS representation of the full wavefunction $|\psi\rangle$. The number of coefficients needed for this representation is $(L-2)d\chi^2+2d\chi \sim Ld\chi^2$, compared to d^L in Eq. (1.53). Given any coefficient tensor $C_{\sigma_1,\sigma_2,\ldots,\sigma_L}$ we can always decompose it into a series of smaller tensors as in Eq. (1.23) and thus provide a MPS representation of the wavefunction. This decomposition is achieved by repeated reshapes, partitions and Singular Value Decompositions (SVDs) of the coefficient tensor. The SVD is a factorisation of any $m \times n$ matrix M via $M = U\Lambda V^T$ where U and V are square unitary matrices whilst Λ is an $m \times n$ diagonal rectangular matrix whose entries are known as the singular values of the SVD. The bond-dimension χ of an MPS is exactly the number of singular values kept during these various SVDs.

The SVD is the workhorse of a number of MPS algorithms and the success of

the MPS formalism and these algorithms hinges on being able to discard/ignore a large number of singular values so that $Ld\chi^2 \ll d^L$ whilst maintaining an accurate representation of the many-body wavefunction. Generally, we should have no reason to believe we can efficiently achieve this for a given wavefunction. However, the ground states of gapped, locally-interacting Hamiltonians satisfy a property known as the 'Area Law' [76, 77, 78, 79] — where the von–Neumann entanglement entropy of the reduced density matrix formed following a bi-partition of the system grows in proportion to the size of the boundary between the two partitions. In a 1D system this means the entanglement entropy will be independent of L and it can be shown that, in an MPS representation of the wavefunction, it is upper bounded by $\log_2\chi$ [80, 81].

Wavefunctions in 1D which satisfy the area law can therefore be faithful represented by an MPS with a bond dimension χ that is independent of the system size L. This representation is very memory efficient as the total size of the tensor no longer scales exponentially with L. Furthermore, typical operators, such as the Hamiltonian and those corresponding to Hermitian observables, can also be efficiently represented in a similar Matrix Product form known as Matrix Product Operators (MPOs). We picture an MPO in its most general form in Fig. 1.5, where the additional physical leg on the on-site tensor reflects the fact that the MPO lives in the operator space $\mathcal{B}(\mathcal{H})$ instead of in the Hilbert space $\mathcal{H}$. These MPOs can easily be applied to MPSs and other MPOs by contracting the exposed tensor indices of the MPSs and MPOs with each other. These contractions, when carefully ordered so as to exploit the MPS structure, then allow a number of 'standard' quantum operations to be performed efficiently, such as the calculation of observables which is pictured in Fig. 1.6.

The DMRG algorithm can effectively be seen as a variational routine that determines the MPS representation of $|\psi\rangle$ which minimises the expectation value $\langle\psi|H|\psi\rangle$, i.e. for a given χ it is an optimisation over the $(L-2)d\chi^2+2d\chi$ coefficients of the MPS. Meanwhile, the TEBD algorithm can then be seen as one which, for a given timestep Δt, dynamically updates the coefficients of the MPS $|\psi(t)\rangle$ to create a new MPS $|\psi'\rangle$ which optimises the overlap $\langle\psi'|e^{-iH\Delta t}|\psi(t)\rangle$. Specifically, the typical TEBD methodology for a nearest-neighbour Hamiltonian is to write it as a sum of local, two-site, Hamiltonians $H = \sum_i H_{i,i+1}$. The propagator is then approximated via

$$e^{-\mathrm{i}H\Delta t} \approx \prod_{i=1}^{L-1} e^{-\mathrm{i}H_{i,i+1}\frac{\Delta t}{2}} \prod_{i=L}^{2} e^{-\mathrm{i}H_{i,i-1}\frac{\Delta t}{2}}. \tag{1.55}$$

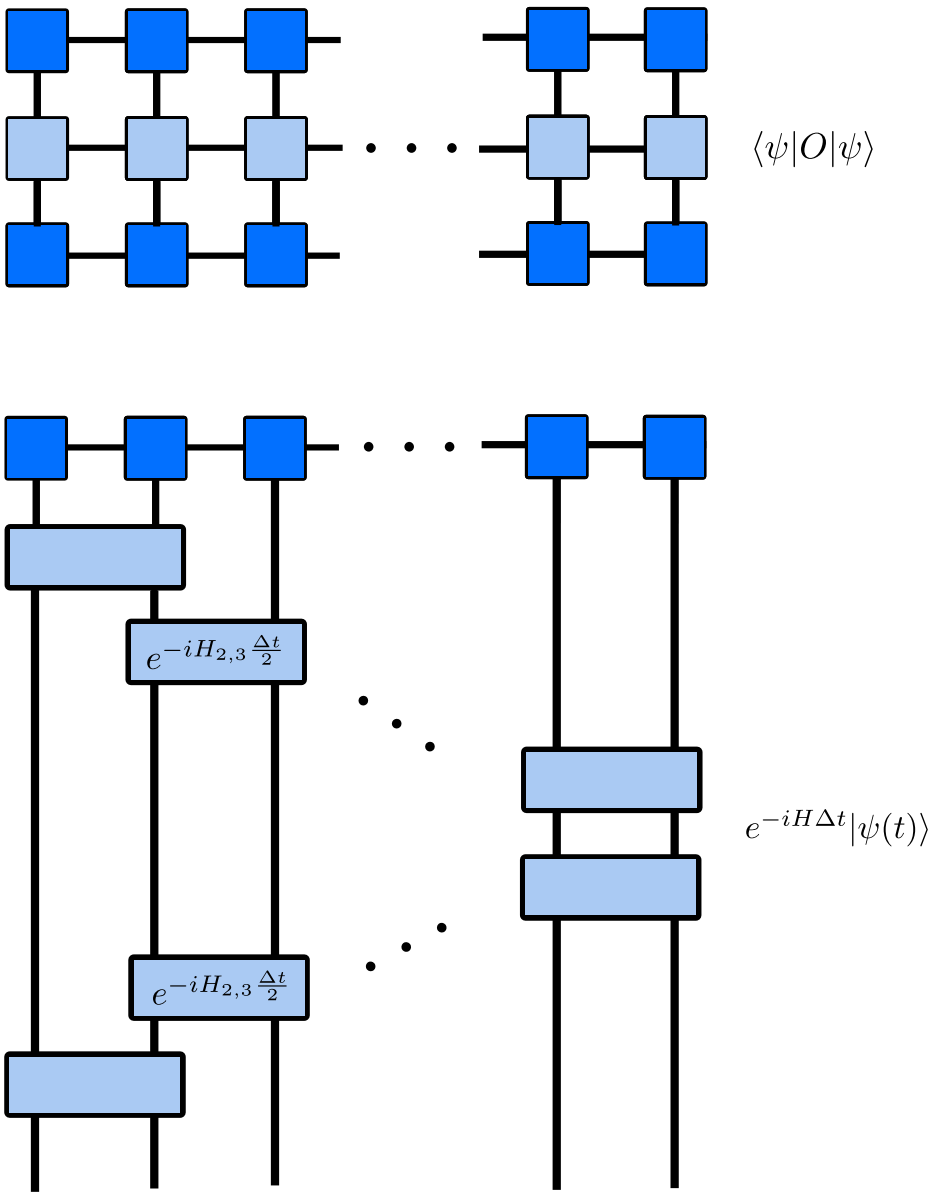

Figure 1.6: Top) Tensor network diagram for the contraction of a Matrix Product State with a Matrix Product Operator to form the scalar $\langle\psi|\, O\, |\psi\rangle$. Connected legs are implicitly summed over. Bottom) Propogation of a Matrix Product State over time Δt with the nearest-neighbour Hamiltonian H. As the Hamiltonian is nearest-neighbour its exponential can be approximated as a product of MPO gates $\exp(-\mathrm{i}H_{i,i+1}\Delta t)$ — see Eq. (1.55) — which can be applied sequentially and locally to neighbouring sites i and $i+1$.

The error on this expansion is of order $\mathcal{O}(\Delta t^3)$ and stems from assuming the local Hamiltonians commute when taking the exponential. Equation (1.55) is known as a 2nd order Suzuki Trotter expansion [82] — higher order, more accurate Suzuki Trotter expansions can also easily be constructed [83]. In the TEBD algorithm the 'gates' $e^{-\mathrm{i}H_{i,i+1}\frac{\Delta t}{2}}$ in Eq. (1.55) are then converted faithfully to simple two-site MPOs and applied in a staircase manner to the MPS $|\psi(t)\rangle$ to propagate it in time [75]. This process is pictured in Fig. 1.6. Longer-range Hamiltonians can be treated by extending the range of the local Hamiltonians and thus the size of the MPO gates, a method which we will apply in chapter 4.

The success of the DMRG and TEBD algorithms stems from this MPS description and in the years since their inception a number of routines have been developed which take advantage of this formalism. For example, methods for constructing efficient MPO representations of thermal states [84, 85], dynamically simulating long-range 1D systems [86, 87, 88], simulating infinite 1D chains [89] and even treating 2D systems [90, 91, 71] have all been developed.

In the case of driven quantum systems, MPS time-evolution methods such as TEBD can be immediately applied to simulate their dynamics. Provided the time-step in the evolution is sufficiently small, then the necessary elements of the MPO which propagates the system simply need to be updated appropriately at each time-step in order to reflect the time-dependence in the Hamiltonian. Care needs to be taken in ensuring the bond dimension is sufficiently large in order to accurately perform the simulation. Driving often causes the excitation of states which do not satisfy the area law, increasing the von-Neumann entanglement entropy in the system and necessitating the use of large bond dimensions to faithfully capture the dynamics. This, in turn, limits the maximum time that can be reached in the simulation.

The aforementioned MPS algorithms have also been shown to be relevant for the simulation of open quantum systems [92, 93]. The 'superket', or vectorized, density matrix $||\rho(t)\rangle\rangle$ can be cast as an MPS with physical dimension d^2 and superoperators can be built as corresponding MPOs — allowing time-evolution methods such as TEBD or DMRG-based algorithms for finding the steady state to be performed within this compressed format [94, 95]. Alternatively, the quantum trajectories approach can naturally be written in the MPS language — with the trajectory wavefunctions represented via MPSs and the jump operators and effective Hamiltonian as MPOs acting upon them.

Whilst MPS algorithms are incredibly successful for the simulation of closed, locally interacting, gapped 1D systems, this does not immediately extend to open quan-

tum systems. The bond dimension χ for the MPO respresentation of a mixed state can no longer be directly related to the entanglement entropy and there is no known area law of entanglement in the steady states of open systems. The intrinsically non-unitary evolution in an open system leads to both classical and quantum correlations appearing in the density matrix and can render time-evolution algorithms inefficient [96]. Whether MPS methods can successfully be used to simulate open systems is therefore dependent upon the problem at hand and requires a careful choice of the appropriate algorithm to use [97].

1.4 Conclusion

In this chapter we have introduced a theoretical description of driven and dissipative quantum systems. We discussed Floquet theory for driven systems and derived various master equations for open systems, including the celebrated GSKL equation. We then moved on to a discussion of the mathematical properties of this equation and detailed how it can be solved numerically — providing a simple example in the form of a harmonic oscillator coupled to a finite temperature bath. Further to this, we introduced the concept of Decoherence Free Subspaces, regions of the Hilbert space which do not decohere when in contact with an external environment, and provided an example in the form of the GSKL equation for a pair of qubits under collective loss. In the last section methods for dealing with more complex instances of driven and dissipative systems — where exact diagonalisation is unfeasible due to memory requirements — were described. Namely, we summarized the Monte-Carlo wavefunction treatment for open quantum systems and the Matrix Product State ansatz for simulating both driven and dissipative quantum systems.

We are now in a position to introduce the first results of this thesis. In the following chapter we will discuss the role of symmetries in quantum systems, allowing us to introduce a novel symmetry-based mechanism which causes a system to dynamically manifest long-range order as it absorbs heat. We will consider heat which originates from either a coherent driving source or an external environment and thus the theory introduced in this chapter will be of fundamental use.

References

[1] E. Butikov, "On the dynamic stabilization of an inverted pendulum," *Am. J. Phys.*, vol. 69, pp. 755–768, 2001.

[2] G. Arioli and F. Gazzola, "A new mathematical explanation of what triggered the catastrophic torsional mode of the Tacoma Narrows Bridge," *Appl. Math. Model.*, vol. 39, no. 2, pp. 901–912, 2015.

[3] T. Oka and S. Kitamura, "Floquet engineering of quantum materials," *Annu. Rev. Condens. Matter Phys.*, vol. 10, pp. 387–408, 2019.

[4] A. Eckardt, "Colloquium: Atomic quantum gases in periodically driven optical lattices," *Rev. Mod. Phys.*, vol. 89, p. 011004, 2017.

[5] G. Teschl, *Ordinary Differential Equations and Dynamical Systems*. American Mathematical Society, Rhode Island USA, 2012.

[6] J. R. Coulthard, S. R. Clark, S. Al-Assam, A. Cavalleri, and D. Jaksch, "Enhancement of superexchange pairing in the periodically driven Hubbard model," *Phys. Rev. B*, vol. 96, p. 085104, 2017.

[7] T. Kuwahara, T. Mori, and K. Saito, "Floquet–Magnus theory and generic transient dynamics in periodically driven many-body quantum systems," *Ann. Phys.*, vol. 367, pp. 96–124, 2016.

[8] T. Kitagawa, E. Berg, M. Rudner, and E. Demler, "Topological characterization of periodically driven quantum systems," *Phys. Rev. B*, vol. 82, p. 235114, 2010.

[9] J. H. Shirley, "Solution of the Schrödinger equation with a Hamiltonian periodic in time," *Phys. Rev.*, vol. 138, pp. B979–B987, 1965.

[10] W. Magnus, "On the exponential solution of differential equations for a linear operator," *Commun. Pure Appl. Math.*, vol. 7, pp. 649–673, 1954.

[11] S. Blanes, F. Casas, J. Oteo, and J. Ros, "The Magnus expansion and some of its applications," *Phys. Rep.*, vol. 470, pp. 151–238, 2009.

[12] B. Marin, D. Luca, and P. Anatoli, "Universal high-frequency behavior of periodically driven systems: from dynamical stabilization to floquet engineering," *Adv. Phys.*, vol. 64, pp. 139–226, 2015.

[13] T. Kuwahara, T. Mori, and K. Saito, "Floquet–Magnus theory and generic transient dynamics in periodically driven many-body quantum systems," *Ann. Phys.*, vol. 367, pp. 96–124, 2016.

[14] L. D'Alessio and M. Rigol, "Long-time behavior of isolated periodically driven interacting lattice systems," *Phys. Rev. X*, vol. 4, p. 041048, 2014.

[15] P. Pedro, C. Anushya, Z. Papić, and D. A. A., "Periodically driven ergodic and many-body localized quantum systems," *Ann. Phys.*, vol. 353, pp. 196–204, 2015.

[16] D. A. Abanin, W. De Roeck, and F. Huveneers, "Theory of many-body localization in periodically driven systems," *Ann. Phys.*, vol. 372, pp. 1–11, 2016.

[17] L. D'Alessio and A. Polkovnikov, "Many-body energy localization transition in periodically driven systems," *Ann. Phys.*, vol. 333, pp. 19–33, 2013.

[18] A. Russomanno, G. E. Santoro, and R. Fazio, "Entanglement entropy in a periodically driven Ising chain," *J. Stat. Mech.: Theory Exp*, vol. 2016, p. 073101, jul 2016.

[19] V. Gritsev and A. Polkovnikov, "Integrable Floquet dynamics," *SciPost Phys.*, vol. 2, p. 021, 2017.

[20] J. V. Neumann and R. Beyer, *Mathematical Foundations of Quantum Mechanics*. Goldstine Printed Materials, Princeton University Press, Princeton, 1955.

[21] C. Gardiner and P. Zoller, *The Quantum World of Ultra-Cold Atoms and Light Book*

III: Ultra-Cold Atoms. World Scientific Europe Ltd, London, 2017.

[22] H. Carmichael, *An open systems approach to quantum optics: Lectures presented at the Université Libre de Bruxelles*. Lecture Notes in Physics, Springer-Verlag, Berlin, 1993.

[23] M. Lewenstein, A. Sanpera, V. Ahufinger, B. Damski, A. Sen De, and U. Sen, "Ultracold atomic gases in optical lattices: Mimicking condensed matter physics and beyond," *Adv. Phys.*, vol. 56, pp. 243–379, 2006.

[24] M. Lewenstein, A. Sanpera, and V. Ahufinger, *Ultracold Atoms in Optical Lattices: Simulating quantum many-body systems*. Oxford University Press, Oxford, 2012.

[25] H. Häffner, C. Roos, and R. Blatt, "Quantum computing with trapped ions," *Phys. Rep.*, vol. 469, pp. 155–203, 2008.

[26] H. Breuer and F. Petruccione, *The Theory of Open Quantum Systems*. Oxford University Press, Oxford, 2002.

[27] Á. Rivas and S. Huelga, *Open Quantum Systems: An Introduction*. SpringerBriefs in Physics, Springer-Verlag, Berlin, 2011.

[28] D. Manzano, "A short introduction to the Lindblad master equation," *AIP Advances*, vol. 10, p. 025106, 2020.

[29] S. Nakajima, "On quantum theory of transport phenomena: Steady diffusion," *Prog. Theor. Phys.*, vol. 20, pp. 948–959, 1958.

[30] R. Zwanzig, "Ensemble method in the theory of irreversibility," *J. Chem. Phys.*, vol. 33, pp. 1338–1341, 1960.

[31] M. Richter and S. Mukamel, "Relaxation processes in systems strongly coupled to a harmonic bath," *J. Mod. Opt.*, vol. 57, pp. 2004–2008, 2010.

[32] E. Ferraro, M. Scala, R. Migliore, and A. Napoli, "On the validity of non-Markovian master equation approaches for the entanglement dynamics of two-qubit systems," *Phys. Scr*, vol. T140, p. 014042, 2010.

[33] M. Xu, Y. Yan, Y. Liu, and Q. Shi, "Convergence of high order memory kernels in the Nakajima-Zwanzig generalized master equation and rate constants: Case study of the spin-boson model," *J. Chem. Phys.*, vol. 148, p. 164101, 2018.

[34] B. Vacchini and H.-P. Breuer, "Exact master equations for the non-Markovian decay of a qubit," *Phys. Rev. A*, vol. 81, p. 042103, 2010.

[35] H. Z. Shen, M. Qin, X.-M. Xiu, and X. X. Yi, "Exact non-Markovian master equation for a driven damped two-level system," *Phys. Rev. A*, vol. 89, p. 062113, 2014.

[36] A. G. Redfield, "On the theory of relaxation processes," *IBM J. Res. Dev.*, vol. 1, pp. 19–31, 1957.

[37] I. Kondov, U. Kleinekathöfer, and M. Schreiber, "Stochastic unraveling of Redfield master equations and its application to electron transfer problems," *J. Chem. Phys.*, vol. 119, pp. 6635–6646, 2003.

[38] C. Kalyanaraman and D. Evans, "Symplectic integrators for the multilevel Redfield equation," *Chem. Phys. Lett.*, vol. 324, pp. 459–465, 2000.

[39] I. Kondov, U. Kleinekathöfer, and M. Schreiber, "Efficiency of different numerical methods for solving Redfield equations," *J. Chem. Phys.*, vol. 114, pp. 1497–1504, 2001.

[40] M. Yang and G. R. Fleming, "Influence of phonons on exciton transfer dynamics: comparison of the Redfield, Förster, and modified Redfield equations," *Chem. Phys.*, vol. 275, pp. 355–372, 2002.

[41] P. Bocchieri and A. Loinger, "Quantum recurrence theorem," *Phys. Rev.*, vol. 107,

pp. 337–338, 1957.
[42] J. Stewart, "Positive definite functions and generalizations, an historical survey," *Rocky Mt. J. Math.*, vol. 6, pp. 409–434, 1976.
[43] R. Edwards, *Fourier Series: A Modern Introduction Volume 1.* Graduate Texts in Mathematics, Springer, New York, 2011.
[44] P. Haikka and S. Maniscalco, "Non-Markovian dynamics of a damped driven two-state system," *Phys. Rev. A*, vol. 81, p. 052103, 2010.
[45] A. L. Daniel, B. Zsolt, and W. K.Birgitta, "From completely positive maps to the quantum markovian semigroup master equation," *Chem. Phys.*, vol. 268, pp. 35–53, 2001.
[46] R. Alicki, "Invitation to quantum dynamical semigroups," *arXiv Preprint: quant-ph/0205188*, 2002.
[47] G. Lindblad, "On the generators of quantum dynamical semigroups," *Commun. Math. Phys.*, vol. 48, pp. 119–130, 1976.
[48] D. A. Lidar, Z. Bihary, and K. Whaley, "From completely positive maps to the quantum Markovian semigroup master equation," *Chem. Phys.*, vol. 268, pp. 35–53, 2001.
[49] M. S. Sarandy and D. A. Lidar, "Abelian and non-Abelian geometric phases in adiabatic open quantum systems," *Phys. Rev. A*, vol. 73, p. 062101, 2006.
[50] J. Ginibre, "Statistical ensembles of complex, quaternion, and real matrices," *J. Math. Phys.*, vol. 6, pp. 440–449, 1965.
[51] A. Buchleitner and K. Hornberger, *Coherent Evolution in Noisy Environments.* Lecture Notes in Physics, Springer-Verlag, Berlin, 2008.
[52] D. Walls and G. Milburn, *Quantum Optics.* Springer-Verlag, Berlin, 2008.
[53] R. Rangel and L. Carvalho, "Algebraic solution of master equations," *arXiv Preprint: quant-ph/0309042*, 2003.
[54] V. Lev and R. Marcos, "Generalized Gibbs ensemble in integrable lattice models," *J. Stat. Mech.: Theory Exp.*, vol. 2016, p. 064007, 2016.
[55] R. Nandkishore and D. A. Huse, "Many-body localization and thermalization in quantum statistical mechanics," *Annu. Rev. Condens. Matter Phys.*, vol. 6, pp. 15–38, 2015.
[56] A. Barenco, A. Berthiaume, D. Deutsch, A. Ekert, R. Jozsa, and C. Macchiavello, "Stabilization of quantum computations by symmetrization," *SIAM J. Comput.*, vol. 26, p. 1541–1557, 1997.
[57] P. Zanardi and M. Rasetti, "Error avoiding quantum codes," *Mod. Phys. Lett. B*, vol. 11, pp. 1085–1093, 1997.
[58] L.-M. Duan and G.-C. Guo, "Preserving coherence in quantum computation by pairing quantum bits," *Phys. Rev. Lett.*, vol. 79, pp. 1953–1956, 1997.
[59] P. Zanardi and M. Rasetti, "Noiseless quantum codes," *Phys. Rev. Lett.*, vol. 79, pp. 3306–3309, 1997.
[60] D. A. Lidar, I. L. Chuang, and K. B. Whaley, "Decoherence-free subspaces for quantum computation," *Phys. Rev. Lett.*, vol. 81, 1998.
[61] A. Beige, D. Braun, B. Tregenna, and P. L. Knight, "Quantum computing using dissipation to remain in a decoherence-free subspace," *Phys. Rev. Lett.*, vol. 85, pp. 2594–2597, 2000.
[62] P. W. Shor, "Fault-tolerant quantum computation," in *Proceedings of 37th Conference on Foundations of Computer Science*, pp. 56–65, 1996.
[63] M. A. Sepiol, A. C. Hughes, J. E. Tarlton, D. P. Nadlinger, T. G. Ballance, C. J. Ballance, T. P. Harty, A. M. Steane, J. F. Goodwin, and D. M. Lucas, "Probing qubit

memory errors at the part-per-million level," *Phys. Rev. Lett.*, vol. 123, p. 110503, 2019.
[64] J. B. Altepeter, P. G. Hadley, S. M. Wendelken, A. J. Berglund, and P. G. Kwiat, "Experimental investigation of a two-qubit decoherence-free subspace," *Phys. Rev. Lett.*, vol. 92, p. 147901, 2004.
[65] Z. J. Deng, M. Feng, and K. L. Gao, "Preparation of entangled states of four remote atomic qubits in decoherence-free subspace," *Phys. Rev. A*, vol. 75, p. 024302, 2007.
[66] D. Kielpinski, V. Meyer, M. A. Rowe, C. A. Sackett, W. M. Itano, C. Monroe, and D. J. Wineland, "A decoherence-free quantum memory using trapped ions," *Science*, vol. 291, pp. 1013–1015, 2001.
[67] A. J. Daley, "Quantum trajectories and open many-body quantum systems," *Adv. Phys.*, vol. 63, pp. 77–149, 2014.
[68] M. B. Plenio and P. L. Knight, "The quantum-jump approach to dissipative dynamics in quantum optics," *Rev. Mod. Phys.*, vol. 70, pp. 101–144, 1998.
[69] J. Dalibard, Y. Castin, and K. Mølmer, "Wave-function approach to dissipative processes in quantum optics," *Phys. Rev. Lett.*, vol. 68, pp. 580–583, 1992.
[70] U. Schollwöck, "The density-matrix renormalization group in the age of matrix product states," *Ann. Phys.*, vol. 326, pp. 96–192, 2011.
[71] R. Orús, "A practical introduction to tensor networks: Matrix product states and projected entangled pair states," *Ann. Phys.*, vol. 349, pp. 117–158, 2014.
[72] F. Verstraete, V. Murg, and J. Cirac, "Matrix product states, projected entangled pair states, and variational renormalization group methods for quantum spin systems," *Adv. Phys.*, vol. 57, pp. 143–224, 2008.
[73] G. K.-L. Chan, A. Keselman, N. Nakatani, Z. Li, and S. R. White, "Matrix product operators, matrix product states, and ab initio density matrix renormalization group algorithms," *J. Chem. Phys.*, vol. 145, p. 014102, 2016.
[74] S. R. White, "Density matrix formulation for quantum renormalization groups," *Phys. Rev. Lett.*, vol. 69, pp. 2863–2866, 1992.
[75] G. Vidal, "Efficient classical simulation of slightly entangled quantum computations," *Phys. Rev. Lett.*, vol. 91, p. 147902, 2003.
[76] J. Eisert, M. Cramer, and M. B. Plenio, "Colloquium: Area laws for the entanglement entropy," *Rev. Mod. Phys.*, vol. 82, pp. 277–306, 2010.
[77] L. Amico, R. Fazio, A. Osterloh, and V. Vedral, "Entanglement in many-body systems," *Rev. Mod. Phys.*, vol. 80, pp. 517–576, 2008.
[78] M. Srednicki, "Entropy and area," *Phys. Rev. Lett.*, vol. 71, pp. 666–669, 1993.
[79] M. M. Wolf, F. Verstraete, M. B. Hastings, and J. I. Cirac, "Area laws in quantum systems: Mutual information and correlations," *Phys. Rev. Lett.*, vol. 100, p. 070502, 2008.
[80] J. Eisert, "Entanglement and tensor network states," *arXiv Preprint: quant-ph/1308.3318*, 2013.
[81] G. Evenbly and G. Vidal, "Tensor network states and geometry," *J. Stat. Phys.*, vol. 145, pp. 891–918, 2011.
[82] M. Suzuki, "Generalized Trotter's formula and systematic approximants of exponential operators and inner derivations with applications to many-body problems," *Commun. Math. Phys.*, vol. 51, pp. 183–190, 1976.
[83] J. R. Coulthard, *Engineering quantum states of fermionic many-body systems.* PhD thesis, University of Oxford, Oxford University Research Archive, 2017.

[84] C. Karrasch, J. H. Bardarson, and J. E. Moore, "Finite-temperature dynamical density matrix renormalization group and the Drude weight of spin-1/2 chains," *Phys. Rev. Lett.*, vol. 108, p. 227206, 2012.

[85] M. Berta, F. G. S. L. Brandão, J. Haegeman, V. B. Scholz, and F. Verstraete, "Thermal states as convex combinations of matrix product states," *Phys. Rev. B*, vol. 98, p. 235154, 2018.

[86] B. Kloss, Y. B. Lev, and D. Reichman, "Time-dependent variational principle in matrix-product state manifolds: Pitfalls and potential," *Phys. Rev. B*, vol. 97, 2018.

[87] J. Haegeman, J. I. Cirac, T. J. Osborne, I. Pižorn, H. Verschelde, and F. Verstraete, "Time-dependent variational principle for quantum lattices," *Phys. Rev. Lett.*, vol. 107, p. 024307, 2011.

[88] P. Secular, N. Gourianov, M. Lubasch, S. Dolgov, S. R. Clark, and D. Jaksch, "Parallel time-dependent variational principle algorithm for matrix product states," *Phys. Rev. B*, vol. 101, p. 235123, 2020.

[89] G. Vidal, "Classical simulation of infinite-size quantum lattice systems in one spatial dimension," *Phys. Rev. Lett.*, vol. 98, p. 070201, 2007.

[90] F. Verstraete and J. I. Cirac, "Renormalization algorithms for quantum-many body systems in two and higher dimensions," *arXiv Preprint: cond-mat.ste-el/0407066*, 2004.

[91] F. Verstraete, M. M. Wolf, D. Perez-Garcia, and J. I. Cirac, "Criticality, the area law, and the computational power of projected entangled pair states," *Phys. Rev. Lett.*, vol. 96, p. 220601, 2006.

[92] F. Verstraete, J. J. García-Ripoll, and J. I. Cirac, "Matrix product density operators: Simulation of finite-temperature and dissipative systems," *Phys. Rev. Lett.*, vol. 93, p. 207204, 2004.

[93] M. Zwolak and G. Vidal, "Mixed-state dynamics in one-dimensional quantum lattice systems: A time-dependent superoperator renormalization algorithm," *Phys. Rev. Lett.*, vol. 93, p. 207205, 2004.

[94] E. Mascarenhas, H. Flayac, and V. Savona, "Matrix-product-operator approach to the nonequilibrium steady state of driven-dissipative quantum arrays," *Phys. Rev. A*, vol. 92, p. 022116, 2015.

[95] J. Cui, J. I. Cirac, and M. C. Bañuls, "Variational matrix product operators for the steady state of dissipative quantum systems," *Phys. Rev. Lett.*, vol. 114, p. 220601, 2015.

[96] A. Datta and G. Vidal, "Role of entanglement and correlations in mixed-state quantum computation," *Phys. Rev. A*, vol. 75, p. 042310, 2007.

[97] D. Jaschke, S. Montangero, and L. D. Carr, "One-dimensional many-body entangled open quantum systems with tensor network methods," *Quantum Sci. Technol.*, vol. 4, p. 013001, 2018.

Chapter 2

The Maximum Entropy States of Symmetric Many-Body Systems

Some of the results in this chapter were inspired by the work in

• B. Buča, J. Tindall, and D. Jaksch *Non-stationary coherent quantum many body dynamics through dissipation*, Nature Communications, **10** (2019)
• J. Tindall, B. Buča, J. R. Coulthard and D. Jaksch, *Heating-Induced Long-Range η-Pairing in the Hubbard Model*, Phys. Rev. Lett, **123** (2019)
• J. Tindall, F. Schlawin, M. Sentef and D. Jaksch, Analytical Solution for the Steady States of the Driven Hubbard model, *Physical Review B* **103**, 035146 (2021).

Contributions to these papers from JT are listed in the introduction.

In this chapter we begin by introducing the concept of symmetries in the context of open and closed quantum systems. In both cases we discuss the consequences symmetries can have on the equilibrium and non-equilibrium properties of the system. This background allows us to demonstrate how the long-time state of a generic system that undergoes continuous heating can be written in the basis which diagonalises the irreducible representation of its symmetries. We discuss how periodic driving or local, Hermitian dephasing are typical mechanisms by which this heating could occur.

We then explore the consequences of this result, first taking a generic many-body system under heating which preserves a U(1) symmetry and showing how the maximum entropy steady states which form in the U(1) subspaces are always featureless in the sense that all two-point correlations in space are zero. This observation is directly related to the local nature of the U(1) operator and we present an explicit example in the form of the XXZ spin chain. Then, in constrast to the U(1) case, we consider an arbitrary system composed of spin $s = 1/2$ particles and prove that the maximum

entropy steady states which form under SU(2) preserving heating will generally (i.e. for the majority of initial states) possess finite, distance-invariant, inter-spin correlations. Our proof uncovers that the ratio of correlated steady states to uncorrelated ones grows in proportion to the system size and we detail how the same arguments can be applied when $s > 1/2$ or for an SU(2) symmetric fermionic system. We term this phenomenon heating-induced order and demonstrate an explicit example in the $s = 1$ driven AKLT model. Finally, we discuss how this mechanism should also be observable in systems with higher order symmetries such as SU(N) with N > 2 and SO(N).

2.1 Symmetries in Quantum Systems

Closed Quantum Systems

Symmetries are central to our understanding of a number of physical phenomena. In classical physics, Noether's theorem tells us that for every symmetry in a system there is a corresponding conserved quantity [1]. Upon identification, these symmetries can help simplify the relevant equations of motion.

In quantum mechanics, symmetries play a similar role. For a closed undriven system symmetries can be identified by their operator representation O commuting with the Hamiltonian H, i.e. $[H, O] = 0$. In a closed driven system, we need O to commute with the time-dependent Hamiltonian $H(t)$ for all times, i.e. $[H(t), O] = 0\ \forall t$. In both cases it immediately follows from the solution of the Schrödinger equation that the quantity $\langle O \rangle$ is a constant of motion. This can simplify things significantly, allowing us to diagonalise H into independent blocks indexed by the distinct eigenvalues of O. The existence of a symmetry also generally leads to degeneracies in the eigenstates of the Hamiltonian, which can have a number of implications. For instance, modulations in the spatial density profile of a cold excitonic ring have been shown to be a signature of degeneracy in the system [2].

Symmetries and conserved quantities are also intimately related to the notion of integrability. In integrable quantum systems a set of maximal, non-trivial, independent operators which commute with the Hamiltonian can be constructed[1] [4, 5]. The existence of these integrals of motion, or charges, is directly related to the eigenvalues of the Hamiltonian possessing Poissonian level statistics [6, 7]. Moreover, these

[1]Non-trivial is usually defined in the sense that these operators are local or few-body [3] — the projectors to the eigenstates of the Hamiltonian form a maximal independent set but would be classed as 'trivial' as they are generally non-local and many-body and thus not sufficient for the system to be integrable.

charges can sometimes render the model soluble via, for example, the celebrated Bethe ansatz [8, 9, 10] which can be used to identify algebraic expressions for the eigenvalues and eigenvectors of the Hamiltonian.

The integrability of a quantum system also has important consequences for its non-equilibrium dynamics. Specifically, following a quench under the Hamiltonian H, the expectation values of observables in an integrable system do not agree with the typical predictions of the Gibbs ensemble $\frac{1}{Z}\exp(-\beta H)$, where Z is the partition function and β is the inverse temperature. Instead, these expectation values are known to relax to the predictions of the Generalized Gibbs Ensemble (GGE) [11, 12, 13] $\frac{1}{Z}\exp(-\sum_q \beta_q C_q)$ where $\{C_q\}$ is the maximal set of independent conserved quantities (including the Hamiltonian H) and $\{\beta_q\}$ is the set of corresponding Lagrange multipliers or inverse temperatures. The GGE is a state of maximum entropy subject to the phase-space constraints imposed by the charges $\{C_q\}$. In the following section we will see how phase-space constraints also dictate the long-time behaviour of quantum systems subject to continuous heating from an external source. Prior to this, we shall introduce a description of symmetries in open quantum systems.

Open Quantum Systems

In open systems, more care needs to be taken when identifying symmetries due to the addition of the interaction between the system and the environment, which can break the symmetries that the Hamiltonian possesses. In this thesis our focus is predominantly on Markovian open systems governed by the GSKL equation. We will therefore discuss the notion of symmetries in this context and consider a system with Hamiltonian H whose density matrix is governed by the GSKL equation

$$\frac{\partial\rho(t)}{\partial t} = \mathcal{L}\rho(t) = -\mathrm{i}[H,\rho(t)] + \sum_j \gamma_j\big(L_j\rho(t)L_j^\dagger - \frac{1}{2}\{L_{ji}^\dagger L_j,\rho(t)\}\big). \tag{2.1}$$

A detailed derivation and description of the various terms in this equation is given in chapter 1. By moving to the equivalent Heisenberg picture, where the operators become time-dependent and the density matrix static, we can describe the time evolution of a generic operator O via

$$\frac{\partial O(t)}{\partial t} = \mathcal{L}^\dagger O(t) = \mathrm{i}[H,O(t)] + \sum_j \gamma_j\big(L_j^\dagger O(t)L_j - \frac{1}{2}\{L_j^\dagger L_j,O(t)\}\big), \tag{2.2}$$

and the equation of motion for the corresponding observable $\langle O(t)\rangle = \mathrm{Tr}(\rho O(t))$ follows immediately by tracing over the product of Eq. (2.2) and the static density matrix ρ.

It is clear from Eq. (2.2) that the condition $[H, O] = 0$ (where we use O to represent $O(0)$) is not sufficient for an operator to be a true symmetry of the system with $\langle O(t) \rangle$ constant $\forall t$. Instead, it is clear that if an operator satisfies

$$[H, O] = [L_j, O] = [L_j^\dagger, O] = 0 \ \forall j, \tag{2.3}$$

it is a true symmetry of the system with $\partial O(t)/\partial t = 0 \ \forall t$ and the corresponding observable constant. In this case, O is known as a 'strong' symmetry of the system[2] [14, 15] which, along with the conservation of the corresponding observable, has significant implications for the eigenmodes of the Liouvillian.

Firstly, assuming O is Hermitian, it follows that the superoperators $\mathcal{L}$, $1 \otimes O^T$, $O \otimes 1$ form a mutually commuting set of observables and so we can diagonalise the Liouvillian into independent blocks which are indexed by the different *distinct* eigenvalues of $1 \otimes O^T$ and $O \otimes 1$. As the distinct eigenvalues of $1 \otimes O^T$ and $O \otimes 1$ are just those of O the blocks will be indexable by the X^2 unique tuples (a, b), with a and b each running through the X distinct eigenvalues of O.

As an example of this, if we return to the master equation from chapter 1 which describes a pair of qubits in the presence of a magnetic field and collective loss

$$\frac{\partial \rho(t)}{\partial t} = \mathcal{L}\rho(t) = -\mathrm{i}\omega[S^z, \rho(t)] + S^-\rho(t)S^+ - \frac{1}{2}\{S^+S^-, \rho(t)\}, \tag{2.4}$$

where $S^{\pm,z} = \sum_{i=1,2} \sigma_i^{\pm,z}$, we can show that the Casimir operator $S^2 = S^+S^- + S^-S^+ + (S^z)^2$ is a strong symmetry of the system. In Fig. 2.1 we plot the elements of the superoperator matrix $\mathcal{L}$ in the basis formed from eigenvectors of the left and right Casimir operators, $1 \otimes S^2$ and $S^2 \otimes 1$. In this basis, the Liouvillian is block-diagonal.

The presence of a strong symmetry also has implications for the steady state degeneracy of the Liouvillian. Namely, it can be shown there always exists at least one steady state of trace unity within each of the blocks where the tuple indices are the same (i.e. $a = b$) [14]. In the case of a single strong symmetry this means the steady state degeneracy must be lower bounded by the number of distinct eigenvalues of the operator O. Meanwhile, the matrix elements in the blocks where $a \neq b$ are all traceless and thus a steady state with finite trace cannot exist there.

In Ref. [15] it was further proved how for systems with multiple non-Abelian strong symmetries[3] the degeneracy can be lower bounded by constructing an irreducible representation for the set of strong symmetries. The steady states of an open

[2]Outside of the Markovian picture we can understand a strong symmetry as an operator that resides in the Banach space of the system and commutes with both the system Hamiltonian and each of the operators A_μ which make up the system-environment interaction $H_{\text{int}} = \sum_\mu A_\mu \otimes B_\mu$.

[3]Non-Abelian means that the operator representations of these symmetries do not commute.

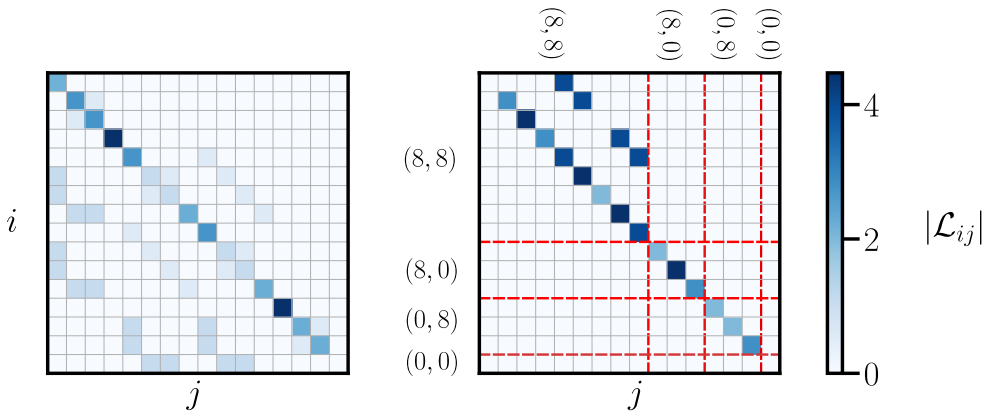

Figure 2.1: Absolute value of the elements of the Liouvillian superoperator matrix for two qubits in a uniform magnetic field with collective loss, see Eq. (2.4). The elements of the matrix are indexed by i and j. Left) Superoperator matrix in the basis formed from the tensor product of two copies of the basis $\{|\uparrow,\uparrow\rangle, |\uparrow,\downarrow\rangle, |\downarrow,\uparrow\rangle, |\downarrow,\downarrow\rangle\}$, which diagonalises S^z. Right) Superoperator matrix in the basis formed from the tensor product of two copies of the eigenvectors of the Casimir operator S^2 $\{|1\rangle, |2\rangle, |3\rangle, |4\rangle\} = \{|\downarrow,\downarrow\rangle_8, (|\uparrow,\downarrow\rangle + |\downarrow,\uparrow\rangle)_8, |\uparrow,\uparrow\rangle_8, (|\uparrow,\downarrow\rangle - |\downarrow,\uparrow\rangle)_0\}$ where the subscript denotes the corresponding eigenvalue. The red lines separate the different blocks which emerge with the numbers inside the tuples reflecting the eigenvalues for the eigenvectors used to construct a given block. As an example, the matrix elements $|1\rangle\langle 4|\langle 4|\langle 4|$, $|2\rangle|4\rangle\langle 4|\langle 4|$ and $|3\rangle|4\rangle\langle 4|\langle 4|$ span the block with the row tuple $(8,0)$ and the column tuple $(0,0)$. The Liouvillian is block-diagonal in this basis, possessing non-zero elements solely within the diagonal blocks.

system often inherit the structure of its strong symmetries leading to the manifestation of unique properties in the long-time limit. One such example is in molecular lattices, where the symmetries can be harnessed to control the flow of current through them [16].

Strong symmetries are not the only type of symmetry that can occur in an open system. For instance the Liouvillian may possess a 'weak' symmetry in the form of a unitary operator U which leaves the action of the Liouvillian on a state invariant, i.e. $\mathcal{L}(U\rho U^\dagger) = U(\mathcal{L}\rho)U^\dagger$ [14]. Despite having no associated conservation law the existence of a weak symmetry can still have significant consequences, often leading to an appropriate block-decomposition of the Liouvillian, as well as having physical implications for the dynamics of the system [17, 18].

2.2 Maximum Entropy States in the Presence of Symmetries

We now consider what happens when a quantum system, with Hamiltonian H, continuously absorbs energy from an external source and reaches a state of maximum entropy whilst still possessing certain symmetries and thus being restricted to a specific subspace of the Hilbert space. It is worth emphasizing that by maximum entropy state we mean the identity matrix, which occupies all available basis states in the given subspace with equal probability and maximises the von-Neumann entropy. In the context of pure states we simply mean a state which mimics the properties of this maximum entropy density matrix when measurements are made of few-body, physical observables.

As typical external sources which could induce such heating we consider either a) continuous periodic driving which realises the time-dependent Hamiltonian $H+H_D(t)$, where $H_D(t)$ is the periodic driving term or b) the presence of a Markovian environment which leads to the system being governed by the GSKL equation in Eq. (2.1). In the driven case the assumption that the system will continuously absorb energy is reasonable for almost all generic periodic driving terms due to the inevitability of Floquet heating [19, 20]. In the dissipative case this will only occur for certain types of jump operators. We will focus on the case of local, Hermitian jump operators as such a type because it can be shown via Eq. (2.2) that if $L_j = L_j^\dagger \ \forall j$ the maximum entropy identity matrix forms a steady state with trace 1 in each of the strong symmetry blocks of the Liouvillian.

We assume that we can identify a set of N operators $C = \{C_1, C_2, ..., C_N\}$, which form a linearly independent, irreducible representation of the symmetries of the heated system with $[C_i, C_k] = 0 \ \forall i, k$. We note that whilst this might not always possible in a general quantum system, for the range of setups we consider in this thesis we are always able to identify the completely commuting set C. For the driven case these operators must satisfy

$$[H + H_D(t), C_i] = 0 \ \forall i, \tag{2.5}$$

and for the dissipative case we assume they form a series of strong symmetries

$$[H, C_j] = [L_j, C_i] = [L_j^\dagger, C_i] = 0 \ \forall i, j. \tag{2.6}$$

As the system evolves towards a state of maximum entropy it is under the constraint that its probability distribution over the eigenspace of any conserved quantities must

be constant. Hence, the long-time state should have the form[4]

$$\lim_{t\to\infty}\rho(t)=\rho_{ss}=\sum_{\alpha=(\alpha_1,\alpha_2,...\alpha_N)}P_\alpha\sum_{\beta=1}^{D_\alpha}|\alpha,\beta\rangle\langle\alpha,\beta|\,, \tag{2.7}$$

with $\sum_\alpha P_\alpha D_\alpha = 1$ and the multi-index/quantum number α running over the different distinct regions of the Hilbert space. A given region is spanned by the D_α degenerate states $|\alpha,\beta\rangle$ — these states are each simultaneously an eigenvector of all the operators in C with the corresponding eigenvalues $(\alpha_1,\alpha_2,...\alpha_N)$, i.e. $C_i|\alpha,\beta\rangle = \alpha_i|\alpha,\beta\rangle$. Finally, we have used P_α to denote the probability of finding the system within a given region/ degenerate subspace. This probability is preserved throughout the time evolution and thus

$$P_\alpha=\sum_{\beta=1}^{D_\alpha}\mathrm{Tr}\big[\rho(0)|\alpha,\beta\rangle\langle\alpha,\beta|\,\big], \tag{2.8}$$

where $\rho(0)$ is the initial state of the system. We note that, unlike in the GGE, the Hamiltonian H does not form one of the conserved quantities, i.e. $H\notin C$ as energy is not conserved. It is also worth mentioning that if the set C is empty, i.e. the system has no symmetries, then the index α is redundant and the states $|\alpha,\beta\rangle\to|\beta\rangle$ can be any orthonormal set which spans the Hilbert space. In this case the steady state is just the featureless identity matrix over the whole Hilbert space and needs no attention.

Meanwhile, assuming that C is not empty, Eq. (2.7) shows that if the system is initialised in a state with a fixed $\alpha = x$, i.e. $P_\alpha = \delta_{\alpha,x}$, then the steady state is the identity matrix in the space spanned by the eigenvectors $\{|x,\beta\rangle\}$ with $\beta = 1...D_x$. If the initial state instead has a non-zero overlap with multiple different sectors then the steady state is just a correspondingly weighted sum over the identity matrix in each of those sectors.

In the following section we will considering several types of symmetries which are common in many-body quantum systems and see that the properties of these identity matrices are not necessarily trivial and are strongly dependent on the symmetries in question.

[4]Whilst in the driven case a pure state will always remain pure we will see that this mixed state ansatz is, at least at the level of measuring few-body observables, reasonable in a many-body system as the energy of the driving will have scrambled the phases of the wavefunction sufficiently to destroy any coherences between different $|\alpha,\beta\rangle$ eigenstates [21].

U(1) Symmetries

The first symmetry we will consider is that of U(1). We can take a general Hamiltonian for a many-body single species system to be a function of local creation and annihilation operators, i.e.

$$H = H(\psi_1, \psi_2, ..., \psi_L, \psi_1^\dagger, \psi_2^\dagger, ..., \psi_L^\dagger), \tag{2.9}$$

where $\psi_i^\dagger$ and ψ_i, respectively, create and annihilate a body/ particle at position i in the system and there are L possible positions. These operators could be those for bosons or fermions and will obey the corresponding commutation relations. The Hamiltonian could also describe a series of $2s+1$ level spins such as qubits ($s = 1/2$), each at a different position i, and the corresponding $\psi_i^\dagger$ and ψ_i would instead be spin raising and lowering operators.

In all cases we say that the Hamiltonian H is $U(1)$ symmetric if it is invariant under the transformation $\psi_i \to e^{\mathrm{i}\phi}\psi_i$ and $\psi_i^\dagger \to e^{-\mathrm{i}\phi}\psi_i^\dagger$, with $\phi \in \mathbb{R}$ and the complex number $e^{\mathrm{i}\phi}$ forming the fundamental representation of the U(1) symmetry [22]. This invariance of H under $e^{\mathrm{i}\phi}$ implies that, for bosons/fermions, the operator $\mathcal{Q} = \sum_i \psi_i^\dagger \psi_i$ commutes with H and represents the total number of particles. For spins this operator will instead be $\mathcal{Q} = \sum_i \psi_i^\dagger \psi_i - \psi_i \psi_i^\dagger$ and represents the total spin along the axis where $\psi_i^\dagger$ creates excitations. This operator $\mathcal{Q}$ forms the 'global' operator representation of the U(1) symmetry and it is often referred to as the total 'charge' of the system [22].

Under heating that preserves the U(1) symmetry the system will reach a long-time state of the form in Eq. (2.7), the states $|\alpha, \beta\rangle$ will simply correspond to the eigenvectors of $\mathcal{Q}$. As $\mathcal{Q}$ is a sum of purely local operators it immediately follows that these eigenvectors can always each be expressed as product states over the different positions in the system. The steady state is diagonal in this basis and so it clearly cannot possess any finite correlations between different positions and is effectively featureless beyond the fixed value of $\langle \mathcal{Q} \rangle$. We note that the same is also true even if we have more than one species of particle in our Hamiltonian — whilst this allows us to have multiple U(1) symmetries the corresponding total charge operators will all commute and be a sum over purely local operators, making the steady state necessarily featureless.

We will now illustrate these ideas with an explicit example in the form of the XXZ Hamiltonian for interacting qubits. The Hamiltonian reads

$$H = \sum_i J\sigma_i^x \sigma_{i+1}^x + J\sigma_i^y \sigma_{i+1}^y + \Delta \sigma_i^z \sigma_{i+1}^z, \tag{2.10}$$

with $\sigma_i^{x,y,z}$ being the corresponding Pauli matrix acting on the ith qubit. The XXZ model is a paradigmatic model of quantum magnetism which has attracted significant attention since its inception. For instance, the Bethe Ansatz was first formulated by Hans Bethe in order to find the exact solutions of the eigenstates of this Hamiltonian [23, 24, 25] and has since been extended to a number of quantum lattice models [26, 27]. Furthermore, the XXZ model was one of the first examples used to demonstrate the power of the Density Matrix Renormalization Group (DMRG) algorithm [28].

For the purpose of analysing the U(1) symmetry this Hamiltonian possesses it is helpful to write it solely in terms of the spin raising and lowering operators $\sigma_i^+ = (1/2)(\sigma_i^x + \mathrm{i}\sigma_i^y)$ and $\sigma_i^- = (1/2)(\sigma_i^x - \mathrm{i}\sigma_i^y)$,

$$H = \sum_i 2J(\sigma_i^+\sigma_{i+1}^- + \sigma_i^+\sigma_{i+1}^-) + \Delta[\sigma_i^+, \sigma_i^-][\sigma_{i+1}^+, \sigma_{i+1}^-]. \tag{2.11}$$

This Hamiltonian is now in the form described by Eq. (2.9) with $\psi_i^\dagger = \sigma_i^+$ and $\psi_i = \sigma_i^-$. It is clearly invariant if we apply the transformation corresponding to a rotation by an angle α around the z-axis via $\sigma_i^+ \to e^{\mathrm{i}\alpha}\sigma_i^+$ and $\sigma_i^- \to e^{-\mathrm{i}\alpha}\sigma_i^-$. This invariance means the system is U(1) symmetric. The total z magnetisation operator $S^z = \sum_i \sigma_i^z = \sum_i \sigma_i^+\sigma_i^- - \sigma_i^-\sigma_i^+$ is the 'global' operator representation for this U(1) symmetry and commutes with H.

We will now consider the addition of periodic driving or dissipation which preserve this U(1) symmetry whilst causing the system to heat up to the steady state described in Eq. (2.7). The $|\alpha, \beta\rangle$ will denote the eigenstates of the S^z - α indexes the different distinct eigenvalues and β indexes the degeneracy of said eigenvalues.

In Fig. 2.2 we use numerical calculations to observe the formation of this steady state exactly. As the initial state we have chosen resides in the subspace with $\langle S^z \rangle = 0$ we can restrict ourselves to this space as S^z is conserved throughout the evolution. In Fig. 2.2a, for the dissipative case, we see the long-time density matrix corresponds to the identity matrix in the space spanned by the 0 eigenvectors of S^z, in agreement with Eq. (2.7). Furthermore, for the driven case in Fig. 2.2b, we observe that the phase differences between the coefficients of the wavefunction in this space are completely scrambled. This creates an effective equivalence between the driven and dissipative cases which is seen in the measured observables, despite the different system sizes used. The similarity between the two system sizes also indicates that boundary effects are not particularly important here. The heating has 'washed out' the geometry of the system, making the steady state independent of the Hamiltonian, where the boundary conditions originated.

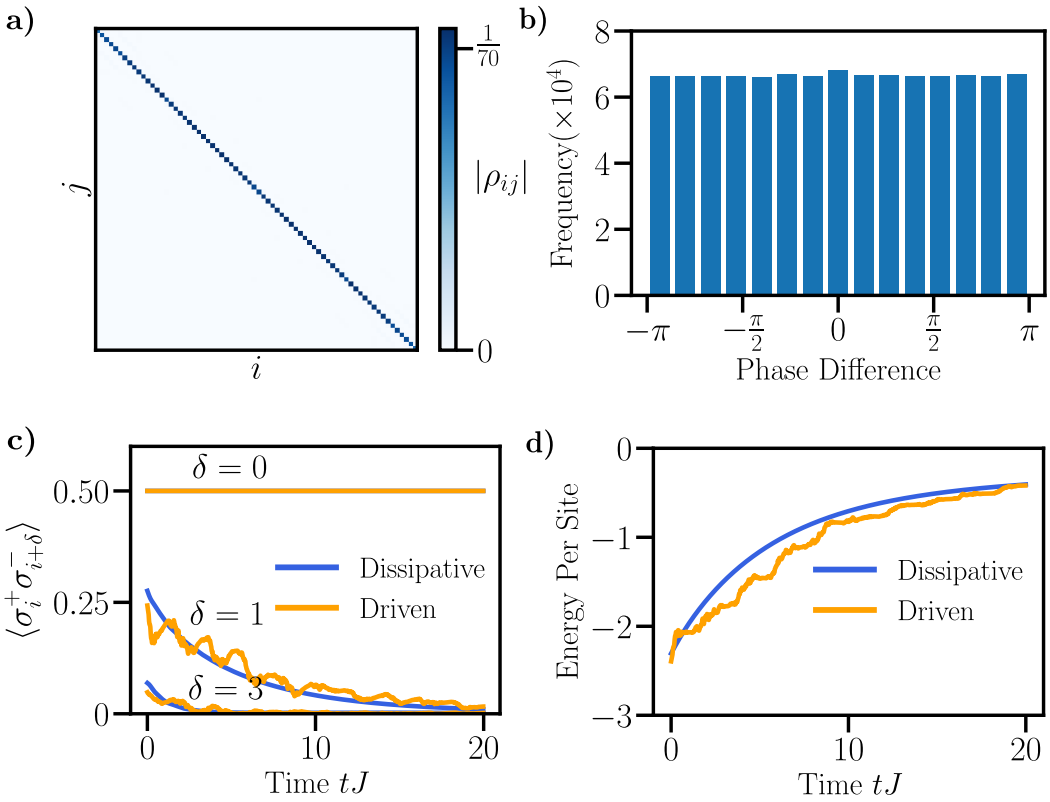

Figure 2.2: Properties of the driven/ dissipative XXZ chain described by the Hamiltonian H in Eq. (2.10) with $\Delta = 2.0J$. We initialise the system in the ground state and time-evolve it under driving or dissipation. In the driven case we take $L = 20$ sites and add an additional time-dependent term $H_D(t) = h \sin(\omega t) \sum_i f(i)\sigma_i^z$ to H, with $h = 10.0J$, $\omega J = 1.5$ and $f(i)$ a random number between 0 and 1. In the dissipative case we take $L = 8$ sites governed by Eq. (2.1) with jump operators $L_j = \gamma \sigma_j^z$, where j runs over the sites of the chain, and $\gamma_j = 0.01J \; \forall j$. We solve the corresponding GSKL equation using a superoperator approach. a) Dissipative case — absolute value of the elements of the density matrix in the number basis with $\langle S^z \rangle = 0$ at time $tJ = 20.0$. b) Driven case — histogram of the phase difference between the coefficients of the wavefunction in the $\langle S^z \rangle = 0$ number basis, 10^3 basis states were randomly sampled to create 10^6 phase differences. c) Time-evolution of the spin-exchange correlations at several distances. d) Time-evolution of the energy per site, defined as $E = \mathrm{Tr}(\rho(t)H)/L$.

Notably, outside of the fixed magnetisation, in Fig. 2.2c we observe that the long-time state is effectively featureless: only the on-site correlations are non-zero and these can be described classically (there is no superposition involved). Upon being driven out of equilibrium the system has rapidly heated up, with any initial inter-qubit correlations decaying away. In Fig. 2.2d we see that, in both cases, the system continuously absorbs energy from the external source and eventually begins

to saturate as it reaches the steady state.

This formation of a featureless steady state as a system with a U(1) symmetry (or one with no symmetries at all) absorbs energy is completely general and independent of the specific model, parameters or initial state we have chosen. As a result, mechanisms such as Floquet heating and Hermitian dephasing are typically seen as obstacles when engineering quantum states of matter, or when realising quantum technologies such as quantum computers.

In the following, however, we will counterpose this and show how heating, and consequently these mechanisms, can actually be used a resource for state engineering in quantum systems. We will see that the preservation of symmetries beyond that of U(1) can lead to the maximum entropy steady states in certain symmetry subspaces containing completely uniform, long-range spatial correlations. The correlations in these long-time states can be significantly amplified in comparison to the equilibrium state out of which the system was driven and thus the heating, counterintuitively, induces and subsequently protects order in the system.

SU(2) Symmetries

The symmetry which we will focus on to exemplify this phenomenon is that of SU(2) — the special unitary group of 2×2 matrices [29]. Their natural representation is that of 3 traceless Hermitian 2×2 matrices, or generators, $\{J^1, J^2, J^3\}$ which satisfy the following SU(2) commutation relations

$$[J^i, J^j] = \mathrm{i}\epsilon_{ijk} J^k, \tag{2.12}$$

where ϵ_{ijk} is the Levi-Civita symbol. The Pauli matrices $\sigma^x, \sigma^y, \sigma^z$ are arguably the most common representation of the SU(2) group [29]. If we consider the many-body XXZ Hamiltonian from Eq. (2.10) we notice that if, and only if, $\Delta = J$ the Hamiltonian commutes with the global representation of the SU(2) operators, i.e $[H(\Delta = J), S^{x,y,z}] = 0$, where $S^{x,y,z} = \sum_i \sigma_i^{x,y,z}$. These global operators, like their local counterparts $\sigma_i^{x,y,z}$, satisfy the SU(2) relations in Eq. (2.12) and hence the Hamiltonian is SU(2) symmetric in this limiting case, a consequence of it being invariant under rotations about any of the spin-axes: x, y or z.

We wish to know what impact such an SU(2) symmetry has on the steady state of a many-body system under heating. We define the many-body system as SU(2) symmetric in the sense that we can identify the 'global' SU(2) operators $\{S^x, S^y, S^z\}$, which obey Eq. (2.12) and are each invariant under their corresponding equation of motion. These operators could be those we defined for spin $s = 1/2$, for a system of

higher spin $s > 1/2$, or even those for a fermionic system — the specific representation is not important. If the heating in the system originates from periodic driving then we require that the SU(2) operators each satisfy Eq. (2.5) in order to be invariant under their equation of motion, whilst if the heating arises from a dissipative process they should satisfy Eq. (2.6) instead.

In our SU(2) setup, we still expect the long-time state to be of the form in Eq. (2.7), but as we have multiple non-commuting integrals of motion care needs to be taken in identifying the relevant eigenbasis $|\alpha, \beta\rangle$. This non-commutativity means we cannot find a basis $|\alpha, \beta\rangle$ which simultaneously diagonalises S^x, S^y and S^z. Despite this, we can form the Casimir operator $S^2 = (S^x)^2 + (S^y)^2 + (S^z)^2$ which commutes with each of these operators. We then introduce the vector $|\alpha_1, \alpha_2\rangle$ which is simultaneously an eigenvector of S^z and S^2, with α_1 and α_2 indexing their respective eigenvalues. It can be proven that these eigenvectors fully span the space generated by the operators $S^{x,y,z}$ and form a complete irreducible representation of the SU(2) symmetry [29, 30]. Hence, in Eq. (2.7), for the steady state of an SU(2) many-body system the multi-index α should run over the possible distinct eigenvalue pairs (α_1, α_2) and β would index the degenerate vectors $|\alpha_1, \alpha_2, \beta\rangle$ for a given pair. For a system initialised in a state with a well-defined (α_1, α_2), the steady state ρ_{ss} is the identity matrix over the corresponding degenerate vectors $|\alpha_1, \alpha_2, \beta\rangle$.

This identity matrix, however, is far from the featureless, uncorrelated state we observed for a U(1) system. The Casimir operator is formed from a summation over non-local operators $S^2 = \sum_{ij} s_i^x s_j^x + s_i^y s_j^y + s_i^z s_j^z$, where $s_i^{x,y,z}$ are the local SU(2) operators. This non-locality, along with the interplay between the three non-commuting generators, has important consequences for ρ_{ss}. Specifically, we can prove that ρ_{ss} will, in general, possess finite, distance-invariant correlations.

For simplicity, we will consider a system composed of a finite, even, number L of spin $s = 1/2$s and then describe how our arguments extend to the thermodynamic limit and apply to other species of particles. First, we observe that $S^z = \sum_i \sigma_i^z$ has $L + 1$ distinct eigenvalues which are $-L, -L + 2, ..., L - 2, L$. The index α_1 will run over these eigenvalues. For a given α_1 the magnetisation of the system is fixed and so, without loss of generality, we can let $S^2 \to (S^x)^2 + (S^y)^2$ and remove the dependency on S^z. The SU(2) commutation relations in Eq. (2.12) can be used to show that the distinct eigenvalues of S^2 for a given α_1 are of the form $4\alpha_2(\alpha_2 + 1) - \alpha_1^2$ where the index α_2 runs from $\frac{|\alpha_1|}{2}, \frac{|\alpha_1|}{2} + 1, ..., \frac{L}{2}$.

For any α_1 and α_2 we can always decompose the Casimir operator into diagonal and off-diagonal parts via

$$S^2 = 2L + \sum_{\substack{i,j=1 \\ i \neq j}}^{N} \sigma_i^x \sigma_j^x + \sigma_i^y \sigma_j^y, \tag{2.13}$$

where we have used the fact that the Pauli matrices are idempotent, i.e. $(\sigma_i^\alpha)^2 \equiv 1$ for $\alpha = x, y$ or z. It then follows from Eq. (2.13) that in order for any given state in the space specified by α_1 and α_2, including the identity matrix, to have all its off-diagonal correlations equal to zero we require $\langle S^2 \rangle = 4\alpha_2(\alpha_2 + 1) - \alpha_1^2 = 2L$. Thus only in the space where α_1 and α_2 satisfy

$$\alpha_2 = -\frac{1}{2}\big(-1 + \sqrt{1 + 2L + \alpha_1^2}\big) \tag{2.14}$$

does the identity matrix possess no inter-spin correlations[5].

For a given L there are $\frac{1}{2}L^2 + L + 1$ distinct pairs (α_1, α_2) and we now know, *at most*, L of those pairs correspond to a space where the identity matrix is uncorrelated. Therefore there are extensively more spaces in which the identity matrix is correlated than uncorrelated. Furthermore, as the identity matrix is preserved under a change of basis it follows that if we are in one of these correlated spaces then we cannot transform the corresponding basis into one completely made up of product states. If we could, then we would have a contradiction as the identity matrix would be uncorrelated. This is the fundamental reason that generally, in a given SU(2) subspace, the identity matrix will be correlated — the basis states which span the space cannot all be written as, or transformed into, product states.

Our arguments do not immediately apply to the case $L \to \infty$ as in this limit the off-diagonal correlations can vanish but their summation in Eq. (2.13) can be non-vanishing. Nonetheless, we can see that for large L the ratio of the number of correlated identity matrices to uncorrelated ones grows proportionally to L. This ratio should maintain continuity as $L \to \infty$ and thus there will be infinitely many more correlated spaces than uncorrelated ones in the thermodynamic limit.

Regardless of the value of L, the correlations in these identity matrices are always invariant with distance. This can be seen from the fact that the Casimir operator is unchanged under a permutation of any of the spins and the identity matrix is just a projector to one of the eigenspaces of the Casimir operator, forcing it to inherit this

[5]The solution where $\alpha_2 < 0$ is invalid as S^2 is a positive valued operator.

symmetry. This has also been proven more formally in the Supplemental Material of [31].

To summarize, these results tell us that for an initial state with a given α_1 and α_2 the maximum entropy steady state which forms under SU(2) preserving heating will generally (for the majority of values of α_1 and α_2) have finite, distance-invariant inter-spin correlations. If the initial state has, instead, an overlap with multiple spaces (α_1, α_2) then, via Eq. (2.7), the steady state will just be a correspondingly weighted sum over the identity matrix in the different spaces. The resulting correlations will be non-zero unless the correlations from the different spaces cancel each other out — which is highly unlikely for an arbitrary initial state.

The methodology we have just used can be directly applied to treat the case $s > 1/2$ or for a system of fermions. The SU(2) commutation relations are obeyed regardless of the representation and so the eigenvalues of S^2 can always be written in a form which is quadratic in terms of the indices α_1 and α_2 [29]. For a given α_1 there will therefore be only one specific value of α_2 where the steady state will be uncorrelated[6]. As the number of possible values of α_2 for a given α_1 grows extensively with the system size then the steady state will, typically, possess finite, uniform, correlations.

An immediate candidate system to directly observe the formation of such correlated steady states is the XXZ Hamiltonian in Eq. (2.10) when $\Delta = J$. In this case, however, any physical mechanism such as periodic driving or dephasing, which we would seek to use to achieve the desired heating, will break the SU(2) symmetry if it is non-trivial. As a result we take the $s = 1$ driven Affleck-Lieb-Kennedy-Tasaki (AKLT) model as our first explicit example, reinforcing the fact the arguments we have just made can be extended to any s.

Driven SU(2) Affleck Lieb Kennedy Tasaki Model — The AKLT model describes a chain of interacting, coupled spin-1s. We denote the basis for a single spin as $\{|\uparrow\rangle, |0\rangle, |\downarrow\rangle\}$ and use this to construct the local spin-1 matrices

$$s^x = \frac{1}{\sqrt{2}}\begin{pmatrix} 0 & 1 & 0 \\ 1 & 0 & 1 \\ 0 & 1 & 0 \end{pmatrix}, \quad s^y = \frac{\mathrm{i}}{\sqrt{2}}\begin{pmatrix} 0 & 1 & 0 \\ -1 & 0 & 1 \\ 0 & -1 & 0 \end{pmatrix}, \quad s^z = \begin{pmatrix} 1 & 0 & 0 \\ 0 & 0 & 0 \\ 0 & 0 & -1 \end{pmatrix}, \tag{2.15}$$

which are analogous to the Pauli matrices for a spin-1/2. In fact, they can be proven to be the adjoint representation of the Pauli matrices [30]. The AKLT Hamiltonian

[6]The second root of the quadratic equation will be unphysical as S^2 is always a positive valued operator.

can be written in terms of these operators via

$$H = \sum_{i=1}^{L-1} \beta_1 \vec{S}_i \cdot \vec{S}_{i+1} + \beta_2 \left(\vec{S}_i \cdot \vec{S}_{i+1} \right)^2, \tag{2.16}$$

where L is the number of sites on the chain and $\vec{S}_i = (S_i^x, S_i^y, S_i^z)$ is the vector of spin-1 operators. These spin-1 operators act as the corresponding spin-1 matrix from Eq. (2.15) on the ith spin and as the identity matrix on all other spins.

The AKLT model has a number of interesting properties. Firstly, it is exactly solvable in the sense that its ground state can be constructed analytically. This ground state consists of the neighbouring spins forming 'valence bonds' or singlet states $\frac{1}{\sqrt{2}}(|\uparrow\downarrow\rangle - |\downarrow\uparrow\rangle)$ [32] and admits a very simple Matrix Product State representation of bond-dimension $\chi = 2$ [33]. Additionally, in the case of an open boundary chain the spins at the ends of the chain are missing a valence bond and thus behave partially as free spins which give rise to topological 'edge' states [34]. The model also serves as an example of Haldane's conjecture, which states that integer spin Heisenberg chains have a gapped excitation spectrum whilst half-integer spin chains (such as the XXZ model introduced earlier) do not [35, 36]. These equilibrium properties of the system have made the AKLT model important for understanding the role of transport, valence-bond order and topology in quantum spin systems.

Here, we will focus on the behaviour of the AKLT model as it is driven out of equilibrium. We will drive the system by introducing a periodic time-dependence in the Hamiltonian, setting $\beta_2 \to \beta_2(t)$ and $H \to H(t)$. This driven Hamiltonian has our desired SU(2) symmetry as the global spin-1 SU(2) operators $S^{x,y,x} = \sum_i S_i^{x,y,z}$ satisfy the relations in Eq. (2.12) and each commute with the Hamiltonian in Eq. (2.16) for all values of β_1 and β_2.

In Fig. 2.3 we demonstrate the consequences of this SU(2) symmetry on the dynamics of the system. At time $t = 0$ the system is initialised in the ground state of $H(0)$ and then time-evolved under $H(t)$ with a periodically modulated β_2. We compute the two-point spin-exchange correlations $\langle S_i^+ S_j^- \rangle$, where the local raising and lowering operators are defined as $S_i^{\pm} = \frac{1}{2}(S_i^x \pm iS_i^y)$ and their corresponding global representations are $S^{\pm} = \frac{1}{2}(S^x \pm iS^y)$. Initially, the spin-exchange correlations decay with distance. As the system heats up we observe that these correlations reorganise themselves and become completely uniform with distance. Due to the conservation of $\langle S^+ S^- \rangle = \sum_{ij} \langle S_i^+ S_j^- \rangle$ during the dynamics this results in a significant amplification of the long-range correlations at the expense of the short range, nearest-neighbour correlations.

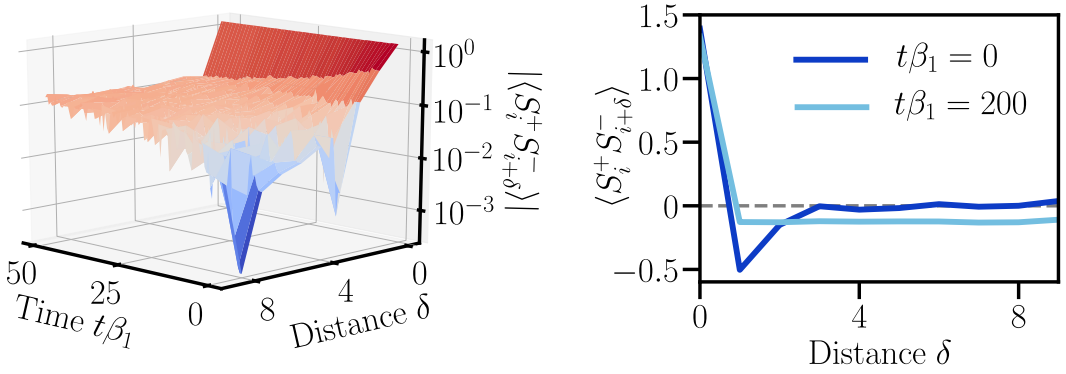

Figure 2.3: Spin-exchange correlations of the $L = 10$ site driven AKLT model described by the Hamiltonian in Eq. (2.16) but with a time-dependent β_2 of the form $\beta_2 = 6\cos(\omega t)\beta_1$ where $\omega\beta_1 = 1$. The system is initialised in the ground state of H with $t = 0$ and then time-evolved under $H(t)$. Left) Magnitude of the spin-exchange correlations $\langle S_i^+ S_{i+\delta}^- \rangle(t)$ versus both time and distance. Right) Spin-Exchange correlations versus distance for both the initial state ($t\beta_1 = 0$) and the long-time ($t\beta_1 = 200$) state under driving.

The results in Fig. 2.3 are a direct consequence of the preservation of the SU(2) symmetry under heating. The system reaches a long-time state which mimics the form in Eq. (2.7) where the eigenstates $|\alpha, \beta\rangle$ are simultaneously those of the Casimir operator S^2 and the magnetisation operator S^z. The steady state has inherited the correlated, translationally invariant nature of these eigenstates. This should be directly contrasted with the example of the driven/dissipative XXZ model, where the sole presence of a U(1) symmetry led to a featureless long-time state.

It is worth mentioning that the formation of such an ordered steady-state under the preservation of an SU(2) symmetry may seem in contrast to the notion that order in Condensed Matter systems is usually associated with a *broken* symmetry. The underlying mechanism — which we will often refer to as 'heating-induced order' — is, however, effectively the dynamical emergence of a uniform, correlated steady state as a result of a *rearrangement* of the available order in the initial state at $t = 0$. There is no spontaneous manifestation of order. Despite this, such a rearrangement can significantly amplify the correlations at certain distances in the system and also ensures they are distance invariant. This has important consequences in the context of superconductivity and synchronisation and, as we will discuss, is relevant for later results and examples in this thesis.

Other Symmetries

This result of heating-induced order is not specific to the presence of an SU(2) symmetry in a many-body system. The group SU(2) is a specific instance of the special unitary group SU(N) which has a fundamental representation of $\mathrm{N}^2 - 1$ Hermitian, traceless N × N matrices or generators $\{\lambda^1, ..., \lambda^{\mathrm{N}^2-1}\}$ which satisfy the SU(N) commutation relations

$$[\lambda^a, \lambda^b] = \sum_{c=1}^{\mathrm{N}^2-1} f_{abc}\lambda^c, \tag{2.17}$$

where f_{abc} are a series of 'structure' constants. For the Pauli Matrices, which form the generators of SU(2), we have $f_{abc} = i\epsilon_{abc}$. In the case of SU(3) the eight, 3×3 'Gell-Mann' matrices form this fundmental representation and are defined as

$$\lambda^1 = \begin{pmatrix} 0 & 1 & 0 \\ 1 & 0 & 0 \\ 0 & 0 & 0 \end{pmatrix}, \quad \lambda^2 = \begin{pmatrix} 0 & -i & 0 \\ i & 0 & 0 \\ 0 & 0 & 0 \end{pmatrix}, \quad \lambda^3 = \begin{pmatrix} 1 & 0 & 0 \\ 0 & -1 & 0 \\ 0 & 0 & 0 \end{pmatrix}, \lambda^4 = \begin{pmatrix} 0 & 0 & 1 \\ 0 & 0 & 0 \\ 1 & 0 & 0 \end{pmatrix},$$
$$\lambda^5 = \begin{pmatrix} 0 & 0 & -i \\ 0 & 0 & 0 \\ i & 0 & 0 \end{pmatrix}, \lambda^6 = \begin{pmatrix} 0 & 0 & 0 \\ 0 & 0 & 1 \\ 0 & 1 & 0 \end{pmatrix}, \lambda^7 = \begin{pmatrix} 0 & 0 & 0 \\ 0 & 0 & -i \\ 0 & i & 0 \end{pmatrix}, \lambda^8 = \frac{1}{\sqrt{3}} \begin{pmatrix} 1 & 0 & 0 \\ 0 & 1 & 0 \\ 0 & 0 & -2 \end{pmatrix}. \tag{2.18}$$

These satisfy the commutation relation in Eq. (2.18) when the appropriate structure constants are used.

The generators for a given N can be used to construct the Casimir operators which commute with each of the generators and are required to form the irreducible representation of the SU(N) symmetry. In the case of SU(3) there are two Casimir operators

$$J_1 = \sum_{a=1}^{8} \lambda_a^2,$$
$$J_2 = \sum_{abc=1}^{8} d_{abc}\lambda_a\lambda_b\lambda_c, \tag{2.19}$$

where the non-zero d_{abc} are

$$d_{118} = d_{228} = d_{338} = -d_{888} = \frac{1}{\sqrt{3}},$$
$$d_{448} = d_{558} = d_{668} = d_{778} = -\frac{1}{2\sqrt{3}},$$
$$d_{146} = d_{157} = -d_{247} = d_{256} = d_{344} = d_{355} = -d_{366} = -d_{377} = \frac{1}{2}. \tag{2.20}$$

More generally, for a given N there are $\mathrm{N}-1$ Casimir operators which are constructed by similar summations and products over the N^2-1 generators. These can be the generators of any representation of the SU(N) symmetry, not just those for the fundamental representation.

We now define an SU(N) symmetric many-body system (with L possible positions/sites) as one whose Hamiltonian commutes with the global SU(N) generators $\lambda^a = \sum_{i=1}^{L} \lambda_i^a$, where λ_i^a is the local (i.e. acting on the ith position) representation of the ath generator. Under SU(N) symmetric heating the steady state will be of the form in Eq. (2.7) where each $|\alpha, \beta\rangle$ is a simultaneous eigenvector of the $2\mathrm{N}-2$ operators which form the irreducible representation of SU(2) symmetry. The first $N-1$ of these operators are the Casimir operators and the remaining $N-1$ operators are the 'diagonal' generators, e.g. λ^3 and λ^8 in Eq. (2.18) for SU(3). The index α in $|\alpha, \beta\rangle$ is then specified by the unique tuple $\alpha = (\alpha_1, ..., \alpha_{2\mathrm{N}-2})$ with α_i being the corresponding eigenvalue for the ith operator — the index β runs over the possible degeneracy for a given α.

For an initial state with a fixed α the steady state which forms under SU(N) symmetric heating is the identity matrix over the D_α states $|\alpha, \beta\rangle$. We proved for SU(2) that, generally, this identity matrix is correlated and not featureless. It is natural to anticipate that this result should hold for $\mathrm{N} > 2$ given the non-local correlated structure of the corresponding Casimir operators and the fact they obey similar commutation relations. Moreover, the correlations in such a state will always be invariant with distance as the SU(N) Casimir operators are unchanged under a permutation of any pair of bodies for all $\mathrm{N} \geq 2$.

There a number of examples of many-body quantum systems which possess SU(N) symmetries with $\mathrm{N} > 2$. These are often exploratory models whose Hamiltonians are constructed to be SU(N) symmetric, as opposed to having any physical motivation. For example, extensions of the AKLT model and other SU(2) spin chains to SU(N) symmetric versions have been considered [37, 38, 39, 40, 41, 42]. Alongside this, SU(N) versions of the Hubbard model have been introduced which involve N different 'flavours' of fermions [43, 44]. Despite the 'toy' nature of these models, optical lattices provide a highly-tunable experimental playground in which such models can be, and already have been, realised by trapping multi-component fermionic and bosonic gases [45, 46, 47].

Although common, SU(N) and U(1) symmetries are not the only type of symmetries present in quantum systems. A full list or treatment of these symmetries is beyond the scope of this thesis. Nonetheless, we emphasize that for any symmetry

operator O in a many-body system, if the eigenvectors for a given eigenvalue of O cannot be written as, or transformed into via a unitary operator, a set of local product states then the maximum entropy state should not be expected to be a featureless state containing no inter-body correlations. Additionally, many symmetry groups are closely related to each other. The SO(N) symmetry group, the special orthogonal group which describes rotations in N dimensional space, is in certain cases isomorphic to the special unitary group. For instance, SU(4) and SO(6) are isomorphic [48] and the Hubbard model, which we will study at length in the next chapter, has two SU(2) symmetries whose product is isomorphic with SO(4) [49].

2.3 Conclusion

In this chapter we have introduced the concept of symmetries in both closed and open quantum systems, discussing the impact that they can have on their equilibrium and non-equilibrium properties. We then used this understanding to write down the steady state of quantum systems under continuous heating in terms of the irreducible representation of their symmetries. By comparing two different symmetries, U(1) and SU(2), we observed how the type of symmetry strongly effects the steady state properties.

Specifically, in the U(1) case, we detailed how the local nature of the corresponding symmetry operator meant the steady state could be written as the identity matrix over a series of product states. This ensures the absence of spatial correlations in the steady state of any U(1) symmetric many-body system under heating. We presented an example in the form of the XXZ chain. Meanwhile, in contrast to this, we proved, for a series of qubits, that the maximum entropy steady state which forms under SU(2) symmetric heating will generally possess finite, distance-invariant spatial correlations. We detailed how the same arguments can be extended to a series of spin $s > \frac{1}{2}$ particles or for a fermionic system and then presented an explicit example in the form of a spin-1 AKLT chain, observing the formation of these distance-invariant correlations under heating.

The presence of uniform, distance-invariant correlations (also known as off-diagonal long-range order - ODLRO) in quantum states underpins a number of phenomena such as superconductivity in fermionic systems and superfluidity in bosonic systems [50, 51, 52, 53]. The physical implications of the results from this chapter are thus significant. In the next chapters we will explore some of these implications in the context of the paradigmatic Hubbard model which has a rich symmetry structure and

is physically relevant for the modelling of strongly-correlated materials and high-T_c superconductivity.

References

[1] E. Noether, "Invariante variationsprobleme (Invariant variation problems)," *Nachr. d. König Gesellsch. d. Wiss. zu Göttingen, Math-phys. Klasse*, pp. 235–257, 1918.

[2] L. S. Levitov, B. D. Simons, and L. V. Butov, "Pattern formation as a signature of quantum degeneracy in a cold exciton system," *Phys. Rev. Lett.*, vol. 94, p. 176404, 2005.

[3] P. Calabrese, F. H. L. Essler, and G. Mussardo, "Introduction to 'quantum integrability in out of equilibrium systems'," *J. Stat. Mech.: Theory Exp*, vol. 2016, p. 064001, jun 2016.

[4] A. Doijou, S. Evangelisti, G. Feverati, and N. Karaiskos, "Introduction to quantum integrability," *Int. J. Mod. Phys. A*, vol. 25, pp. 3307–3351, 2010.

[5] J.-S. Caux and J. Mossel, "Remarks on the notion of quantum integrability," *J. Stat. Mech.: Theory Exp.*, vol. 2011, p. P02023, 2011.

[6] J. A. Scaramazza, B. S. Shastry, and E. A. Yuzbashyan, "Integrable matrix theory: level statistics," *Phys. Rev. E*, vol. 94, p. 032106, 2016.

[7] Z. Cheng and J. L. Lebowitz, "Statistics of energy levels in integrable quantum systems," *Phys. Rev. A*, vol. 44, pp. 1350–1353, 1991.

[8] M. Karbach, G. Müller, H. Gould, and J. Tobochnik, "Introduction to the Bethe ansatz part 1," *Comput. Phys.*, vol. 11, pp. 36–43, 1997.

[9] A. A. Zvyagin, "Bethe ansatz solvable multi-chain quantum systems," *J. Phys. A: Math. Gen.*, vol. 34, pp. R21–R53, 2001.

[10] M. Ogata and H. Shiba, "Bethe-ansatz wave function, momentum distribution, and spin correlation in the one-dimensional strongly correlated Hubbard model," *Phys. Rev. B*, vol. 41, pp. 2326–2338, 1990.

[11] L. Vidmar and M. Rigol, "Generalized Gibbs ensemble in integrable lattice models," *J. Stat. Mech.: Theory Exp.*, vol. 2016, p. 064007, 2016.

[12] M. Rigol, V. Dunjko, V. Yurovsky, and M. Olshanii, "Relaxation in a completely integrable many-body quantum system: An ab initio study of the dynamics of the highly excited states of 1D lattice hard-core bosons," *Phys. Rev. Lett.*, vol. 98, p. 050405, 2007.

[13] M. Rigol, A. Muramatsu, and M. Olshanii, "Hard-core bosons on optical superlattices: Dynamics and relaxation in the superfluid and insulating regimes," *Phys. Rev. A*, vol. 74, p. 053616, 2006.

[14] B. Buča and T. Prosen, "A note on symmetry reductions of the Lindblad equation: Transport in constrained open spin chains," *New J. Phys.*, vol. 14, p. 073007, 2012.

[15] Z. Zhang, J. Tindall, J. Mur-Petit, D. Jaksch, and B. Buča, "Stationary state degeneracy of open quantum systems with non-Abelian symmetries," *J. Phys. A: Math. Theor.*, vol. 53, p. 215304, 2020.

[16] J. Thingna, D. Manzano, and J. Cao, "Dynamical signatures of molecular symmetries in nonequilibrium quantum transport," *Sci. Rep.*, vol. 6, p. 28027, 2016.

[17] G. Benenti, G. Casati, T. Prosen, D. Rossini, and M. Žnidarič, "Charge and spin transport in strongly correlated one-dimensional quantum systems driven far from equilibrium," *Phys. Rev. B*, vol. 80, p. 035110, 2009.

[18] M. Žnidarič, "Spin transport in a one-dimensional anisotropic Heisenberg model," *Phys. Rev. Lett.*, vol. 106, p. 220601, 2011.

[19] L. D'Alessio and M. Rigol, "Long-time behavior of isolated periodically driven interacting lattice systems," *Phys. Rev. X*, vol. 4, p. 041048, 2014.

[20] P. Ponte, A. Chandran, Z. Papić, and D. A. Abanin, "Periodically driven ergodic and many-body localized quantum systems," *Ann. Phys.*, vol. 353, pp. 196–204, 2015.
[21] A. Lazarides, A. Das, and R. Moessner, "Equilibrium states of generic quantum systems subject to periodic driving," *Phys. Rev. E*, vol. 90, p. 012110, 2014.
[22] P. Woit, *Quantum Theory, Groups and Representations: An Introduction*. Springer International Publishing, New York, 2017.
[23] R. I. Nepomechie, "Functional relations and Bethe ansatz for the XXZ chain," *J. Stat. Phys.*, vol. 111, pp. 1363–1376, 2003.
[24] O. Babelon, H. de Vega, and C. Viallet, "Analysis of the Bethe ansatz equations of the XXZ model," *Nucl. Phys. B*, vol. 220, pp. 13–34, 1983.
[25] A. N. Kirillov and N. Y. Reshetikhin, "Exact solution of the Heisenberg XXZ model of spin s," *J. Sov. Math.*, vol. 35, pp. 2627–2643, 1986.
[26] R. Yue and T. Deguchi, "Analytic Bethe ansatz for 1D Hubbard model and twisted coupled XY model," *J. Phys. A: Math. Gen.*, vol. 30, pp. 849–865, 1997.
[27] B. Buca, C. Booker, M. Medenjak, and D. Jaksch, "Dissipative Bethe ansatz: Exact solutions of quantum many-body dynamics under loss," *arXiv Preprint: cond-mat.stat-mech/2004.05955*, 2020.
[28] S. R. White, "Density matrix formulation for quantum renormalization groups," *Phys. Rev. Lett.*, vol. 69, pp. 2863–2866, 1992.
[29] Y. Kosmann-Schwarzbach and S. Singer, *Groups and Symmetries: From Finite Groups to Lie Groups*. Springer New York, New York, 2009.
[30] B. Hall, *Lie Groups, Lie Algebras, and Representations: An Elementary Introduction*. Graduate Texts in Mathematics, Springer International Publishing, New York, 2015.
[31] J. Tindall, B. Buča, J. R. Coulthard, and D. Jaksch, "Heating-induced long-range η pairing in the Hubbard model," *Phys. Rev. Lett.*, vol. 123, p. 030603, 2019.
[32] I. Affleck, T. Kennedy, E. H. Lieb, and H. Tasaki, "Rigorous results on valence-bond ground states in antiferromagnets," *Phys. Rev. Lett.*, vol. 59, pp. 799–802, 1987.
[33] U. Schollwöck, "The density-matrix renormalization group in the age of matrix product states," *Ann. Phys.*, vol. 326, pp. 96–192, 2011.
[34] M. Hagiwara, K. Katsumata, I. Affleck, B. I. Halperin, and J. P. Renard, "Observation of S=1/2 degrees of freedom in an S=1 linear-chain Heisenberg antiferromagnet," *Phys. Rev. Lett.*, vol. 65, pp. 3181–3184, 1990.
[35] F. D. M. Haldane, "Nonlinear field theory of large-spin Heisenberg antiferromagnets: Semiclassically quantized solitons of the one-dimensional easy-axis Néel state," *Phys. Rev. Lett.*, vol. 50, pp. 1153–1156, 1983.
[36] L.-H. Pan and C.-D. Gong, "A note on Haldane's conjecture," *J. Phys. Condens. Matter*, vol. 20, p. 215232, 2008.
[37] S. Gozel, D. Poilblanc, I. Affleck, and F. Mila, "Novel families of SU(N) AKLT states with arbitrary self-conjugate edge states," *Nucl. Phys. B*, vol. 945, p. 114663, 2019.
[38] T. Morimoto, H. Ueda, T. Momoi, and A. Furusaki, "$\mathcal{F}_3$ symmetry-protected topological phases in the SU(3) AKLT model," *Phys. Rev. B*, vol. 90, p. 235111, 2014.
[39] S. Rachel, R. Thomale, M. Führinger, P. Schmitteckert, and M. Greiter, "Spinon confinement and the Haldane gap in SU(N) spin chains," *Phys. Rev. B*, vol. 80, p. 180420, 2009.
[40] Y. Y. Kiselev, S. A. Parameswaran, and D. P. Arovas, "Order and disorder in SU(N) simplex solid antiferromagnets," *J. Stat. Mech.: Theory Exp.*, vol. 2016, p. 013105, 2016.

[41] R. K. Kaul, "Quantum criticality in SU(3) and SU(4) antiferromagnets," *Phys. Rev. B*, vol. 84, p. 054407, 2011.
[42] R. Bondesan and T. Quella, "Infinite matrix product states for long-range SU(N) spin models," *Nucl. Phys. B*, vol. 886, pp. 483–523, 2014.
[43] W. Nie, D. Zhang, and W. Zhang, "Ferromagnetic ground state of the SU(3) Hubbard model on the Lieb lattice," *Phys. Rev. A*, vol. 96, p. 053616, 2017.
[44] B. Hou, D. Peng, and R. Yue, "The exact solution of the SU(3) Hubbard model," *Nucl. Phys. B*, vol. 575, pp. 561–578, 2000.
[45] U. Bornheimer, C. Miniatura, and B. Grémaud, "SU(3) topological insulators in the honeycomb lattice," *Phys. Rev. A*, vol. 98, p. 043614, 2018.
[46] C. Honerkamp and W. Hofstetter, "Ultracold fermions and the SU(N) Hubbard model," *Phys. Rev. Lett.*, vol. 92, p. 170403, 2004.
[47] P. Azaria, S. Capponi, and P. Lecheminant, "Three-component Fermi gas in a one-dimensional optical lattice," *Phys. Rev. A*, vol. 80, p. 041604, 2009.
[48] K. J. Barnes, J. Hamilton-Charlton, and T. R. Lawrence, "How orbits of SU(N)) can describe rotations in SO(6)," *J. Phys. A: Math. Gen.*, vol. 34, pp. 10881–10900, 2001.
[49] F. Kazuyuki, O. Hiroshi, and S. Tatsuo, "More on the isomorphism SU(2) x SU(2) = SO(4)," *Int. J. Geom. Methods Mod. Phys.*, vol. 4, pp. 471–485, 2011.
[50] C. N. Yang, "Concept of off-diagonal long-range order and the quantum phases of liquid He and of superconductors," *Rev. Mod. Phys.*, vol. 34, pp. 694–704, 1962.
[51] O. Penrose and L. Onsager, "Bose-Einstein condensation and liquid helium," *Phys. Rev.*, vol. 104, pp. 576–584, 1956.
[52] C. N. Yang, "η pairing and off-diagonal long-range order in a Hubbard model," *Phys. Rev. Lett.*, vol. 63, pp. 2144–2147, 1989.
[53] G. L. Sewell, "Off-diagonal long-range order and the Meissner effect," *J. Stat. Phys.*, vol. 61, pp. 415–422, 1990.

Chapter 3

The Correlated Steady States of the Hubbard Model

A number of the results in this chapter were first published as

- B. Buča, J. Tindall, and D. Jaksch *Non-stationary coherent quantum many body dynamics through dissipation*, Nature Communications, **10** (2019)
- J. Tindall, B. Buča, J. R. Coulthard and D. Jaksch, *Heating-Induced Long-Range η-Pairing in the Hubbard Model*, Phys. Rev. Lett, **123** (2019)
- J. Tindall, F. Schlawin, M. Sentef and D. Jaksch, Analytical Solution for the Steady States of the Driven Hubbard model, Physical Review B **103**, (2021).

Contributions to these papers from JT are listed in the introduction.

In this chapter we begin by introducing the fermionic Hubbard model, describing its origin and relevance as a physical description of solid-state electronic behaviour. We then detail the symmetries of the model, discussing their dependence on the lattice structure and how they influence the equilibrium and non-equilibrium properties of the system. Following this, we perform a simultaneous diagonalisation of the model's two possible SU(2) symmetries and analytically construct the different maximum entropy steady states which form upon heating the system. These states possess finite, uniform long-range correlations in the symmetry sectors which are preserved by the heating and, through our methodology, we quantify these correlations for a wide range of lattice structures, fillings, Hamiltonian parameters and initial states.

We end the chapter by detailing how the experimental setup necessary for observing such correlated states could be realised with current technology in both quantum material and optical lattice systems. The desired heating can be induced by either coherent periodic driving or coupling with an external environment.

3.1 Introduction to the Hubbard Model

The Hubbard Hamiltonian

The Hubbard model is a simplified description of electronic behaviour in solid-state systems. Generally, quantum materials are incredibly complicated to describe, with a number of competing degrees of freedom and electronic bands present. The Hubbard model, which was introduced by J. Hubbard in 1963 [1], provides a simplified single-band description on a discrete lattice structure. In this model there are only two competing terms in the Hamiltonian — a kinetic term describing the tunnelling of particles between lattice sites and an on-site interaction term.

This discretised Hamiltonian can be derived from a continuum description of electrons moving in the potential formed from a static ionic lattice [2], with the minima of the potential landscape forming the lattice sites in the Hamiltonian. A number of assumptions are necessary in this derivation:

- All the energy bands are sufficiently separated so that they do not overlap and the Fermi surface lies within a single one of these bands. We can then project the Hamiltonian onto this band.
- The electron-electron interactions are sufficiently screened by the ionic potential so that only local interactions need to be retained.
- The electrons are *tightly-bound*, i.e. they are strongly localised to their respective ionic cores. This leads to the electronic hopping processes being dominated by nearest-neighbour tunnelling.

Following these assumptions leads to the second-quantised Hubbard Hamiltonian

$$H = -J \sum_{\langle ij \rangle} \sum_{\sigma \in \{\uparrow,\downarrow\}} c^{\dagger}_{\sigma,i} c_{\sigma,j} + \text{H.c.} + U \sum_{i} n_{\uparrow,i} n_{\downarrow,i}, \tag{3.1}$$

where the first term is the hopping term between neighbouring sites $\langle ij \rangle$, with strength J and the second is the on-site interaction term between fermions of opposite spin with strength U. The operators $c^{\dagger}_{\sigma,i}$, $c_{\sigma,i}$ are the creation and annihilation operators for a fermion of spin $\sigma \in \{\uparrow,\downarrow\}$ on site i which obey the anti-commutation relations

$$\{c_{\sigma,i}, c^{\dagger}_{\sigma',j}\} = \delta_{\sigma,\sigma'}\delta_{i,j}, \quad \{c^{\dagger}_{\sigma,i}, c^{\dagger}_{\sigma',j}\} = \{c_{\sigma,i}, c_{\sigma',j}\} = 0, \tag{3.2}$$

and can be used to form the number operator $n_{\sigma,i} = c^{\dagger}_{\sigma,i} c_{\sigma,i}$ for a fermion of spin σ on site i. In Fig. 3.1 we picture the Hamiltonian and the action of the kinetic and interaction terms.

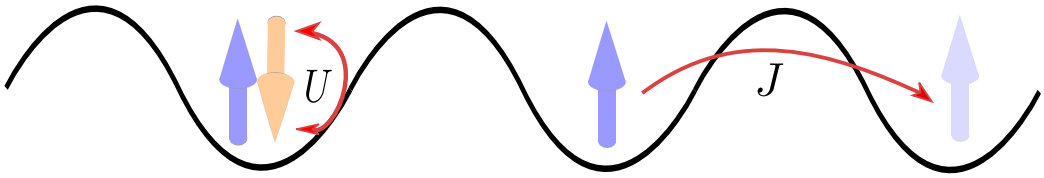

Figure 3.1: Schematic of the Hubbard Model on a 1D chain. The fermions, of which there are two species (spin up and spin down), reside in a lattice structure generated by the minima of a potential energy landscape. The fermions can hop to neighbouring sites with an energy J, whilst fermions of opposite spin on the same site interact with an energy U.

Despite its simplicity, the equilibrium properties of the Hubbard Hamiltonian are very rich and strongly dependent on a number of factors such as the lattice structure, the fermionic density, the temperature and the Hamiltonian parameters. In a hypercubic lattice at zero temperature, half-filling and positive U the ground state is typically anti-ferromagnetic and insulating, with the electrons highly localised and having opposite spin to their neighbours. With increasing temperature the system will become more metallic, whilst changes in the electron filling or sign of U can stabilise various superconducting, fermi-liquid or superfluid phases [3, 4, 5]. Meanwhile, for different geometries, the equilibrium landscape can vary drastically and in triangular lattice structures various exotic magnetically ordered phases emerge which are not stable in hypercubic realisations of the Hubbard model [6, 7].

Due to the many-body complexity of the Hamiltonian H, an analytical solution has only been obtained for the case of a 1D chain [8] and a number of open questions on the different phases, and the inter-phase transitions, of the model remain. Nonetheless, the Hubbard model has found significant success as a description of solid-state electronic behaviour. For example, various analytical and numerical methods on an infinite dimensional Hubbard lattice have successfully captured the metal-insulator transition [9, 10, 11] which commonly occurs in three-dimensional oxides [12, 13]. More generally, there are a number of materials, such as Sr_2CuO_3 [14, 15, 16], $TMTSF_2$ salts [17] and high-T_c superconducting cuprates [18, 19], whose electronic properties are considered to be described by 'Hubbard-like' models — i.e. features of their electronic behaviour can be captured by the Hubbard Hamiltonian, or extensions thereof[1].

The Hubbard model has also attracted attention due to advances in the field of ultracold atoms. Optical lattices provide a highly tunable playground in which various

[1]For example by including longer-range interactions or additional bands/ orbitals.

quantum Hamiltonians can be accurately realised and manipulated. The Hubbard model is no exception and a number of experiments have accurately realised the Hamiltonian by loading a cold gas of fermionic atoms into a lattice potential generated through the interference pattern of standing-wave laser beams [3, 20, 21]. These experiments provide a controlled environment in which the physics of this Hamiltonian, such as the Mott-insulating phase for low temperature and finite U, can be observed [22, 23]. Furthermore, the continued advancement of laser technology has meant that the tools available for controlling and making measurements in these environments is ever expanding — allowing more complicated experiments to be undertaken. The non-equilibrium response of the system when exposed to coherent driving or an external bath is such an experiment and in the last decade this type of setup has attracted a significant amount of attention from researchers working on strongly correlated systems.

In the dissipative case, a number of theoretical works have shown how the influence of an environment can be used to control the flow of transport in a system [24] or induce the formation of desirable, correlated steady states [25, 26, 27]. In the context of the Hubbard model, examples of the latter include using non-local jump operators to guide the system towards pure, superconducting eigenstates of the Hamiltonian [28, 29] or controlling and inducing magnetic correlations with two body loss [30]. These proposals all rely on coupling the system to very carefully engineered Markovian environments. Whilst this is typically not possible in a quantum material, in optical lattice setups the high degree of control available means it is much easier to induce or suppress various system-environment couplings — with a recent experiment realising a 1D Hubbard chain with Markovian particle loss [31].

Meanwhile, in the case of driven Hubbard systems, theoretical investigations are even more numerous. By subjecting the system to a carefully-tuned periodic field the effective Hamiltonian can be modified to one which transiently favours various different pairing mechanisms, or is able to control competing types of order [32, 33, 34, 35, 36, 37, 38, 39]. These studies are motivated by the opportunities that arise from having dynamical time-dependent Hubbard Hamiltonians, which have been realised experimentally in optical lattice setups via modulation of the standing wave interference pattern [40] and in strongly-correlated materials by exposing them to intense mid-infrared laser pulses [41, 42, 43, 44].

The features induced by the effective Hamiltonian in these driven systems are, however, in competition with the energy absorbed from the driving field [45, 46]. This

absorption of energy will inevitably dominate the long-time dynamics and, in the absence of certain symmetries, realise a featureless infinite temperature state. This puts constraints on the time-scales and parameter regimes available in the aforementioned setups, as care needs to be taken to ensure the heating rate is minimal and the desired features observable on some intermediate time-scale.

Here we will show that these precautions, or the aforementioned engineering of specific system-environment couplings in dissipative setups, are not necessary for realising ordered states in the Hubbard model. The rich symmetry structure of the model means it is a perfect environment for observing the mechanism of heating-induced order introduced in the previous chapter — with robust, correlated long-time states realisable for a range of different dissipative and driving setups. The only requirement for this mechanism to occur is that heat is supplied to the system whilst preserving the requisite symmetries.

Symmetries of the Hubbard Model

We will start by detailing the symmetry structure of the Hubbard Hamiltonian. In order to be as general as possible we define the Hamiltonian over an arbitrary connected[2] graph $\mathcal{G} = \mathcal{G}(V, E)$ where the vertices V correspond to the lattice sites and the edges E are the nearest-neighbour bonds. We also define L as the total number of vertices and for simplicity assume it is even. The Hubbard Hamiltonian over this arbitrary lattice[3] is then

$$H = -J \sum_{V,V' \in E} \sum_{\sigma} (c^{\dagger}_{\sigma,V} c_{\sigma,V'} + \text{H.c}) + U \sum_{V} n_{\uparrow,V} n_{\downarrow,V}, \tag{3.3}$$

with the first summation running over all the edges in the graph and kinetically coupling the two vertices V, V' on that edge. The second summation represents an on-site interaction term and runs over all the vertices of the graph. We depict this Hamiltonian and some example graphs that we will use for our subsequent numerics in Fig. 3.2.

We can introduce the first SU(2) symmetry of this Hamiltonian via the global

[2] i.e. it is possible to get from any vertex to any another via the edges of the graph, which represent the electron hopping.

[3] Although mathematically distinct we will abuse terminology and use 'graph' and 'lattice' interchangeable here, with both terms referring to the collection of sites and inter-site/ nearest-neighbour bonds which define the geometry of the system.

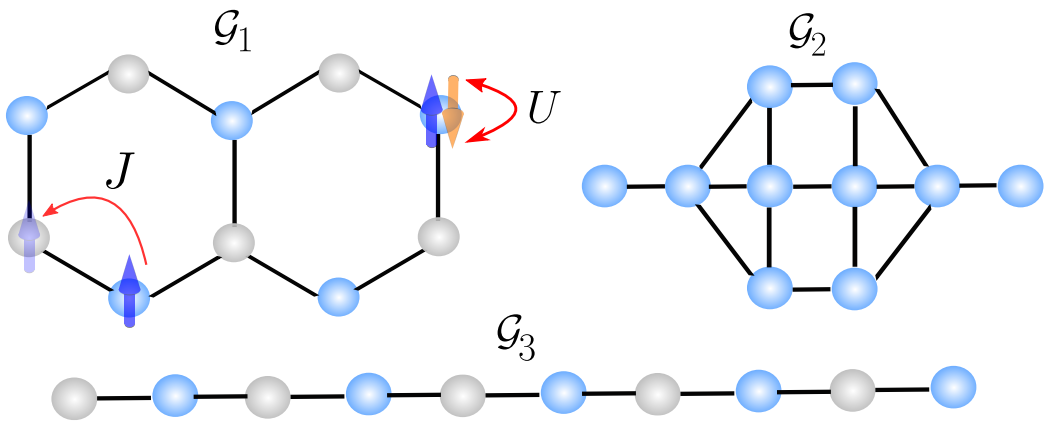

Figure 3.2: Fermionic Hubbard model on a graph $\mathcal{G} = \mathcal{G}(V, E)$ where V are the vertices, indicated by the circles and E are the black edges which connect the vertices. The L vertices form the lattice sites on which the fermions reside and interact with strength U whilst the edges form the nearest-neighbour bonds over which the fermions can hop with constant amplitude J. The three graphs $\mathcal{G}_1$, $\mathcal{G}_2$ and $\mathcal{G}_3$ are those we use in our numerics and the blue vs grey sites represent a bi-partite splitting for graphs $\mathcal{G}_1$ and $\mathcal{G}_3$.

representations of the 'spin' number, raising and lowering operators

$$S^z = \sum_V s^z_V = \sum_V (n_{\uparrow,V} - n_{\downarrow,V}),$$
$$S^+ = \sum_V s^+_V = \sum_V c^\dagger_{V,\uparrow} c_{V,\downarrow}, \qquad S^- = \sum_V s^-_V = \sum_V c^\dagger_{V,\downarrow} c_{V,\uparrow}. \tag{3.4}$$

These operators act on singlons (single fermions occupying a given lattice site, $\sigma \in \{\uparrow, \downarrow\}$) and obey the SU(2) commutation relations introduced in the previous chapter. Through the relations in Eq. (3.2), these operators can be shown to commute with H $\forall \mathcal{G}$, meaning the Hamiltonian has a permanent spin SU(2) symmetry when defined over any lattice. The operator S^z represents the total magnetisation of the system (i.e. the difference between the total number of 'up' fermions and 'down' fermions), which is conserved by $H_\mathcal{G}$ as part of the spin SU(2) symmetry.

We can also introduce a second, possible, SU(2) symmetry via the global representation of the η number, raising and lowering operators

$$\eta^z = \sum_V \eta^z_V = \sum_V (n_{\uparrow,V} + n_{\downarrow,V} - 1),$$
$$\eta^+ = \sum_V \eta^+_V = \sum_V f(V) c^\dagger_{V,\uparrow} c^\dagger_{V,\downarrow}, \qquad \eta^- = \sum_V \eta^-_V = \sum_V f(V) c_{V,\downarrow} c_{V,\uparrow}, \tag{3.5}$$

where $f(V)$ is a real-valued function whose domain is the vertices of the graph. These operators act on doublons and holons (locally paired fermions and empty

sites, $\sigma \in \{\uparrow\downarrow, \text{vac}\}$) within the lattice and commute with the spin SU(2) operators: $[\eta^{\pm,z}, S^{\pm,z}] = 0$. We can show that $[H_{\mathcal{G}}, \eta^z] = 0\ \forall \mathcal{G}$ and so η^z, which effectively constitutes the total particle number, is also a permanent symmetry for all lattice structures. Combined with the S^z symmetry this tells us that the Hubbard Hamiltonian independently conserves the number of $\uparrow$ fermions ($N_\uparrow = \sum_V n_{\uparrow,V}$) and $\downarrow$ fermions ($N_\downarrow = \sum_V n_{\downarrow,V}$).

The relationship between $H_{\mathcal{G}}$ and $\eta^\pm$ is, however, more complicated and depends on whether $\mathcal{G}$ is bi-partite or not. If $\mathcal{G}$ is bi-partite then, by definition, the vertices V can be split into two sets and the edges of the graph only connect vertices in different sets and none of the vertices in the same set. In this bi-partite case we set $f(V) = \pm 1$ depending on whether V is in the first or second set, which results in

$$[H, \eta^\pm] = \pm U \eta^\pm \implies [H - UN/2, \eta^\pm] = 0, \tag{3.6}$$

where $N = N_\uparrow + N_\downarrow$ is the total number operator. As N is conserved by the Hamiltonian then, for a fixed total particle number, $-UN/2$ is just a constant term which has a trivial effect on the eigenspectrum of H. Consequently, we can say that if $\mathcal{G}$ is bi-partite then H has an η SU(2) symmetry alongside its spin SU(2) symmetry and is thus SU(2) $\times$ SU(2) symmetric. If, instead, $\mathcal{G}$ is not bi-partite then the η SU(2) symmetry is broken and only the spin SU(2) symmetry and the U(1) symmetry in η^z are present, i.e. the system is U(1) $\times$ SU(2) symmetric.

Interestingly, there are certain triangular lattice structures where an η SU(2) symmetry can still be identified despite the lattice not being bi-partite [47] . This, however, requires the hopping integral J to be inhomogeneous and complex, with different phases on different edges of the lattice. In this thesis we always focus on a real valued hopping integral.

The spin and η SU(2) symmetries play an important role in the physics of the Hubbard model. The η symmetry was first identified by C. N. Yang in Ref. [48] and there it was noted that the η raising operator can be used to construct various excited eigenstates of the Hubbard Hamiltonian which have uniform off-diagonal long-range particle-hole order (ODLRO) and are superconducting [49, 50]. These states can be built via repeated application of η^+ to the vacuum state, for example $|\psi\rangle \propto (\eta^+)^{L/2} |\text{vac}\rangle$ is such a state and, for any given L, has $\langle \eta_V^+ \eta_{V'}^- \rangle$ constant and non-zero for all $V \neq V'$. Additionally, both symmetries play a fundamental role in the Bethe ansatz solution for the 1D Hubbard chain which provides algebraic expressions for the eigenstates and eigenspectrum of the Hamiltonian [8].

In the following section, we will use these symmetries extensively and exploit them to write down the various maximum entropy states of the Hubbard model which form under heating. By the same arguments from the previous chapter, these states will be capable of hosting finite off-diagonal order.

3.2 Constructing the Correlated Steady States

Building a Complete SU(2) × SU(2) Basis

In order to construct these states we will form a complete basis in which the irreducible representations of the spin and η SU(2) symmetries on an arbitrary graph with fixed values of $N_\uparrow$ and $N_\downarrow$ are diagonal. The full basis for any particle number can then be trivially identified through a direct sum of the different bases for the range of possible values of $N_\uparrow$ and $N_\downarrow$. In order to simplify some of the equations that follow we define the quantities $\alpha = (L - N)/2$ and $\beta = (N_\uparrow - N_\downarrow)/2$, alongside assuming that L, $N_\uparrow$ and $N_\downarrow$ are even so that α and β are both integers.

The two commuting SU(2) Casimir operators $\eta^2 = \eta^+\eta^- + \eta^-\eta^+ + (\eta^z)^2$ and $S^2 = S^+S^- + S^-S^+ + (S^z)^2$, and the corresponding z operators η^z and S^z, form the representation that we wish to diagonalise. As we have fixed the particle numbers we have already removed the dependency on the 'z' operators and can focus on identifying states which simultaneously diagonalise $\eta^+\eta^- + \eta^-\eta^+$ and $S^+S^- + S^-S^+$. We note, however, that for fixed values of $N_\uparrow$ and $N_\downarrow$ any eigenvector of O^+O^- is also an eigenvector of O^-O^+ where O can be either η or S. Hence, we can reduce the problem to identifying a basis which simultaneously diagonalises S^+S^- and $\eta^+\eta^-$ for given particle numbers.

Our next step is to notice that these two operators both commute with the total doublon operator $N_d = \sum_V n_{\uparrow,V} n_{\downarrow,V}$ and thus we can simultaneously reduce them into block matrices with the blocks indexed by i, the number of doublons on the graph, which can range from $\mathrm{Max}(0, -2\alpha)$ to $\mathrm{Min}(N_\uparrow, N_\downarrow)$. For a given value of i, we observe that there must be $L + i - N$ holons in the graph and so the remaining vertices, or sites, will be occupied by $N_\uparrow - i$ and $N_\downarrow - i$ singlons of spin $\uparrow$ and $\downarrow$ respectively.

We then arrange the sites of our lattice into two sets, with the first set (A) containing $L + 2i - N$ sites and the second set (B) containing the remaining $N - 2i$ sites. There are $\binom{L}{N-2i}$ different ways in which the sites can be arranged in this manner and in A we place all of the doublons and holons whilst in B we place all of the singlons.

If the operator $S^+_V S^-_{V'}$ ($\eta^+_V \eta^-_{V'}$) acts on a vertex which is in set A (B) then it will immediately annihilate any given state and thus we can let

$$\eta^+\eta^- \to (\eta^+\eta^-)' = \sum_{V,V'\in A} \eta^+_V \eta^-_{V'}, \qquad S^+S^- \to (S^+S^-)' = \sum_{V,V'\in B} S^+_V S^-_{V'}, \tag{3.7}$$

and ignore the other terms in these two operators. If we can now construct a state $|\eta\rangle$, within A, which is an eigenvector of $(\eta^+\eta^-)'$ with eigenvalue λ_η and a state $|S\rangle$ within B which is an eigenvector of $(S^+S^-)'$ with eigenvalue λ_S then their tensor product $|\eta\rangle \tilde{\otimes} |S\rangle$ [4] will simultaneously be an eigenvector of both $\eta^+\eta^-$ and S^+S^-, with respective eigenvalues λ_η and λ_S, on the full graph $\mathcal{G}$.

We now need to determine the eigenspectrum of $(\eta^+\eta^-)'$ and $(S^+S^-)'$. Crucially, we know that $(\eta^+\eta^-)'$ and $(S^+S^-)'$ correspond to the SU(2) Casimir operators in a, respectively, $L + 2i - N$ and $N - 2i$ fold tensor product representation of the fundamental representation of SU(2) [51, 52]. By exploiting the ladder-like structure of SU(2) representations we can determine the eigenvalues of $(\eta^+\eta^-)'$ and $(S^+S^-)'$ as

$$\begin{aligned} \lambda_\eta(k) &= k(k+1) - \alpha(\alpha+1), \qquad k = |\alpha|, |\alpha|+1, ...\alpha + i, \\ \lambda_S(m) &= m(m+1) - \beta(\beta+1), \qquad m = |\beta|, |\beta|+1, ..., N/2 - i. \end{aligned} \tag{3.8}$$

These eigenvalues have the following degeneracies

$$\begin{aligned} D_\eta(k,i) &= C(\alpha + i + k, \alpha + i - k - \delta_k), \\ D_s(m,i) &= C(N/2 - i + m, N/2 - i - m - \delta_m), \end{aligned} \tag{3.9}$$

where the function $C(x,y)$ corresponds to the Catalan Triangle Number [53]

$$C^x_y = \begin{cases} \frac{(x+y)!(x-y+1)}{y!(x+1)!} & x, y > 0, \\ 1 & \text{Otherwise.} \end{cases} \tag{3.10}$$

With this knowledge we can denote $|\eta_{k,l}\rangle$ and $|S_{m,n}\rangle$ as the eigenvectors of $(\eta^+\eta^-)'$ and $(S^+S^-)'$ where k and m index the respective eigenvalues and l and n run through the degenerate eigenvectors for a given k and m. The state $|\psi\rangle = |\eta_{k,l}\rangle \hat{\otimes} |S_{m,n}\rangle$ is then an eigenvector of $\eta^+\eta^-$ and S^+S^- on the full graph $\mathcal{G}$. We provide all the relevant indices for $|\psi\rangle$ with the notation $|\psi_{i,j,k,l,m,n}\rangle$ where i is the number of doublons, j indexes the $\binom{L}{N-2i}$ ways in which the lattice can be split into the two sets, k and l index the eigenvectors of $(\eta^+\eta^-)'$ whilst m and n do the same for $(S^+S^-)'$.

The states $|\psi\rangle$ form a complete basis which diagonalises $\eta^+\eta^-$ and S^+S^- for the given filling as the following statements are true

[4] The tilde on the tensor product means we will take into account the way the sets were formed and re-order the lattice sites back to their original order.

- Orthonormality: $\langle\psi_{i,j,k,l,m,n}|\psi_{i',j',k',l',m',n'}\rangle = \delta_{i,i'}\delta_{j,j'}\delta_{k,k'}\delta_{l,l'}\delta_{m,m'}\delta_{n,n'}$,
- Completeness: $\sum_{i=\mathrm{Max}(0,-2\alpha)}^{\mathrm{Min}(N_\uparrow,N_\downarrow)} \binom{L}{N-2i} \sum_{k=|\alpha|}^{\alpha+i} D_\eta(k,i) \sum_{m=|\beta|}^{N/2-i} D_s(m,i) = \binom{L}{N_\uparrow}\binom{L}{N_\downarrow}$,
- $\eta^+\eta^- \left|\psi_{i,j,k,l,m,n}\right\rangle = \lambda_\eta(k) \left|\psi_{i,j,k,l,m,n}\right\rangle$,
- $S^+S^- \left|\psi_{i,j,k,l,m,n}\right\rangle = \lambda_S(m) \left|\psi_{i,j,k,l,m,n}\right\rangle$.

Analytical Expression for the Steady States

We can use these results to construct the steady states of the Hubbard model for fixed filling on an arbitrary graph under external heating. Following the methodology of chapter 2, and assuming the two SU(2) symmetries are the only relevant symmetries in the system, these steady states will be diagonal in the basis we have just constructed. This assumption does rely on the heating mechanism either breaking any *polygon* symmetries of the lattice[5], or the fact that these symmetries can be ignored due to their sufficiently small effect on the steady states. We will see that these are reasonable assumptions for the setups we consider.

Following this assumption, the steady states will have the form

$$\rho_\infty = \frac{1}{Z} \sum_{i=\mathrm{Max}(0,-2\alpha)}^{\mathrm{Min}(N_\uparrow,N_\downarrow)} \sum_{k=|\alpha|}^{\alpha+i} \sum_{m=|\beta|}^{N/2-i} P_{k,m} \sum_{l=1}^{D_\eta(k,i)} \sum_{n=1}^{D_s(m,i)} \sum_{j=1}^{\binom{L}{N-2i}} \left|\psi_{i,j,k,l,m,n}\right\rangle \left\langle\psi_{i,j,k,l,m,n}\right|, \quad (3.11)$$

where Z is the partition function which can be immediately determined by the normalisation condition $\mathrm{Tr}(\rho_\infty) = 1$ and $P_{k,m}$ are a series of probabilities which are related to the following projectors

$$\begin{aligned}
\mathcal{P}_k^\eta &= \sum_{i,j,m,n,l} \left|\psi_{i,j,k,l,m,n}\right\rangle \left\langle\psi_{i,j,k,l,m,n}\right|, \\
\mathcal{P}_m^S &= \sum_{i,j,k,n,l} \left|\psi_{i,j,k,l,m,n}\right\rangle \left\langle\psi_{i,j,k,l,m,n}\right|, \\
\mathcal{P}_{m,k}^{S,\eta} &= \sum_{i,j,n,l} \left|\psi_{i,j,k,l,m,n}\right\rangle \left\langle\psi_{i,j,k,l,m,n}\right|, \qquad (3.12)
\end{aligned}$$

with the indices ranging in the same manner as in Eq. (3.11). We have not yet stated which (if any) of the SU(2) symmetries the heating or lattice structure breaks. This is intentional and can be reflected entirely within the relationship between the probabilities $P_{k,m}$ and the projectors in Eq. (3.12), which we summarize in Table. 3.1.

[5]By *polygon* symmetries we mean spatial symmetries which the lattice may possess: for example a 1D chain possesses a reflection symmetry about the central site, whilst on more complex geometries there may be mutiple reflection and translational symmetries [2]

Symmetries Preserved	Form of Probabilities
Spin and η	$P_{m,k} = \mathrm{Tr}(\rho(0)\mathcal{P}^{S,\eta}_{m,k})$
η Only	$P_{m,k} = P_m P_k, \quad P_k = \mathrm{Tr}(\rho(0)\mathcal{P}^{\eta}_{k}) \quad P_m = \text{const.}$
Spin Only	$P_{m,k} = P_m P_k, \quad P_k = \text{const.}, \quad P_m = \mathrm{Tr}(\rho(0)\mathcal{P}^{S}_{m})$
Neither	$P_{m,k} = \text{const.}$

Table 3.1: Form of the probabilities $P_{k,m}$ which characterise the maximum entropy steady state of the Hubbard model under continuous heating. The probabilities are defined by their relationship to the initial state $\rho(0)$ and the projectors $\mathcal{P}^{\eta}_{k}$, $\mathcal{P}^{S}_{m}$ and $\mathcal{P}^{S,\eta}_{m,k}$, which are defined in Eq. (3.12). This relationship changes depending on which of the two SU(2) symmetries are preserved by the governing equation of motion as the system heats up.

Symmetries Preserved	Driving Term	Jump Operator
Spin and η	$A\cos(\omega t)\sum_V n_{\uparrow,V} n_{\downarrow,V}$	None Possible
η Only	$A\cos(\omega t)\sum_V g(V)(n_{\uparrow,V} - n_{\downarrow,V})$	$L_V = n_{\uparrow,V} - n_{\downarrow,V}$
Spin Only	$A\cos(\omega t)\sum_V g(V)(n_{\uparrow,V} + n_{\downarrow,V})$	$L_V = n_{\uparrow,V} + n_{\downarrow,V}$
Neither	$A\cos(\omega t)\sum_V g(V) n_{\uparrow,V}$	$L_V = n_{\uparrow,V}$

Table 3.2: Examples of driving terms and local jump operators which preserve the SU(2) symmetries of the Hubbard model and, when combined with the Hubbard Hamiltonian in Eq. (3.1) will induce the formation of the corresponding maximum entropy states in the long-time limit. The function $g(V)$ can be any real-valued inhomogeneous function of V whilst the jump operators correspond to examples of local, Hermitian operators which can make up the dissipative term of the GSKL equation — with a separate jump operator L_V acting on each site V of the lattice. Notably, there is no non-trivial (i.e. not the identity matrix) local Hermitian operator which preserves both the η and spin SU(2) symmetries.

Table 3.1, alongside Eq. (3.11), allows us to classify and write down the steady states of the Hubbard model under heating on an arbitrary graph. This classification is based on which of the SU(2) symmetries are broken/ preserved by the system as it heats up. A number of possible mechanisms could be used to provide the symmetry-preserving heating we need to form these correlated steady states. Here we focus on heating which originates from either periodic driving or local dephasing from a Markovian bath. In Table 3.2 we provide examples of such driving terms and dephasing terms which preserve/break the possible SU(2) symmetries of the Hubbard model. In the following section we will explicitly use these terms in our numerical calculations to demonstrate the formation of these steady states. Moreover, these terms can also be realised experimentally in quantum setups with current technology, a process which we will discuss in detail in section 3.3.

The projectors in Eq. (3.12) are essentially just the identity matrices for a given SU(2) subspace. The same arguments from chapter 2 apply here and so these identity matrices will generally not be featureless, instead possessing distance-invariant non-zero inter-site correlations. For $\mathcal{P}_k^\eta$ and $\mathcal{P}_m^S$ these correlations will be of the form $\eta_V^+\eta_{V'}^-$ and $S_V^+S_{V'}^-$ respectively whilst for $\mathcal{P}_{m,k}^{S,\eta}$ *both* $\eta_V^+\eta_{V'}^-$ and $S_V^+S_{V'}^-$ will be finite and distance-invariant. The steady state is a weighted summation over these identity matrices and, for the symmetries which are preserved, these weights will be non-uniform and thus the steady state will generally possess finite, distance-invariant correlations in the corresponding observables ($\langle\eta_V^+\eta_{V'}^-\rangle$ if η symmetry is preserved and $\langle S_V^+S_{V'}^-\rangle$ if spin symmetry is preserved). For any broken symmetries, the uniform distribution of weights will instead ensure all excitations in that symmetry sector are equally likely and the corresponding inter-site correlations will be zero.

Given the probabilities $P_{k,m}$, Eq. (3.11) can be used to calculate a number of properties of ρ_∞. As all of the basis states we constructed are eigenstates of the doublon number operator we can immediately deduce its moments as

$$\begin{aligned}\langle N_d^\alpha\rangle &= \frac{1}{Z}\sum_i i^\alpha f(i),\\ f(i) &= \sum_{k,m} P_{k,m} D_\eta(k,i) D_s(m,i)\binom{L}{N-2i}.\end{aligned} \tag{3.13}$$

These equations are useful because we can take advantage of the distance-invariance of correlations in the steady state[6] and use the first moment of the doublon number

[6]It is worth stating that the particle-hole correlations $\langle c_{V,\uparrow}^\dagger c_{V\downarrow}^\dagger c_{V',\downarrow} c_{V',\uparrow}\rangle$ in this state are technically only distance invariant once we apply the prefactor $f(V)f(V')$, which is naturally built into the η operators as $\langle\eta_V^+\eta_{V'}^-\rangle = f(V)f(V')\langle c_{V,\uparrow}^\dagger c_{V\downarrow}^\dagger c_{V',\downarrow} c_{V',\uparrow}\rangle$.

($\alpha = 1$), along with the initial value $\langle \eta^+ \eta^- \rangle$ and $\langle S^+ S^- \rangle$, to directly extract values for both the steady state off-diagonal spin-exchange and particle-hole order, $\langle S^+_V S^-_{V'} \rangle$ and $\langle \eta^+_V \eta^-_{V'} \rangle$ respectively - with $V \neq V'$. Specifically, we have

$$\langle \eta^+ \eta^- \rangle = \langle N_d^1 \rangle + M(M-1) \langle \eta^+_V \eta^-_{V'} \rangle, \tag{3.14}$$

and a similar equation follows for $\langle S^+ S^- \rangle$. It is worth stating that this equation is our fermionic analogue of Eq. (2.13) in chapter 2: it tells us that if the η symmetry is preserved the steady state off-diagonal η correlations can only be zero if the value of $\langle \eta^+ \eta^- \rangle$ in the initial state happens to be equal to $\langle N_d^1 \rangle$, the total number of doublons that the steady state will possess, which is unlikely. The same is true of the spin sector (with $\langle N_d^1 \rangle$ being replaced by the total number of singlons of spin $\uparrow$). Higher moments of the doublon number provide access to multi-point correlators in the η and spin symmetry sectors (for example we can show that $\langle n_{\uparrow,V} n_{\downarrow,V} n_{\uparrow,V'} n_{\downarrow,V'} \rangle \propto \langle N_d^2 \rangle - \langle N_d^1 \rangle$).

In principle, in order to calculate $\langle N_d^\alpha \rangle$ we would need to know the full distribution of values of the $P_{k,m}$s. For certain initial states, such as the ground state on a bipartite lattice, this is straightforward enough as it resides in a fixed subspace (i.e. $P_{k,m}$ is only non-zero for a specific k and m) by virtue of being an eigenstate of the SU(2) symmetric Hamiltonian. In other, more general, cases this could be quite complicated and would involve taking a number of projective measurements on the initial state. We find from our equations, however, that the first moment of the doublon number is only dependent on the $P_{k,m}$s through its relationship to $\langle \eta^+ \eta^- \rangle$ and $\langle S^+ S^- \rangle$ and thus knowledge of these two values, and the graph size and filling, is enough to calculate $\langle N_d^1 \rangle$. The steady state off-diagonal order parameters $\langle \eta^+_V \eta^-_{V'} \rangle$ and $\langle S^+_V S^-_{V'} \rangle$ then follow immediately from Eq. (3.14) and its corresponding 'spin' version.

The off-diagonal order parameters $\langle \eta^+_V \eta^-_{V'} \rangle$ and $\langle S^+_V S^-_{V'} \rangle$ are particularly important because when finite and non-decaying in the thermodynamic limit the system can be said to possess off-diagonal long-range order (ODLRO) [54] in the corresponding channel. In the steady state we know these correlations will not just be non-decaying but completely uniform with distance. A finite, distance-invariant value of $\langle \eta^+_V \eta^-_{V'} \rangle$ in the equilibrium state of a macroscopically large many-body system has been proven to imply the existence of the Meissner effect and flux quantisation [49, 50]. As our steady states are in equilibrium with respect to the Hubbard Hamiltonian (they commute with H in Eq. (3.1)) then, if $\langle \eta^+_V \eta^-_{V'} \rangle$ is finite for $L \to \infty$, we can expect them to exhibit these phenomenon. The Meissner effect and flux quantisation are

characteristic features of a superconductor, suggesting these steady states *may*[7] also be superconducting. Meanwhile, a finite value of $\langle S_V^+ S_{V'}^- \rangle$ implies a large degree of mobility in the transport of spin through the system and so that the corresponding steady states can, potentially, host a frictionless spin current.

Scaling of the Steady State Correlations

By performing numerical calculations of the driven/dissipative Hubbard model we can observe the formation of the states described in Eq. (3.11) and such charge and spin order. We will use exact diagonalisation routines in both the driven and dissipative case — adopting a quantum trajectories approach for the open system to relieve the memory overhead[8]. Whilst these routines are limited to relatively small systems we can use them to directly witness the evolution of the system and verify our earlier analytical results for sufficiently large times. We will then confidently be able to use these analytical results for system sizes which cannot be treated numerically.

To help with our analysis we introduce the graph measure $d(V, V')$ which is the minimum number of edges that must be traversed to move between the vertices V and V'. With this the correlation function

$$O(\delta) = \frac{1}{\mathcal{N}} \sum_{\substack{\langle V,V' \rangle \\ d(V,V')=\delta}} \langle O_V^+ O_{V'}^- \rangle, \tag{3.15}$$

can be defined. Here, $O = S$ or $O = \eta$, the summation is over all pairs of vertices where $d(V, V') = \delta$ and $\mathcal{N}$ is the number of pairs of vertices which satisfy $E(V, V') = \delta$. Hence, $O(\delta)$ measures the average of the spin-exchange or particle-hole correlations at a distance δ for any given graph. We can then easily define the quantity $\overline{|O(\delta)|}_{\delta>l}$ as the magnitude of the average of these correlations over distances greater than l.

Single SU(2) Symmetry Preservation - We start off by considering the case in which one of the SU(2) symmetries is broken during the time evolution whilst the other is preserved. This breaking could occur via the external heating mechanism or, in the case of a broken η symmetry, through the non-bipartite nature of the lattice.

[7] Definitively determining this is beyond the scope of this thesis and would require explicit calculation of the excitation spectrum of the governing Hamiltonian in the vicinity of these states.

[8] Whilst these calculations could be performed using Matrix Product State methods, the large number of excitations induced by the driving/dissipation, and our desire to witness the evolution of the system over a large time window, would require us to use very large bond dimensions. A direct attempt to solve for the steady state of an MPO representation of the superoperator may work in the dissipative case [55] — but would require encoding multiple SU(2) symmetries into the relevant MPS routines and dealing with on-site dimensions of $d = 16$.

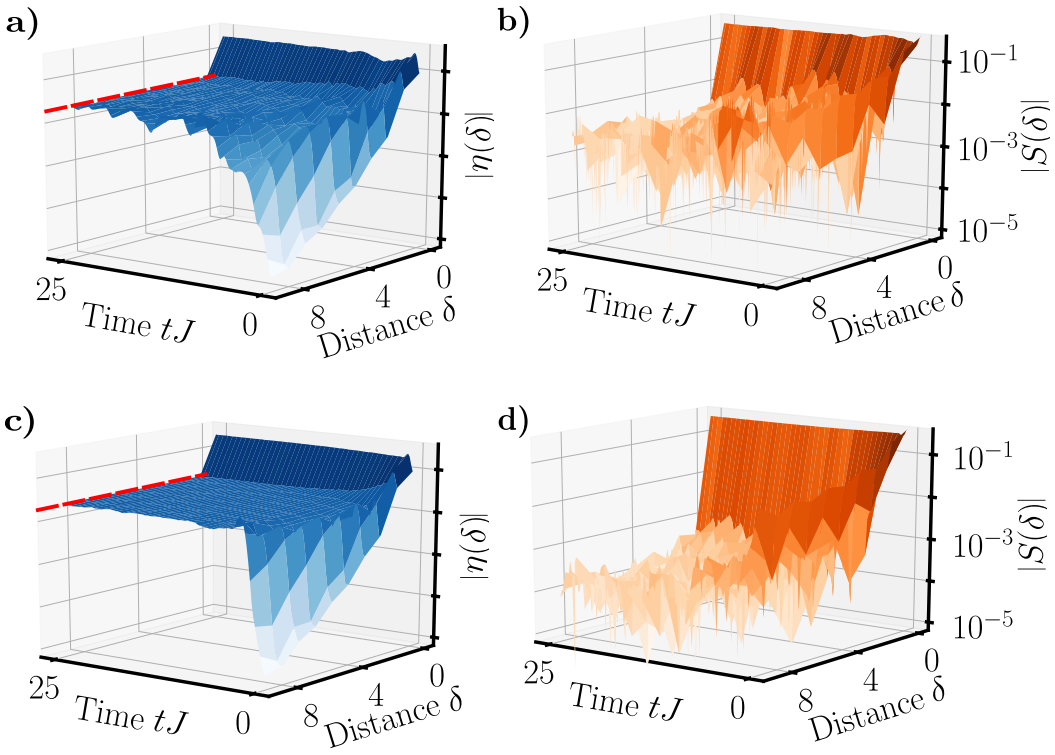

Figure 3.3: Spin and η correlations versus both time and distance for the half-filled Hubbard model on the graph $\mathcal{G}_1$: an $L = 10$ site chain. The bare Hamiltonian is defined in Eq. (3.3) and the system is initialised in the ground state of H with $U = 4.0J$. The red dotted lines correspond to analytical predictions. Top row) Dynamics under the Hamiltonian $H(t) = H + H_D(t)$ where $H_D(t) = A\sin(\omega t)\sum_V V s^z_V$, $A = 2U$, $\omega J = 1.0$ and the vertex index V runs along the chain from 1 to 10. Bottom row) Dynamics under the GSKL master equation with Hamiltonian H and jump operators $L_V = \sqrt{\gamma} s^z_V$ on each site, setting $\gamma = J$. The dynamics were calculated by averaging over 500 quantum trajectories, with the relative error $\frac{\Delta(\langle O(\delta)\rangle)}{\langle O(\delta)\rangle)} < 0.1$ for both $O = \eta$ and $O = S$ and for all times and distances.

In Figure 3.3 we break the spin SU(2) symmetry and preserve the η symmetry. We plot the dynamics of the spin and η-exchange correlations for a half-filled chain under either $H_D(t) = A\sin(\omega t)\sum_V V s^z_V$ or jump operators of the form $L_V = \sqrt{\gamma} s^z_V$. In both cases the time dynamics manifests identical, uniform long-range order in the η sector, which is not present in the initial ground state of the system at $t = 0$. The order we observe is in complete agreement with the equations we have derived previously and in the spin sector no long-time order is induced and the off-diagonal correlations are decaying away. Whilst still evident, the decay of the spin correlations is less pronounced in the driven system than the dissipative one. This is because the finite system size places a limit on the extent to which the coefficients in the pure state can dephase and mimic the density matrix we have constructed in Eq. (3.11).

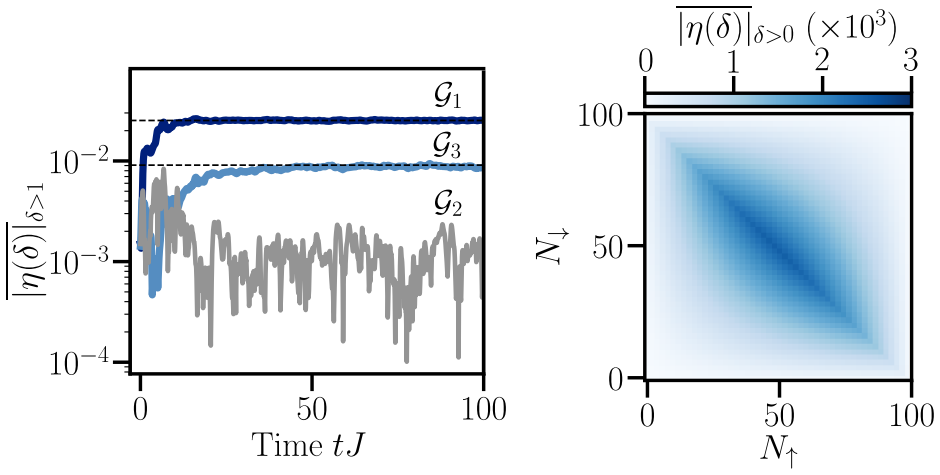

Figure 3.4: Left) Magnitude of the off-diagonal, non nearest-neighbour η correlations versus time for the three graphs $\mathcal{G}_1$, $\mathcal{G}_2$ and $\mathcal{G}_3$ with particle fillings $N_\uparrow = N_\downarrow = 5$, $N_\uparrow = N_\downarrow = 4$ and $N_\uparrow = N_\downarrow = 3$ respectively. The graphs are initialised in the ground state of H with $U = 4.0J$ and time-evolved under the Hamiltonian $H(t) = H + H_D(t)$ where $H_D(t) = A\sin(\omega t)\sum_V V s_V^z$, $A = 2U$, $\omega J = 1.0$ and the vertex index V runs over the site numbers. The black-dotted lines represent the analytical predictions. Right) Long-time off-diagonal η correlations versus particle numbers for a bi-partite system initialised in the subspace where $\langle \eta^+ \eta^- \rangle = 0$ and time evolved under external heating which breaks the spin symmetry whilst preserving the η symmetry.

In Fig. 3.4 we demonstrate the generality of the results we have derived. We consider several different particle densities and all 3 lattices from Fig. 3.2 and show how our equations still hold. Periodic driving is used which breaks the spin symmetry and induces the formation of finite η order in the two bi-partite lattices, $\mathcal{G}_1$ and $\mathcal{G}_3$, as they heat up. Meanwhile, the non bi-partite nature of $\mathcal{G}_2$ means that the system cannot establish long-time η order due to the lack of the requisite symmetry. The more connected nature of $\mathcal{G}_1$ versus $\mathcal{G}_3$ likely explains why the system's approach to the correlated steady state is faster in the former. Additionally, the different fillings in $\mathcal{G}_1$ and $\mathcal{G}_3$ explains the different values for the induced η order; as they are both bi-partite graphs with equal numbers of vertices in each subgraph the lattice structure is irrelevant to the size of the long-time order.

In Fig. 3.4b we use our analytical results to show how the long-time η order, when starting in the lowest eigenspace of $\langle \eta^+ \eta^- \rangle$, is affected by the values of the particle numbers $N_\uparrow$ and $N_\downarrow$ on the lattice. We observe that the long-time order is maximised around the symmetric point $N_\uparrow = N_\downarrow = L/2$, whilst trailing towards 0 as these quantities move towards either L or 0. This can be understood from the fact that the system can support a maximum, and equal, number of doublon and holons

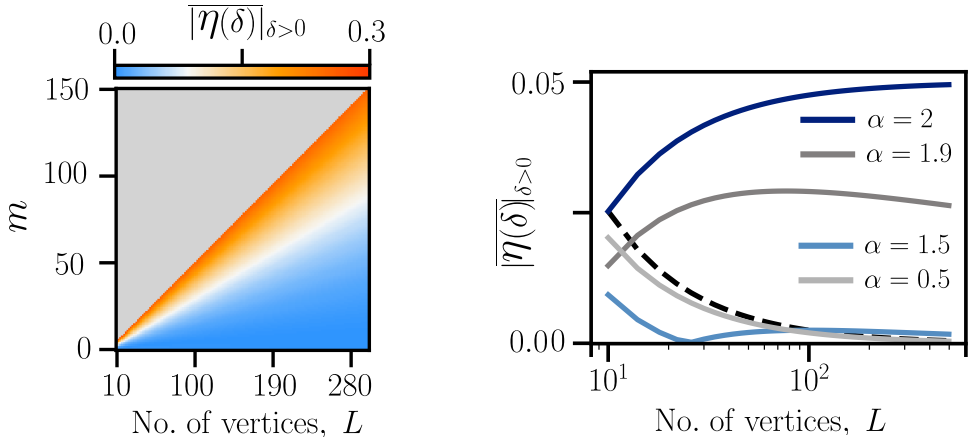

Figure 3.5: Off-diagonal η-correlations in the maximum entropy steady state of the heated, half-filled Hubbard model on an arbitrary bi-partite graph, with the governing equation of motion preserving the η SU(2) symmetry whilst breaking the spin SU(2) symmetry. Left) Map of these correlations versus both system size L and m, with m calculated from the initial state $\rho(0)$ via $m = (-1 + \sqrt{1 + 4\mathrm{Tr}(\rho(0)\eta^+\eta^-)})/2$. Right) Scaling of these correlations versus system size for various different initial values of $\mathrm{Tr}(\rho(0)\eta^+\eta^-)$. For the solid lines we have set $\mathrm{Tr}(\rho(0)\eta^+\eta^-) = L^\alpha/20$. The black-dashed line corresponds to $\mathrm{Tr}(\rho(0)\eta^+\eta^-) = 0$.

at the symmetric point. These two types of quasiparticle are equally necessary for a non-zero value of $\langle \eta^+_V \eta^-_{V'} \rangle$ and at the edges of the plot the system cannot support them both simultaneously — preventing order from emerging in the steady state.

One of the most immediate questions about the order we have observed is how it scales with system size. Whilst our numerics are severely limited in this respect, our analytical calculations are not. In Fig. 3.5 we plot the steady state η order as a function of both the system size and the initial value of $\langle \eta^+\eta^- \rangle$. These results apply to any bi-partite graph in which the applied heating breaks the spin symmetry and preserves the η symmetry. We immediately notice that, as the system size L increases, the ratio of states with $\eta^+_V \eta^-_{V'} > a$ versus those with $\eta^+_V \eta^-_{V'} < a$, where a is some constant is growing. This reinforces our results from chapter 2 where we found that the ratio of correlated to uncorrelated maximum entropy steady states in an SU(2) symmetric system should grow extensively with system size.

We can easily argue from Eq. (3.14) that these correlations will be finite in the thermodynamic limit if, and only if, the initial state satisfies $\langle \eta^+\eta^- \rangle \propto L^2$. As the eigenvalues of $\eta^+\eta^-$ are directly proportional to $m(m+1)$, where $m = 0, ..., L/2$ it is clear that as $L \to \infty$ the ratio of the number of possible values of m where this

condition is satisfied compared to values where it is not infinite. Although the initial states in the subspaces with $\langle \eta^+ \eta^- \rangle \propto L^2$ are already likely to have finite long-range η correlations, the heating will still act to renormalize these correlations and make them completely uniform with distance. Only when these correlations are uniform can it be argued that the Meissner effect and flux quantisation can be observed [49, 50].

Furthermore, this mechanism of heating-induced order could act to protect the system against unwanted decoherence mechanisms which break the η symmetry. Specifically, if the magnitude of the term which implements the desired heating into the system is made to be much larger than the size of any unwanted symmetry breaking terms then the Quantum Zeno effect could occur [56]. Any dynamics induced by these unwanted terms would be 'frozen' out due to their small size in comparison to that of the desired heating. Such a process was directly observed in Ref. [57].

In Fig. 3.3 we initialised our system in the ground state. For half-filled hypercubic graphs it can always be proved that the ground state satisfies $\langle \eta^+ \eta^- \rangle = 0$ [58] and so the induced long-range order decays away as $1/L$ to 0 (see Fig. 3.5) — preventing the formation of a superconductor in the thermodynamic limit. This order does, however, remain finite for any finite-size system and despite the ground state possessing the smallest possible value of $\langle \eta^+ \eta^- \rangle$ the magnitude of this long-time order is larger than any other initial states which have finite $\langle \eta^+ \eta^- \rangle < (L-1)/2$. This is because the steady state off-diagonal η order $\langle \eta_V^+ \eta_{V'}^- \rangle$ is a monotonic function of $\langle \eta^+ \eta^- \rangle$ but is negative for finite L and $\langle \eta^+ \eta^- \rangle < L/4$, at which point it changes sign. Hence, the ground state η order is the most negative and it can be shown from our equations that the magnitude of this order is larger than that for any of the other states in the range $0 < \langle \eta^+ \eta^- \rangle < (L-1)/2$.

As we saw in Fig. 3.3, in a finite system the dynamics which follow from driving such a ground state out of equilibrium involves a drastic amplification of the long-range correlations at the expense of the shorter-range ones in order to reach a finite value for the long-range order. This signals a significant enhancement in the mobility of the charge-carrying doublons throughout the lattice, which could be reflected in conductivity measurements of the system.

Meanwhile, on an unbalanced bi-partite graph, i.e. one in which the number of vertices in different subgraphs is unequal, Lieb's theorems [58] can be used to argue that for $U < 0$ the ground state will satisfy the condition $\langle \eta^+ \eta^- \rangle \propto L^2$ for observing finite, uniform η order in the steady state in the thermodynamic limit. Such ground states will likely have long-range η order already but previous literature has shown that it will be inhomogeneous and staggered with sign as a function of distance

[59, 60]. Heating which preserves the η symmetry will thus force these correlations to become uniform with distance and potentially realise a macroscopic superconductor. This remarkable result is the subject of the recent preprint, Ref. [61] and we will study an example of such a lattice where this can occur in the next chapter.

All of these results are completely analogous to the case in which the spin SU(2) symmetry is preserved and the η symmetry is broken. In this case the steady state predictions for the off-diagonal spin-exchange order will be identical to those for the η order we presented here. Interestingly, in Ref. [32], a type of spin SU(2) preserving periodic driving was studied for the 1D Hubbard chain in the thermodynamic limit. There it was shown how, when starting in the ground state, this driving can renormalize the exchange parameters in the system and transiently enhance long-range singlet pairing. Even though our calculations show the long-time spin-exchange order will be 0, our results here suggest this transient response could be a result of the dynamic preservation of $\langle S^+S^-\rangle$. This constraint forces a drastic reorganisation of the spin degrees of freedom, which will likely lead to a transient enhancement of the long-range correlations at the expense of the shorter ones, before they mutually decay away to 0 as $t \to \infty$.

Dual SU(2) Symmetry Preservation - We now consider the case in which both SU(2) symmetries are preserved under the heating applied to the lattice. We will focus our numerics on the periodically driven Hubbard model as non-trivial dissipative terms which preserve both symmetries would have to be highly non-local and thus may not induce the desired heating. In Fig. 3.6a-b we start in a half-filled thermal state on the three different graphs and apply a periodic time-dependence to the Hubbard parameters, preserving both SU(2) symmetries. For the two bi-partite graphs we observe the manifestation of order in both symmetry sectors with the quantitative value agreeing with the predictions of our equations. The long-time state therefore uniquely supports both finite, uniform spin-exchange and particle-hole order simultaneously. In the graph $\mathcal{G}_2$ the system cannot sustain η order because it is not bi-partite.

Again, we can take advantage of our equations and analyse these dual symmetric long-time states for systems much larger than those available by exact calculations. In Fig. 3.6c-d we plot maps of the long-time η and spin correlations as a function of the initial values of $\langle \eta^+\eta^-\rangle$ and $\langle S^+S^-\rangle$ for a bi-partite graph with $L = 100$ nodes. For the majority of initial states, finite spin and η order co-exist and in the inset we provide examples of the uniform correlations in these states. Identically to the single symmetry case, in the thermodynamic limit, the condition $\langle \eta^+\eta^-\rangle \propto L^2$ or $\langle S^+S^-\rangle \propto L^2$ is necessary to observe finite ODLRO in the η and spin sectors,

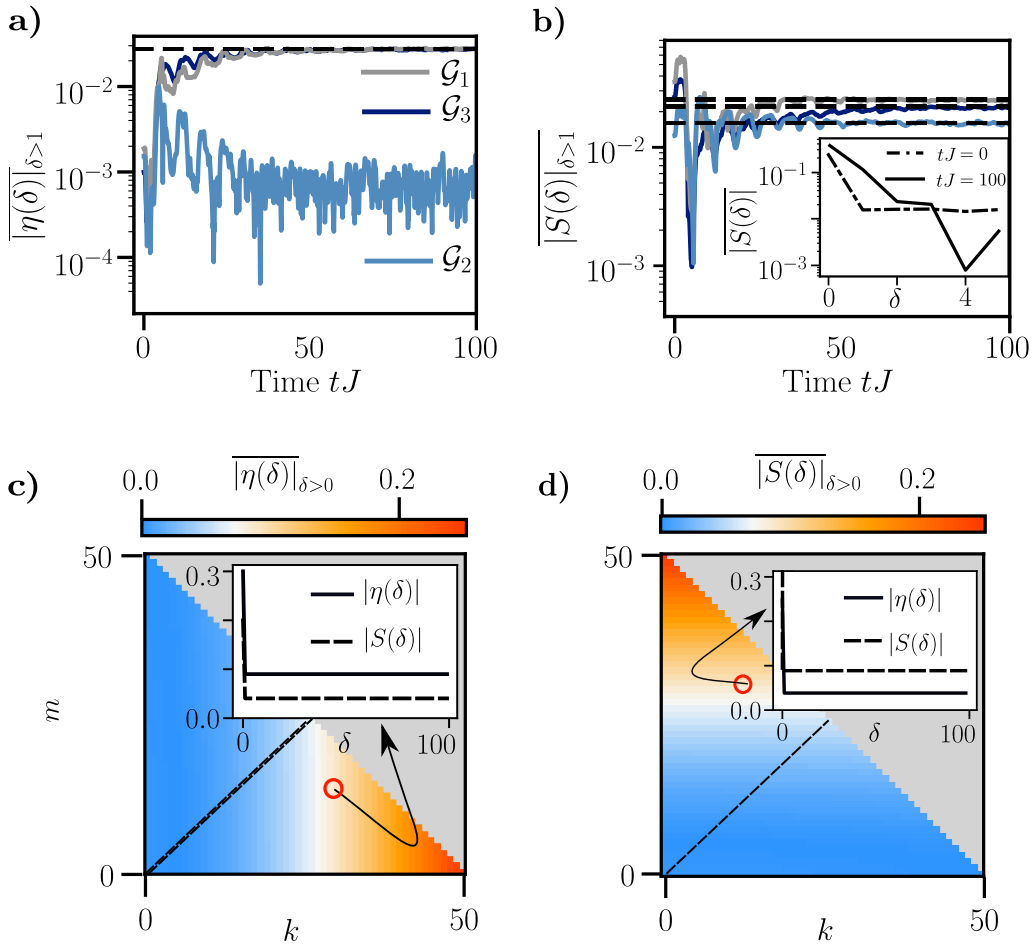

Figure 3.6: Top) Off-Diagonal Spin and η Correlations versus time for 3 different half-filled 10 site Hubbard graphs $\mathcal{G}_1$, $\mathcal{G}_2$ and $\mathcal{G}_3$ (see Fig. 3.2) with driving of the form $H_D = \delta U \cos(\omega t) \sum_V n_{\uparrow,V} n_{\downarrow,V}$ and the bare Hamiltonian H as defined in Eq. (3.3) with $U = 4.0J$. The system is initialised, at time $tJ = 0$, in the thermal state $\rho \propto \exp(-\beta H)$ with $\beta J = 5$ and then time-evolved under H with $U = 4.0J$, $\delta U = 1.5J$ and $\omega = 1.0J$. Black-Dotted lines represent the long-time analytical predictions for the 3 respective graphs. Inset) Spin-correlations versus distance at times $tJ = 0$ and $tJ = 100$ for the lattice $\mathcal{G}_2$. Bottom) Maps of the doublon and spin order of steady states of the Hubbard model on a 100 node bi-partite graph under continuous heating which preserves both SU(2) symmetries. The indices m and k are dependent on the initial values of the spin and η Casimir operators via $m = (-1 + \sqrt{1 + 4\langle S^+ S^- \rangle})/2$ and $k = (-1 + \sqrt{1 + 4\langle \eta^+ \eta^- \rangle})/2$. The two maps are related via a reflection over the black-dotted line. Insets: doublon (solid line) and spin (dashed line) order for the long-time state at the circled point on the map.

respectively. These two conditions are not, however, mutually exclusive and lead us to show how we can use heating to form a unique spin-η condensate from two independent condensates.

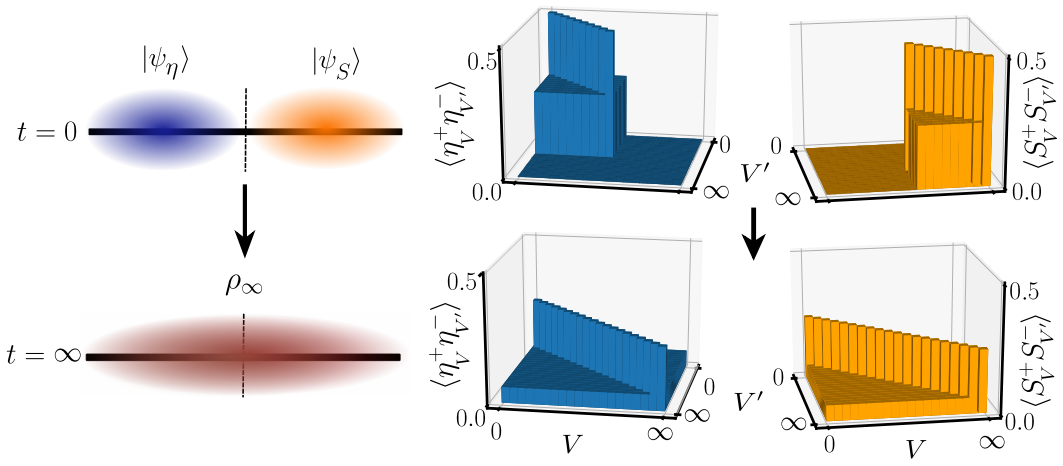

Figure 3.7: Merging of two condensates under heating. A graph hosting two species of fermionic particles is initialised in two independent halves which contain an η condensate, $|\psi_\eta\rangle \propto (\eta^+)^{L/4}|\text{vac}\rangle$ and spin-wave condensate, $|\psi_S\rangle \propto (S^+)^{L/4}|\downarrow\downarrow, ..., \downarrow\rangle$, respectively. The system is then time-evolved under the Hubbard Hamiltonian and a heating mechanism which commutes with $\eta^+\eta^-$ and S^+S^-, causing it to reach a maximum entropy state where the two condensates have merged into a single hybrid spin-η condensate. Left) Pictorial depiction of the merging of the two condensates. Right) Matrices of η and spin- exchange correlations for the whole lattice in the thermodynamic limit ($L \to \infty$) at times $t = 0$ and $t = \infty$. The indices V and V' run over the sites of the graph.

Heating-induced formation of an η-spin condensate - Consider a graph of L sites which hosts the initial state $(S^+)^{L/4}|\chi_A\rangle \otimes (\eta^+)^{L/4}|\chi_B\rangle$, where $|\chi_A\rangle = |\downarrow, \downarrow, ..., \downarrow\rangle$ over $L/2$ of the sites and $|\chi_B\rangle$ is the vacuum state over the other $L/2$ sites. This state consists of two independent condensates — a spin-wave and particle-hole condensate — each confined to one half of the graph. Under the Hubbard Hamiltonian and heating which preserves both the η and spin SU(2) symmetries these condensates will merge and phase-lock into a single, larger condensate which possesses both particle-hole and spin-wave uniform, off-diagonal order. Specifically, our equations show $\lim_{L\to\infty} = \overline{|\eta(\delta)|}_{\delta>0} = \overline{|S(\delta)|}_{\delta>0} = 0.0625$ for $i \neq j$ and $i, j = 1...L$. This process is pictured in Fig. 3.7. The actual graph structure is not important and occurs under the application of SU(2) preserving heating to independent fermionic condensates which are initialised on two halves of *any* bi-partite graph. This process could also be used to merge two condensates of the same type, such as states of the form $(S^+)^{L/4}|\chi_A\rangle \otimes (S^+)^{L/4}|\chi_A\rangle$ or $(\eta^+)^{L/4}|\chi_B\rangle \otimes (\eta^+)^{L/4}|\chi_B\rangle$. In this case the heating only needs to preserve the relevant SU(2) symmetry in order to manifest a larger η or spin condensate.

3.3 Experimental Implementations of SU(2) Symmetric Heating in the Hubbard Model

We have seen how the introduction of SU(2) preserving heating can guide the Hubbard model into various correlated steady states. Periodic driving or Hermitian local dephasing can achieve this desired heating and here we will show how these processes can be implemented in an experimental realisation of the Hubbard Hamiltonian.

We will start by considering the case in which only a single SU(2) symmetry is preserved, and the other is broken. In a cold atom setting, dissipation induced via immersion of the optical lattice into a large, homeogeneous Bose-Einstein Condensate (BEC) provides an opportunity to realise the desired setup. We will demonstrate this by outlining a derivation of the GSKL master equation for this system, closely following the methodology of Refs. [62, 63]. We start by writing the Hamiltonian of the Hubbard optical lattice + Bose-Einstein condensate

$$\begin{aligned} H_{\text{tot}} &= H_L + H_I + H_{\text{BEC}}, \\ H_L &= H, \\ H_I &= \int \left(\kappa_\uparrow \chi_\uparrow^\dagger(\mathbf{r})\chi_\uparrow(\mathbf{r})\phi^\dagger(\mathbf{r})\phi(\mathbf{r}) + \kappa_\downarrow \chi_\downarrow^\dagger(\mathbf{r})\chi_\downarrow(\mathbf{r})\phi^\dagger(\mathbf{r})\phi(\mathbf{r})\right) d\mathbf{r}, \\ H_{\text{BEC}} &= \int \phi^\dagger(\mathbf{r})\left[-\frac{\nabla^2}{2m_b} + V_{\text{ext}}(\mathbf{r}) + \frac{g}{2}\phi^\dagger(\mathbf{r})\phi(\mathbf{r})\right]\phi(\mathbf{r}) d\mathbf{r}, \end{aligned} \tag{3.16}$$

with H_L, H_{BEC} and H_I being the lattice (see Eq. (3.3)), BEC and lattice-BEC interaction Hamiltonian respectively. The operators $\chi_\uparrow(\mathbf{r})$ and $\chi_\downarrow(\mathbf{r})$ are the field operators of the two fermionic levels at position $\mathbf{r}$ which couple to the bosonic field $\phi^\dagger(\mathbf{r})$ with amplitudes $\kappa_\uparrow$ and $\kappa_\downarrow$ respectively. The mass of a condensate atom is given by m_b, V_{ext} is an external trapping potential for the BEC and g is the interaction strength between the condensate atoms.

In order for the condensate to affect the dynamics of the lattice solely in one of the symmetry sectors we require the coupling strengths to satisfy $\kappa_\uparrow = \pm\kappa_\downarrow$ with the '+' leading to dephasing in the η sector and the '$-$' leading to dephasing in the spin sector. This relationship could be achieved via Feshbach resonances [64, 65] which allow the tuning of atomic scattering lengths over a wide range of values. It is also necessary that $|\kappa_\uparrow| \ll g n^0 \epsilon^D$, where n_0 is the BEC density in the centre of the trap, ϵ is the healing length and D is the system dimension [62]. By solving the Gross-Pitaevskii equation and treating the resulting deformations in the BEC as coherent states of phonons an effective, discretized, Hamiltonian for the system can be derived.

We can then trace out the phonon degrees of freedom, invoking the rotating wave, Born and Markov approximations to arrive at the following master equation for the density matrix of the lattice $\rho_L(t)$

$$\partial_t \rho_L(t) = -\mathrm{i}[H_g, \rho_L(t)] + \sum_{V,V'=1}^{L} f_{V,V'}(t)\big(O_V O_{V'}\rho_L(t) + \rho_L(t) O_V O_{V'} - 2O_V \rho_L(t) O_{V'}\big),$$

$$H_g = H^{'} - \sum_{V,V'=1}^{L} g_{V,V'}(t) O_V O_{V'}. \tag{3.17}$$

In this equation $H^{'}$ is the Hubbard Hamiltonian (the prime denotes that the parameters have been slightly modified due to the BEC presence), $f_{V,V'}(t)$ and $g_{V,V'}(t)$ are a pair of time-dependent, short-range (based on 'typical' parameters for a BEC) functions which become time-independent as $t \to \infty$. The operator O_V is either $n_V = n_{\uparrow,V} + n_{\downarrow,V}$ or $s^z_V = n_{\uparrow,V} - n_{\downarrow,V}$ depending on whether we set $\kappa_\uparrow = \kappa_\downarrow$ or $\kappa_\uparrow = -\kappa_\downarrow$ respectively. The explicit form of the functions $f_{V,V'}(t)$ and $g_{V,V'}(t)$ is not important and when $\kappa_\uparrow = \kappa_\downarrow$ the master equation preserves the spin SU(2) symmetry whilst the η SU(2) symmetry is instead preserved when $\kappa_\uparrow = -\kappa_\downarrow$.

The short-range nature of the functions f and g means that the dissipation will be relatively local and, as the operator O_V is Hermitian, should induce the desired heating. Provided two-point correlations can be measured in the lattice[9] then this experimental setup provides the possibility of witnessing the onset of long-range order that our equations predict. This could be done by initialising the lattice in its equilibrium state, immersing it into the BEC and then probing some finite region on a transient timescale.

We will now consider the possibility of preserving both symmetries under heating. This can be achieved by periodically modulating at least one of the Hamiltonian parameters in time. In an ultracold atomic lattice the Hubbard interaction and hopping strengths have a well defined relationship with the depth and separation of the potential minima which form the lattice sites. These quantities can therefore be directly controlled, and made to oscillate, by modulating the standing-wave interference pattern which generates the potential landscape — a process which has already led to the experimental realisation of a time-dependent Hubbard Hamiltonian [40] and could be used to realise the unique states we have observed here.

[9]Spin correlations are measurable via direct in-situ measurements with quantum gas microscopy [66] whilst η correlations could be measured by allowing the η pairs to associate into molecules and performing time-of-flight measurements [67].

In a quantum materials setting it is not possible to gain such precise control over the parameters of the Hamiltonian as in an optical lattice. Nonetheless, a number of experiments have exposed materials to strong infrared laser pulses, resonantly exciting their vibrational modes and dynamically altering the electronic degrees of freedom of the underlying Hamiltonian [68, 69, 70, 71, 72, 73, 74, 75]. In the following chapter we will focus on one such experiment, showing how the mechanism of heating-induced order could be used to explain the experimental observation of photo-induced superconductivity in this setup.

3.4 Conclusion

In this chapter we have focussed on the single-band Hubbard model — a physical, tight binding description of electronic behaviour in solid state materials. We have directly applied our results from chapter 2, showing how the rich symmetry structure of the Hubbard Hamiltonian can constrain the dynamics of the system as it heats up and induce the formation of ordered, correlated maximum entropy states. By diagonalising the irreducible representation of the Hamiltonian's symmetry structure we have been able to analytically construct these states and make a number of quantitative predictions about them. These predictions vary based on the size, structure and filling of the underlying lattice as well as the properties of the initial state that was driven out of equilibrium. Finally, we identified a number of experimental setups which could achieve the desired conditions required for observing the formation of these ordered states.

We should emphasize that the formation of the correlated fermionic steady states studied in this chapter is not specifically dependent on the single-band Hubbard Hamiltonian. The application of driving/dissipation to this Hamiltonian simply offers an example of a concrete, physical and experimentally realisable setup in which these states can form. More generally, for *any* many-body system comprised of two fermionic species, an evolution process which is non-local and heats the system up whilst preserving the relevant Casimir operator(s) will create the steady states studied here. For systems with more than two fermionic species then the preservation of the corresponding SU(N > 2) Casimir operators will induce exotic steady states with uniform correlations involving each distinct pair of species.

In the next chapter we will maintain our focus on the two-species single-band setup in order to consider a recent experiment which observed photo-induced superconductivity in the organic compound $\kappa - (\mathrm{BEDT} - \mathrm{TTF})_2\mathrm{Cu}[\mathrm{N}(\mathrm{CN})_2]\mathrm{Br}$. By forming a

simplified description of the experiment with a non-bipartite driven two-rung triangular Hubbard model we will show how the mechanism of heating-induced order can manifest itself via a unique pathway. This mechanism initiates the formation of the correlated steady states we have observed in this chapter and thus provides a possible explanation for the results of this experiment.

References

[1] J. Hubbard, "Electron correlations in narrow energy bands," *Proc. R. Soc. Lond. A*, vol. 276, pp. 238–257, 1963.

[2] F. H. L. Essler, H. Frahm, F. Göhmann, A. Klümper, and V. E. Korepin, *The One-Dimensional Hubbard Model*. Cambridge University Press, Cambridge, 2005.

[3] L. Tarruell and L. Sanchez-Palencia, "Quantum simulation of the Hubbard model with ultracold fermions in optical lattices," *C. R. Phys.*, vol. 19, pp. 365–393, 2018.

[4] T. Esslinger, "Fermi-Hubbard physics with atoms in an optical lattice," *Annu. Rev. Condens. Matter Phys.*, vol. 1, pp. 129–152, 2010.

[5] E. Cocchi, L. A. Miller, J. H. Drewes, M. Koschorreck, D. Pertot, F. Brennecke, and M. Köhl, "Equation of state of the two-dimensional Hubbard model," *Phys. Rev. Lett.*, vol. 116, p. 175301, 2016.

[6] A. Yamada, "Magnetic properties and Mott transition in the Hubbard model on the anisotropic triangular lattice," *Phys. Rev. B*, vol. 89, p. 195108, 2014.

[7] M. Laubach, R. Thomale, C. Platt, W. Hanke, and G. Li, "Phase diagram of the Hubbard model on the anisotropic triangular lattice," *Phys. Rev. B*, vol. 91, p. 245125, 2015.

[8] M. Ogata and H. Shiba, "Bethe-ansatz wave function, momentum distribution, and spin correlation in the one-dimensional strongly correlated Hubbard model," *Phys. Rev. B*, vol. 41, pp. 2326–2338, 1990.

[9] A. Georges, G. Kotliar, W. Krauth, and M. J. Rozenberg, "Dynamical mean-field theory of strongly correlated fermion systems and the limit of infinite dimensions," *Rev. Mod. Phys.*, vol. 68, pp. 13–125, 1996.

[10] R. Bulla, "Zero temperature metal-insulator transition in the infinite-dimensional Hubbard model," *Phys. Rev. Lett.*, vol. 83, pp. 136–139, 1999.

[11] K. Held, G. Keller, V. Eyert, D. Vollhardt, and V. I. Anisimov, "Mott-Hubbard metal-insulator transition in paramagnetic V_2O_3: An LDA+DMFT(QMC) study," *Phys. Rev. Lett.*, vol. 86, pp. 5345–5348, 2001.

[12] D. B. McWhan, A. Menth, J. P. Remeika, W. F. Brinkman, and T. M. Rice, "Metal-insulator transitions in pure and doped V_2O_3," *Phys. Rev. B*, vol. 7, pp. 1920–1931, 1973.

[13] J. M. Honig and L. L. V. Zandt, "The metal-insulator transition in selected oxides," *Annu. Rev. Mater. Sci.*, vol. 5, pp. 225–278, 1975.

[14] H. Fujisawa, T. Yokoya, T. Takahashi, S. Miyasaka, M. Kibune, and H. Takagi, "Angle-resolved photoemission study of Sr_2CuO_3," *Phys. Rev. B*, vol. 59, pp. 7358–7361, 1999.

[15] R. Neudert, M. Knupfer, M. S. Golden, J. Fink, W. Stephan, K. Penc, N. Motoyama, H. Eisaki, and S. Uchida, "Manifestation of spin-charge separation in the dynamic dielectric response of one-dimensional Sr_2CuO_3," *Phys. Rev. Lett.*, vol. 81, pp. 657–660, 1998.

[16] H. Rosner, H. Eschrig, R. Hayn, S.-L. Drechsler, and J. Málek, "Electronic structure and magnetic properties of the linear chain cuprates Sr_2CuO_3 and Ca_2CuO_3," *Phys. Rev. B*, vol. 56, pp. 3402–3412, 1997.

[17] A. Schwartz, M. Dressel, G. Grüner, V. Vescoli, L. Degiorgi, and T. Giamarchi, "On-chain electrodynamics of metallic $(TMTSF)_2x$ salts: Observation of Tomonaga-Luttinger liquid response," *Phys. Rev. B*, vol. 58, pp. 1261–1271, 1998.

[18] P. Anderson, *The Theory of Superconductivity in the High-Tc Cuprate Superconductors*. Princeton Series in Physics, Princeton University Press, Princeton, 2017.

[19] J. Kaczmarczyk, J. Spałek, T. Schickling, and J. Bünemann, "Superconductivity in the two-dimensional Hubbard model: Gutzwiller wave function solution," *Phys. Rev. B*, vol. 88, p. 115127, 2013.

[20] R. A. Hart, P. M. Duarte, T.-L. Yang, X. Liu, T. Paiva, E. Khatami, R. T. Scalettar, N. Trivedi, D. A. Huse, and R. G. Hulet, "Observation of antiferromagnetic correlations in the Hubbard model with ultracold atoms," *Nature*, vol. 519, pp. 211–214, 2015.

[21] M. Köhl, H. Moritz, T. Stöferle, K. Günter, and T. Esslinger, "Fermionic atoms in a three dimensional optical lattice: Observing Fermi surfaces, dynamics, and interactions," *Phys. Rev. Lett.*, vol. 94, p. 080403, 2005.

[22] U. Schneider, L. Hackermüller, S. Will, T. Best, I. Bloch, T. A. Costi, R. W. Helmes, D. Rasch, and A. Rosch, "Metallic and insulating phases of repulsively interacting fermions in a 3D optical lattice," *Science*, vol. 322, pp. 1520–1525, 2008.

[23] R. Jördens, N. Strohmaier, K. Günter, H. Moritz, and T. Esslinger, "A Mott insulator of fermionic atoms in an optical lattice," *Nature*, vol. 455, pp. 204–207, 2008.

[24] F. Damanet, E. Mascarenhas, D. Pekker, and A. J. Daley, "Controlling quantum transport via dissipation engineering," *Phys. Rev. Lett.*, vol. 123, p. 180402, 2019.

[25] S. Dutta and N. R. Cooper, "Long-range coherence and multiple steady states in a lossy qubit array," *Phys. Rev. Lett.*, vol. 125, p. 240404, 2020.

[26] C. D. Parmee and N. R. Cooper, "Steady states of a driven dissipative dipolar XXZ chain," *J. Phys. B*, vol. 53, p. 135302, 2020.

[27] B. Kraus, H. P. Büchler, S. Diehl, A. Kantian, A. Micheli, and P. Zoller, "Preparation of entangled states by quantum Markov processes," *Phys. Rev. A*, vol. 78, p. 042307, 2008.

[28] S. Diehl, A. Micheli, A. Kantian, B. Kraus, H. P. Büchler, and P. Zoller, "Quantum states and phases in driven open quantum systems with cold atoms," *Nat. Phys.*, vol. 4, pp. 878–883, 2008.

[29] S. Diehl, W. Yi, A. J. Daley, and P. Zoller, "Dissipation-induced d-wave pairing of fermionic atoms in an optical lattice," *Phys. Rev. Lett.*, vol. 105, p. 227001, 2010.

[30] M. Nakagawa, N. Tsuji, N. Kawakami, and M. Ueda, "Dynamical sign reversal of magnetic correlations in dissipative Hubbard models," *Phys. Rev. Lett.*, vol. 124, p. 147203, 2020.

[31] K. Sponselee, L. Freystatzky, B. Abeln, M. Diem, B. Hundt, A. Kochanke, T. Ponath, B. Santra, L. Mathey, K. Sengstock, and C. Becker, "Dynamics of ultracold quantum gases in the dissipative Fermi–Hubbard model," *Quantum Sci. Technol.*, vol. 4, p. 014002, 2018.

[32] J. R. Coulthard, S. R. Clark, S. Al-Assam, A. Cavalleri, and D. Jaksch, "Enhancement of superexchange pairing in the periodically driven Hubbard model," *Phys. Rev. B*, vol. 96, p. 085104, 2017.

[33] M. A. Sentef, A. F. Kemper, A. Georges, and C. Kollath, "Theory of light-enhanced phonon-mediated superconductivity," *Phys. Rev. B*, vol. 93, p. 144506, 2016.

[34] M. Knap, M. Babadi, G. Refael, I. Martin, and E. Demler, "Dynamical Cooper pairing in nonequilibrium electron-phonon systems," *Phys. Rev. B*, vol. 94, p. 214504, 2016.

[35] T. Kaneko, T. Shirakawa, S. Sorella, and S. Yunoki, "Photoinduced η pairing in the Hubbard model," *Phys. Rev. Lett.*, vol. 122, p. 077002, 2019.

[36] M. A. Sentef, A. Tokuno, A. Georges, and C. Kollath, "Theory of laser-controlled competing superconducting and charge orders," *Phys. Rev. Lett.*, vol. 118, p. 087002, 2017.

[37] D. M. Kennes, E. Y. Wilner, D. R. Reichman, and A. J. Millis, "Transient superconductivity from electronic squeezing of optically pumped phonons," *Nat. Phys.*, vol. 13, pp. 479–483, 2017.

[38] Y. Murakami, N. Tsuji, M. Eckstein, and P. Werner, "Nonequilibrium steady states and transient dynamics of conventional superconductors under phonon driving," *Phys. Rev. B*, vol. 96, p. 045125, 2017.

[39] M. W. Cook and S. R. Clark, "Controllable finite-momenta dynamical quasicondensation in the periodically driven one-dimensional Fermi-Hubbard model," *Phys. Rev. A*, vol. 101, p. 033604, 2020.

[40] M. Messer, K. Sandholzer, F. Görg, J. Minguzzi, R. Desbuquois, and T. Esslinger, "Floquet dynamics in driven Fermi-Hubbard systems," *Phys. Rev. Lett.*, vol. 121, p. 233603, 2018.

[41] N. Tancogne-Dejean, M. A. Sentef, and A. Rubio, "Ultrafast modification of Hubbard u in a strongly correlated material: Ab initio high-harmonic generation in NiO," *Phys. Rev. Lett.*, vol. 121, p. 097402, 2018.

[42] T. Ishikawa, Y. Sagae, Y. Naitoh, Y. Kawakami, H. Itoh, K. Yamamoto, K. Yakushi, H. Kishida, T. Sasaki, S. Ishihara, Y. Tanaka, K. Yonemitsu, and S. Iwai, "Optical freezing of charge motion in an organic conductor," *Nat. Comm.*, vol. 5, p. 5528, 2014.

[43] S. Wall, D. Brida, S. R. Clark, H. P. Ehrke, D. Jaksch, A. Ardavan, S. Bonora, H. Uemura, Y. Takahashi, T. Hasegawa, H. Okamoto, G. Cerullo, and A. Cavalleri, "Quantum interference between charge excitation paths in a solid-state Mott insulator," *Nat. Phys.*, vol. 7, pp. 114–118, 2011.

[44] R. Singla, G. Cotugno, S. Kaiser, M. Först, M. Mitrano, H. Y. Liu, A. Cartella, C. Manzoni, H. Okamoto, T. Hasegawa, S. R. Clark, D. Jaksch, and A. Cavalleri, "THz-frequency modulation of the Hubbard u in an organic Mott insulator," *Phys. Rev. Lett.*, vol. 115, p. 187401, 2015.

[45] L. D'Alessio and M. Rigol, "Long-time behavior of isolated periodically driven interacting lattice systems," *Phys. Rev. X*, vol. 4, p. 041048, 2014.

[46] P. Ponte, A. Chandran, Z. Papić, and D. A. Abanin, "Periodically driven ergodic and many-body localized quantum systems," *Ann. Phys.*, vol. 353, pp. 196–204, 2015.

[47] H. Zhai, "Two generalizations of η pairing in extended Hubbard models," *Phys. Rev. B*, vol. 71, p. 012512, 2005.

[48] C. N. Yang, "η pairing and off-diagonal long-range order in a Hubbard model," *Phys. Rev. Lett.*, vol. 63, pp. 2144–2147, 1989.

[49] G. L. Sewell, "Off-diagonal long-range order and the Meissner effect," *J. Stat. Phys.*, vol. 61, pp. 415–422, 1990.

[50] H. T. Nieh, G. Su, and B.-H. Zhao, "Off-diagonal long-range order: Meissner effect and flux quantization," *Phys. Rev. B*, vol. 51, pp. 3760–3764, 1995.

[51] P. Woit, *Quantum Theory, Groups and Representations: An Introduction.* Springer International Publishing, New York, 2017.

[52] A. Barut and R. Raczka, *Theory of Group Representations and Applications.* Polish Scientific Publishers, Warsaw, 1980.

[53] D. F. Bailey, "Counting arrangements of 1s and -1s," *Math. Mag.*, vol. 69, pp. 128–131, 1996.

[54] C. N. Yang, "Concept of off-diagonal long-range order and the quantum phases of liquid He and of superconductors," *Rev. Mod. Phys.*, vol. 34, pp. 694–704, 1962.

[55] J. Cui, J. I. Cirac, and M. C. Bañuls, "Variational matrix product operators for the

steady state of dissipative quantum systems," *Phys. Rev. Lett.*, vol. 114, p. 220601, 2015.

[56] W. M. Itano, D. J. Heinzen, J. J. Bollinger, and D. J. Wineland, "Quantum Zeno effect," *Phys. Rev. A*, vol. 41, pp. 2295–2300, 1990.

[57] J. Tindall, B. Buča, J. R. Coulthard, and D. Jaksch, "Heating-induced long-range η pairing in the Hubbard model," *Phys. Rev. Lett.*, vol. 123, p. 030603, 2019.

[58] E. H. Lieb, "Two theorems on the Hubbard model," *Phys. Rev. Lett.*, vol. 62, pp. 1201–1204, 1989.

[59] S.-Q. Shen, Z.-M. Qiu, and G.-S. Tian, "Ferrimagnetic long-range order of the Hubbard model," *Phys. Rev. Lett.*, vol. 72, pp. 1280–1282, 1994.

[60] H. Yoshida and H. Katsura, "Rigorous results on the ground state of the attractive SU(n) Hubbard model," *Phys. Rev. Lett.*, vol. 126, p. 100201, Mar 2021.

[61] J. Tindall, F. Schlawin, M. Sentef, and D. Jaksch, "Lieb's theorem and maximum entropy condensates," *arXiv Preprint: cond-mat.str-el/2103.04687*, 2021.

[62] A. Klein, M. Bruderer, S. R. Clark, and D. Jaksch, "Dynamics, dephasing and clustering of impurity atoms in Bose–Einstein condensates," *New J. Phys.*, vol. 9, p. 411, 2007.

[63] M. Bruderer, A. Klein, S. R. Clark, and D. Jaksch, "Polaron physics in optical lattices," *Phys. Rev. A*, vol. 76, p. 011605, 2007.

[64] M. Theis, G. Thalhammer, K. Winkler, M. Hellwig, G. Ruff, R. Grimm, and J. H. Denschlag, "Tuning the scattering length with an optically induced Feshbach resonance," *Phys. Rev. Lett.*, vol. 93, p. 123001, 2004.

[65] S. Inouye, M. R. Andrews, J. Stenger, H.-J. Miesner, D. M. Stamper-Kurn, and W. Ketterle, "Observation of Feshbach resonances in a Bose–Einstein condensate," *Nature*, vol. 392, pp. 151–154, 1998.

[66] M. F. Parsons, A. Mazurenko, C. S. Chiu, G. Ji, D. Greif, and M. Greiner, "Site-resolved measurement of the spin-correlation function in the Fermi-Hubbard model," *Science*, vol. 353, no. 6305, pp. 1253–1256, 2016.

[67] A. Kantian, A. J. Daley, and P. Zoller, "η condensate of Fermionic atom pairs via adiabatic state preparation," *Phys. Rev. Lett.*, vol. 104, p. 240406, Jun 2010.

[68] M. Mitrano, A. Cantaluppi, D. Nicoletti, S. Kaiser, A. Perucchi, S. Lupi, P. Di Pietro, D. Pontiroli, M. Riccò, S. Clark, D. Jaksch, and A. Cavalleri, "Possible light-induced superconductivity in K_3C_{60} at high temperature," *Nature*, vol. 530, pp. 461–464, 2016.

[69] D. Fausti, R. I. Tobey, N. Dean, S. Kaiser, A. Dienst, M. C. Hoffmann, S. Pyon, T. Takayama, H. Takagi, and A. Cavalleri, "Light-induced superconductivity in a stripe-ordered cuprate," *Science*, vol. 331, pp. 189–191, 2011.

[70] W. Hu, S. Kaiser, D. Nicoletti, C. R. Hunt, I. Gierz, M. C. Hoffmann, M. Le Tacon, T. Loew, B. Keimer, and A. Cavalleri, "Optically enhanced coherent transport in $YBa_2Cu_3O_{6.5}$ by ultrafast redistribution of interlayer coupling," *Nat. Mat.*, vol. 13, pp. 705–711, 2014.

[71] D. Nicoletti, E. Casandruc, Y. Laplace, V. Khanna, C. R. Hunt, S. Kaiser, S. S. Dhesi, G. D. Gu, J. P. Hill, and A. Cavalleri, "Optically induced superconductivity in striped $La_{2-x}Ba_xCuO_4$ by polarization-selective excitation in the near infrared," *Phys. Rev. B*, vol. 90, p. 100503, 2014.

[72] M. Budden, T. Gebert, M. Buzzi, G. Jotzu, E. Wang, T. Matsuyama, G. Meier, Y. Laplace, D. Pontiroli, M. Riccò, F. Schlawin, D. Jaksch, and A. Cavalleri, "Evidence for metastable photo-induced superconductivity in K_3C_{60}," *Nat. Phys.*, 2021.

[73] K. A. Cremin, J. Zhang, C. C. Homes, G. D. Gu, Z. Sun, M. M. Fogler, A. J. Millis, D. N. Basov, and R. D. Averitt, "Photoenhanced metastable c-axis electrodynamics in stripe-ordered cuprate $La_{1.885}Ba_{0.115}CuO_4$," *Proc. Natl. Acad. Sci.*, vol. 116, pp. 19875–19879, 2019.

[74] A. Cantaluppi, M. Buzzi, G. Jotzu, D. Nicoletti, M. Mitrano, D. Pontiroli, M. Riccò, A. Perucchi, P. Di Pietro, and A. Cavalleri, "Pressure tuning of light-induced superconductivity in K_3C_{60}," *Nat. Phys.*, vol. 14, pp. 837–841, 2018.

[75] D. Nicoletti and A. Cavalleri, "Nonlinear light–matter interaction at terahertz frequencies," *Adv. Opt. Photon.*, vol. 8, pp. 401–464, 2016.

Chapter 4

Dynamical Superconductivity in a Frustrated Many-Body System

A number of the results in this chapter were first published as

- M. Buzzi, D. Nicoletti, M. Fechner, N. Tancogne-Dejean, MA. Sentef, A. Georges, M. Dressel, A. Henderson, T. Siegrist, J.A. Schlueter, K. Miyagawa, K. Kanoda, M-S. Nam, A. Ardavan, J. Coulthard, J. Tindall, F. Schlawin, D. Jaksch, A. Cavalleri, *Photo-molecular high temperature superconductivity*, Physical Review X, **10** (2020)
- J. Tindall, F. Schlawin, M. Buzzi, D. Nicoletti, JR. Coulthard, H. Gao, A. Cavalleri, M.A Sentef and D. Jaksch, *Dynamical Superconductivity in a Frustrated Many-Body System*, Physical Review Letters, **123** (2020)

Contributions to these papers from JT are listed in the introduction.

In this chapter we investigate the mechanism of heating-induced order in a driven, two-rung triangular Hubbard lattice. Our motivation comes from both the opportunity to study the out-of-equilibrium dynamics of a frustrated many-body system and a recent experiment that transiently observes superconductivity by photo-exciting the vibrational modes of the charge transfer salt $\kappa - (\mathrm{BEDT} - \mathrm{TTF})_2\mathrm{Cu}[\mathrm{N}(\mathrm{CN})_2]\mathrm{Br}$.

We begin the chapter by introducing this experiment: discussing its motivation, setup and the key observations made. We then provide a simplified description of the transfer salt's Hamiltonian via a quasi-1D triangular Hubbard lattice. By performing Density Matrix Renormalization Group (DMRG) calculations on this Hamiltonian we uncover several unique ground-state phases separated by first-order transitions. A time-dependence is then introduced into the Hamiltonian, which is reflective of the excitation of the phonon modes in $\kappa - (\mathrm{BEDT} - \mathrm{TTF})_2\mathrm{Cu}[\mathrm{N}(\mathrm{CN})_2]\mathrm{Br}$. We study the properties of the system as these ground-state phases are driven out-of-equilibrium

by this time-dependence. Within one of these phases we observe the dynamical formation of uniform particle-hole correlations despite the lattice lacking the requisite η SU(2) symmetry. This remarkable result originates from the interplay between the driving and irregular geometry of the lattice which effectively causes the particle-hole excitation channel to shut down, allowing the mechanism of heating-induced order to occur. We discuss how the particle-hole correlations induced via this unique pathway may therefore be connected with the experimental observation of light-induced superconductivity in $\kappa - (\mathrm{BEDT} - \mathrm{TTF})_2\mathrm{Cu}[\mathrm{N}(\mathrm{CN})_2]\mathrm{Br}$. More generally, these results lead to the exciting possiblity of observing such rich dynamical behaviour in other systems which possess complex, non-hypercubic geometries.

4.1 Photo-Induced Superconductivity in $\kappa - (\mathrm{BEDT} - \mathrm{TTF})_2\mathrm{Cu}[\mathrm{N}(\mathrm{CN})_2]\mathrm{Br}$

Background

In the last decade, a number of experiments have been performed which subject specific phonon modes of strongly correlated materials to intense THz laser pulses, dynamically altering the material's electronic degrees of freedom and inducing a number of striking non-equilibrium properties [1, 2, 3, 4, 5, 6, 7, 8]. Measurements taken following this excitation have then indicated the presence of superconducting-like features such as perfect reflectivity, vanishing resistivity and an inverse-frequency divergence of the imaginary part of the optical conductivity. These induced features typically decay away over a timescale on the order of several picoseconds and, remarkably, appear when exciting the material at temperatures well above their equilibrium critical temperature T_c.

These results have opened up a new route to achieving superconductivity in solid-state systems and have moved researchers closer to the distant, tantalising goal of creating a room temperature superconductor. Theoretical attempts to understand these observations of light-induced superconductivity have identified a number of possible mechanisms that could be involved. For example, it has been suggested that the light field directly melts away order which competes with and suppresses the superconductivity in the system [9, 10, 11]. Other approaches have discussed the possibility of the laser field reducing the phase fluctuations that prevent superconductivity [12] or, alternatively, energetically overcoming the Coulomb interaction and creating attraction and pairing between fermions in the material [13]. None of

these approaches, however, successfully explain how this remarkable phenomenon of 'light-induced superconductivity' occurs in such a variety of different materials and experimental setups.

In this chapter we focus on a recent experiment observing light-induced superconductivity [14] in the compound $\kappa-(\mathrm{BEDT}-\mathrm{TTF})_2\mathrm{Cu}[\mathrm{N}(\mathrm{CN})_2]\mathrm{Br}$. We take the Hubbard model on a quasi-1D triangular lattice as a simplified description of the photo-excited material and identify a unique pathway, based on the geometry of the system, by which the mechanism of heating-induced order can occur in the presence of an intense laser field. Our results draw a possible connection between this mechanism and the superconducting observations of this recent experiment. More generally, our results provide an understanding of how lattice geometry can create unique pathways for realising ordered states under driving. We discuss how this should apply in a range of driven systems which possess complex, non-hypercubic lattice structures and not just the lattice considered here.

Experiment and Numerical Model

In the experiment of Ref. [14], specific vibrational modes of the organic charge transfer salt $\kappa-(\mathrm{BEDT}-\mathrm{TTF})_2\mathrm{Cu}[\mathrm{N}(\mathrm{CN})_2]\mathrm{Br}$ (which we will shorten to $\kappa-\mathrm{Br}$) were excited with intense, mid-infrared radiation. Following excitation of the molecular crystal, a number of signatures of superconductivity were observed: perfect reflectivity of low frequency radiation, an opening of a gap in the real part of the optical conductivity and an inverse frequency divergence of the imaginary part of the optical conductivity. These features were observed at temperatures several times higher than the crystal's critical temperature $T_c = 12.5K$ and, additionally, the opening of a gap in the real part of the optical conductivity is not a feature seen when cooling the molecule below T_c. This suggests a distinctively different superconducting mechanism is at play compared to that which occurs upon lowering the material's temperature.

The geometry and equilibrium properties of organic compounds of the form $\kappa-\mathrm{X}$ have been studied extensively due to the superconducting properties of these materials when in equilibrium [15, 16, 17, 18]. The molecule $\kappa-\mathrm{Br}$ has the largest T_c in this family. In $\kappa-\mathrm{Br}$, whose structure is pictured in Fig. 4.1, the $\mathrm{BEDT}-\mathrm{TTF}$ molecules form dimers which create conducting layers perpendicular to insulating layers of $\mathrm{Cu}[\mathrm{N}(\mathrm{CN})_2]\mathrm{Br}$ molecules. Within these conducting in-plane layers, the dimerised $\mathrm{BEDT}-\mathrm{TTF}$ molecules form a triangular lattice structure which is well described by a Hubbard model with on-dimer interaction strength U and two hopping strengths J and J' [19, 20, 21].

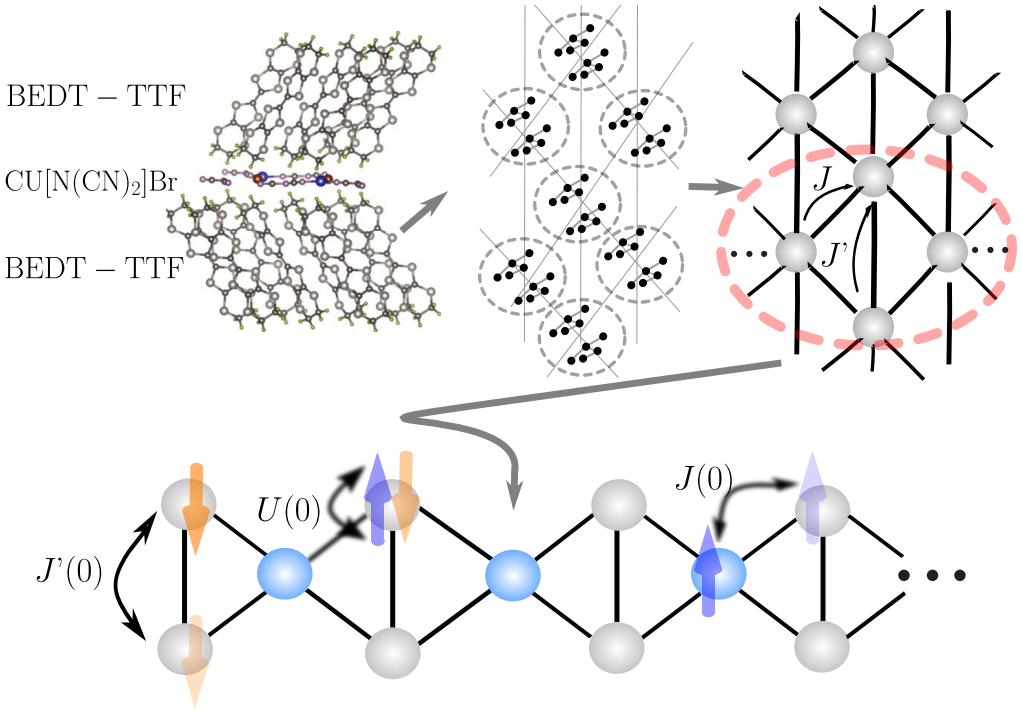

Figure 4.1: Successively zoomed in snapshots of the molecule $\kappa-(\mathrm{BEDT-TTF})_2\mathrm{Cu[N(CN)_2]Br}$. Top Left) Reproduced from Ref. [14], layered structure of the molecular compound $\kappa-(\mathrm{BEDT-TTF})_2\mathrm{Cu[N(CN)_2]Br}$. Top middle) Bird's eye view of a single layer of $\mathrm{BEDT-TTF}$ with pairs of BEDT-TTF molecules circled. Top right) The pairs of $\mathrm{BEDT-TTF}$ molecules form dimers which can be approximated as the sites of a triangular Hubbard lattice with competing hopping strengths J' and J. Bottom) A single extensive axis of the triangular Hubbard model is then taken to form a numerically tractable model for the experiment in Ref. [14]

.

For the experiment in Ref. [14] the drastic change in the material properties were observed from in-plane conductivity measurements and, hence, to form a tractable, theoretical model we focus on a single layer of the $\mathrm{BEDT-TTF}$ dimers, describing it with a triangular Hubbard Hamiltonian. We further simplify our model by restricting the triangular geometry to be extensive in only a single dimension; the lattice sites can then be reordered into a one-dimensional Hubbard chain which will be amenable to Matrix Product State algorithms.

In Fig. 4.1 we picture this simplification process for modelling the conducting layer of $\kappa-(\mathrm{BEDT-TTF})_2\mathrm{Cu[N(CN)_2]Br}$. We first sketch the full molecular structure of the compound and then successively zoom in on: a single layer of $\mathrm{BEDT-TTF}$ molecules, the dimerized triangular Hubbard structure they form and the single axis

triangular Hubbard model we use in this work. The Hamiltonian for this model is

$$H = -J(0) \sum_{ij\in\langle \text{diag}\rangle,\sigma} (c^{\dagger}_{\sigma,i} c_{\sigma,j} + \text{H.c}) \; - J'(0) \sum_{ij\in\langle \text{vert}\rangle,\sigma} (c^{\dagger}_{\sigma,i} c_{\sigma,j} + \text{H.c}) + U(0) \sum_{i} n_{i,\uparrow} n_{i,\downarrow}, \tag{4.1}$$

where the fermionic operators are defined in the same manner as the previous chapter and we opt to use the indices i and j to refer to the sites of the lattice. The first summation in Eq. (4.1) runs over the sites coupled by a diagonal bond and the second runs over those coupled by a vertical bond (see Fig. 4.1)). The final term runs over all the lattice sites and represents a homogeneous on-site interaction term of strength $U(0)$. We refer to the sites along the outside of the lattice (grey sites, Fig. 4.1) as 'outer' sites and the remaining sites as 'centre' sites.

4.2 Simulation of the Driven Quasi-1D Triangular Hubbard Lattice

Ground State Properties

Before we simulate any dynamics, it is important to explore the properties of the ground state of the Hamiltonian, as this is the state which will be driven out of equilibrium by phonon excitation. Whilst the experiment was performed at a small finite temperature, here we will assume that $T = 0$K in order to simplify our numerical calculations. We can then apply the Density Matrix Renormalization Group (DMRG) algorithm [23] to the Hamiltonian in Eq. (4.1), adapting the algorithm to include the next nearest-neighbour hopping term which appears in the Hamiltonian [24]. With these calculations we can observe the ground state properties of the system as a function of U and J' for system sizes much larger than those available with exact diagonalisation routines.

To aid our analysis we reintroduce the Hubbard spin and η operators $S^{\pm} = \sum_i s_i^{\pm,z}$ and $\eta^{\pm} = \sum_i f(i)\eta_i^{\pm}$ from the previous chapter, where we have set the function $f(i)$ to take the value +1 (-1) depending on whether the site i is a central or outer site. Using the spin operators, the following structure factors can be defined

$$S_{\pm}(q) = \sum_{jk} e^{\mathrm{i}(j-k)q} \langle S_j^{+} S_k^{-} \rangle, \qquad S_z(q) = \sum_{jk} e^{\mathrm{i}(j-k)q} \langle S_j^{+} S_k^{-} \rangle, \tag{4.2}$$

where the quasi-momentum q ranges in discrete steps of $(2\pi/L)$ from $-\pi$ to π. We also utilise the distance dependent order parameter from the previous chapter

$$O(\delta) = \frac{1}{\mathcal{N}} \sum_{\substack{\langle i,j \rangle \\ d(i,j)=\delta}} \langle O_i^+ O_j^- \rangle, \tag{4.3}$$

where O can now be η, S or S^z (for the latter we simply set $O^+ = O^- = S^z$) — with $d(i,j)$ referring to the shortest path (by traversal of the edges/ black bonds in Fig. 4.1) between sites i and j. The quantity $\overline{|O(\delta)|}_{\delta>l}$ is then, as before, the magnitude of the average of these two-point correlations over distances greater than l.

In Fig. 4.2 we plot the quantities $\langle S^+S^- \rangle$ and $\langle \eta^+\eta^- \rangle$ for a range of U and J'. The operator S^+S^- is a symmetry of the Hubbard Hamiltonian on any graph (even in the presence of inhomogeneous hopping), and this leads to the ground state of the system possessing discrete values of $\langle S^+S^- \rangle$ which coincide with the eigenvalues of S^+S^-. Meanwhile, $\eta^+\eta^-$ is not a symmetry of the system (aside from the limiting bi-partite case $J'(0) = 0$) and so the ground state possesses non-discrete values of $\langle \eta^+\eta^- \rangle$. The upper plots in Fig. 4.2 demonstrate a rich phase diagram in the quantities $\langle \eta^+\eta^- \rangle$ and $\langle S^+S^- \rangle$ and through this plot we identify three key equilibrium phases of the system, I, II and III. In the remainder of Fig. 4.2 we analyse the magnetic observables which characterise these phases.

Within phase I the ground state of the system resides in the lowest eigenspace of $\langle \eta^+\eta^- \rangle$ despite the corresponding operator not being conserved. Here, the system displays the properties of a spin-wave condensate through the large value of $\langle S^+S^- \rangle$ which is underpinned by long-range spin-exchange order and a sharp zero-momentum peak in the corresponding structure factor. There are, additionally, two peaks of opposite momenta which correspond to interference in the condensate order. This interference comes from the reduced correlations between the central and outer sites of the lattice, which are significantly suppressed compared to those solely in the outer sites of the lattice.

As $J'(0)$ increases, the value of the condensate order parameter $\langle S^+S^- \rangle$ jumps discontinuously and there is a spontaneous SU(2) symmetry breaking as the system transitions into phase II. In this phase, some of the vertically-bonded sites localise and form singlets separate from the rest of the system, depleting the condensate order observed in the previous phase. For even higher $J'(0)$ the system undergoes another transition into phase III. Here, the vertical hopping is sufficiently large to create a spin-dimerized phase where all the vertically-bonded sites form singlets decoupled from the central sites and the condensate is completely depleted.

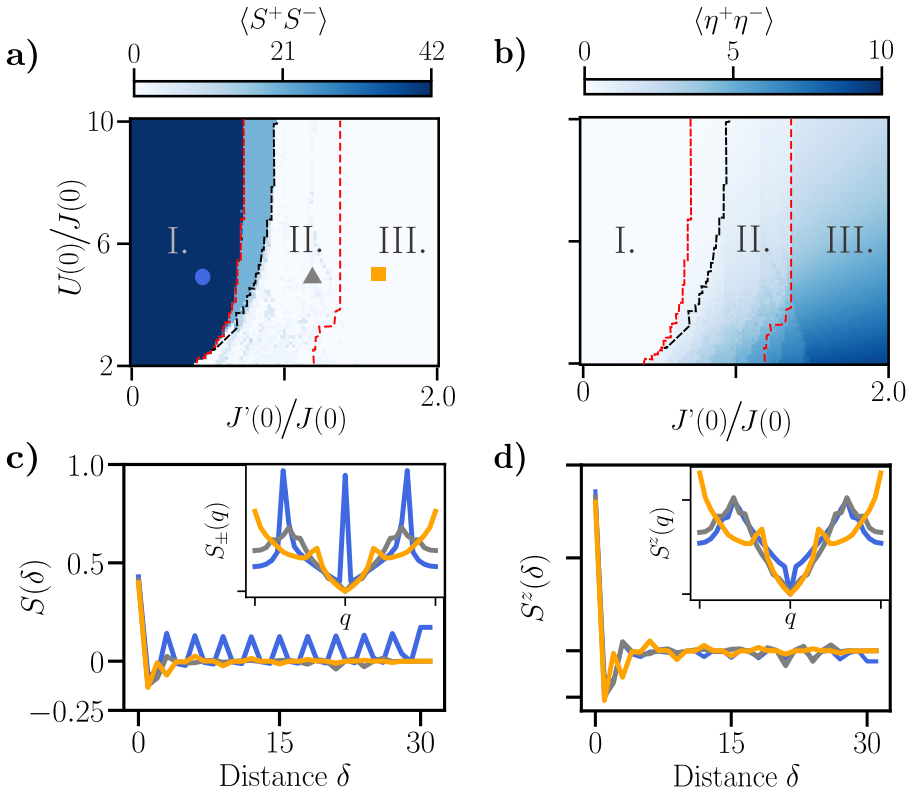

Figure 4.2: a-b) Expectation value of $\langle S^+S^-\rangle$ and $\langle \eta^+\eta^-\rangle$ for the ground state of the half-filled $L = 32$ two-rung triangular Hubbard model, see Eq. (4.1), as a function of $U(0)$ and $J'(0)$. The red dotted lines separate the three distinct phases/regions — I, II and III — observed for this system size. Their properties are described in the text. In the thermodynamic limit the width of region I changes and the I - II transition instead occurs along the black dotted line. c-d) Spin-exchange $S(\delta)$ and magnetic $S_z(\delta)$ correlations, see Eq. (4.3), versus distance δ. Insets) Spin-exchange and magnetic structure factors, see Eq. (4.2), versus quasi-momenta q. The blue, grey and orange lines correspond, respectively, to the points in phases I, II and III marked on the top left plot.

These results were calculated for a system with $L = 32$ lattice sites. It is important to determine whether the distinct phases we have observed persist in the thermodynamic limit $L \to \infty$. Whilst we cannot directly perform calculations in this limit, we can perform a finite-size scaling analysis (FSA) and extrapolate. In Fig. 4.3 we do exactly this, focussing on the value $U(0) = 5.0J(0)$ and plotting various ground state quantities for a range of L and $J'(0)$. Crucially, we observe 3 discontinuous jumps in these quantities, pointing to the existence of several first-order phase transitions. The first discontinuity appears around $J'(0) = 0.69J(0)$ and is diminishing with L,

whilst the size of the second and third, which occur at around $J'(0) = 0.9J(0)$ and $J'(0) = 1.35J(0)$, appear to be stable or increasing with system size. This suggests that the latter two points are first-order transitions in the thermodynamic limit and we can associate these with the transitions $\mathrm{I} - \mathrm{II}$ and $\mathrm{II} - \mathrm{III}$. We therefore expect as $L \to \infty$ the $\mathrm{I} - \mathrm{II}$ transition will move from the red-dotted line in Fig. 4.2 to the black-dotted line and the properties of the system in the light-blue region will converge from those in phase II to those in phase I. This is evidenced in Fig. 4.3 where we plot the spin-wave condensate parameter $\langle S^+S^-\rangle$ and observe this approach directly, finding an exact polynomial fit for this quantity as a function of system size.

Fig. 4.3 shows that the order parameter $\langle S^+S^-\rangle/L^2$ will be finite in phase I in the thermodynamic limit before discontinuously jumping to 0 as $J'(0)$ moves across the $\mathrm{I} - \mathrm{II}$ transition line. At $J'(0) = 0$, the value of $\langle S^+S^-\rangle/L^2$ is in direct agreement with Lieb's theorem for the ground state spin of unbalanced[1] bi-partite lattices [25]. The properties of the ground state of the system at this point, i.e. a staggered, long-range correlation pattern along the spin x and y axes can be attributed to this finite value and are consistent with the long-range ferrimagnetic correlations which have previously been observed in the ground state of unbalanced bi-partite lattices [26, 27]. Such properties are not possible in hypercubic Hubbard lattices as the ground state always satisfies $\langle S^+S^-\rangle = 0 \ \ \forall L$ and are directly tied to the unbalanced nature of the system.

Remarkably, we find that in our system the finite value of $\langle S^+S^-\rangle/L^2$, and the related long-range ferrimagnetic correlations, persist for all finite $J'(0) < 0.9J(0)$. Thus it appears that some aspects of Lieb's theorem are clearly still manifest even in this frustrated, non-bipartite regime. In the following we will see that this has important ramifications when the system is driven out of equilibrium.

Out-of-Equilibrium Dynamics

In Ref. [14], density functional theory (DFT) [28, 29] was applied to the triangular lattice description of the dimerised $\mathrm{BEDT} - \mathrm{TTF}$ molecules and used to determine its ground state and band structure. By fitting a tight-binding, single band model to these results the effective Hubbard parameters $J(0), J'(0)$ and $U(0)$ were determined and found to be consistent with previous literature [15]. Following this, the phonon modes of the isolated $\mathrm{BEDT} - \mathrm{TTF}$ dimers were determined and, by systematically

[1] Unbalanced in the sense that the number of sites in the two sublattices are unequal.

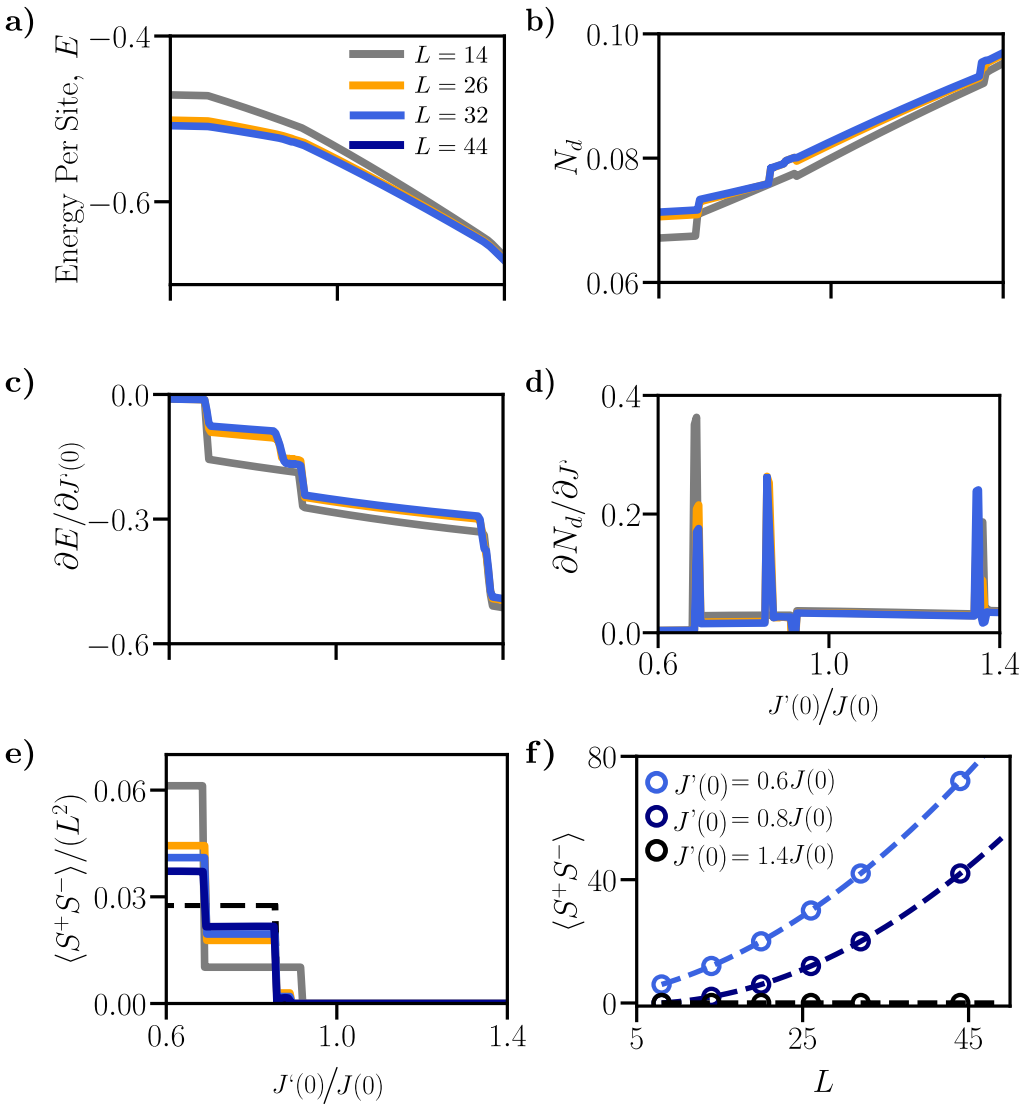

Figure 4.3: a-b) Energy per site and average doublon occupancy N_d versus $J'(0)$ for the ground state of the half-filled two-rung triangular Hubbard model described in Eq. (4.1) with $U(0) = 5.0J(0)$. Several system sizes are plotted. c-d) Derivative of the above plots with respect to $J'(0)$. e) $\langle S^+S^- \rangle/L^2$ versus $J'(0)$. The black dotted line in the top right plot is an extrapolation to the thermodynamic limit. f) Scaling of $\langle S^+S^- \rangle$ with L for several $J'(0)$. Dotted Lines correspond to the polynomials $\langle S^+S^- \rangle = L^2/36 + 7L/18 + 10/9$, $\langle S^+S^- \rangle = L^2/36 - 5L/18 + 4/9$ and $\langle S^+S^- \rangle = 0$ for the respective $J'(0)$.

displacing the ionic co-ordinates of the system, the electronic parameters of the single band Hamiltonian were recalculated based on this translated lattice structure. Through these calculations it was found that, when certain vibrational modes are excited, the electronic parameters $J(0)$ and $U(0)$ vary quadratically with the induced displacement whilst $J'(0)$ is affected minimally. The phonon modes are treated as

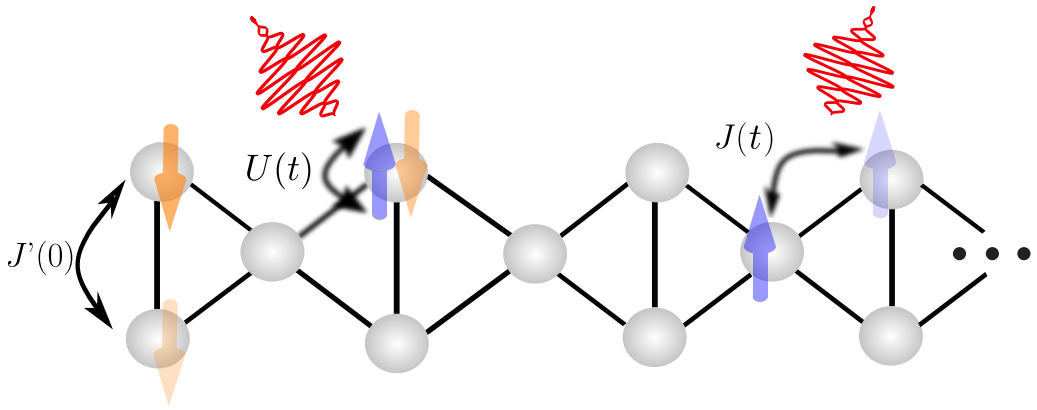

Figure 4.4: Time-dependent two-rung triangular Hubbard system, see Eqs. (4.4) and (4.5), used to model the THz irradiation of the organic compound $\kappa-\mathrm{Br}$ [14].

harmonic oscillators and so the displacement induced by the laser field is taken to be a sinusoidal function of time with a frequency Ω.

With this information we can write down an effective non-equilibrium version of our single axis triangular Hamiltonian

$$H(t) = -J(t) \sum_{ij\in\langle \mathrm{diag}\rangle,\sigma} (c^{\dagger}_{\sigma,i}c_{\sigma,j} + \mathrm{H.c}) \; - J'(0) \sum_{ij\in\langle \mathrm{vert}\rangle,\sigma} (c^{\dagger}_{\sigma,i}c_{\sigma,j} + \mathrm{H.c}) + U(t) \sum_{i} n_{i,\uparrow}n_{i,\downarrow}, \tag{4.4}$$

which reflects the effect the intense THz radiation, and the ensuing vibrational excitations, had on the $\kappa-\mathrm{Br}$ compound in Ref [14]. The introduced time-dependence in Eq. (4.4) is of the form

$$\begin{aligned} J(t) &= J(0)\big(1 + A_J \sin^2(\Omega t) \exp\big(-(t-T_p)^2/(2T_w^2)\big)\big), \\ U(t) &= U(0)\big(1 + A_U \sin^2(\Omega t) \exp\big(-(t-T_p)^2/(2T_w^2)\big)\big), \end{aligned} \tag{4.5}$$

where the constants A_U and A_J are the amplitudes of the modulation of U and J relative to their equilibrium values. The frequency of the oscillations is Ω, whilst T_p and T_w describe the offset and width of the Gaussian envelope containing these oscillations — which has been incorporated to reflect the limited duration and strength of the laser pulse used in the experiment. In Fig. 4.4 we picture this non-equilibrium version of the Hamiltonian and the vibrational excitation of the system due to the external driving.

Whilst the driving in Eq. (4.5), when the appropriate parameters are used, reflects the experiment in Ref. [14] we emphasize that it also describes a fairly general periodic time-dependence of the Hamiltonian parameters. We are always free to fix

one parameter of a Hamiltonian and so the lack of a time-dependence on J' is inconsequential. We therefore stress that the results we will present here extend beyond their relationship to the experiment on $\kappa - \mathrm{Br}$ and have important consequences for our understanding of the dynamical behaviour of irregular, non-hypercubic frustrated lattice structures.

In order to interpret our numerical results in the context of the mechanism of heating-induced order, we need to know the symmetry structure of the time-dependent Hamiltonian in Eq. (4.4). The following relations are obeyed by $H(t)$

$$\begin{aligned} &[H(t), S^{\pm,z}] = [H(t), \eta^z] = 0 \ \forall t, \\ &[H(t), \eta^+\eta^-] \propto J'(0), \end{aligned} \tag{4.6}$$

where the lack of commutation with $\eta^+\eta^-$ is a direct result of the 'vertical' hopping term $H_{\mathrm{V}} = \sum_{ij\in\langle \mathrm{vert}\rangle,\sigma}(c^\dagger_{\sigma,i}c_{\sigma,j} + \mathrm{h.c})$ which disrupts the bi-partite nature of the lattice. Equation (4.6) tells us that the driven system has a permanent SU(2) spin symmetry but no SU(2) η symmetry outside of the limiting case $J'(0) = 0$.

In the previous chapter we showed how the initial state condition $\langle S^+S^-\rangle \propto L^2$ is necessary for the manifestation of uniform, finite long-range spin-exchange order in the thermodynamic limit under heating which preserves the spin SU(2) symmetry. The plots in Fig. 4.3 indicate that the ground state for $J'(0) < J'(0)_c$ satisfies this condition and we can therefore expect the driving to rearrange the staggered ground state correlations seen in Fig. 4.2, making them completely uniform with distance and allowing the system to form a spin-wave condensate without the interference pattern. Meanwhile, in the particle-hole sector the absence of the requisite symmetry means we should expect that, for any system size, the particle-hole correlations will decay to zero as the system heats up under the driving.

We investigate this directly in Fig. 4.5, applying the time-evolving-block-decimation (TEBD) algorithm [30] — adapted to include next-nearest-neighbour hopping — to drive the system out of the ground state with a strong pulse of unlimited duration. The dynamics in the spin-exchange sector is what we expect, with the staggered correlations reorganising themselves to be relatively uniform with distance. The fact that they are not exactly uniform is due to the limitations on the time-scales we are able to reach with our numerics. Nonetheless, we can see that this uniform order is forming and, moreover, our analytical works from the previous chapter tell us that in the thermodynamic limit this order will take the value $S(\delta) = 1/36$. The driving has established completely uniform ODLRO and fixed any imperfections in the spin-wave nature of the ground state.

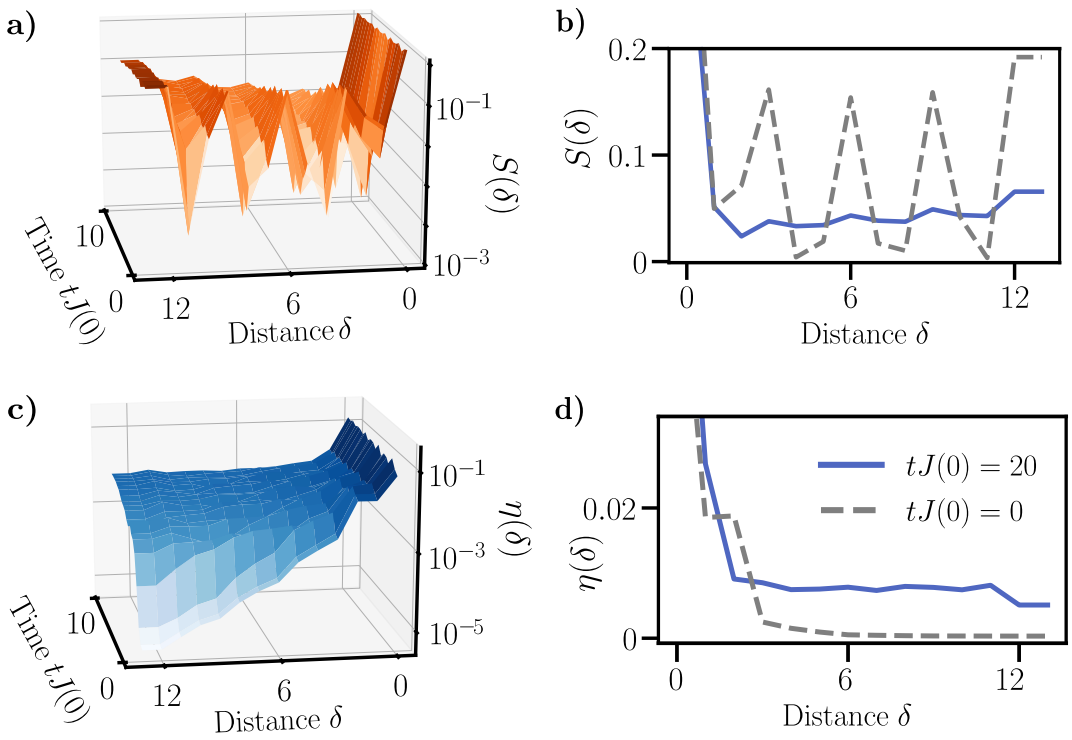

Figure 4.5: Spin-exchange and particle-hole order versus time and distance for the strongly driven two-rung triangular Hubbard model. The system is initialised in the half-filled ground state of Eq. (4.1) with $U(0) = 5J(0)$ and $J'(0) = 0.2J(0)$ and then time evolved under the driven Hamiltonian in Eq. (4.4) with $A_U = 2A_J = 0.7$, $\Omega J(0) = 2.5$, $T_w = \infty$ and $T_p = 0$. a) Spin-exchange order versus distance and time. b) Spin-exchange order versus distance for the two times $tJ(0) = 0$ and $tJ(0) = 20$. c) Particle-hole order versus distance and time. d) Particle-hole order versus distance for the same two times as b).

Meanwhile, in contrast to the spin dynamics, the system's response in the particle-hole sector is completely unexpected. There has been a colossal amplification in the long-range particle-hole correlations and uniform off-diagonal order has begun to form in this sector despite the fact the lattice is not bi-partite and the time-dependent Hamiltonian does not possess an η SU(2) symmetry. This is in direct contradiction to our symmetry-based predictions.

We investigate this remarkable result further by varying the value of $J'(0)$ and plotting the dynamical response of the key observables in the particle-hole channel, alongside the impact the vertical hopping term H_V (which should directly break the η symmetry) has on the state of the system. We plot our observations in Fig. 4.6 and find that there is a critical value $J'(0)_c \approx 0.69J(0)$ of the vertical hopping strength $J'(0)$ beneath which particle-hole excitations are prevented and the system acts as if it has an approximate η SU(2) symmetry. The heating from the driving induces off-

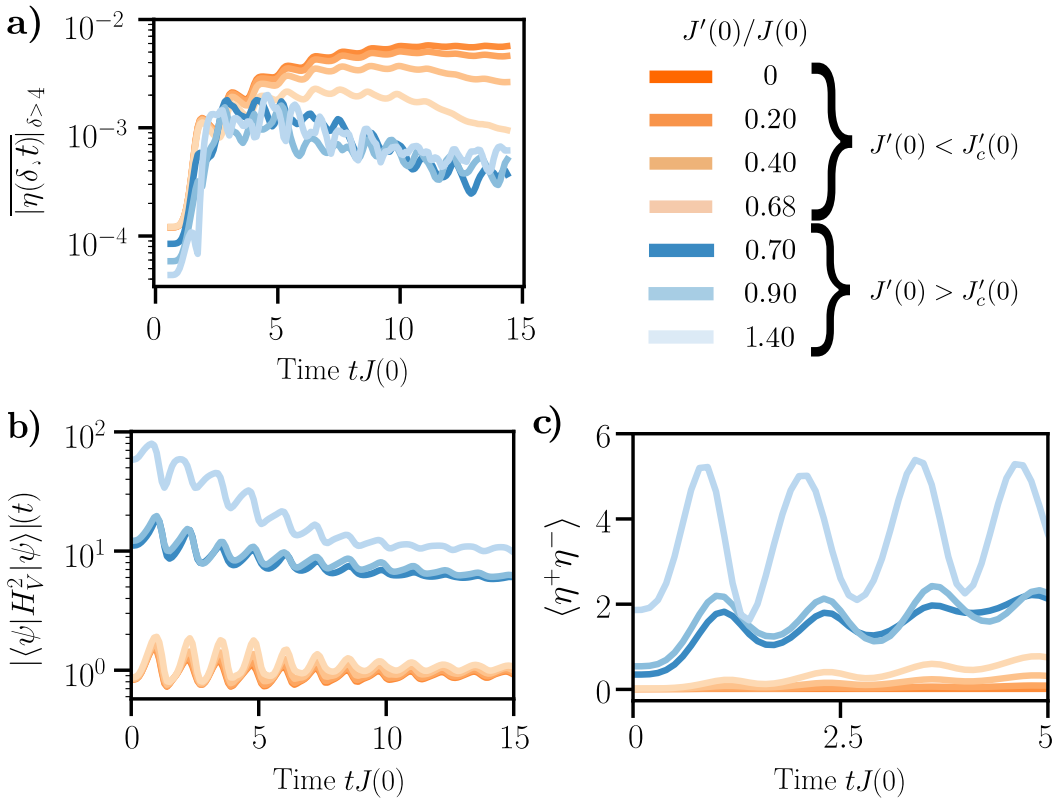

Figure 4.6: Dynamics of the strongly driven two-rung triangular Hubbard model. The system is initialised in the half-filled ground state of Eq. (4.1) with $U(0) = 5J(0)$ for various $J'(0)$ and then time evolved under the driven Hamiltonian in Eq. (4.4) with $A_U = 2A_J = 0.7$, $\Omega J(0) = 2.5$, $T_w = \infty$ and $T_p = 0$. a) Long-range particle-hole order versus time. b) Expectation value of the square of the vertical hopping term H_V, where $J'(0)H_V$ is defined as the second term in Eq. (4.1), versus time. c) Expectation value of $\langle\eta^+\eta^-\rangle$ versus time.

diagonal order amongst the available excitations. Above this critical value of $J'(0)$ the system's response changes dramatically, with $\langle\eta^+\eta^-\rangle$ suddenly varying significantly in time. This results in the system failing to dynamically establish robust particle-hole order — with any available correlations rapidly decaying away for $tJ(0) > 5$ due to the creation of a large number of additional, incommensurate excitations by the driving.

Figure 4.6b hints at the origin of this critical behaviour, with the vertical hopping term effectively annihilating the state for $J'(0) < J'(0)_c$, which results in H_V having no role in the dynamics and $\langle\eta^+\eta^-\rangle$ being approximately conserved. The critical value $J'(0)_c$ lies directly on the first red dotted line in Fig. 4.2, which marks the transition between phases I and II in a finite-size system. As a result we can assume this annihilative action of H_V is tied to the properties of the ground state of the

system in phase I, which is the state that was driven out of equilibrium.

In phase I, the system forms a spin-wave condensate with an additional interference pattern in the form of supressed correlations between the central and outer sites of the lattice. The operator H_V, however, only acts on the outer part of the lattice, where there are large, positive, uniform long-range spin-exchange correlations. The two-site reduced density matrix (RDM) in this sub-lattice will therefore be dominated by spin-exchange terms such as $(|\uparrow,\downarrow\rangle+|\downarrow,\uparrow\rangle)(\langle\uparrow,\downarrow|+\langle\downarrow,\uparrow|)$. This term is annihilated by a Hubbard hopping operator acting from either the left or the right.

More rigorously, our numerics show that in phase I the average two-site RDM within the outer sub-lattice is approximately of the form [31]

$$\rho \propto c_1(|\uparrow\downarrow,0\rangle\langle\uparrow\downarrow,0| + |0,\uparrow\downarrow\rangle\langle 0,\uparrow\downarrow|) + c_2\big(|\uparrow,\downarrow\rangle + |\downarrow,\uparrow\rangle\big)\big(\langle\uparrow,\downarrow| + \langle\downarrow,\uparrow|\big), \qquad (4.7)$$

with the constants c_1 and c_2 at least an order of magnitude larger than any other terms in the matrix. This RDM is annihilated by a hopping term and is exactly what is obtained upon tracing out all but two sites of the perfect spin-wave condensate $(S^+)^{X/2}|\downarrow_1\downarrow_2 ... \downarrow_X\rangle$ on an X site lattice. Thus, we can see that the initial action of H_V as an annihilation operator, and the resulting induction of particle-hole order we observe for $J'(0) < J'(0)_c$, is a direct result of the spin-condensed ferrimagnetic nature of the ground state of the system which we drove out of equilibrium. For $J'(0) > J'(0)_c$ the system is instead in phase II, where the spin-condensate is depleted due to some of the vertically bonded sites forming localised singlets. The operator H_V has a significant effect on these singlets, leading to the particle-hole SU(2) symmetry being truly broken and a lack of induced order in that channel under driving.

It could be argued that H_V should only act as an annihilation operator on a very short timescale as the driving will have caused a significant change in the initial wavefunction after a reasonably short period of time. This is not what we observe and in Fig. 4.6 we see that H_V acts as an annihilation operator over fairly long periods of time, resulting in the approximate conservation of $\langle\eta^+\eta^-\rangle$ and the buildup of particle-hole order. We understand this from the fact that, transiently, driving with the parameters we have used mainly causes changes in the longer-range spin-exchange correlations in the system — as opposed to more local, nearest-neighbour correlations. This is directly reflected in Fig. 4.5b, where the nearest-neighbour correlations (which are those H_V acts on) are effectively unchanged by the drive. Hence, the two-site RDM for the vertically bonded sites is transiently stable and so is the action of H_V and the formation of long-range particle-hole order under driving.

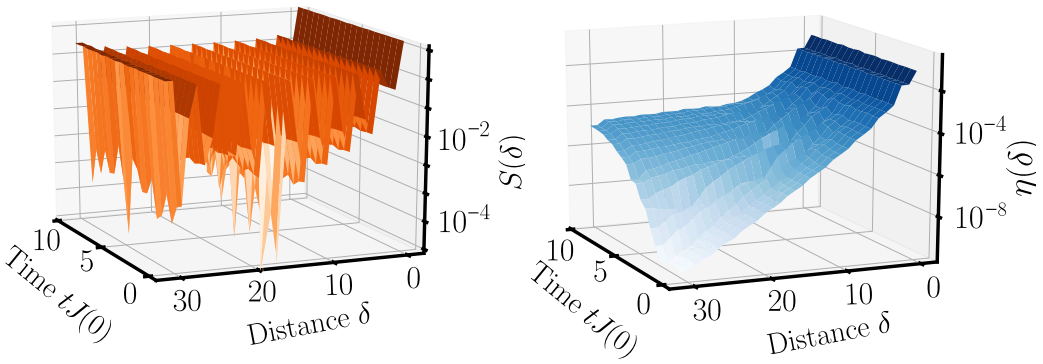

Figure 4.7: Dynamics of the strongly driven two-rung triangular Hubbard model. The system is initialised, at $t = 0$, in the half-filled ground state of the Hamiltonian in Eq. (4.1), with $U(0) = 5J(0)$ and $J'(0) = 0.25J(0)$, and then time evolved with the same Hamiltonian, setting $A_U = -2A_J = 0.3$, $\Omega J(0) = 2.5$, $T_w = 2.5J(0)$ and $T_p = 5.0J(0)$. Left) Spin-exchange order versus distance and time. Right) Particle-hole order versus distance and time.

Some of the parameters used in Figs 4.5 and 4.6 (specifically $U(0), J'(0), J(0)$ and Ω) reflect the values extracted from the frozen-phonon calculations in Ref. [14] and thus the electronic properties of $\kappa - \mathrm{Br}$. We used values for the amplitudes A_U and A_J, however, that were much larger than those suggested by the DFT calculations and we also used an infinite-width, infinite-duration pulse as opposed to a more physical one of finite duration. Whilst this was done in order to definitively determine the response of the system as it absorbs a large amount of energy from the pulse it may mean that the behaviour we have observed will not occur when more reasonable pulse parameters are used.

To this end, in Fig. 4.7, all the numerical parameters directly reflect those extracted from the DFT modelling of the $\kappa - \mathrm{Br}$ compound. We also adopt a larger system size and use a timescale that reflects that of the experiment in Ref. [14]. Figure 4.7 shows that the spin-exchange dynamics are affected minimally by the driving, with only some of the correlations between the outer and central sites changing significantly in time. The drastic re-organisation of the spin degrees of freedom seen in Fig. 4.5 is not present. This is likely due to the robustness of the ground state, the transient timescales, and the small amplitude of the driving.

This absence of spin dynamics means that in the spin-exchange sector the system will remain close to the ground state — which is annihilated by H_V. As a result, there is an approximate particle-hole SU(2) symmetry and, due to the mechanism of heating-induced order, uniform long-range order begins to manifest in the particle-

hole channel, with a colossal increase (many orders of magnitude) in the corresponding correlations.

As this dynamical formation of charge order still occurs for these more realistic parameters, our results offer a potential explanation for the observations of superconductivity in Ref. [14] — with a unique interplay between the geometry of the system and the driving allowing the available charge carrying doublons to establish long-range order. This effect is noticeable even on intermediate time-scales and with relatively small driving amplitudes.

4.3 Conclusion and Open Questions

In this chapter we investigated a recent experiment observing photo-induced superconductivity in the organic compound $\kappa - (\mathrm{BEDT-TTF})_2\mathrm{Cu}[\mathrm{N(CN)_2}]\mathrm{Br}$, forming a simplified description of the experiment with a non-bipartite driven two-rung triangular Hubbard model. We showed how the interaction between the driving and the initial equilibrium state shuts down the particle-hole excitation pathway and allows the system to manifest off-diagonal, uniform particle-hole correlations as it heats up. This unexpected pathway to heating-induced order provides a possible explanation for the results of this recent experiment.

This work has raised a number of open questions. Firstly, we have approximated the conducting BEDT − TTF layer with a single-axis triangular system. To establish a more definitive connection with the experiment it would be necessary to perform our calculations with a fully 2D triangular Hubbard model instead. Such a process is currently not feasible outside of exact diagonalisation on small lattices. Future advances in algorithms for Projected Entangled Pair States (the two-dimensional analogue of Matrix Product States) [32, 33] may make this a possibility.

The second, pertinent, question concerns the amplitude of the induced particle-hole correlations. In the thermodynamic limit, for sufficiently long times, this will go to zero by the scaling arguments from the previous chapter. What happens transiently, however, is unclear and there may well still be a significant amplification and reordering of the long-range correlations under driving before they mutually decay to zero. Moreover, the measurements taken in the experiment in Ref. [14] were over a finite-size region of the material and so it is possible to argue that our dynamical finite-size calculations are valid. Ideally we would also resolve this issue by performing numerics on a much larger, 2D, triangular lattice and the optical conductivity (as opposed to the particle-hole correlations) would be measured over a finite region on

the relevant timescales in order to make a more direct, quantitative, comparison with the experimental observations.

More generally, our single axis triangular Hubbard model allowed us to study the dynamics of a driven, geometrically frustrated lattice structure. We anticipate that other systems which possess geometries characterised by frustration, inhomogeneous co-ordination numbers and anisotropic hopping terms — such as optical quasi-crystalline structures[2] [34, 35, 36, 37], doped cuprates [38, 39, 40, 41] and Kagomé lattices [42, 43] — could display similarly rich physics upon being driven out-of-equilibrium.

Along these lines, the Kagomé lattice is similar to the single-axis triangular setup we have studied here as it can be formed by taking an unbalanced bi-partite lattice and adding additional hopping terms which frustrate it away from the bi-partite regime. If the additional hopping terms on the Kagomé lattice are sufficiently small then a finite value of $\langle S^+S^-\rangle/L^2$ may still be manifest in this frustrated regime and the ground state will possess staggered, long-range spin-exchange correlations like those observed here. Uniform, long-range charge order will then form under the appropriate driving, despite the system not possessing the requisite symmetry.

In the next chapter we shift our focus to identify how symmetries in open systems can be exploited to induce long-time *non-stationary* coherent dynamics. We will find that these non-stationary dynamics can be related to the mechanism of heating-induced order and the corresponding emergence of long-range, ordered states we have witnessed in these last few chapters.

[2]Optical quasi-crystalline are, however, known to demonstrate features of localisation in certain regimes which could significantly slow the affect of heating-induced order.

References

[1] M. Mitrano, A. Cantaluppi, D. Nicoletti, S. Kaiser, A. Perucchi, S. Lupi, P. Di Pietro, D. Pontiroli, M. Riccò, S. Clark, D. Jaksch, and A. Cavalleri, "Possible light-induced superconductivity in K_3C_{60} at high temperature," *Nature*, vol. 530, pp. 461–464, 2016.

[2] D. Fausti, R. I. Tobey, N. Dean, S. Kaiser, A. Dienst, M. C. Hoffmann, S. Pyon, T. Takayama, H. Takagi, and A. Cavalleri, "Light-induced superconductivity in a stripe-ordered cuprate," *Science*, vol. 331, pp. 189–191, 2011.

[3] W. Hu, S. Kaiser, D. Nicoletti, C. R. Hunt, I. Gierz, M. C. Hoffmann, M. Le Tacon, T. Loew, B. Keimer, and A. Cavalleri, "Optically enhanced coherent transport in $YBa_2Cu_3O_{6.5}$ by ultrafast redistribution of interlayer coupling," *Nat. Mat.*, vol. 13, pp. 705–711, 2014.

[4] D. Nicoletti, E. Casandruc, Y. Laplace, V. Khanna, C. R. Hunt, S. Kaiser, S. S. Dhesi, G. D. Gu, J. P. Hill, and A. Cavalleri, "Optically induced superconductivity in striped $La_{2-x}Ba_xCuO_4$ by polarization-selective excitation in the near infrared," *Phys. Rev. B*, vol. 90, p. 100503, 2014.

[5] M. Budden, T. Gebert, M. Buzzi, G. Jotzu, E. Wang, T. Matsuyama, G. Meier, Y. Laplace, D. Pontiroli, M. Riccò, F. Schlawin, D. Jaksch, and A. Cavalleri, "Evidence for metastable photo-induced superconductivity in K_3C_{60}," *Nat. Phys.*, 2021.

[6] K. A. Cremin, J. Zhang, C. C. Homes, G. D. Gu, Z. Sun, M. M. Fogler, A. J. Millis, D. N. Basov, and R. D. Averitt, "Photoenhanced metastable c-axis electrodynamics in stripe-ordered cuprate $La_{1.885}Ba_{0.115}CuO_4$," *Proc. Natl. Acad. Sci.*, vol. 116, pp. 19875–19879, 2019.

[7] A. Cantaluppi, M. Buzzi, G. Jotzu, D. Nicoletti, M. Mitrano, D. Pontiroli, M. Riccò, A. Perucchi, P. Di Pietro, and A. Cavalleri, "Pressure tuning of light-induced superconductivity in K_3C_{60}," *Nat. Phys.*, vol. 14, pp. 837–841, 2018.

[8] D. Nicoletti and A. Cavalleri, "Nonlinear light–matter interaction at terahertz frequencies," *Adv. Opt. Photon.*, vol. 8, pp. 401–464, 2016.

[9] A. Cavalleri, "Photo-induced superconductivity," *Contemp. Phys.*, vol. 59, pp. 31–46, 2018.

[10] A. Patel and A. Eberlein, "Light induced enhancement of superconductivity via melting of competing bond-density wave order in underdoped cuprates," *Phys. Rev. B*, vol. 93, p. 195139, 2016.

[11] M. A. Sentef, A. Tokuno, A. Georges, and C. Kollath, "Theory of laser-controlled competing superconducting and charge orders," *Phys. Rev. Lett.*, vol. 118, p. 087002, 2017.

[12] R. Höppner, B. Zhu, T. Rexin, A. Cavalleri, and L. Mathey, "Redistribution of phase fluctuations in a periodically driven cuprate superconductor," *Phys. Rev. B*, vol. 91, p. 104507, 2015.

[13] D. M. Kennes, E. Y. Wilner, D. R. Reichman, and A. J. Millis, "Transient superconductivity from electronic squeezing of optically pumped phonons," *Nat. Phys.*, vol. 13, pp. 479–483, 2017.

[14] M. Buzzi, D. Nicoletti, M. Fechner, N. Tancogne-Dejean, M. A. Sentef, A. Georges, T. Biesner, E. Uykur, M. Dressel, A. Henderson, T. Siegrist, J. A. Schlueter, K. Miyagawa, K. Kanoda, M.-S. Nam, A. Ardavan, J. Coulthard, J. Tindall, F. Schlawin, D. Jaksch, and A. Cavalleri, "Photomolecular high-temperature superconductivity," *Phys. Rev. X*, vol. 10, p. 031028, 2020.

[15] H. C. Kandpal, I. Opahle, Y.-Z. Zhang, H. O. Jeschke, and R. Valentí, "Revision of

model parameters for κ-type charge transfer salts: An ab initio study," *Phys. Rev. Lett.*, vol. 103, p. 067004, 2009.

[16] J. Müller and T. Thomas, "Low-frequency dynamics of strongly correlated electrons in (BEDT-TTF)$_2$X studied by fluctuation spectroscopy," *Crystals*, vol. 8, p. 166, 2018.

[17] A. Lebed, *The Physics of Organic Superconductors and Conductors*. Springer Series in Materials Science, Springer-Verlag, Berlin, 2008.

[18] J. Caulfield, W. Lubczynski, F. L. Pratt, J. Singleton, D. Y. K. Ko, W. Hayes, M. Kurmoo, and P. Day, "Magnetotransport studies of the organic superconductor κ -(BEDT-TTF)$_2$Cu(NCS)$_2$ under pressure: The relationship between carrier effective mass and critical temperature," *J. Phys. Condens. Matter*, vol. 6, pp. 2911–2924, 1994.

[19] A. Fortunelli and A. Painelli, "On the ab initio evaluation of Hubbard parameters. ii. the κ-(BEDT-TTF)$_2$CuN(CN)$_2$Br crystal," *J. Chem. Phys.*, vol. 106, pp. 8051–8058, 1997.

[20] R. H. McKenzie, "A strongly correlated electron model for the layered organic superconductors κ -(BEDT-TTF)$_2$X," *arXiv Preprint: cond-mat.str-el/9802198*, 1998.

[21] Y. Shimizu, K. Miyagawa, K. Kanoda, M. Maesato, and G. Saito, "Spin liquid state in an organic Mott insulator with a triangular lattice," *Phys. Rev. Lett.*, vol. 91, p. 107001, 2003.

[22] T. Isono, T. Terashima, K. Miyagawa, K. Kanoda, and S. Uji, "Quantum criticality in an organic spin-liquid insulator κ-(BEDT-TTF)$_2$Cu$_2$(CN)$_3$," *Nat. Comm.*, vol. 7, pp. 13494–13494, 2016.

[23] S. R. White, "Density matrix formulation for quantum renormalization groups," *Phys. Rev. Lett.*, vol. 69, pp. 2863–2866, 1992.

[24] S. Daul and R. M. Noack, "Dmrg study of ferromagnetism in a one-dimensional Hubbard model," *Z. Phys. B Condens. Matter*, vol. 103, pp. 293–295, 1996.

[25] E. H. Lieb, "Two theorems on the Hubbard model," *Phys. Rev. Lett.*, vol. 62, pp. 1201–1204, 1989.

[26] H. Yoshida and H. Katsura, "Rigorous results on the ground state of the attractive SU(n) Hubbard model," *Phys. Rev. Lett.*, vol. 126, p. 100201, Mar 2021.

[27] S.-Q. Shen, Z.-M. Qiu, and G.-S. Tian, "Ferrimagnetic long-range order of the Hubbard model," *Phys. Rev. Lett.*, vol. 72, pp. 1280–1282, 1994.

[28] C. Fiolhais, F. Nogueira, and M. Marques, *A Primer in Density Functional Theory*. Lecture Notes in Physics, Springer-Verlag, Berlin, 2003.

[29] E. Gross and R. Dreizler, *Density Functional Theory*. Nato Science Series B, Springer-Verlag, New York, 2013.

[30] G. Vidal, "Efficient classical simulation of slightly entangled quantum computations," *Phys. Rev. Lett.*, vol. 91, p. 147902, 2003.

[31] J. Tindall, F. Schlawin, M. Buzzi, D. Nicoletti, J. R. Coulthard, H. Gao, A. Cavalleri, M. A. Sentef, and D. Jaksch, "Dynamical order and superconductivity in a frustrated many-body system," *Phys. Rev. Lett.*, vol. 125, p. 137001, 2020.

[32] F. Verstraete, V. Murg, and J. Cirac, "Matrix product states, projected entangled pair states, and variational renormalization group methods for quantum spin systems," *Adv. Phys.*, vol. 57, pp. 143–224, 2008.

[33] F. Verstraete, M. M. Wolf, D. Perez-Garcia, and J. I. Cirac, "Criticality, the area law, and the computational power of projected entangled pair states," *Phys. Rev. Lett.*, vol. 96, p. 220601, 2006.

[34] K. Viebahn, M. Sbroscia, E. Carter, J. Yu, and U. Schneider, "Matter-wave diffraction

from a quasicrystalline optical lattice," *Phys. Rev. Lett.*, vol. 122, p. 110404, 2019.
[35] M. Sbroscia, K. Viebahn, E. Carter, J.-C. Yu, A. Gaunt, and U. Schneider, "Observing localization in a 2d quasicrystalline optical lattice," *Phys. Rev. Lett.*, vol. 125, p. 200604, 2020.
[36] A. Szabó and U. Schneider, "Non-power-law universality in one-dimensional quasicrystals," *Phys. Rev. B*, vol. 98, p. 134201, 2018.
[37] K. Singh, K. Saha, S. A. Parameswaran, and D. M. Weld, "Fibonacci optical lattices for tunable quantum quasicrystals," *Phys. Rev. A*, vol. 92, p. 063426, 2015.
[38] N. P. Armitage, P. Fournier, and R. L. Greene, "Progress and perspectives on electron-doped cuprates," *Rev. Mod. Phys.*, vol. 82, pp. 2421–2487, 2010.
[39] G. Deutscher and P.-G. de Gennes, "A spatial interpretation of emerging superconductivity in lightly doped cuprates," *C. R. Phys.*, vol. 8, pp. 937–941, 2007.
[40] G. Li, L. You, W. Wei, Y. Lu, J. Ju, A. Wannberg, H. Rundlöf, Zou, T. Yang, Tian, Liao, N. Toyota, and Lin, "$La_4Cu_{3-x}Zn_xMoO_{12}$: Zinc-doped cuprates with Kagomé lattices," *J. Am. Chem. Soc.*, vol. 127, pp. 14094–14099, 2005.
[41] E. H. da Silva Neto, B. Yu, M. Minola, R. Sutarto, E. Schierle, F. Boschini, M. Zonno, M. Bluschke, J. Higgins, Y. Li, G. Yu, E. Weschke, F. He, M. Le Tacon, R. L. Greene, M. Greven, G. A. Sawatzky, B. Keimer, and A. Damascelli, "Doping-dependent charge order correlations in electron-doped cuprates," *Sci. Adv.*, vol. 2, 2016.
[42] I. Syôzi, "Statistics of Kagomé Lattice," *Prog. Theor. Phys.*, vol. 6, pp. 306–308, 1951.
[43] T. Ohashi, N. Kawakami, and H. Tsunetsugu, "Mott transition in Kagomé lattice Hubbard model," *Phys. Rev. Lett.*, vol. 97, p. 066401, 2006.

Chapter 5

Dissipation-Induced Non-Stationarity in Many-Body Quantum Systems

A number of the results in this chapter were first published as

• B. Buča, J. Tindall, and D. Jaksch *Non-stationary coherent quantum many body dynamics through dissipation*, Nature Communications, **10** (2019)

Contributions to this paper from JT are listed in the introduction.

In this chapter our focus is on non-stationarity in quantum systems. We begin by detailing some established mechanisms by which many-body quantum systems relax to a stationary equilibrium state. This leads us to describe several novel processes, such as many-body localisation and quantum scarring, where this anticipated relaxation is avoided and the system enters an exotic, non-equilibrium phase.

We then introduce the central result of this chapter: an entirely new type of symmetry — the strong dynamical symmetry (SDS) — which, when present in an open system, prevents it from relaxing and instead forces it to undergo indefinite, coherent oscillations. We write down the set of simple, mathematical conditions — which are independent of any microscopic details — required for this operator to exist in an open system governed by the GSKL equation. We then explore this major result in detail, providing an intuitive picture of the symmetry structure of the superoperator space in a system possessing a SDS and showing how this new concept subsumes, and goes beyond, the well-established notion of a Decoherence Free Subspace.

Finally, we take the number-dephased Hubbard model as a central example of an open system with a SDS and numerically observe the induction of coherent non-

stationary spin dynamics in the long-time limit. We discuss how the non-stationary states which arise in this system are intrinsically related to the correlated maximum entropy states we observed in the previous chapters.

5.1 Background

Equilibration and Thermalisation

Understanding how a closed many-body system can reach equilibrium is a fundamental topic in modern physics. In classical mechanics this is largely understood, with the initial state of a generic system spreading out and exploring the whole of phase space as it evolves in time [1, 2]. This notion of ergodicity means that the time-average of a given observable can be directly connected to its statistical average, with the long-time behaviour of the system effectively independent of all properties of the initial state other than its energy.

In a many-body quantum system, however, the linearity of the Schrödinger equation and the exponential size of the Hilbert space means that the wavefunction will never, on any reasonable time-scale, explore the whole of this space. This issue can be neatly summarised by considering a closed system with Hamiltonian H and corresponding eigenvalues and vectors $\{E_\alpha\}$ and $\{|E_\alpha\rangle\}$. Given an initial state $|\psi(0)\rangle$ the expectation of an observable A at time t is

$$\langle\psi(t)|A|\psi(t)\rangle = \langle A(t)\rangle = \sum_{\alpha,\beta} c_\alpha c_\beta^* e^{\mathrm{i}(E_\alpha - E_\beta)t}\langle E_\alpha|A|E_\beta\rangle, \tag{5.1}$$

where the coefficients c_α are those for the initial state in the energy eigenbasis, i.e. $c_\alpha = \langle E_\alpha|\psi(0)\rangle$. In a generic many-body system the energies $\{E_\alpha\}$ will be numerous and incommensurate[1] and so, when taking the time-averaged expectation value, the off-diagonal terms will interfere with each other and we have[2]

$$\overline{\langle A(t)\rangle} = \lim_{T\to\infty}\frac{1}{T}\int_0^T \langle A(t)\rangle dt \approx \sum_\alpha |c_\alpha|^2\langle E_\alpha|A|E_\alpha\rangle. \tag{5.2}$$

We see that this time-averaged expectation value is still strongly dependent on the coefficients of the initial state and thus the question of how it can mimic the statistical, microcanonical average $\langle A\rangle_{\mathrm{MC}} \propto \sum_\alpha \langle E_\alpha|A|E_\alpha\rangle$, which is independent of these coefficients, immediately arises.

[1] In the sense that the ratios $E_\alpha/E_{\alpha'}$ do not possess any simple structure, or pattern.

[2] Occasionally, time-averaging is not used here and $\langle A(t)\rangle$ is suggested to, in the long-time limit, be approximately equal to the RHS of Eq. (5.2) for all values of t [3].

One of the earliest efforts to resolve this question came when John von Neumann introduced the Quantum Ergodic Theorem (QET) [4, 5, 6, 7]. The QET provides a quantum notion of 'ergodicity' or 'normality' whereby, for a typical macroscopically large quantum system, almost every initial state $|\psi(0)\rangle$ will have $|c_\alpha|^2 \approx$ const. in some macroscopically large energy shell of the Hilbert space. This then means that Eq. (5.2) will agree with the desired satistical prediction.

Despite these efforts, criticisms have been made of the QET, suggesting that it is 'vacuous' and more a statement of the mathematical structure of the Hilbert space, as opposed to anything physical [8, 9]. In the late 20th century, work by Deutsch and Srednicki introduced the 'Eigenstate Thermalisation Hypothesis' (ETH) which offered a new explanation, departing from the notion of ergodicity, of how a quantum system can equilibrate [3, 10, 11, 12]. Instead of making a statement about the initial state of the system, the ETH focuses on the observable matrix elements $\langle E_\alpha|A|E_\alpha\rangle$ in Eq. (5.2), suggesting that, for 'local' observables[3], they are often relatively constant over a given energy window, allowing the equivalence to be made between $\overline{\langle A(t)\rangle}$ and $\langle A\rangle_{\text{MC}}$. The ETH has been verified for a number of quantum systems [13, 14, 15, 16] and is widely accepted as a route via which a quantum system can reach thermal equilibrium.

The question of how driven and dissipative quantum systems can equilibrate is more straightforward than for closed systems due to the lack of energy conservation. When periodically driven, a quantum system will continuously absorb energy from the driving field causing all available eigenstates to be equally excited and the system to reach an effectively infinite temperature state within the symmetry sectors that it was initialised in. This Floquet heating is typical for almost all driving fields and we saw numerous examples in chapters 2, 3 and 4. Meanwhile, in open quantum systems, the system-environment coupling can open up a number of possible pathways to equilibrium. For example, in the case of coupling to a bath which induces local, Hermitian dephasing the system will thermalise in the same manner as a periodically driven system. Alternatively, for baths which induce both the loss and gain of quanta in the system some equilibrium, or balance, between these two processes will be found [17, 18, 19], which we saw for the harmonic oscillator coupled to a thermal bath in chapter 1.

[3]Local in the sense that they are few-body or act within some non-extensive region of the system.

Preventing Relaxation in Quantum Systems

The process of equilibration in quantum systems is fundamentally related to the emergence of macroscopic phenomena from microscopic quantum behaviour, which serves as an important link between the foundational theories of quantum and statistical mechanics. Moreover, understanding how quantum systems reach equilibrium helps us to identify situations where they do not and, instead, non-equilibrium behaviour emerges.

In previous chapters we have already seen how the presence of certain symmetries can prevent the typical featureless equilibration of a quantum system as it heats up and instead guide it towards a non-trivial, correlated steady state. In this case the system has still relaxed to equilibrium, but within a constrained subspace of the Hilbert space where correlations are necessarily manifest. In this chapter we focus upon the case in which the system does not relax at all, i.e. it does not reach a stationary state — whether thermal equilibrium or some other fixed point — in the long-time limit and there is persistent dynamical behaviour.

This 'non-stationarity' or 'absence of relaxation' has been observed in a variety of quantum setups. In closed systems one of the most notable examples comes from many-body localisation (MBL). In MBL, the presence of disorder in the potential landscape can freeze the local degrees of freedom and prevent the system from reaching thermal equilibrium on any finite time-scale [20, 21, 22]. The eigenstates of an MBL Hamiltonian do not satisfy the ETH [23] and this localisation phenomena has a number of promising applications, with examples including heat engines [24] or protecting coherences and quantum information in qubit arrays [25].

Another significant example arises from quantum scarring [26, 27, 28, 29, 30, 31]. In this scenario there exist special eigenstates of the Hamiltonian, known as 'scars', which do not obey the ETH. When dynamically evolving initial states which have a non-zero overlap with these scars, thermalisation can be prevented and the system will often display unique dynamical behaviour which reflects the properties of these scars — for example, in the form of robust oscillations in the system's entanglement entropy [27, 28].

There are also a number of cases where driving or dissipation have been used to prevent relaxation in a quantum system — despite the fact that they will generically expedite this process. Returning to the example of quantum scarring, carefully tuned periodic driving has been shown to control the weight of scars in a chain of atoms, effectively determining the extent to which the system thermalises or enters a 'scarred

regime' where information is protected and persistent oscillations occur [32]. Furthermore, periodic 'rotations' of a chain of trapped ions with a carefully engineered laser pulse have been shown to generate a persistent subharmonic response in the magnetisation [33].

In the context of open systems, many-body spin chains undergoing collective loss in the thermodynamic limit have been shown to exhibit a dissipative phase transition between a unique time-periodic steady state and a stationary ensemble [34, 35]. Meanwhile, dissipation induced into a cavity-confined Bose Einstein Condensate was recently observed to cause the condensate to rotate coherently between two different spatial modes [36]. Additionally, an important example that we will compare with the results of this chapter is that of a decoherence free subspace (DFS) [37, 38, 39, 40, 41]: a region of the Hilbert space of an open system which is free from the influence of the environment. If the projection of the Hamiltonian into this subspace is of a sufficiently simple structure, or the subspace dimension is relatively small, then there should be no equilibration and coherent non-stationary dynamics can occur.

These results are of fundamental interest to the scientific community and provide opportunities to understand and harness the exotic properties of these quantum systems. Moreover, identification of equilibrium-preventing mechanisms which are independent of any microscopic details allow such states, and other unique non-equilibrium phases, to be observed in a variety of systems — as opposed to a single, specific setup.

In the following section we achieve this in the context of open quantum systems. We will introduce a set of conditions which, when satisfied, guarantee that an open system will not reach a stationary steady state and instead coherently oscillate in the long-time limit. These conditions make no statements about the microscopic details of the system and are instead based solely on symmetry arguments — meaning they can be applied to a variety of different systems in order to realise exotic out-of-equilibrium quantum states of matter. Furthermore, we will show these conditions encapsulate, and go beyond, the concept of a DFS.

5.2 Symmetry-Based Conditions for Preventing Relaxation in an Open Quantum System

The Strong Dynamical Symmetry Operator

Here our focus is on the Markov description of an open quantum system but we emphasize that these results can be applied outside of the Markovian picture [42]. The GSKL equation, which we derived and introduced in chapter 1, reads

$$\frac{\partial}{\partial t}\rho(t) = \mathcal{L}\rho = -\mathrm{i}[H,\rho] + \sum_j \gamma_j\big(L_j\rho L_j^\dagger - \frac{1}{2}\{L_j^\dagger L_j, \rho(t)\}\big), \tag{5.3}$$

with the meaning of the operators unchanged. The eigenvalues and eigenvectors of the Liouvillian $\mathcal{L}$ completely determine the dynamics of the system as we have

$$||\rho(t)\rangle\rangle = \sum_i c_i e^{\lambda_i t}\,||i_R\rangle\rangle\,, \qquad c_i = \langle\langle i_L|\rho(0)\rangle\rangle, \tag{5.4}$$

where $\langle\langle i_L||$ and $\langle\langle i_R||$ are the left and right eigenvectors (in superket form) of $\mathcal{L}$, λ_i is the corresponding eigenvalue and $||\rho(t)\rangle\rangle$ is the vectorized density matrix. As we have $\mathrm{Re}(\lambda_i) \leq 0\ \forall i$ the dynamics in the limit $t \to \infty$ are completely determined by the eigenvectors with $\mathrm{Re}(\lambda_i) = 0$. If all of these eigenvectors also have $\mathrm{Im}(\lambda_i) = 0$ then the system will reach a stationary, equilibrium state. This is clearly the case in Fig. 5.1 where we plot the eigenspectrum for a Liouvillian built from random jump operators and a random Hamiltonian. This 'stationary' spectrum is typical for random Liouvillians [43, 44] as well as for a number of interacting, many-body systems [45, 46, 47].

We can, however, identify a set of conditions which guarantee that this is not the case, without making any statements about the microscopic details of the system. Specifically, if we can identify an operator A which satisfies

$$[H, A] = \Omega A,\ \Omega \in \mathbb{R}_{>0} \qquad [L_j, A] = [L_j^\dagger, A] = 0 \qquad \forall j, \tag{5.5}$$

then it immediately follows by substitution into Eq. (5.3) that there exists a series of imaginary eigenmodes of the form

$$\rho_{n,m} = (A)^n\rho_\infty(A^\dagger)^m, \qquad \mathcal{L}\rho_{n,m} = \Omega_{n,m}\rho_{m,n}, \qquad \Omega_{n,m} = \mathrm{i}(m-n), \tag{5.6}$$

where ρ_∞ is a steady state of the system, i.e. $\mathcal{L}\rho_\infty = 0$. There is always at least one steady state of $\mathcal{L}$ and thus provided the conditions in Eq. (5.5) are satisfied for some operator A we can say that $\mathcal{L}$ possesses a series of purely imaginary eigenvalues.

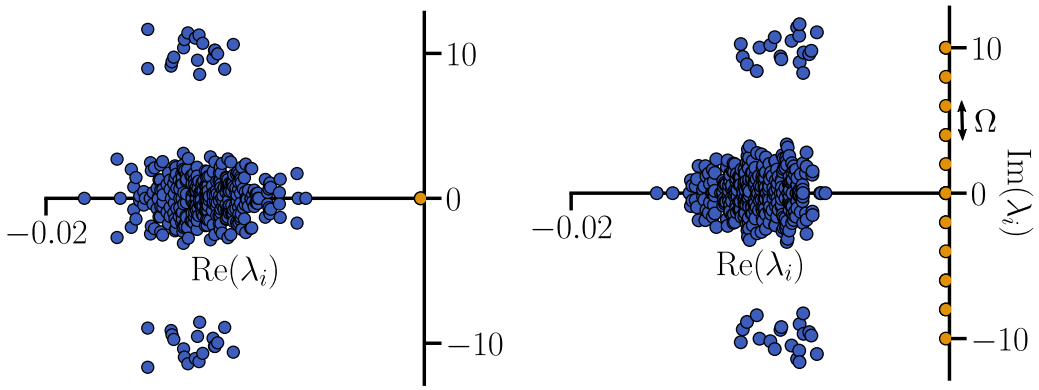

Figure 5.1: Spectrum of eigenvalues of the Liouvillian $\mathcal{L}$ of an open quantum system described by the GSKL equation. Eigenvalues with real part equal to zero are marked in orange. Left) Taken from chapter 1 Fig. 1: spectrum of a Liouvillian built from random jump operators and a random Hamiltonian. There are no purely imaginary eigenvalues and the only eigenvalue on the imaginary axis corresponds to the steady state eigenvalue $\lambda_i = 0$. Right) Spectrum of a Liouvillian with a strong dynamical symmetry operator A which is defined in Eq. (5.5). Due to the existence of this operator a series of equally spaced eigenvalues has formed on the imaginary axis with spacing Ω.

The possible values for the integers m and n are dependent on the system at hand, but provided that $(A)^n\rho_\infty(A^\dagger)^m \neq 0$ for some $n \neq m$ then there will be at least one imaginary eigenvalue of $\mathcal{L}$. The restriction $\Omega \in \mathbb{R}_{>0}$ in Eq. (5.5) is a natural one because for $\Omega = 0$ or $\Omega \in \mathbb{C}$ the modes $\rho_{n,m}$ are clearly no longer imaginary whilst, given the existence of the operator A, the case when $\Omega \in \mathbb{R}_{<0}$ is trivially satisfied by $A^\dagger$, the adjoint of A.

We can also determine the corresponding left 'imaginary' eigenmode of $\mathcal{L}$ given the right 'imaginary' eigenmode $\rho_{n,m}$. By taking the adjoint of the Liouvillian and then applying it to ρ and taking the adjoint again we get the equation of motion

$$\rho'\mathcal{L} = -\mathrm{i}[H,\rho'] + \sum_j \gamma_j\big(L_j^\dagger\rho' L_j - \frac{1}{2}\{L_j^\dagger L_j,\rho'\}\big), \tag{5.7}$$

for 'left' density matrices ρ'. From this it follows that $\rho'_{n,m} = (A)^n\rho'_\infty(A^\dagger)^m$ is the corresponding left eigenmode for $\rho_{n,m}$ because, by substituting it into Eq. (5.7) we find $\rho'_{n,m}\mathcal{L} = i\Omega(m-n)\rho'_{n,m}$. We have defined ρ'_∞ as the matrix representation of the left steady state, i.e. ρ'_∞ satisfies $\rho'_\infty\mathcal{L} = 0$ whilst the right steady state ρ_∞ satisfies $\mathcal{L}\rho_\infty = 0$.

The operator A in Eq. (5.5) is referred to as a 'strong dynamical symmetry' (SDS) of the system. In Fig. 5.1 we also plot an example of the spectrum of a Liouvillian with

a SDS, observing how the imaginary eigenvalues form a commensurate, equidistant spectrum because of this operator. This has significant implications for the dynamics of the system as $t \to \infty$. Specifically, if we consider an open system with a single SDS operator A then, assuming that the only imaginary eigenvalues are those originating from the existence of A, the long-time dynamics can be written as

$$\begin{aligned}
&\lim_{t\to\infty} \rho(t) = \sum_{m,n} \sum_{k} c^{(k)}_{m,n} d^{(k)}_{m,n} e^{\mathrm{i}\Omega(m-n)t} (A)^n \rho^{(k)}_{\infty} (A^\dagger)^m, \\
&c^{(k)}_{m,n} = \mathrm{Tr}(\rho(0)(A)^m \rho'^{(k)}_{\infty} (A^\dagger)^n), \\
&d^{(k)}_{m,n} = 1/\mathrm{Tr}\big((A)^n \rho^{(k)}_{\infty} (A^\dagger)^m (A)^m \rho'^{(k)}_{\infty} (A^\dagger)^n\big),
\end{aligned} \tag{5.8}$$

where k is used to index the different steady states of the system[4]. It then follows from tracing over the product of Eq. (5.8) and some operator X that the long-time dynamics of a given observable $\langle X \rangle$ can be written as a Fourier series and will thus be non-stationary as long as both the initial state and X have non-zero overlap with at least one of the $\rho_{n,m}$ when $m \neq n$.

This is a significant result, especially when considering that typical many-body systems will relax to stationarity due to the incommensurate nature of their spectrum and that the added influence of an external environment will usually expedite this relaxation rather than preventing it. Additionally, these SDS conditions are purely based on symmetry and make no statements about any microscopic details — suggesting they could be satisfied by a number of different systems. Later on in this chapter, and in the next chapter, we will provide specific examples of quantum setups which possess a SDS. Before this, we will try to develop a stronger physical intuition for the symmetry structure of an open quantum system with a SDS. We will then compare and contrast this structure with that which arises when an open system possesses a Decoherence Free Subspace (DFS).

Structure of an Open Quantum System with a Strong Dynamical Symmetry Operator

It is instructive to understand the connection between the SDS conditions in Eq. (5.5) and the conditions for a strong symmetry in an open system, which we introduced in chapter 2. If we recall, a strong symmetry in the context of the GSKL equation is an operator satisfying [48]

$$[H, S] = 0, \qquad [L_j, S] = [L_j^\dagger, S] = 0 \qquad \forall j, \tag{5.9}$$

[4]We will see shortly that the existence of A means that there are likely to be multiple steady states.

which is the limiting scenario $\Omega \to 0$ of Eq. (5.5). In the case when such an operator can be identified the Liouvillian matrix is block-diagonalisable into a series of subspaces indexed by the $\mathcal{N}^2$ distinct pairs of eigenvalues (a, b) of the elevated symmetry operators $1 \otimes S^T$ and $S \otimes 1$. As the eigenvalues of these operators are just those of S but with extra degeneracies, we can simplify this by just saying that a and b each run over the $\mathcal{N}$ distinct eigenvalues of S. Within the subspaces where $a = b$ there must be at least one steady state with trace unity [48].

Strong dynamical symmetries are fundamentally related to strong symmetries. Specifically, it is straightforward to show from Eq. (5.5) that if a system satisfies the conditions for a SDS operator A then it possesses a strong symmetry of the form $S = AA^\dagger + A^\dagger A$.

This strong symmetry is important in order to understand the form of the imaginary modes $\rho_{n,m}$ and steady states that the system will possess. Due to the existence of S the Liouvillian can be block diagonalised in the aforementioned manner and, within each of the subspaces where $a = b$, there will be a trace one steady state ρ_∞ which is of the form $\rho_\infty = \sum_{ij} \rho_{ij} |i\rangle \langle j|$ with $S|i\rangle = a|i\rangle$ and $S|j\rangle = a|j\rangle$. Meanwhile, in each of the subspaces where $a \neq b$ there will be an imaginary eigenmode of the system which can be constructed from the aforementioned steady states via $\rho_{n,m} = (A)^n \rho_\infty (A^\dagger)^m$ with $n \neq m$. These imaginary modes will be traceless as they are of the form $\rho_{n,m} = \sum_{ij} c_{ij} |i\rangle \langle j|$ where $\langle i|S|i\rangle \neq \langle j|S|j\rangle$. In the case that $n = m$ then we find that we have instead constructed another steady state of the system as we have simply moved to a different block with $a = b$. Hence, the operators A and $A^\dagger$ allow us to move between the different disconnected subspaces of the Banach space $\mathcal{B}(\mathcal{H})$ and create a defining relationship between the steady states and the imaginary eigenmodes of the Liouvillian which exist within these subspaces.

In Fig. 5.2 we picture this, providing a block-diagonalised representation of a Liouvillian with a SDS and showing how the eigenvalues of the corresponding strong symmetry $S = AA^\dagger + A^\dagger A$ can be used to index these blocks. For clarity we only picture the case where there are two distinct eigenvalues of S, but this can be trivially extended to any number of distinct eigenvalues.

In order to observe non-stationarity in the system in the limit $t \to \infty$ it is necessary for the initial state to contain coherences between states with a different value of $\langle S \rangle$. This will then correspond to a non-zero 'weight' of the initial density matrix in the superblocks where $a \neq b$ and an overlap with the corresponding imaginary modes. This overlap does not decay away, instead it picks up a time-dependent phase factor which is the source of the observable non-stationary behaviour. Importantly, the

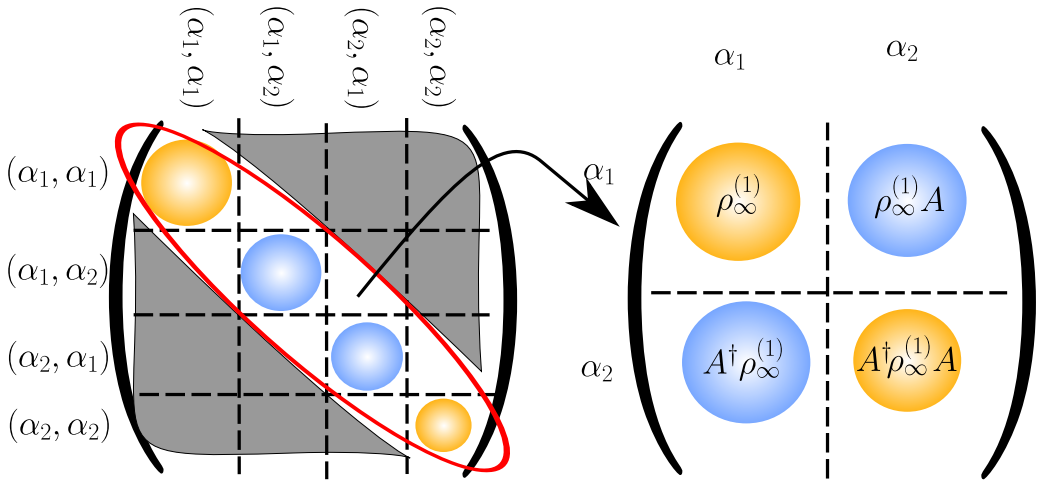

Figure 5.2: Symmetry structure of the Liouvillian superoperator for a system with a strong dynamical symmetry operator A. Left) The existence of A immediately implies a strong symmetry of the form $S = AA^\dagger + A^\dagger A$ and so the Liouvillian can be diagonalised into subspaces, or blocks, indexed by the $\mathcal{N}^2$ pairs (a, b) where a and b run over the $\mathcal{N}$ distinct eigenvalues of S. Here, for simplicity, we set $\mathcal{N} = 2$ and use α_1 and α_2 to denote the two distinct eigenvalues of S. Right) Within each of the subspaces where $a = b$ there is a trace 1 stationary state ρ_∞ and within each of the subspaces where $a \neq b$ there is at least one traceless, purely imaginary eigenmode of the Liouvillian. The operators A and $A^\dagger$ can be used to move between the subspaces and define the relationship between the stationary states and imaginary eigenmodes.

imaginary modes are traceless and thus are not 'attractors' — any overlap the system has with these fixed points will be unchanging in time. Meanwhile the steady states ρ_∞ are attractors as they have trace and so the overlap the system has with them can grow as it evolves under $\mathcal{L}$.

What we have discussed here provides a strong intuition for the structure of an open system with a SDS. The specific physical properties of these states and the corresponding non-stationary oscillations will, of course, be dependent on the finer, microscopic details of the Hamiltonian, the jump operators and the SDS operator A.

Comparison with Decoherence Free Subspaces

Before we move on to a specific example of a system with a SDS we will compare this new concept with the established notion of a Decoherence Free Subspace (DFS) [37, 38, 39, 40, 41]. We described the DFS in chapter 1 as a region of the Hilbert space of an open system which is free from the effects of the environment and where

coherences are preserved. Specifically, in the context of the GSKL equation, a DFS is spanned by the set of states $\{|\psi_i\rangle\}$ whose members are degenerate eigenvectors of each of the jump operators (i.e. $L_j |\psi_i\rangle = c_j |\psi_i\rangle \ \forall i,j$) and are mapped by the Hamiltonian H into a linear superposition of the other members of the set (i.e. H does not map the $|\psi_i\rangle$ out of the DFS). The conditions for a DFS make statements at the level of pure states of the open system. It is clear that this subspace is completely unaffected by the dissipative part of the Liouvillian as $D(|\psi_i\rangle \langle\psi_k|) = 0 \ \forall i,k$ and thus the dynamics within it are unitary and governed solely by the Hamiltonian H.

We can show that in the GSKL picture any non-stationarity in a DFS can be described in terms of a series of strong dynamical symmetry operators. For a given DFS, we have the projector $\mathcal{P} = \sum_i |\psi_i\rangle \langle\psi_i|$ which can be used to form the DFS Hamiltonian $H' = \mathcal{P}H\mathcal{P}$. The eigenvectors $|\lambda_i\rangle$ of this projected Hamiltonian form a new basis which spans the DFS and satisfy the following conditions

$$\begin{aligned} \big[H, |\lambda_i\rangle \langle\lambda_k|\big] &= (\lambda_i - \lambda_k) |\lambda_i\rangle \langle\lambda_k|, \\ \big[L_j, |\lambda_i\rangle \langle\lambda_k|\big] &= \big[L_j^\dagger, |\lambda_i\rangle \langle\lambda_k|\big] = 0 \ \ \forall i,k, \end{aligned} \tag{5.10}$$

where λ_i is the corresponding eigenvalue for $|\lambda_i\rangle$, i.e. $H|\lambda_i\rangle = H'|\lambda_i\rangle = \lambda_i |\lambda_i\rangle$. We see that the existence of a DFS therefore implies the existence of $\frac{N}{2}(N-1)$ unique SDS operators of the form $A = |\lambda_i\rangle \langle\lambda_k|$ (or $A^\dagger = |\lambda_k\rangle \langle\lambda_i|$), where $\lambda_i \neq \lambda_k$ and N is the number of distinct eigenvalues of the projected Hamiltonian H'. These operators govern the non-stationary behaviour in the DFS. Meanwhile, for any degenerate eigenvalues of H', i.e. $\lambda_i = \lambda_k$, the corresponding operators $|\lambda_i\rangle \langle\lambda_k|$ are just strong symmetries of the system.

As an example, recall the master equation from chapter 1 for two qubits under collective loss,

$$\frac{\partial\rho(t)}{\partial t} = -\mathrm{i}\omega[S^z, \rho(t)] + S^-\rho(t)S^+ - \frac{1}{2}\{S^+S^-, \rho(t)\}. \tag{5.11}$$

This system has a DFS spanned by the two states $|\uparrow\downarrow\rangle - |\downarrow\uparrow\rangle$ and $|\downarrow\downarrow\rangle$. The projected Hamiltonian H' is already diagonal in this basis and so this DFS is equivalent to the existence of the SDS operator $|\downarrow\downarrow\rangle (\langle\uparrow\downarrow| - \langle\downarrow\uparrow|)$ and its adjoint. As there is only one unique SDS operator, coherent oscillations emerge at a frequency of 2ω — the difference in energy between the two eigenvalues of H'.

In general, whether or not non-stationary behaviour emerges in a DFS is dependent on the structure of the eigenvalues of the projected Hamiltonian — just like in a closed system. If they are numerous and incommensurate then the multiple SDS

operators are likely to interfere with each other, preventing the emergence of non-stationary. If, instead, they are equidistant or there are only a few of them then non-stationary behaviour will emerge.

Whilst any dynamics in a DFS can be described in terms of strong dynamical symmetry operators it is important to recognise that the opposite is not true. The existence of a SDS, and the corresponding dynamics, does not imply the existence of a DFS. The imaginary modes $\rho_{n,m}$ and steady states ρ_∞ generated by a SDS span the space which governs the long-time dynamics of the system and are generally mixed as they have been influenced by the environment. This mixedness enforces itself on the long-time non-stationary state of the system and if the environment is removed the structure of this space and corresponding dynamics of the system will be altered.

Meanwhile, a DFS is always spanned solely by pure states: which means that a pure state initialised inside of it will retain its purity under the action of the Liouvillian and its dynamics will be completely independent of the presence of the environment. The DFS thus does not generally encapsulate the SDS formalism. The only exception is if the SDS operator(s) are of the particularly simple 'pure' form described in Eq. (5.10) which can be identified by the SDS operator A satisfying $\mathrm{Tr}((AA^\dagger)^n) = 1,\ \forall n \in \mathbb{Z}^+$.

In the following section we will introduce an example of a many-body open system satisfying the SDS conditions. The resulting dynamics involve a unique interplay between coherent oscillations and dissipation and cannot be captured within the DFS formalism. Furthermore we will see that when the environment is removed, these coherent oscillations become noisy — the presence of the environment is *necessary* for the coherent response observed.

5.3 Example: Non-Stationary Coherent Dynamics in the Dissipative Hubbard Model

Model and Symmetry Structure

In chapter 3 we took an in-depth look at the Hubbard model, describing its origin and success as a description of solid-state electronic behaviour. We then detailed its rich dual SU(2) symmetry structure and showed how heating in the presence of these symmetries leads to robust, maximum entropy steady states with off-diagonal long-range correlations. Here we return to the model, considering the additional presence

of several homogeneous fields and focussing on a 1D chain. The Hamiltonian reads

$$H(B,\mu) = -J\sum_{\langle ij\rangle,\sigma}\left(c^{\dagger}_{\sigma,i}c_{\sigma,j}+\text{H.c.}\right)+U\sum_{i}n_{\uparrow,i}n_{\downarrow,i}+\frac{B}{2}\sum_{i}(n_{\uparrow,i}-n_{\downarrow,i})+\mu\sum_{i}(n_{\uparrow,i}+n_{\downarrow,i}), \tag{5.12}$$

where the operators retain their usual meaning and the index i runs over the sites of the chain with $\langle ij\rangle$ denoting nearest-neighbour pairs of sites. The added third term describes the interaction of the fermions with an external magnetic field of strength B which splits the energy of the two spin states $|\uparrow\rangle$ and $|\downarrow\rangle$. Meanwhile, the final term describes a homogeneous chemical potential of strength μ which makes the energy of the system dependent on the total particle number. For simplicity and numerical ease, we have fixed the geometry to be that of a 1D chain but emphasize that the following results apply for *any* bi-partite Hubbard lattice.

The additional terms in Eq. (5.12) have modified the symmetry structure of the Hamiltonian because if we reintroduce the spin and η generators defined in chapter 3 we find

$$\begin{aligned}
&[H(B,\mu),\eta^{\pm}] = \pm(2\mu+U)\eta^{\pm},\\
&[H(B,\mu),S^{\pm}] = \pm BS^{\pm},\\
&[H(B,\mu),\eta^{z}] = [H(B,\mu),S^{z}] = 0.
\end{aligned} \tag{5.13}$$

The relationships in Eq. (5.13) tell us that, in the presence of finite B or μ (with $\mu \neq -U/2$), the operators S^{+} and η^{+} respectively form raising operators of the Hamiltonian $H(B,\mu)$. We emphasize, however, that the spin and η Casimir operators $S^{+}S^{-}$ and $\eta^{+}\eta^{-}$ still commute with $H(B,\mu)$.

We now take the Hubbard Hamiltonian in Eq. (5.12) to be weakly coupled to a Markovian environment and thus governed by the GSKL master equation in Eq. (5.3) — with $H = H(B,\mu)$. It follows from Eq. (5.13) that if B is finite and the conditions $[L_j, S^{+}] = [L_j^{\dagger}, S^{+}] = 0\ \forall j$ are satisfied then S^{+} is a SDS operator for this open system, whilst if μ is finite (and $\mu \neq -U/2$) and the conditions $[L_j,\eta^{+}] = [L_j^{\dagger},\eta^{+}] = 0\ \forall j$ are satisfied then η^{+} is a SDS operator. If we let the jump operators be of the form $L_j = n_{\uparrow,j}+\kappa n_{\downarrow,j}$ where j runs over the sites of the chain (i.e. there is a jump operator corresponding to each site) then we see that the former conditions are satisfied if $\kappa = 1$ whilst the latter are satisfied if $\kappa = -1$. For $\kappa = 1$ we have that $[L_j,\eta^{+}\eta^{-}] \neq 0$ and so we have broken the η SU(2) symmetry of the open system. For $\kappa = -1$ we will have instead broken the spin SU(2) symmetry as $[L_j, S^{+}S^{-}] \neq 0$.

These two situations correspond to local number dephasing and local spin dephasing respectively and in chapter 3 we showed how both cases could be implemented

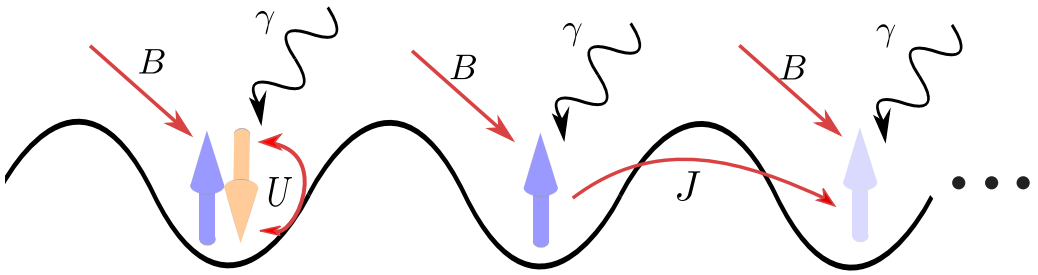

Figure 5.3: Schematic of the Hubbard model on a 1D chain, with hopping and interaction strengths J and U respectively. A constant magnetic field of strength B has been applied to the system, alongside homogeneous local number-dephasing of strength γ. The system is described by the Liouvillian in Eq. (5.14), setting $\gamma_i = \gamma\ \forall i$.

experimentally by immersing a Hubbard optical lattice into a Bosonic condensate and tuning the interaction between the condensate atoms and fermionic spin states with Feshbach resonances.

In the case of local spin dephasing and a finite chemical potential μ the imaginary modes of the system will be of the form $\rho_{n,m} = (\eta^+)^n \rho_\infty (\eta^-)^m$ where the steady state ρ_∞ lives in the $a = b$ suspaces of the Liouvillian. In this case, the imbalance $n \neq m$ means the $\rho_{n,m}$ will contain coherences between states of different fermion number and so we would require initial wavefunctions which are in a superposition of different number states in order to excite the $\rho_{n,m}$. For systems of electrons, such initial states are unphysical due to the charge superselection rule and so we will fix the total particle number, allowing us to ignore the effect of any homogeneous chemical potentials and focus solely on finite B. Our system is thus governed by the master equation

$$\frac{\partial}{\partial t}\rho(t) = \mathcal{L}\rho = -\mathrm{i}[H(B,0),\rho] + \sum_i \gamma_i \big(n_i \rho n_i - \frac{1}{2}\{n_i n_i, \rho(t)\}\big), \quad n_i = n_{\uparrow,i} + n_{\downarrow,i} \tag{5.14}$$

with the operator S^+ satisfying the SDS conditions in Eq. (5.5) with $\Omega = B$ and i running over the sites of the chain. The imaginary modes of this Liouvillian are of the form $\rho_{n,m} = (S^+)^n \rho_\infty (S^-)^m$ and can be excited with initial wavefunctions which are in a superposition of states of different magnetisation. In Fig. 5.3 we picture this setup, showing the Hubbard chain in the presence of a homogeneous magnetic field and local number dephasing.

The Liouvillian in Eq. (5.14) has three strong symmetry operators: the total particle number N, the total z magnetisation S^z and the Casimir operator $S^2 = S^+S^- + S^-S^+$. We already have a strong understanding of this system as, in chapter

3, we treated the same setup but with both the magnetic field and chemical potential set to zero. There we were focussed on the steady state properties of the system and so we fixed the values of $\langle N \rangle$ and $\langle S^z \rangle$. This led to the Liouvillian being block-diagonalised into a series of subspaces indexed by the unique tuples (a, b) where a and b run over the distinct eigenvalues of S^2. Within each of the diagonal spaces (where $a = b = \alpha$) there is a trace one steady state which corresponds to an infinite temperature state over the basis formed from the eigenstates of S^2 with eigenvalue α. By the arguments of chapter 2 and the calculations of chapter 3 we know these steady states will generally contain uniform, finite, off-diagonal spin-wave order.

In this chapter we wish to observe the consequences of the imaginary eigenmodes which form alongside these steady states due to the additional presence of the homogeneous magnetic field in the Hamiltonian. As a result we need to consider the structure of the Liouvillian without fixing the z magnetisation. This is straightforward and we can simply block-diagonalise the Liouvillian into a series of subspaces indexed by the tuples (a_1, b_1, a_2, b_2) where a_1 and b_1 each run over the distinct eigenvalues of S^2 and a_2 and b_2 each run over those of S^z. The steady states, again, live in the spaces where $a_1 = b_1$ and $a_2 = b_2$ and are exactly the same steady states we have just discussed — except that we have an additional index which allows us to move between steady states of different magnetisation. Crucially, the off-diagonal spaces are now important as these are where the imaginary modes $\rho_{n,m}$ reside and involve density matrix elements which describe coherences between states of different z magnetisation and different values of S^2. If we initialise our system in a state with such coherences we should excite these imaginary modes and be able to observe their impact on the dynamics of the system.

It is worth noting that the Liouvillian structure we have just described seems slightly more complicated than that introduced in section 6.2 for a generic system with a SDS operator A. This is because our open Hubbard system has an additional strong symmetry S^z whose expectation value changes upon the action of S^+ on a given state. Nonetheless, the intuition is still the same, we have just had to invoke an extra degree of freedom due to the SU(2) nature of the strong dynamical symmetry.

Numerical Results

We are now ready to explicitly observe the consequences of this SDS on the dynamics of our open Hubbard system. In Fig. 5.4 we take an initial state, which is in a superposition of states of different magnetisation, and time evolve it under the Liouvillian in Eq. (5.14). We measure the single point and two point x magnetisation on

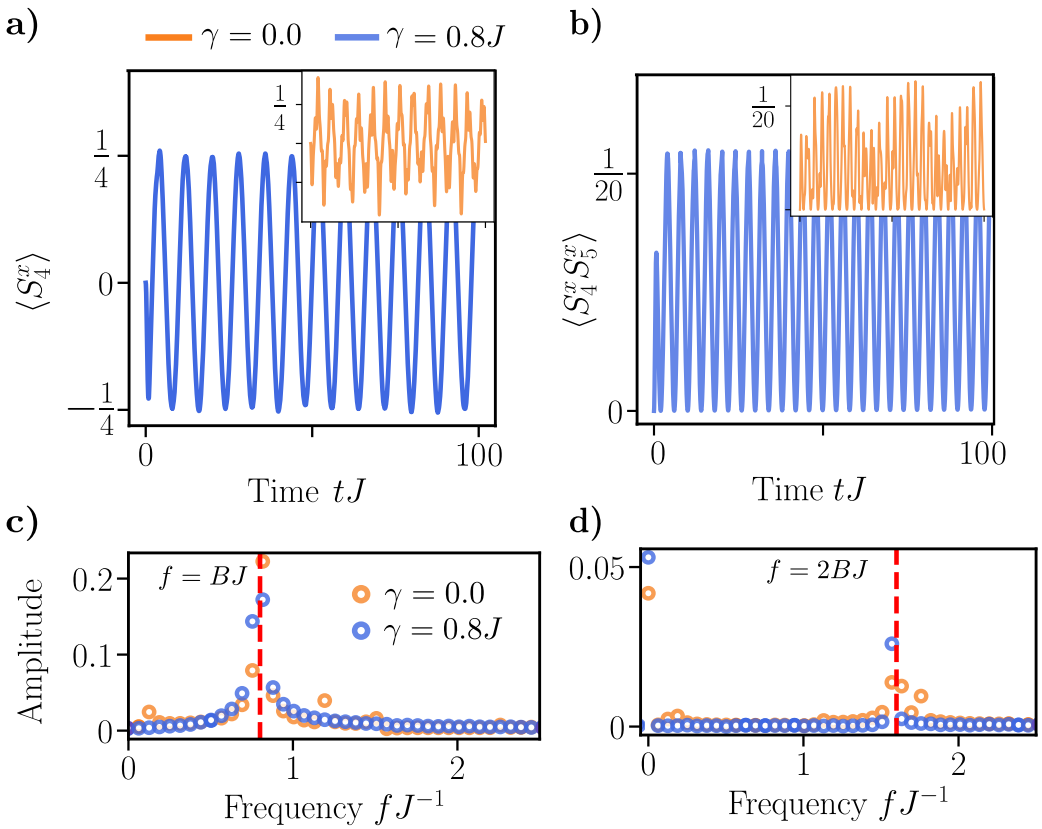

Figure 5.4: Dynamics of the number-dephased Hubbard model described by the master equation in Eq. (5.14). The system is initialised in the state $|\leftarrow \text{vac} \leftarrow \text{vac}...\rangle$ on an 8 site chain where $|\leftarrow\rangle = (1/\sqrt{2})(|\uparrow\rangle - |\downarrow\rangle)$ and $|\text{vac}\rangle$ is an empty site. This state is then time-evolved under $\mathcal{L}$ with $U = 4.0J$, $B = 0.8J$ and $\gamma_i = \gamma \ \forall i$ — the two values of γ used are specified in the legend. a) Single point x magnetisation $\langle S_4^x \rangle$ versus time. b) Two point x magnetisation $\langle S_4^x S_5^x \rangle$ versus time. c) Fourier transform of the single point magnetisation. d) Fourier transform of the two point magnetisation. The red dotted lines correspond to integer multiples of the magnetic field strength B.

the specified sites, choosing these observables as they have a non-zero overlap with the imaginary eigenmodes $\rho_{n,m}$. We can clearly see that as the open system evolves, coherent oscillations form in both measured observables and persist indefinitely. The oscillations occur at integer multiples of the magnetic field strength B which correlates with the structure of the imaginary eigenvalues of the Liouvillian. We also plot the dynamics in the corresponding closed system (i.e. $\gamma_i = 0 \ \forall i$) where the oscillatory response is still present but is less coherent and noisier.

This contrast between the open and closed system is remarkable, with the dephasing actively stabilising and 'cleaning' the noisy oscillatory response of the system. Conventional wisdom would suggest that the presence of an environment should

destroy coherences in a quantum system, as opposed to enhancing them. From a mathematical perspective we are able to understand this remarkable effect. In the open system, the presence of a SDS operator has meant that the eigenvalues of the Liouvillian on the imaginary axis are equidistant and so the long-time dynamics can only involve coherent oscillations at integer multiples of B. The dynamics due to any other eigenvalues of the Liouvillian will decay away as they do not lie on the imaginary axis. In the closed system the operator S^+ is still a raising operator and thus still generates equidistant eigenvalues. The crucial difference to the open setup is that there are also a number of additional frequencies in the eigenspectrum which do not decay and are incommensurate with those generated by S^+. These frequencies are relevant at all timescales of the dynamics, leading to the noisier response observed.

In Fig. 5.4 we also see that the dynamics of $\langle S_4^x \rangle$ contains only a single frequency $\omega = B$ whilst the dynamics of $\langle S_4^x S_5^x \rangle$ contains the frequency $\omega = 2B$ as well as a constant offset. We know, however, that the operator S^+ generates a series of imaginary eigenmodes $\rho_{n,m}$ with frequencies $B(m-n)$ and that n and m can take values up to, and including, L as $(S^{\pm})^x \neq 0,\ x \leq L$. The fact that the observables in Fig. 5.4 only involve a single frequency is because of their overlap with the imaginary eigenmodes. We can show this explicitly by considering the operator $X = \prod_{i \in P} S_i^x$ where P is a set of M distinct sites of the lattice. Using $S_i^x = S_i^+ + S_i^-$ and performing a multinomial expansion of X the overlap with $\rho_{n,m}$ can then be written as a series of traces involving products of the steady state ρ_∞ and the operators S_i^+ and S_i^- on various sites. These traces are each only non-zero when the number of raising operators is equal to the number of lowering operators. We can identify the frequencies involved in the long-time dynamics of X based on the imaginary modes that it shares a non-zero overlap with, i.e. the modes where at least one of these traces is non-zero. From this, we find that the frequencies can only be integer multiples of B with the same parity (odd or even) as $|M|$ and those integers cannot exceed M. This is exactly what we observe in Fig. 5.4.

As our results are based on the spin SU(2) symmetry structure of the Liouvillian the coherent oscillatory behaviour we observe should be robust to any additional terms which preserve this symmetry. Examples of such terms include an arbitrary inter-site density-density interaction, i.e. $\sum_{i \neq j} f(i,j) n_i n_j$ [49] (where $f(i,j)$ is some real-valued function) and a disordered chemical potential. In Fig. 5.5 we plot the dynamics of the Liouvillian in Eq. (5.14) but with the inclusion of the latter term in the Hamiltonian. When γ is finite we observe the same coherent, oscillatory spin dynamics as before because the inhomogeneous chemical potential term commutes

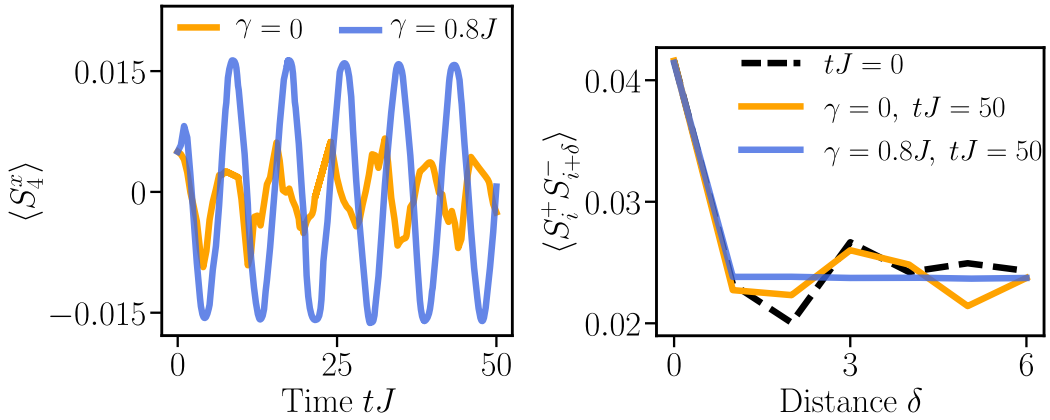

Figure 5.5: Dynamics of the number dephased Hubbard model described by the master equation in Eq. (5.14) but with the addition of a disordered chemical potential, i.e. $H(B,0) \to H(B,0) + \sum_i \epsilon_i n_i$. The system is initialised in the ground state of the Hamiltonian on a 7 site chain with 5 total particles, $U = 5.0J$, $B = 0$ and $\epsilon_i = 0\ \forall i$. This state is then time-evolved under $\mathcal{L}$ with $U = 6.0J$, $B = 0.8J$ and ϵ_i a random number uniformly drawn from the interval $[-0.5, 0.5]J$. The value of γ_i is taken to be the same on all sites and the two values used are specified in the legend. Left) Dynamics of $\langle S_4^x \rangle$. Right) Spin-exchange correlations $\langle S_i^+ S_{i+\delta}^- \rangle$ versus distance δ for the initial state at time $tJ = 0$ and the state at time $tJ = 50$ for both values of γ.

with the spin SU(2) symmetry. In the closed system the additional term has induced further noise in the system's dynamics, creating an even stronger distinction between the open and closed setups.

In Fig. 5.5 we also plot the spin-exchange correlations versus distance for the initial state and the long-time state in both the open and closed setups. We see that, in the open system, the dephasing has re-ordered these correlations to be completely uniform with distance. This is the mechanism of heating-induced order at play: the local, Hermitian jump operators have caused the system to continuously absorb energy whilst preserving the SU(2) spin structure. The homogeneous magnetic field and initial coherences between the spin SU(2) symmetry sectors has meant that, instead of relaxing to equilibrium as in the previous chapters, the system reaches a non-stationary, maximum entropy regime with the phase of those initial coherences continuously evolving in time.

Finally, it is important to discuss how this coherent oscillatory behaviour we have observed scales with the system size — we focused our numerics on small systems as they can be treated with quantum trajectories and an explicit construction of the Hamiltonian and jump operator matrices. We know that the long-time observables in

the open system are all independent of the sites that they are measured over because the imaginary modes and steady states are completely translationally symmetric. This means that if we can identify the behaviour of, for example, the global operator $S^x = \sum_i S_i^x$ then we can immediately determine the dynamics of the corresponding local operator from $L\langle S_i^x\rangle = \langle S^x\rangle$. The dynamical behaviour of S^x follows from the Heisenberg equation of motion where we find

$$\frac{\partial S^x}{\partial t} = \mathrm{i}B[S^z, S^x], \tag{5.15}$$

as S^x commutes with all the jump operators and all parts of the Hubbard Hamiltonian other than the magnetic field in the z direction. This equation tell us that the dynamics of S^x is simply equivalent to that of a big spin in a homogeneous magnetic field and the solution will therefore be $\langle S^x(t)\rangle = \langle S^x(0)\rangle \cos(Bt)$. It then follows that if the initial value $\langle S^x(0)\rangle$ grows, at least, linearly in L then the coherent oscillatory dynamics of S_i^x on a given site will be finite in the thermodynamic limit. Initial states which satisfy this requirement are numerous and examples include the state $\lim_{L\to\infty} \otimes_{i=1}^{L/2} |\leftarrow \mathrm{vac}\rangle$ which we used for finite L in Fig. 5.4. Alongside this, we can make similar arguments and identify initial states where observables such as $\langle S_i^x S_j^x\rangle$ will oscillate coherently in the thermodynamic limit of the open system [42].

In the closed system Eq. (5.15) still holds and so the total spin S^x will also coherently oscillate as $\langle S^x(0)\rangle \cos(Bt)$. Despite this, we cannot generally make the assumption that local observables are independent of the sites they are measured over and thus the dynamics on an individual site are not guaranteed to undergo noise-free coherent oscillations, which we saw explicitly in Figs 5.4 and 5.5. Any disorder in the Hamiltonian or inhomogeneity in the lattice (e.g. not all sites possessing the same co-ordination number) will prevent the Hamiltonian from being translationally invariant and observables such as S_i^x being independent of the site i. In the open Hubbard system, as long as the SDS is present, we can always make such an argument as the heating induced by the dephasing will render the long-time dynamics independent of the lattice geometry or any SU(2)-preserving disorder in the Hamiltonian.

The fact that, in the open system, the oscillatory dynamics of $\langle S_i^x\rangle$ are completely independent of the site i is significant. Given an arbitrary initial state, where the reduced state of the system will generally vary from site to site, the long-time oscillatory dynamics on each site will be identical in both phase and frequency. This phase and frequency locking of multiple distinct bodies is the hallmark of synchronisation [50, 51, 52, 53] and thus the SDS in our open Hubbard model has induced synchronisation in a quantum many-body system. In the following chapter we will explore

this idea in detail, showing how the interplay between an SU(2) SDS operator and heating in an open interacting many-body system can guarantee perfect quantum synchronisation.

5.4 Conclusion

In this chapter we have introduced a series of conditions which, when satisfied, imply the existence of a strong dynamical symmetry (SDS) operator in an open quantum system. The presence of this operator guarantees that the Liouvillian will possess commensurate purely imaginary modes and thus, instead of relaxing to stationarity, the system will undergo coherent oscillations as $t \to \infty$. These conditions are based purely on symmetry and place no constraints on the microscopic details of the system, providing a pathway to avoiding relaxation in a range of quantum systems.

We showed how the satisfaction of the SDS conditions immediately implies the existence of a strong symmetry which can be used to block-diagonalise the super-operator space, with the SDS operator coupling together the different spaces. We then introduced an example of a physical system with a SDS: the number dephased Hubbard model in the presence of an external magnetic field. Here, the presence of a SDS resulted in coherent oscillations in the spin degrees of freedom which persist indefinitely. When the dephasing was switched off, the imaginary eigenvalues of the Liouvillian were no longer commensurate with each other and noise was introduced into the oscillations. Thus the system-environment interaction is necessary for ensuring coherent, non-stationary dynamics in this setup. Finally, we discussed how these dynamics are underpinned by the same steady states and off-diagonal long-range order which we observed in the number-dephased Hubbard model in chapter 3. Here, the addition of a homogeneous magnetic field has introduced an extra time-dependent phase into the state of the system and prevented relaxation to stationarity.

These results open up the possibility of identifying further open systems which possess a SDS and will thus fail to equilibrate in the long-time limit. A number of recent works have observed this avoided relaxation in open systems, for example in the rotation between two different spatial modes in a pair of Bose-Einstein Condensates [54] or in the thermodynamic limit of a lossy collection of qubits [34, 35]. Connecting this behaviour to the presence of a SDS would greatly enhance our understanding of these systems and, in the former example, progress has already been made in this direction [55].

In the next chapter we will present a new avenue of research opened up by the SDS conditions introduced here. Specifically, we will show how the presence of a SDS operator, in tandem with the mechanism of heating-induced order, can lead to a new route via which perfect synchronisation can occur between the constituents of a many-body open quantum system.

References

[1] L. Boltzmann, *Lectures on Gas Theory* (*Reprinted*). Dover Publications, New York, 1995.

[2] D. Szász, *Boltzmann's Ergodic Hypothesis, a Conjecture for Centuries?*, pp. 421–446. Berlin, Heidelberg: Springer-Verlag, Berlin, 2000.

[3] J. M. Deutsch, "Quantum statistical mechanics in a closed system," *Phys. Rev. A*, vol. 43, pp. 2046–2049, 1991.

[4] J. V. Neumann, "Beweis des ergodensatzes und des H-theorems in der neuen mechanik (Proof of the ergodic theorem and the H-theorem in quantum mechanics)," *Z. Physic*, vol. 57, pp. 30–70, 1929.

[5] J. v. Neumann, "Proof of the quasi-ergodic hypothesis," *Proc. Natl. Acad. Sci.*, vol. 18, pp. 70–82, 1932.

[6] M. J. Klein, "The ergodic theorem in quantum statistical mechanics," *Phys. Rev.*, vol. 87, pp. 111–115, 1952.

[7] S. Goldstein, J. Lebowitz, C. Mastrodonato, R. Tumulka, and N. Zanghi, "Normal typicality and von Neumann's quantum ergodic theorem," *Proc. R. Soc. A*, vol. 466, p. 3203–3224, 2009.

[8] P. Bocchieri and A. Loinger, "Ergodic foundation of quantum statistical mechanics," *Phys. Rev.*, vol. 114, pp. 948–951, 1959.

[9] I. E. Farquhar and P. T. Landsberg, "On the quantum-statistical ergodic and H-theorems," *Proc. R. Soc. A*, vol. 239, p. 134–144, 1957.

[10] M. Rigol, V. Dunjko, and M. Olshanii, "Thermalization and its mechanism for generic isolated quantum systems," *Nature*, vol. 452, pp. 854–858, 2008.

[11] M. Srednicki, "Chaos and quantum thermalization," *Phys. Rev. E*, vol. 50, pp. 888–901, 1994.

[12] J. M. Deutsch, "Eigenstate thermalization hypothesis," *Rep. Prog. Phys.*, vol. 81, p. 082001, 2018.

[13] V. Alba, "Eigenstate thermalization hypothesis and integrability in quantum spin chains," *Phys. Rev. B*, vol. 91, p. 155123, 2015.

[14] H. Kim, T. N. Ikeda, and D. A. Huse, "Testing whether all eigenstates obey the eigenstate thermalization hypothesis," *Phys. Rev. E*, vol. 90, p. 052105, 2014.

[15] M. Rigol, V. Dunjko, and M. Olshanii, "Thermalization and its mechanism for generic isolated quantum systems," *Nature*, vol. 452, pp. 888–901, 2008.

[16] R. Steinigeweg, A. Khodja, H. Niemeyer, C. Gogolin, and J. Gemmer, "Pushing the limits of the eigenstate thermalization hypothesis towards mesoscopic quantum systems," *Phys. Rev. Lett.*, vol. 112, p. 130403, 2014.

[17] M. Žnidarič, "Exact solution for a diffusive nonequilibrium steady state of an open quantum chain," *J. Stat. Mech.: Theory Exp.*, vol. 2010, p. L05002, 2010.

[18] X. Xu, C. Guo, and D. Poletti, "Interplay of interaction and disorder in the steady state of an open quantum system," *Phys. Rev. B*, vol. 97, p. 140201, 2018.

[19] T. Prosen, "Open XXZ spin chain: Nonequilibrium steady state and a strict bound on ballistic transport," *Phys. Rev. Lett.*, vol. 106, p. 217206, 2011.

[20] R. Nandkishore and D. A. Huse, "Many-body localization and thermalization in quantum statistical mechanics," *Annu. Rev. Condens. Matter Phys.*, vol. 6, pp. 15–38, 2015.

[21] X. Li, S. Ganeshan, J. H. Pixley, and S. Das Sarma, "Many-body localization and quantum nonergodicity in a model with a single-particle mobility edge," *Phys. Rev. Lett.*, vol. 115, p. 186601, 2015.

[22] S. Gopalakrishnan and S. Parameswaran, "Dynamics and transport at the threshold of many-body localization," *Phys. Rep.*, vol. 862, pp. 1–62, 2020.
[23] F. Alet and N. Laflorencie, "Many-body localization: An introduction and selected topics," *C. R. Phys.*, vol. 19, pp. 498–525, 2018.
[24] N. Yunger Halpern, C. D. White, S. Gopalakrishnan, and G. Refael, "Quantum engine based on many-body localization," *Phys. Rev. B*, vol. 99, p. 024203, 2019.
[25] N. Y. Yao, C. R. Laumann, and A. Vishwanath, "Many-body localization protected quantum state transfer," *arXiv Preprint: quant-ph/1508.06995*, 2015.
[26] E. J. Heller, "Bound-state eigenfunctions of classically chaotic Hamiltonian systems: Scars of periodic orbits," *Phys. Rev. Lett.*, vol. 53, pp. 1515–1518, 1984.
[27] C. J. Turner, A. A. Michailidis, D. A. Abanin, M. Serbyn, and Z. Papić, "Weak ergodicity breaking from quantum many-body scars," *Nat. Phys.*, vol. 14, pp. 745–749, 2018.
[28] S. Chattopadhyay, H. Pichler, M. D. Lukin, and W. W. Ho, "Quantum many-body scars from virtual entangled pairs," *Phys. Rev. B*, vol. 101, p. 174308, 2020.
[29] W. W. Ho, S. Choi, H. Pichler, and M. D. Lukin, "Periodic orbits, entanglement, and quantum many-body scars in constrained models: Matrix product state approach," *Phys. Rev. Lett.*, vol. 122, p. 040603, 2019.
[30] H. Bernien, S. Schwartz, A. Keesling, H. Levine, A. Omran, H. Pichler, S. Choi, A. S. Zibrov, M. Endres, M. Greiner, V. Vuletić, and M. D. Lukin, "Probing many-body dynamics on a 51-atom quantum simulator," *Nature*, vol. 551, pp. 579–584, 2017.
[31] C.-J. Lin and O. I. Motrunich, "Exact quantum many-body scar states in the Rydberg-blockaded atom chain," *Phys. Rev. Lett.*, vol. 122, p. 173401, 2019.
[32] B. Mukherjee, S. Nandy, A. Sen, D. Sen, and K. Sengupta, "Collapse and revival of quantum many-body scars via Floquet engineering," *Phys. Rev. B*, vol. 101, p. 245107, 2020.
[33] J. Zhang, P. W. Hess, A. Kyprianidis, P. Becker, A. Lee, J. Smith, G. Pagano, I.-D. Potirniche, A. C. Potter, A. Vishwanath, N. Y. Yao, and C. Monroe, "Observation of a discrete time crystal," *Nature*, vol. 543, pp. 217–220, 2017.
[34] F. Lemini, A. Russomanno, J. Keeling, M. Schirò, M. Dalmonte, and R. Fazio, "Boundary time crystals," *Phys. Rev. Lett.*, vol. 121, p. 035301, 2018.
[35] G. Piccitto, M. Wauters, F. Nori, and N. Shammah, "Symmetries and conserved quantities of boundary time crystals in generalized spin models," *arXiv Preprint: quant-ph/2101.05710*, 2021.
[36] N. Dogra, M. Landini, K. Kroeger, L. Hruby, T. Donner, and T. Esslinger, "Dissipation-induced structural instability and chiral dynamics in a quantum gas," *Science*, vol. 366, pp. 1496–1499, 2019.
[37] A. Barenco, A. Berthiaume, D. Deutsch, A. Ekert, R. Jozsa, and C. Macchiavello, "Stabilization of quantum computations by symmetrization," *SIAM J. Comput.*, vol. 26, pp. 1541–1557, 1997.
[38] P. Zanardi and M. Rasetti, "Error avoiding quantum codes," *Mod. Phys. Lett. B*, vol. 11, pp. 1085–1093, 1997.
[39] L.-M. Duan and G.-C. Guo, "Preserving coherence in quantum computation by pairing quantum bits," *Phys. Rev. Lett.*, vol. 79, pp. 1953–1956, 1997.
[40] P. Zanardi and M. Rasetti, "Noiseless quantum codes," *Phys. Rev. Lett.*, vol. 79, pp. 3306–3309, 1997.
[41] D. A. Lidar, I. L. Chuang, and K. B. Whaley, "Decoherence-free subspaces for quantum

computation," *Phys. Rev. Lett.*, vol. 81, pp. 2594–2597, 1998.
[42] B. Buča, J. Tindall, and D. Jaksch, "Non-stationary coherent quantum many-body dynamics through dissipation," *Nat. Comm.*, vol. 10, p. 1730, 2019.
[43] T. Can, V. Oganesyan, D. Orgad, and S. Gopalakrishnan, "Spectral gaps and midgap states in random quantum master equations," *Phys. Rev. Lett.*, vol. 123, p. 234103, 2019.
[44] L. Sá, P. Ribeiro, and T. Prosen, "Spectral and steady-state properties of random Liouvillians," *J. Phys. A: Math. Theor.*, vol. 53, p. 305303, 2020.
[45] M. Nakagawa, N. Kawakami, and M. Ueda, "Exact Liouvillian spectrum of a one-dimensional dissipative Hubbard model," *arXiv Preprint: cond-mat.quant-gas/2003.14202*, 2020.
[46] M. V. Medvedyeva, T. Prosen, and M. Žnidarič, "Influence of dephasing on many-body localization," *Phys. Rev. B*, vol. 93, p. 094205, 2016.
[47] M. van Caspel and V. Gritsev, "Symmetry-protected coherent relaxation of open quantum systems," *Phys. Rev. A*, vol. 97, p. 052106, 2018.
[48] B. Buča and T. Prosen, "A note on symmetry reductions of the Lindblad equation: Transport in constrained open spin chains," *New J. Phys.*, vol. 14, p. 073007, 2012.
[49] K. Chinzei and T. N. Ikeda, "Time crystals protected by Floquet dynamical symmetry in Hubbard models," *Phys. Rev. Lett.*, vol. 125, p. 060601, 2020.
[50] A. Pikovsky, M. Rosenblum, J. Kurths, and J. Kurths, *Synchronization: A Universal Concept in Nonlinear Sciences*. Cambridge Nonlinear Science Series, Cambridge University Press, Cambridge, 2003.
[51] L. M. Pecora, T. L. Carroll, G. A. Johnson, D. J. Mar, and J. F. Heagy, "Fundamentals of synchronization in chaotic systems, concepts, and applications," *Chaos*, vol. 7, pp. 520–543, 1997.
[52] A. Roulet and C. Bruder, "Synchronizing the smallest possible system," *Phys. Rev. Lett.*, vol. 121, p. 053601, 2018.
[53] G. Manzano, F. Galve, G. L. Giorgi, E. Hernández-García, and R. Zambrini, "Synchronization, quantum correlations and entanglement in oscillator networks," *Sci. Rep.*, vol. 3, p. 1439, 2013.
[54] N. Dogra, M. Landini, K. Kroeger, L. Hruby, T. Donner, and T. Esslinger, "Dissipation-induced structural instability and chiral dynamics in a quantum gas," *Science*, vol. 366, pp. 1496–1499, 2019.
[55] B. Buča and D. Jaksch, "Dissipation induced nonstationarity in a quantum gas," *Phys. Rev. Lett.*, vol. 123, p. 260401, 2019.

Chapter 6

Quantum Synchronisation Enabled by Heating and Symmetries

A number of the results in this chapter were first published as

- J. Tindall, C. Sánchez Muñoz, B. Buča, and D. Jaksch, *Quantum synchronisation enabled by dynamical symmetries and dissipation*, New Journal of Physics, **22** 013026, (2020)

Contributions to this paper from JT are listed in the introduction.

In this chapter our focus is on quantum synchronisation in many-body systems. We begin with a discussion on the definition of synchronisation in both a classical and quantum setting – detailing notable examples of this co-operative phenomena and recent progress that has been made on our understanding of synchronisation in the quantum regime.

We then introduce the main result of this chapter. We show how, in an open system, the satisfaction of the conditions for a strong dynamical symmetry (SDS), alongside the mechanism of heating induced order, can ensure that a many-body system becomes completely synchronised in the long-time limit. We use first order perturbation theory to show how this novel, symmetry-based synchronisation is robust to a whole class of perturbations in the Hamiltonian of the system. Finally, using extensive analytical and numerical calculations, we present two examples where this mechanism for robust synchronisation can be observed: the many-body number dephased Hubbard model and a small chain of qutrits. We discuss how the SU(2) nature of the SDS operator and the heating in the system means that the synchronisation is underpinned by off-diagonal, long-range correlations.

6.1 Background: Synchronisation in Quantum and Classical Systems

Synchronisation is a fascinating, cross-disciplinary topic in modern science, focussed on understanding how groups of individual bodies adjust their rhythms and phases via their interactions with each other and the environment [1, 2, 3, 4, 5]. In a remarkable display of co-operation, this adjustment can lead to a variety of phenomena such as the 'winking' of fireflies, the behavioural synchrony of strangers or the coupling of pendulums through a common support [6, 7, 8].

Naturally, the study of synchronisation in quantum systems has also attracted significant attention [9, 10, 11, 12, 13, 14, 15]. In the quantum regime, synchronisation takes on a fairly broad definition due to the variety of cooperative, entangled behaviours that can occur [16]. For example, a Bose-Einstein condensate (BEC) could be considered a perfectly synchronised state due to the collective condensation of the bosonic atoms into the same mode [17]. In closer analogy with classical systems, models of self-sustained quantum oscillators, such as quantum Van der Pol oscillators [13, 18, 19] or micromasers [20], have been shown to lock phases and reach coupled limit cycles. Quantum effects play a crucial part in either enhancing [21, 22] or hindering [23] this synchronicity.

There has been a recent focus on observing synchronisation in the limit cycles of quantum systems which do not have a classical analogue [9, 10, 11]. The qutrit (i.e. a three level quantum system) has been proposed as a logical candidate for this and recent work has shown how it can be entrained to an external signal [9, 11] or phase-locked and entangled with a second qutrit [10]. In these single or two body systems, synchronisation emerges due to careful control over the Hamiltonian and dissipation parameters and is witnessed through both the phase space portrait and entanglement profile of the spins.

One of the most remarkable features of synchronisation in the classical regime, however, is that it occurs in such a broad range of systems — with vastly different sizes and structures [6, 7, 8, 24]. This diversity, in turn, leads to rich, observable, complex behaviour. Hence, instead of identifying specific quantum systems and regions of phase space where synchronisation can be observed, we think it is pertinent to determine, more generally, conditions which will ensure synchronisation can happen in a quantum system.

In this chapter we adopt this approach, identifying these conditions and detailing a novel mechanism which guarantees synchronisation in a generic open quantum system,

independent of its microscopic details. Specifically, we show how the coaction of heating-induced order and a strong dynamical symmetry operator can guarantee the formation of a translationally invariant long-time state which undergoes continuous limit cycles underpinned off-diagonal correlations. These cycles capture the essence of synchronisation, describing oscillations where the constituents of the system are locked to a common phase and frequency. Moreover, they also feature the same off-diagonal long-range order we observed under symmetry-constrained heating in the previous chapters indicating the synchronisation is of a truly quantum nature.

It is important to note that quantum synchronisation is sometimes viewed in terms of a locking in phase space of self-sustained oscillators, measured through the Husimi-Q or Wigner phase space distributions [9, 10, 19]. In this thesis we have instead opted for a different approach: to focus on the explicit limit cycles of the bodies in the system and plot them alongside various quantum synchronisation measures such as the negativity and total off-diagonal coherences. This is in order to reflect our intuition of quantum synchronisation as an intrinsically rhythmic process characterised by properties not available in classical systems.

6.2 Quantum Synchronisation Enabled by Heating and Symmetries

Requirements

Let us consider a many-body open quantum system described by the GSKL equation

$$\frac{\partial}{\partial t}\rho(t) = \mathcal{L}\rho = -i[H,\rho] + \sum_j \gamma_j \big(L_j \rho L_j^\dagger - \frac{1}{2}\{L_j^\dagger L_j, \rho(t)\}\big), \tag{6.1}$$

which we derived in chapter 1. We take the Hilbert space to be constructed from the tensor product of multiple, identical spaces/ sites, i.e. $\mathcal{H} = \otimes_i \mathcal{H}_i$ with $\dim(\mathcal{H}_i) = d \; \forall i$ and the Hamiltonian will contain terms which couple these local spaces together. We will assume that this system possesses a strong dynamical symmetry (SDS), i.e. we can identify an operator A which satisfies

$$[H, A] = \Omega A, \;\; \Omega \in \mathbb{R}_{>0} \qquad [L_j, A] = [L_j^\dagger, A] = 0 \qquad \forall j. \tag{6.2}$$

We will also assume that the imaginary eigenmodes and steady states of the Liouvillian originate solely due to the existence of A, i.e., they are all of the form $\rho_{n,m} \propto (A)^n \rho_\infty (A^\dagger)^m$, where ρ_∞ is a steady state of the system and exists in one of the blocks indexed by the distinct eigenvalues of the strong symmetry $S = AA^\dagger + A^\dagger A$.

The dynamics as $t \to \infty$ is thus completely governed by the steady state mode(s) ρ_∞ and the corresponding imaginary eigenmodes $\rho_{n,m}$ and will involve the system undergoing coherent, oscillatory limit cycles. The properties of these cycles are solely dependent on the structure of these long-time modes. For example, if the SDS operator A and the steady states are translationally invariant, then it immediately follows that in the long-time limit the expectation value of any local observable will be independent of the site where it is measured. Thus the system will undergo identical limit cycles at all points in space, i.e. it will be perfectly synchronised.

The immediate question is, in what situation will the operator A and the steady states be translationally invariant? This is where we reintroduce the mechanism of heating-induced order. Specifically, we will first assume that the operator A is SU(2) by nature, i.e. the operators A, $A^\dagger$ and $[A, A^\dagger]$ form the generators J^1, J^2, J^3 which satisfy the SU(2) relations

$$[J^i, J^j] = \mathrm{i}\epsilon_{ijk} J^k. \tag{6.3}$$

The SU(2) Casimir operator $AA^\dagger + A^\dagger A$ is the corresponding strong symmetry S for A. As we are in a truly many-body system (i.e. one which contains non-trivial interactions) we can assume that we are working with a 'global' representation of the SU(2) symmetry.

We then introduce heat into the system via local, homogeneous, Hermitian dephasing — i.e. we let the jump operators form a set of purely local operators $\{L_j\}$ with $L_j \equiv L_j^\dagger$. Here, j runs over all the sites in the systems, and the L_j are identical outside of the fact that they reside on different sites. Homogeneity is ensured by setting $\gamma_j = \gamma \; \forall j$. We know from earlier chapters that this type of dephasing means the system continuously absorbs energy from its environment with the resulting steady states simply forming the identity matrix in each of the SU(2) subspaces.

We also know from our work in chapter 2 that these steady states are translationally invariant and will contain finite, completely uniform off-diagonal correlations. The imaginary modes will inherit the properties of these steady states via $(A)^n \rho_\infty (A^\dagger)^m$ and the limit cycles in the system will thus be underpinned by these quantum correlations and correspond to coherences between the SU(2) subspaces. As the steady state is translationally invariant the spatial dependence of these limit cycles will be completely controlled by A. If A is also translationally invariant then they will be necessarily identical at every point in space and we have perfect synchronisation. This is the case we are focussed on here and as A is a global representation

of SU(2) in a many-body setup it is not unreasonable to assume that it will be translationally invariant[1]. We thus expect the combination of heating-induced order and an SDS to give us perfect synchronisation.

It is worth mentioning that if we consider system-environment couplings that do not heat the system up then we might have steady states which possess alternative types of spatial symmetries such as antisymmetry under an exchange of the constituents or translational invariance but only amongst certain 'clusters' of the constituents. This would lead to examples of anti-synchronisation, or clustered synchronisation, enabled by an SDS[2]. In this chapter we are focussed on the case of perfect synchronisation enabled by an SDS and heating-induced order and note that alternative types of SDS-enabled synchronisation would be a natural extension of this work.

Robustness to Perturbation

Before we treat specific examples of systems where our synchronisation can be observed it is important to consider how robust this setup is to perturbations. In any realistic setting there will always be unwanted influences which force us away from the ideal regime and for our synchronisation mechanism to be observable it should, to some degree, be robust to this.

We will begin by being as general as possible. Let us imagine that we have a Liouvillian $\mathcal{L} = \mathcal{L}^{(0)}$ which is defined via the GSKL equation in Eq. (6.1). We then assume that our open system is subject to some perturbation which alters the Liouvillian to become

$$\mathcal{L} \to \mathcal{L}^{(0)} + \epsilon\mathcal{L}^{(1)}, \tag{6.4}$$

where ϵ is dimensionless and describes the magnitude of the perturbation. We denote the left and right eigenvectors (in superket form) of the unperturbed Liouvillian $\mathcal{L}^{(0)}$ via $|\rho_i^{(0)}\rangle$ and $\langle\sigma_i^{(0)}|$, with $\lambda_i^{(0)}$ the corresponding eigenvalue and i indexing all the different possible eigenvectors. Now, assuming $\epsilon \ll 1$, we can expand the eigenvectors

[1]The only exception which comes to mind is the η operators in the Hubbard model. The checkerboard pattern of $+1$ and -1 these operators possess would instead lead to perfect synchronisation between the sites in the same sublattice and anti-synchronisation between those in different sublattices.

[2]For instance, in Fig. 1 of Ref. [25] the observed anti-synchronisation can be directly related to the fact that one of the steady states is anti-symmetric under an exchange of the qubits.

of the perturbed Liouvllian $\mathcal{L}$ in terms of the unperturbed Liouvillian, i.e.

$$\begin{aligned}|\rho_j\rangle\rangle &= |\rho_j^{(0)}\rangle\rangle + \epsilon|\rho_j^{(1)}\rangle\rangle + \epsilon^2|\rho_j^{(2)}\rangle\rangle + \dots,\\ \langle\langle\sigma_j| &= \langle\langle\sigma_j^{(0)}| + \epsilon\langle\langle\sigma_j^{(1)}| + \epsilon^2\langle\langle\sigma_j^{(2)}| + \dots,\\ \lambda_j &= \lambda_j^{(0)} + \epsilon\lambda_j^{(1)} + \epsilon^2\lambda_j^{(2)} + \dots.\end{aligned} \tag{6.5}$$

We also know that the orthonormality condition $\langle\langle\sigma_j|\rho_k\rangle\rangle = \mathrm{Tr}(\sigma_j^\dagger\rho_k) = \delta_{j,k}$ must hold $\forall\epsilon$, where we have defined σ_j and ρ_k as the matrix forms of the corresponding superket and superbras. Using this condition, to 0th and 1st order, we have

$$\mathrm{Tr}\left(\left(\sigma_j^{(0)}\right)^\dagger\rho_k^{(0)}\right) = \mathrm{Tr}\left(\left(\sigma_j^{(1)}\right)^\dagger\rho_k^{(0)} + \left(\sigma_j^{(0)}\right)^\dagger\rho_k^{(1)}\right) = \delta_{jk}. \tag{6.6}$$

We then simplify the known expression $\langle\langle\sigma_j|\mathcal{L}|\rho_j\rangle\rangle = \lambda_j\langle\langle\sigma_j|\rho_j\rangle\rangle$ by subsitituting the expansions in Eq. (6.5), converting to matrix form and applying Eq. (6.6). As a result we obtain the first order correction to any given eigenvalue:

$$\lambda_j^{(1)} = \mathrm{Tr}\left(\left(\sigma_j^{(0)}\right)^\dagger\mathcal{L}^{(1)}\rho_j^{(0)}\right), \tag{6.7}$$

which is general and applies to any Liouvillian where the perturbation is sufficiently small.

Now we consider specifics relevant to the problem at hand. We are focussing on how perturbations affect the synchronisation in the long-time limit of a system with a SDS, interactions and homogeneous, Hermitian, local dephasing. We thus focus solely on the perturbations to the eigenvalues which have $\mathrm{Re}(\lambda_j) = 0$ and so the $|\rho_j^{(0)}\rangle$ and $\langle\sigma_j^{(0)}|$ that we are considering will be either steady states or purely imaginary eigenmodes.

We take the scenario in which the perturbation in the Liouvillian is due to some inhomogeneous field in the Hamiltonian, i.e.

$$\mathcal{L}^{(1)} = -\mathrm{i}\Big[\sum_i \delta_i f_i, \bullet\Big], \tag{6.8}$$

where the summation is over the constituents of the system with the δ_i being the field strengths and the f_i being Hermitian field operators. Our first order perturbation to the eigenvalues on the imaginary axis is then

$$\lambda_j^{(1)} = -\mathrm{i}\sum_i \delta_i \mathrm{Tr}\Big((\sigma_j^{(0)})^\dagger f_i\rho_j^{(0)} - (\sigma_j^{(0)})^\dagger\rho_j^{(0)}f_i\Big). \tag{6.9}$$

We can simplify this by observing that $\sigma_j^{(0)} = \rho_j^{(0)}$ for our system. This is because our jump operators are Hermitian and so the 'left' and 'right' GSKL equations are

identical and any 'right' eigenvector is automatically a 'left' eigenvector and vice-versa. This leads us to

$$\lambda_j^{(1)} = -\mathrm{i}\sum_i \delta_i \mathrm{Tr}\Big((\rho_j^{(0)})^\dagger f_i \rho_j^{(0)} - (\rho_j^{(0)})^\dagger \rho_j^{(0)} f_i\Big), \tag{6.10}$$

which we note immediately evaluates to 0 if $\left(\rho_j^{(0)}\right)^\dagger = \rho_j^{(0)}$ and is the case for the trace one steady states as they are necessarily Hermitian. Meanwhile, for the non-Hermitian imaginary eigenmodes $\rho_j^{(0)}$ the trace in Eq. (6.10) is independent of i because, for our system, they are all translationally invariant. Hence, if we have $\sum_i \delta_i = 0$ then the first order correction for all the long-time modes is zero and the synchronisation is, to first order, robust to the inhomogeneous field.

This type of inhomogeneous field covers some important cases. For example, in any realistic setup, there will be some disorder in the on-site Hamiltonian terms such as the chemical potential. As the disorder is typically driven by external fluctuations the average will be zero so the system will be robust to this. Secondly, and particularly relevant to our synchronisation scenario, the SDS of our system is likely to arise due to some homogeneous field in the Hamiltonian, i.e. $[\sum_i \omega f_i, A] \propto \omega A$. The observed synchronisation of the system thus corresponds to a phase locking — the frequency locking occurs trivially because all the sites share the same natural frequency ω. We know, however, from the perturbation theory presented above that the synchronisation is robust to a small amount of disorder in ω and so we anticipate frequency locking can occur if the sites have slightly different natural frequencies. This will only happen transiently because eventually higher order effects will manifest and cause the imaginary modes, and corresponding synchronisation, to decay away. In the following examples we will observe this transient synchronisation explicitly, validating the results we have derived here.

Finally, it is also worth mentioning that even in the case of a perturbation where the correction $\lambda_j^{(1)}$ is finite it will always be purely imaginary if the corresponding field operators are real-valued. This covers the majority of physical scenarios and the first order correction will only be in the frequency of the system's limit cycles and will not correspond to any decay of the synchronisation.

6.3 Examples

Synchronisation Witnesses - In order to help us interpret the following numerical results we introduce several synchronisation measures. The first, and most direct, of

these is the time-dependent Pearson correlation factor [14, 26] which measures the correlation between two functions f and g over the domain $[t, t+\Delta t]$:

$$C_{f,g}^{\Delta t}(t) = \frac{\int_t^{t+\Delta t}(f-\bar{f})(g-\bar{g})dt}{\sqrt{\int_t^{t+\Delta t}(f-\bar{f})^2 dt \int_t^{t+\Delta t}(g-\bar{g})^2 dt}}, \tag{6.11}$$

with the function average $\bar{f} = \frac{1}{\Delta t}\int_t^{t+\Delta t} f dt$. This correlation factor is maximal (minimal) or 1 (-1) when the two signals f and g are perfectly synchronised (anti-synchronised), and 0 when they display no correlations. Whilst this allows us to directly quantify how similar the oscillations undergone by the constituents of our system are, it does not tell us whether they are truly correlated; for example, it would give a value of 1 for two independent qubits in a homogeneous magnetic field if they are initialised in the same state. Hence, we introduce two additional measures which can be used to capture the quantum nature of the correlations in the system. These are the negativity $\mathcal{N}$ [27] and off-diagonal coherence $\mathcal{C}$ [11]

$$\begin{aligned} \mathcal{N}_i(\rho) &= \frac{||\rho^{T_i}|| - 1}{2}, \\ \mathcal{C} &= \sum_{j\neq k} |\rho_{jk}|, \end{aligned} \tag{6.12}$$

with T_i indicating the partial transpose with respect to site i and $||X|| = \mathrm{Tr}\sqrt{X^\dagger X}$ denoting the trace norm of an operator. The negativity can be seen as a measure of the degree to which site j is entangled with the rest of the system. It is a proper measure of entanglement as it is an entanglement monotone and vanishes for separable states [27]. Meanwhile, the coherence quantifier $\mathcal{C}$ describes the total magnitude of the off-diagonal elements in the system's density matrix.

Number Dephased Hubbard Model

With these measures in hand we return to the number dephased Hubbard model from the previous chapter which is described by the master equation

$$\frac{\partial}{\partial t}\rho(t) = \mathcal{L}\rho = -i[H,\rho] + \sum_i \gamma_i\big(n_i\rho n_i - \frac{1}{2}\{n_i^\dagger n_i, \rho(t)\}\big), \quad n_i = n_{\uparrow,i} + n_{\downarrow,i}. \tag{6.13}$$

For generality we will take the chemical potential and magnetic field in the Hamiltonian to be disordered, i.e.

$$H = -J\sum_{\langle ij\rangle}\sum_\sigma c_{\sigma,i}^\dagger c_{\sigma,j} + \text{H.c.} + U\sum_i n_{\uparrow,i}n_{\downarrow,i} + \sum_i B_i(n_{\uparrow,i} - n_{\downarrow,i}) + \sum_i \mu_i(n_{\uparrow,i} + n_{\downarrow,i}). \tag{6.14}$$

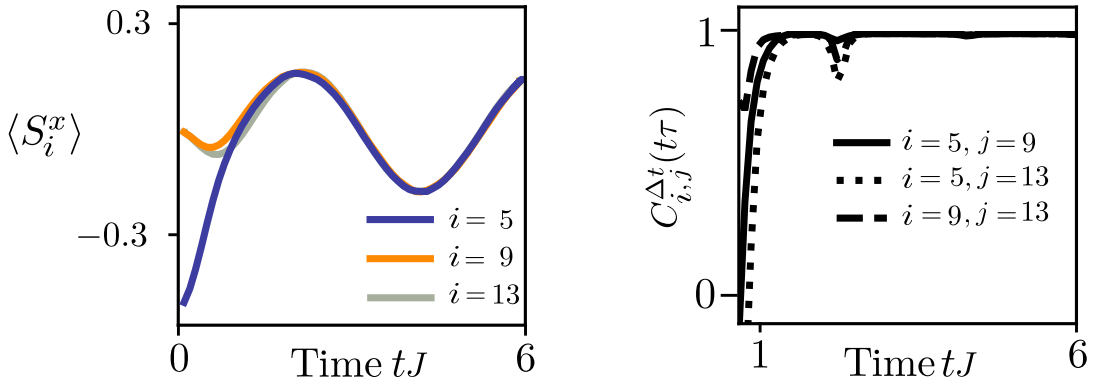

Figure 6.1: Left) Dynamics of $\langle S_i^x \rangle$ for a quench of the $L = 15$ site number-dephased Hubbard chain described by the master equation in Eq. (6.13) and with the Hamiltonian defined in Eq. (6.14). Parameters are $\gamma = 2.5J$, $U = 1.0J$, $B_i = 1.5J\ \forall i$, $\mu_i \in [0.0, 0.2]J$ where $[0.0, 0.2]$ is a uniformly-drawn random number on the specified interval and the plotted dynamics represent a single shot (i.e. a single evolution and instance of $\mu_1, ..., \mu_L$). Synchronisation emerges in the long-time limit for any given shot. The initial state is $|\psi(0)\rangle = \otimes_{i=1}^{5} |\chi\rangle$ where $|\chi\rangle = |\leftarrow\downarrow\uparrow\rangle$ and $\leftarrow, \uparrow$ and $\downarrow$ correspond to each site being polarised in the negative x-direction, positive z and negative z-direction respectively. Right) Pearson time-correlation coefficient for each possible pair of functions from the left plot. The time-averaged window is a rolling window with width $\Delta t = 0.5tJ$ centred at time tJ.

This system satisfies our desired synchronisation conditions when $B_i = B\ \forall i$: there is a SDS operator S^+ which generates an SU(2) algebra, the dephasing is induced by homogeneous, Hermitian operators and (for $U, J \neq 0$) there are non-trivial interactions making the system truly many-body. These interactions are two-fold: in the form of the necessary hopping term which couples sites together and in the form of the interaction term which couples the electrons together. For numerical tractability we are considering a 1D chain as our lattice but emphasize that these results will apply on *any* graph.

In Fig. 6.1 we plot the dynamics of $\langle S_j^x \rangle$ on various sites of the lattice. The specified sites are initially out of phase but they quickly lock together and undergo completely identical limit cycles, with the Pearson coefficient C saturating to unity; the dip at $tJ \approx 2$ is a transient effect which occurs at the first turning point in the magnetisation. Whilst we have specified only three of the fifteen sites on the lattice we emphasize that this synchronised behaviour can be observed in the x magnetisation of any of the sites, with the Pearson coefficient for any given pair saturating to its maximal value. Furthermore, this behaviour can be observed for any system size.

The initial state satisfies $\langle S^x \rangle \propto L$ and so, due to the translational invariance of the long-time dynamics, the limit cycle for each site will have finite amplitude even as $L \to \infty$.

We now consider the case when the magnetic field is not homogeneous, i.e. $B_i \neq$ const. Whilst the operator S^+ is technically no longer a SDS we know from our perturbation theory results that if the inhomogeneity is sufficiently small the corresponding imaginary modes should remain to first order. In Figs. 6.2a-b we plot the quantum synchronisation witnessess $\mathcal{N}_i$ and C as a function of time and of the detuning δ, which quantifies the inhomogeneity of the field. As we anticipate, these quantities are at their largest and do not decay away when there is no detuning in the field and the system exactly satisfies the SDS conditions in Eq. (6.2). Here, the limit cycles of the system survive indefinitely and these plots demonstrate that they are characterised by entanglement and off-diagonal coherences which are intrinsically quantum properties. These properties are related to each other and share the same origin: the off-diagonal long-range order that has been induced in the steady state by the preservation of an SU(2) symmetry under heating.

Strikingly, in Figs. 6.2a-b, there is a band of finite detunings where these quantum effects survive on exceptionally long time-scales and this suggest that the system is still able to synchronise, despite not exactly satisfying the SDS condition. This can be seen in Figs. 6.2c-d where we plot the spin dynamics over time for a specific detuned setup and observe how the limit cycles of the considered spins lock together despite possessing different frequencies and initial phases. The locked frequency is the average of their natural frequencies which is in agreement with our perturbation theory. Whilst in this detuned case the oscillations in $\langle S_i^x \rangle$ are decaying away, they survive for many hopping times.

Spin-Agnostic XXZ Spin-1 Chain

We now move away from the Hubbard model and consider a second example of SDS enabled synchronisation in the form of a chain of spin-1s or qutrits — demonstrating that our results and understanding of this mechanism are general and not specific to a single setup or model. The local basis for each spin-1 is spanned by the three states $\{|\downarrow\rangle, |0\rangle, |\uparrow\rangle\}$. The key operators S_i^+, S_i^- and S_i^z are, respectively, the spin-1 raising, lowering and magnetisation operators for a given spin i. The x and y components of the spin-1 operator can be formed from the raising and lowering operators via $S_i^x = (1/2)(S_i^+ + S_i^-)$, $S_i^y = (\mathrm{i}/2)(S_i^- - S_i^+)$. As usual, by dropping the site subscript we denote the total of an operator, e.g. $S^z = \sum_i S_i^z$.

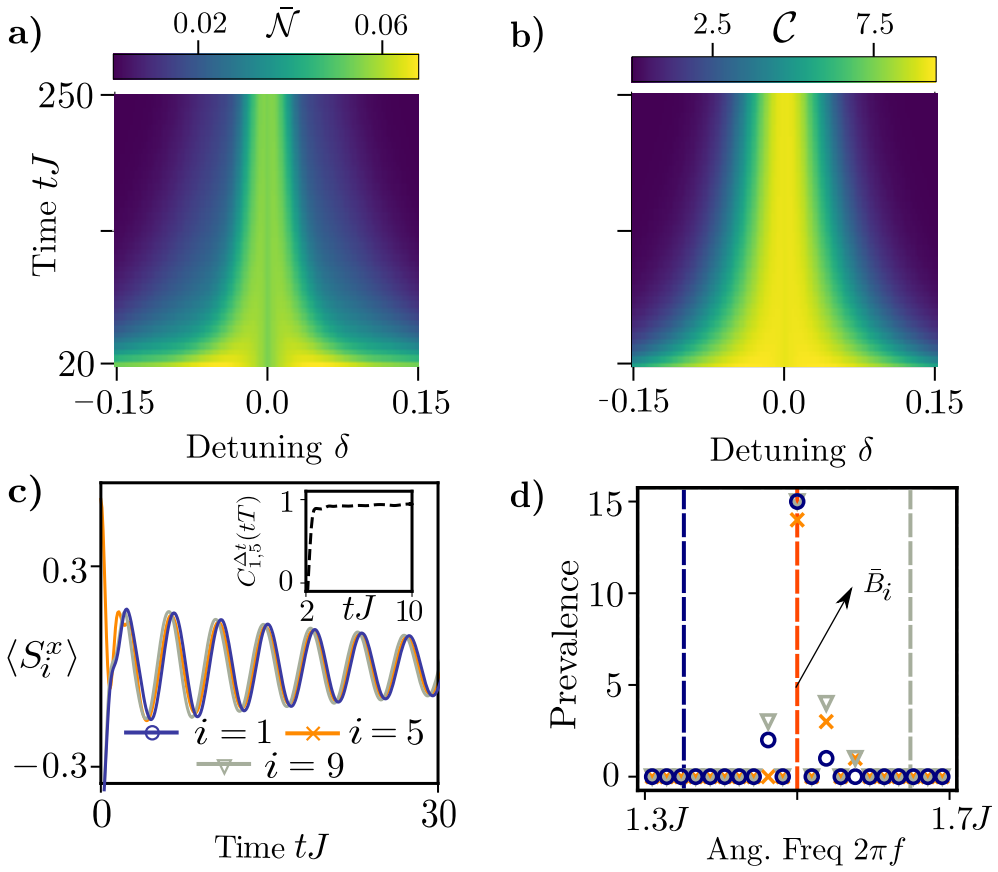

Figure 6.2: a-b) Synchronisation witnesses vs time and detuning for the charge-dephased Hubbard model with $L = 5$ sites, described by Eq. (6.13) with H defined in Eq. (6.14). The system is initialised as $|\psi(0)\rangle = |{\rightarrow}{\uparrow}{\rightarrow}{\uparrow}{\rightarrow}\rangle$ where $\rightarrow, \leftarrow$ and $\uparrow$ correspond to each site being polarised in the positive x, negative x and positive z directions respectively. The system is then evolved with parameters $\gamma = 2.0J, U = 0.5J$ and $\mu_i \in [0, 0.2]J$ — with a different, random, set of μ_i drawn for each detuning strength. The site-dependent magnetic field strengths are $\{B_1, B_2, B_3, B_4, B_5\} = \{1.0 - \delta, 1.0 - \delta/2, 1.0, 1.0 + \delta/2, 1.0 + \delta\}J$. a) Average negativity $\bar{\mathcal{N}} = (1/3)\sum_i \mathcal{N}_i$. b) Total magnitude of the off-diagonal coherences. c) Example dynamics of $\langle S_i^x \rangle$ for $L = 9$. The field strengths are: $\{B_1, B_2, ...B_L\} = \{1.35, 1.3875, ..., 1.65\}J$ and we set $\gamma = 0.5J$, $U = J$, $\mu_i \in [0.0, 0.2]J$ and $|\psi(0)\rangle = \otimes_{i=1}^{3} |\chi\rangle$ where $|\chi\rangle = |{\rightarrow}{\leftarrow}{\rightarrow}\rangle$. Inset) Time-dependent Pearson coefficient for the two functions $\langle S_1^x \rangle$ and $\langle S_5^x \rangle$ with a rolling window of $\Delta t = 2.0tJ$. d) Prevalence of frequencies, extracted from the distribution of angular frequencies created using the time-periods between successive turning points for the oscillations in c) but up to $tJ = 90.0$. Blue and green dashed lines indicate the expected delta function in the prevalence based on the natural frequency of spins 1 and 9. Red dashed line indicates the average of the magnetic field strengths.

The Hamiltonian for our system is that of a spin-1 anisotropic Heisenberg model in a chain geometry [28]

$$H = \sum_{i=1}^{L} \omega_i S_i^z + \sum_{i=1}^{L-1} J\left(S_i^+ S_{i+1}^- + S_i^- S_{i+1}^+\right) + \Delta S_i^z S_{i+1}^z, \tag{6.15}$$

where the spins each have natural frequency ω_i and nearest-neighbour coupling strengths J and $\Delta \neq 0$. The system is then immersed in a bath which induces homogeneous local, quadratic dephasing in a spin-agnostic manner. The ensuing dynamics are described by the master equation

$$\frac{\partial \rho}{\partial t} = \mathcal{L}\rho = -i[H, \rho] + \gamma \sum_{i=1}^{N} (S_i^z)^2 \rho (S_i^z)^2 - \frac{1}{2}\{(S_i^z)^4, \rho\}. \tag{6.16}$$

In Fig. 6.3 we picture this locally dephased spin-1 chain.

In the 'frequency-matched' case of this Liouvillian (i.e. $\omega_i = \omega \ \forall i$) we are able to show that there exists a SDS and derive an analytical expression for the steady states and the imaginary eigenmodes of the chain. Here the Liouvillian has a steady state degeneracy of $2L + 2$ with all but one of these states originating from the magnetisation S^z forming a strong symmetry of the system. These $2L+1$ states thus correspond to the identity matrix in each of the magnetisation sectors: i.e. they are of the form $\rho_{ss} = \sum_j |m_j\rangle \langle m_j|$, where $|m_j\rangle$ is an eigenvector of S^z with eigenvalue m and j indexes the possible eigenvectors for each m. The additional steady state is in the zero magnetisation sector and takes the form $\sum_0 |0_j\rangle \langle 0'_j|$ where we have defined $|-m'_j\rangle = \mathrm{SF}\,|m_j\rangle$, with $\mathrm{SF} = \otimes_{i=1}^{N}\left(|\uparrow\rangle\langle\downarrow| + |\downarrow\rangle\langle\uparrow| + |0\rangle\langle 0|\right)$ being the spin-flip operator. For example if $|2_1\rangle = |0\uparrow\uparrow\rangle$ then $|-2'_1\rangle = |0\downarrow\downarrow\rangle$, or if $|0_3\rangle = |0\uparrow\downarrow\rangle$ then $|0'_3\rangle = |0\downarrow\uparrow\rangle$. Knowing this, we can then write down a general expression for a steady state of the system as

$$\rho_{ss} = \sum_{m=-L}^{L} \lambda_m \left(\sum_j |m_j\rangle \langle m_j| \right) + \lambda'_0 \sum_j |0_j\rangle \langle 0'_j|, \tag{6.17}$$

where the elements $\{\lambda_m\}$ and λ'_0 must satisfy the equation

$$\lambda'_0 + \sum_{m=-L}^{L} \lambda_m \sum_{s=0}^{L} \binom{L}{s} \binom{L-s}{(N-s+m)/2} = 1. \tag{6.18}$$

in order for $\mathrm{Tr}(\rho_{ss}) = 1$.

We can also see that the operators

$$A_m = \sum_j |m_j\rangle \langle -m'_j|, \quad m \neq 0, \ m = -L, ..., L, \tag{6.19}$$

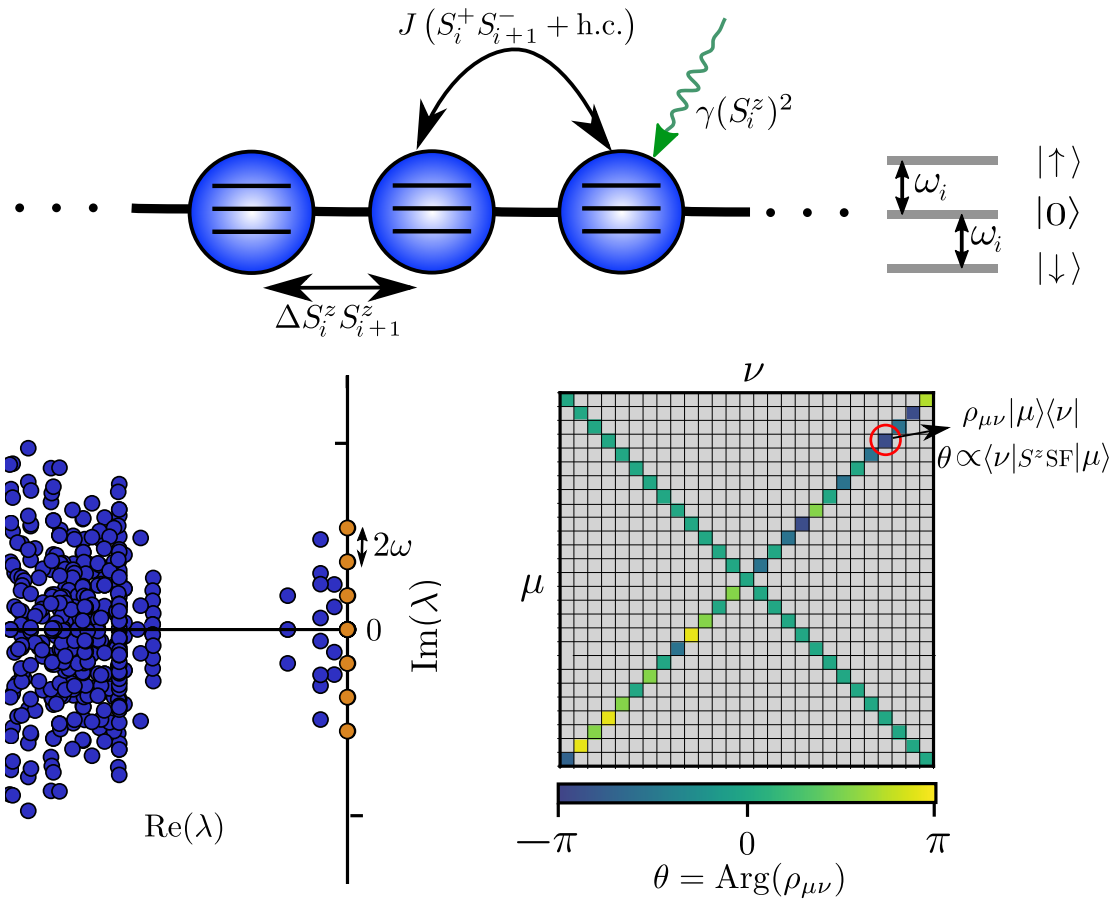

Figure 6.3: a) Series of spin-1s in a chain geometry. The system is governed by the Hamiltonian in Eq. (6.15) with on-site dephasing of the form $L_i = (S_i^z)^2$. The resulting dynamics are described by the master equation in Eq. (6.16). b) Eigenvalues $\{\lambda\}$ close to the real axis for the Liouvillian superoperator. Parameters used are $L = 3,\ \omega_i = \omega = 1.0J\ \forall i,\ \Delta = 0.5J,\ \gamma = 2.0J$. Eigenvalues with $\text{Re}(\lambda) = 0$ are marked in orange, all others are marked in blue. c) Structure of the density matrix in the Fock basis which diagonalises S^z as $t \to \infty$ for $N = 3$. The colour indicates the phase of each complex element $\rho_{\mu\nu}$, the grey colour indicates $\text{Abs}(\rho_{\mu\nu}) = 0$ and so the phase is not plotted. The indices μ and ν run over the basis vectors of the Hilbert space in lexicographic order when they are converted to ternary strings with $\uparrow = 2,\ 0 = 1,\ \downarrow = 0$. As an example when $\mu = 1$ this corresponds to the basis vector $|\uparrow\uparrow\uparrow\rangle = |222\rangle$ and when $\mu = 27$: $|\downarrow\downarrow\downarrow\rangle = |000\rangle$. Example element (ringed in red) has a phase which evolves in time as $\theta = 2m\omega t$ where $m = \langle\nu|\, S^z\text{SF}\, |\mu\rangle$, with $\text{SF} = \otimes_{i=1}^{N}\left(\,|\uparrow\rangle\langle\downarrow| + |\downarrow\rangle\langle\uparrow| + |0\rangle\langle 0|\,\right)$. This phase is only non-zero for elements along the anti-diagonal.

are linearly independent and *each* satisfy the SDS conditions as

$$[H, A_m] = 2m\omega A_m, \quad [L_i, A_m] = [L_i^\dagger, A_m] = 0, \quad \forall i. \tag{6.20}$$

These operators are extensive (i.e. acting over the full system) and each generates an SU(2) algebra as A_m, $A_m^\dagger$ and $[A_m, A_m^\dagger]$ satisfy Eq. (6.3) for any given m. Interestingly, the SU(2) generator A_m cannot be written as a sum over local operators. Nontheless it is still a true representation of SU(2) and is translationally invariant, which is what we require for our synchronisation.

Through the SDS operators A_m we can then construct a series of imaginary eigenmodes

$$\rho^m \propto A_m \rho_{ss} \propto A_m, \qquad \mathcal{L}\rho^m = -2\mathrm{i}m\omega. \tag{6.21}$$

Notably, we have only considered a single application of A_m in generating these modes; further multiplication is redundant as $A_n A_m = 0 \; \forall n, m$. Each SDS operator therefore creates a unique conjugate pair of imaginary eigenmodes through $A_m \rho_{ss}$ and $\rho_{ss} A_m^\dagger$. These modes form an equidistant spectrum as the index m runs in integer steps from $-L$ to L and so the structure of the spectrum is equivalent to having a single SDS which can be applied to the steady state multiple times. This is evidenced numerically in Fig. 6.3.

It might appear problematic that we have multiple SDS operators. These operators, however, are completely independent of each other because they act in sectors of different magnetisation m. Thus in a given region of the Hilbert space which contains the states of magnetisation m and $-m$ we have the conjugate pair of SU(2) SDS operators A_m and $A_m^\dagger$, together with heating and interactions. As S^z is a strong symmetry, regions with different values of m do not interact under the Liouvillian and each one independently satisfies our requirements for synchronisation. The direct sum of all regions (i.e. the total system) will consequently be synchronised.

The steady state and imaginary eigenmodes in Eqs. (6.17) and (6.19) form a complete basis for the long-time dynamics of Eq. (6.16) and so, in this limit, the density matrix can be expressed as a superposition of these modes. This is seen in Fig. 6.3, where we plot an example of the long-time density matrix of the system in the Fock basis which diagonalises S^z. In this product state basis the excited imaginary modes correspond to off-diagonal matrix elements with a time-dependent phase and describe coherences between sectors of opposite magnetisation. Therefore, we require initial states which are in a superposition of states of different magnetisation to excite them. Meanwhile, the steady state modes correspond to time-independent diagonal matrix elements.

Our system contains the necessary ingredients for synchronisation: an extensive SU(2) SDS operator (in this case multiple, independent SU(2) SDS operators), heating and interactions. As a consequence, the steady states and imaginary eigenmodes are completely translationally invariant which can be seen directly in Eqs. (6.17) and (6.19). Any observable will therefore be independent of the sites it is measured over, allowing us to anticipate perfect synchronisation in the case $\omega_i = \omega$. In addition, when the frequencies are slightly detuned we can expect our results from perturbation theory to hold and, to first order, perfect synchronisation will be manifest.

We now use exact diagonalisation on small chains to demonstrate this explicitly. We start with the frequency matched case $\omega_i = \omega \ \forall i$ and observe the synchronisation and coherent limit cycles which occur in the square of the local magnetisation $\langle (S_i^x)^2 \rangle$. In Fig. 6.4a we observe the system when both the dephasing and interactions are switched on. The qutrits are initialised in a random product state and so are initially out of phase. Under the action of the Liouvillian in Eq. (6.16) they synchronise perfectly and undergo identical, coherent limit cycles with a Pearson coefficient of unity. The frequency of these cycles is equal to 2ω because we have that $\mathrm{Tr}((S_i^x)^2 A_m) = 0$ unless $m = 0$ or $m = 2$. In order to observe higher frequencies we can, instead, measure multi-point correlation functions, as we demonstrated in Ref. [29].

In Figs. 6.4b-c we consider the dynamics of the same system but with the $z - z$ interaction strength Δ and dephasing strength γ, respectively, set to 0. In the former we observe coherent limit cycles but there is an absence of phase locking between the spins. This is because, whilst the imaginary eigenmodes and steady states we wrote down in Eqs. (6.17) and (6.19) are still present, the Liouvillian is much simpler[3] and there are additional steady states which are not completely translationally invariant and prevent perfect synchronisation from occurring. By switching on the $z - z$ interaction we can eliminate these steady states and force the qutrits to synchronise. Meanwhile in the closed system where $\gamma = 0$ there are no coherent limit cycles and the dynamics are completely chaotic and noisy as the spectrum of the system is now incommensurate. The system-environment interaction is thus necessary for coherent dynamics, one of the remarkable consequences of a strong dynamical symmetry. We also emphasize that the results in this figure (i.e. the synchronisation for $\Delta, \gamma \neq 0$, lack of phase-locking for $\Delta = 0$ and chaos for $\gamma = 0$) are independent of the specifics

[3]It is in fact no longer many-body as it can be mapped, via a Jordan-Wigner transform, into a system of free particles.

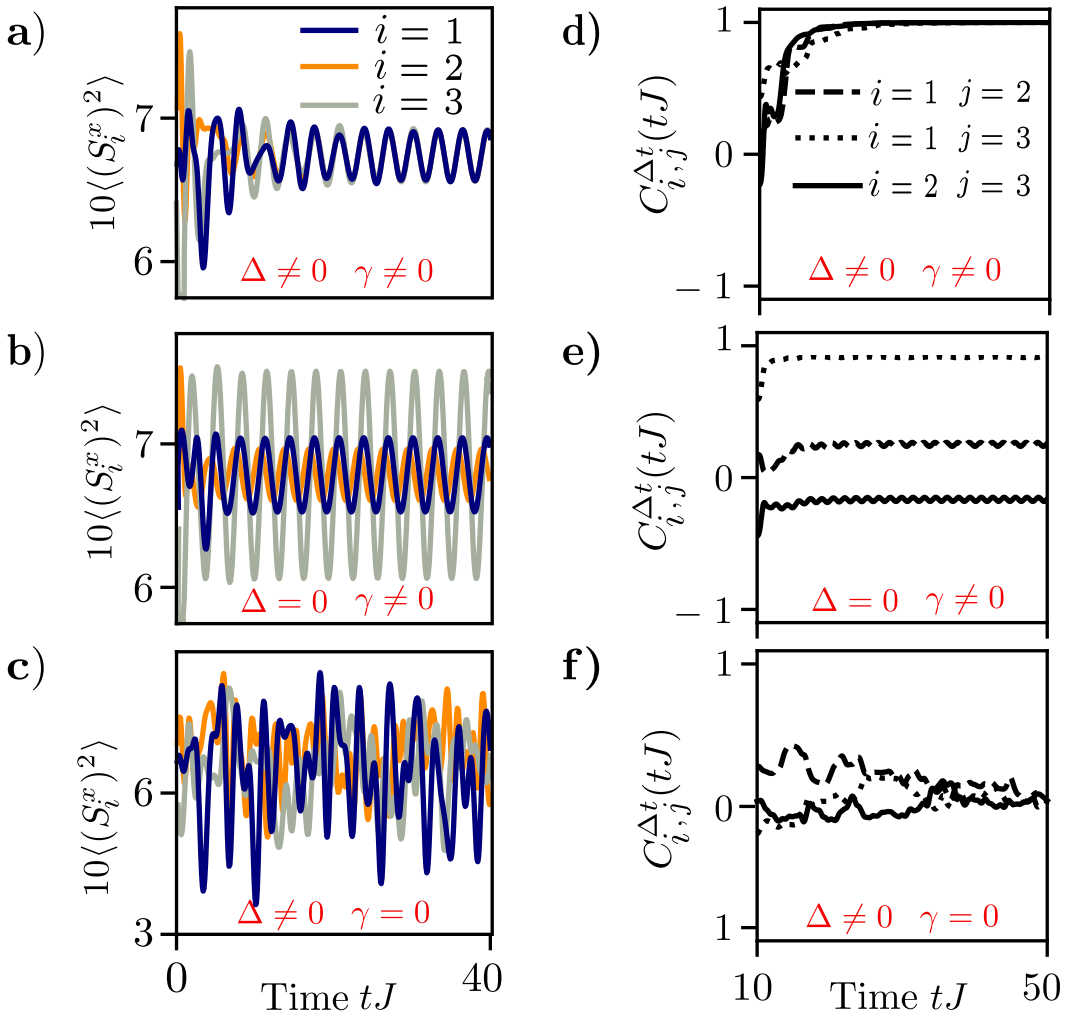

Figure 6.4: (a-c) Dynamics of $\langle(S_i^x)^2\rangle$ for a quench from a randomly drawn product state under the map in Eq. (6.16) with $L = 3$, $\omega_i = 1.0J\ \forall i$. a) $\Delta = 0.5J$, $\gamma = 1.0J$, b) $\Delta = 0$, $\gamma = 2.0J$ c) $\Delta = 0.5J$, $\gamma = 0$. d - f) Pearson time-correlation coefficient for each possible pair of functions from the respective plots in a-c). The time-averaged window is a rolling window with width $\Delta t = 10.0tJ$ centred at time tJ.

of the initial state and subsequent draws from the distribution of random product states will yield the same qualitative results.

Whilst the plots in Fig. 6.4a demonstrate that the spins are able to perfectly lock phases they do not capture the collective origin of this synchronisation. In order to achieve this, in Figs. 6.5a-b, we consider the behaviour in the frequency detuned case and invoke our collective synchronisation witnesses from Eq. (6.12). We observe the same characteristic features as in the number dephased Hubbard model: there is a tongue-like band of detunings where our witnesses are finite and survive on exceptionally long timescales, indicating the collective, quantum nature of the synchronisation and its robustness. The entanglement and correlations underpinning this synchronisation are observable in these plots and can be directly attributed to the mechanism of heating-induced order and the SU(2) nature of the SDS operators.

For the plots in Fig. 6.5a-b, we have also taken cross-sections and find that, at a given time, these measures form a Gaussian curve as a function of detuning whilst, at a given detuning, these measures decay away as an exponential function of time. The coefficient of this decay is proportional to the square of the detuning [29] and thus these cross-sections provide strong evidence that the system is robust to the detuning to first order.

In Figs. 6.5c-d we plot a specific example of the dynamics of $\langle (S_j^x)^2 \rangle$, observing that despite the detuning the qutrits are able to transiently lock their dynamics — with a frequency set by their average frequency — before mutually decaying to zero as $t \to \infty$. This transient synchronisation happens because the deviation of the imaginary eigenmodes from the imaginary axis is proportional to the square of the detuning strength and is much smaller than the Liouvillian gap which occurs when the detuning strength is zero [29]. This means that, for sufficiently small detuning, there is an intermediate timescale where all dynamics other than those relating to the almost-imaginary modes and steady states has decayed away and synchronisation can occur. On extremely long-time scales the deviation of these almost-imaginary modes from the imaginary axis comes into play and they decay away.

Finally, it is worth considering how this synchronisation scales with the size of the chain L. All of our analytical results are valid for any arbitrary length chain of L spin-1s under the Liouvillian in Eq. (6.16). We have focused on a trio of spin-1s because as the system sizes increase, for generic initial states (e.g. product states), the diagonal correlations become increasingly dominant in the long-time limit compared to the off-diagonal coherences, reducing the amplitude of the synchronisation measures in the system. This amplitude will remain finite for any finite-size system

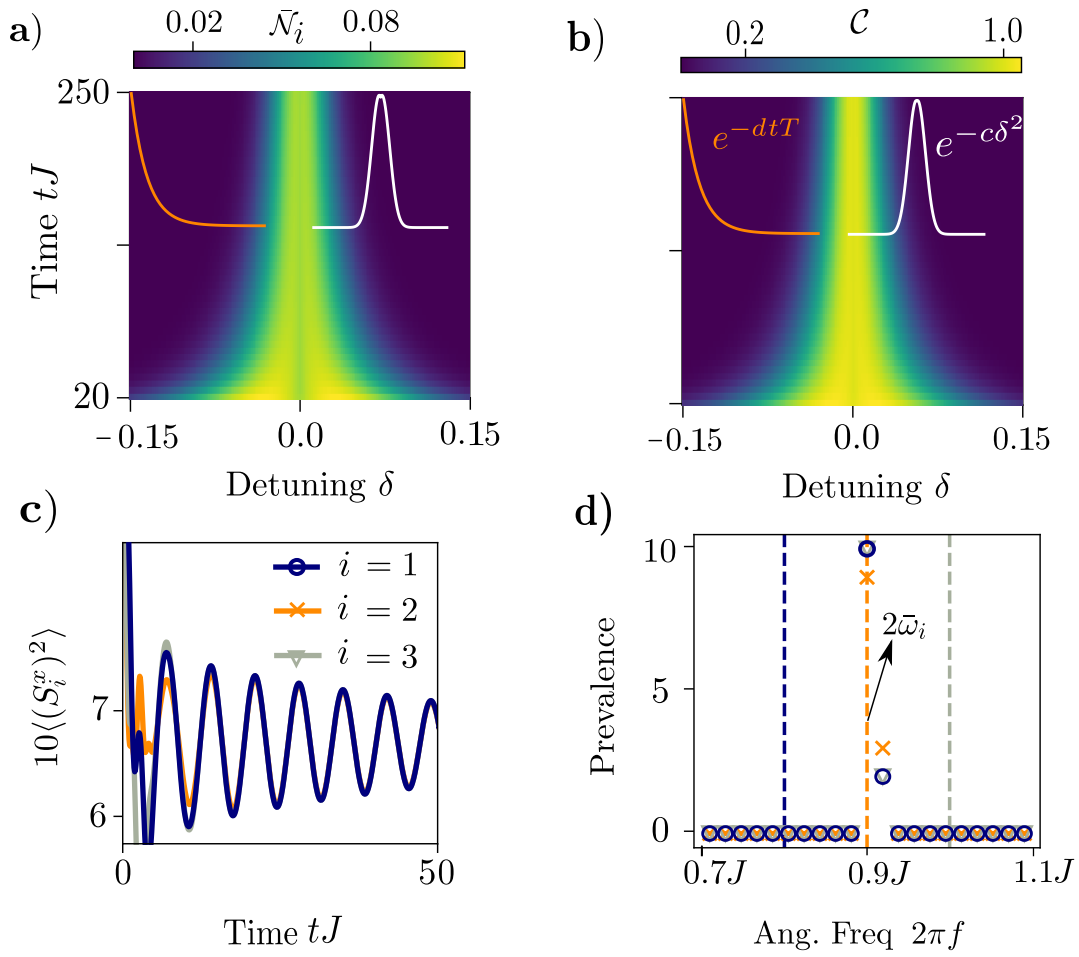

Figure 6.5: a-b) Respectively, plots of average negativity on each site and the total magnitude of the off-diagonal coherences vs time and detuning for the master equation in Eq. (6.16) with $L = 3$. The system is initialised in the state $|\psi(0)\rangle = |{\rightarrow}00\rangle$, where $|{\rightarrow}\rangle = \frac{1}{\sqrt{2}}(|{\uparrow}\rangle + |{\downarrow}\rangle)$, and evolved in time with parameters $\{\omega_1, \omega_2, \omega_3\} = \{1.0 - \delta, 1.0, 1.0 + \delta\}J$, $\gamma = 2.0J, \Delta = 0.5J$. Insets) Cross-section (orange) of these measures versus time at detuning $\delta = -0.075$. Top-right) Cross-section (white) of these measures versus detuning at time $tJ = 250.0$. The parameters d and c are constants used to parametrise the cross-sections. c) Example dynamics of $\langle(S_i^x)^2\rangle$ for the same system except with specific natural frequencies $\{\omega_1, \omega_2, \omega_3\} = \{0.4, 0.45, 0.5\}J$ and dephasing $\gamma = 1.0J$. d) Prevalence of angular frequencies, extracted from the distribution of angular frequencies created using the time-periods between successive turning points for the oscillations in c) but up to $tJ = 100.0$. Dashed lines indicate the expected delta function in the prevalence, based on each spin's natural frequency. The central line is twice the average of the natural frequencies $\bar{\omega}_i$.

but decay to zero in the thermodynamic limit and thus, unlike our Hubbard example, we cannot identify any non-trivial initial state where the observed synchronisation will persist in the thermodynamic limit. The combination of our two examples thus serves to emphasize how this symmetry-induced synchronisation occurs in systems of varying size and structure and provides a novel mechanism for observing truly quantum synchronisation.

6.4 Conclusion

In this chapter we have shown how the conditions for a strong dynamical symmetry, in tandem with the mechanism of heating-induced order, provide a pathway for perfect synchronisation in an interacting open quantum system. Specifically, if the jump operators are Hermitian and purely local and the SDS operator generates an SU(2) algebra then the limit cycles which occur at different position in the system will be necessarily locked in both phase and frequency. This synchronisation is, to first order, robust to a range of perturbations and we presented a pair of example systems — the number dephased Hubbard model and a quadratically dephased chain of qutrits — where our conditions are satisfied and this robust symmetry and heating enabled synchronisation can be observed. In both examples, the synchronisation was characterised by off-diagonal, quantum correlations and of a truly quantum nature.

Whilst we focussed on the case where the SDS is translationally invariant and the system undergoes perfect synchronisation, we can say more generally that the synchronisation in the system inherits the permutational invariance of the SDS. Thus, identifying setups where the SDS operator possesses more complicated permutational invariances could lead to quantum examples where clusters, or subspaces, of the system synchronise separately to each other.

Finally, we wish to state that here we have provided sufficient conditions for observing synchronisation in an open quantum system. These conditions are not dependent on any particular microscopic parameters and should be applicable to a range of systems. Naturally, it is worth considering whether the work here can be extended to find a more general set of conditions which are *necessary* for observing quantum synchronisation. This has possibly been achieved in the context of open systems with finite dimensional Hilbert spaces in Ref. [30], which builds upon a number of the results in this chapter and the work in Ref. [29].

References

[1] A. Pikovsky, M. Rosenblum, and J. Kurths, *Synchronization: A Universal Concept in Nonlinear Sciences*. Cambridge Nonlinear Science Series, Cambridge University Press, Cambridge, 2003.

[2] S. H. Strogatz and I. Stewart, "Coupled oscillators and biological synchronization," *Sci. Am.*, vol. 269, pp. 102–109, 1993.

[3] L. M. Pecora, T. L. Carroll, G. A. Johnson, D. J. Mar, and J. F. Heagy, "Fundamentals of synchronization in chaotic systems, concepts, and applications," *Chaos*, vol. 7, pp. 520–543, 1997.

[4] Y. Kuramoto, "Self-entrainment of a population of coupled non-linear oscillators," in *International Symposium on Mathematical Problems in Theoretical Physics*, pp. 420–422, Springer-Verlag, Berlin, 1975.

[5] S. H. Strogatz, "From Kuramoto to Crawford: Exploring the onset of synchronization in populations of coupled oscillators," *Physica D*, vol. 143, pp. 1–20, 2000.

[6] J. Buck, "Synchronous rhythmic flashing of fireflies. ii.," *Q. Rev. Biol.*, vol. 63, pp. 265–289, 1988.

[7] T. Vacharkulksemsuk and B. L. Fredrickson, "Strangers in sync: Achieving embodied rapport through shared movements," *J. Exp. Soc. Psychol.*, vol. 48, pp. 399–402, 2012.

[8] J. P. Ramirez, L. A. Olvera, H. Nijmeijer, and J. Alvarez, "The sympathy of two pendulum clocks: Beyond Huygens' observations," *Sci. Rep.*, vol. 6, p. 23580, 2016.

[9] A. Roulet and C. Bruder, "Synchronizing the smallest possible system," *Phys. Rev. Lett.*, vol. 121, p. 053601, 2018.

[10] A. Roulet and C. Bruder, "Quantum synchronization and entanglement generation," *Phys. Rev. Lett.*, vol. 121, p. 063601, 2018.

[11] N. Jaseem, M. Hajdušek, V. Vedral, R. Fazio, L.-C. Kwek, and S. Vinjanampathy, "Quantum synchronization in nanoscale heat engines," *Phys. Rev. E*, vol. 101, p. 020201, 2020.

[12] G. Qiao, H. Gao, H. Liu, and X. X. Yi, "Quantum synchronization of two mechanical oscillators in coupled optomechanical systems with Kerr nonlinearity," *Sci. Rep.*, vol. 8, p. 15614, 2018.

[13] S. Walter, A. Nunnenkamp, and C. Bruder, "Quantum synchronization of two Van der Pol oscillators," *Annalen der Physik*, vol. 527, pp. 131–138, 2015.

[14] G. L. Giorgi, F. Galve, G. Manzano, P. Colet, and R. Zambrini, "Quantum correlations and mutual synchronization," *Phys. Rev. A*, vol. 85, p. 052101, 2012.

[15] G. Manzano, F. Galve, G. L. Giorgi, E. Hernández-García, and R. Zambrini, "Synchronization, quantum correlations and entanglement in oscillator networks," *Sci. Rep.*, vol. 3, p. 1439, 2013.

[16] G. L. Giorgi, A. Cabot, and R. Zambrini, "Transient synchronization in open quantum systems," in *Advances in Open Systems and Fundamental Tests of Quantum Mechanics*, pp. 73–89, Springer International Publishing, New York, 2019.

[17] H. Ohadi, Y. d. V.-I. Redondo, A. J. Ramsay, Z. Hatzopoulos, T. C. H. Liew, P. R. Eastham, P. G. Savvidis, and J. J. Baumberg, "Synchronization crossover of polariton condensates in weakly disordered lattices," *Phys. Rev. B*, vol. 97, p. 195109, 2018.

[18] C. D. Tilley, C. K. Teoh, and A. D. Armour, "Dynamics of many-body quantum synchronisation," *New J. Phys.*, vol. 20, p. 113002, 2018.

[19] T. E. Lee and H. R. Sadeghpour, "Quantum synchronization of quantum van der Pol oscillators with trapped ions," *Phys. Rev. Lett.*, vol. 111, p. 234101, 2013.

[20] C. Davis-Tilley and A. D. Armour, "Synchronization of micromasers," *Phys. Rev. A*, vol. 94, p. 063819, 2016.
[21] S. Sonar, M. Hajdušek, M. Mukherjee, R. Fazio, V. Vedral, S. Vinjanampathy, and L. Kwek, "Squeezing enhances quantum synchronization," *Phys. Rev. Lett.*, vol. 120, p. 163601, 2018.
[22] N. Lörch, E. Amitai, A. Nunnenkamp, and C. Bruder, "Genuine quantum signatures in synchronization of anharmonic self-oscillators," *Phys. Rev. Lett.*, vol. 117, p. 073601, 2016.
[23] N. Lörch, S. E. Nigg, A. Nunnenkamp, R. P. Tiwari, and C. Bruder, "Quantum synchronization blockade: Energy quantization hinders synchronization of identical oscillators," *Phys. Rev. Lett.*, vol. 118, p. 243602, 2017.
[24] M. Ballerini, N. Cabibbo, R. Candelier, A. Cavagna, E. Cisbani, I. Giardina, A. Orlandi, G. Parisi, A. Procaccini, M. Viale, and V. Zdravkovic, "Empirical investigation of starling flocks: A benchmark study in collective anim. behav.," *Anim. Behav.*, vol. 76, pp. 201–215, 2008.
[25] G. Karpat, i. Yalçınkaya, and B. Çakmak, "Quantum synchronization of few-body systems under collective dissipation," *Phys. Rev. A*, vol. 101, p. 042121, 2020.
[26] F. Galve, G. L. Giorgi, and R. Zambrini, "Quantum correlations and synchronization measures," in *Lectures on General Quantum Correlations and their Applications*, pp. 393–420, Springer International Publishing, New York, 2017.
[27] G. Vidal and R. F. Werner, "Computable measure of entanglement," *Phys. Rev. A*, vol. 65, p. 032314, 2002.
[28] L.-H. Pan and C.-D. Gong, "A note on Haldane's conjecture," *J. Phys. Condens. Matter*, vol. 20, p. 215232, 2008.
[29] J. Tindall, C. S. Muñoz, B. Buča, and D. Jaksch, "Quantum synchronisation enabled by dynamical symmetries and dissipation," *New J. Phys.*, vol. 22, p. 013026, 2020.
[30] B. Buca, C. Booker, and D. Jaksch, "Algebraic theory of quantum synchronization and limit cycles under dissipation," *arXiv Preprint: quant-ph/2103.01808*, 2021.

Conclusions and Outlook

At many points in this thesis we have stated the importance of identifying mechanisms which guide quantum systems away from their anticipated equilibrium states and into regimes where quantum properties, such as entanglement, long-range off-diagonal order and coherence, are manifest. These properties are characteristic of superfluids, superconductors and other states of matter where quantum phenomena are observable at the macroscopic level. Identifying novel pathways to realise these states is crucial to the development of technologies such as high temperature superconductors, quantum computers [1, 2, 3] and quantum metrological instruments [4, 5, 6].

Summary of Work

It is within this narrative that this thesis fits and has made a number of contributions to its progress, the most significant of which we summarize here:

- In chapter 2 we introduced a new mechanism by which the presence of certain symmetries, such as SU(N), in a quantum system can prevent it from reaching a featureless infinite temperature ensemble under heating. For the case of SU(2) we were able to explicitly prove that, in an arbitrary many-body system, the maximum entropy states which form due to this symmetry preserving heating will possess finite, uniform off-diagonal correlations. We termed this mechanism 'heating-induced order' and discussed how the desired symmetry-preserving heating could be induced by periodic driving or coupling of the system to an external environment. We then demonstrated an explicit example via the driven spin-1 Affleck-Kenedy-Lieb-Tasaki model.

- In chapter 3 we focused on the Hubbard model whose dual SU(2) symmetries make it a rich model for exploring this mechanism of heating-induced order. We performed a simultaneous diagonalisation of the operators associated with these SU(2) symmetries, a process which then allowed us to analytically construct the various maximum entropy off-diagonal spin-wave or η-paired steady

states which can arise under heating. In the thermodynamic limit, finite uniform off-diagonal η-paired order in the Hubbard model can be directly related to superconducting characteristics such as the Meissner effect and flux quantisation. We discussed how a number of the states constructed will exhibit these characteristics and may therefore be superconducting. Finally, we discussed how driven or dissipative experimental setups where these states could be formed are possible with current technologies.

- In chapter 4 we focussed on a recent experiment observing photo-induced superconductivity in the organic compound
  $\kappa - (\mathrm{BEDT-TTF})_2\mathrm{Cu[N(CN)_2]Br}$ [7]. By introducing a simplified Hubbard description of this driven system we showed how the interplay between the irregular lattice geometry and the driving facilitates the mechanism of heating-induced order via a unique pathway. The induced order is in the form of long-range η-pair correlations and thus this mechanism offers a possible explanation for the results of Ref. [7].

- In chapter 5 we introduced a new type of symmetry — the Strong Dynamical Symmetry (SDS) — in the context of open systems governed by the GSKL equation. We detailed the conditions necessary for this symmetry to exist and showed how it guarantees that the spectrum of the Liouvillian will contain a set of equidistant imaginary eigenvalues. These eigenvalues prevent the system from relaxing to stationarity in the long-time limit and force it to undergo coherent oscillations instead. The aforementioned conditions make no statements about the miscroscopic details of the system and thus form a novel environment-assisted route to preventing stationarity and equilibration in a many-body system. We showed how the notion of a SDS both subsumes and goes beyond the established notion of a Decoherence Free Subspace and provided an example in the form of the number dephased Hubbard model.

- In chapter 6 we showed how perfect synchronisation arises in an open system when the satisfaction of the conditions for a SDS occurs alongside the mechanism of heating-induced order. We provided two examples where this unique process can be observed: the number dephased Hubbard model and a spin-1 Heisenberg model. In both cases the interplay between the SU(2) algebra generated by the SDS operator and the heating meant that the synchronisation was underpinned by off-diagonal correlations and entanglement and thus of a truly

quantum nature. We also proved how this type of synchronisation is robust to a whole class of perturbations in the system's Hamiltonian.

Outlook and Open Questions

In this thesis we have also discussed a number of open questions and avenues of future research which have stemmed from these results. Here, we emphasize and elaborate on those we consider the most significant.

The results presented in chapter 5 have led to a number of open questions on non-stationarity in quantum systems, some of which are currently being investigated. Most prominently, the SDS conditions introduced form a set of sufficient conditions for the Liouvillian of an open system described by the GSKL equation to possess imaginary eigenvalues. It would be pertinent to identify whether a more general version of these conditions can be formulated which are necessary for the existence of such imaginary eigenvalues. Such an extension to our work is the subject of Ref. [8], which achieves this in the context of finite-size Hilbert spaces.

The results of Ref. [8], however, do not apply in the thermodynamic limit as there the matrices are of infinite size which leads to convergence issues when evaluating the commutators necessary for identifying the presence of a SDS. This limit is important as it is at the heart of determining whether several recent observations of non-stationarity in open quantum systems in the semi-classical regime [9, 10] can be encapsulated within the SDS formalism. Attempting to extend the SDS formalism to this limit is therefore an open and important avenue of research and could help improve our understanding of these recent results.

Meanwhile, our work in chapter 6 on synchronisation induced by heating and a strong dynamical symmetry motivates the discovery of further systems where similar symmetry-enabled phenomena can be observed. In this thesis we focussed on a specific class of dissipation which enforced heating and ensured that the imaginary eigenmodes generated by the SDS are completely symmetric in space, leading to perfect synchronisation. More generally, however, the synchronisation of the system will reflect the symmetry of the SDS operator and the Liouvillian's steady states and thus in open systems with more complex, spatial symmetries we may observe phenomena such as anti-synchronisation or clustered synchronisation enabled by a SDS.

The mechanism of heating-induced order introduced in chapter 2 has also opened up a number of important research pursuits. Firstly, it would be natural to try to identify further systems with rich symmetry structures where this mechanism would

occur and lead to the formation of novel states of matter under heating. Extensions of the Hubbard model to include multiple fermionic species or multiple orbitals are notable candidates as these have higher order symmetries such as SU(N) with $N > 2$ [11]. Moreover, this mechanism of heating-induced order may explain some recent results where a lossy array of hardcore bosons were shown to possess a series of steady states with off-diagonal order [12, 13]. Definitively establishing this connection could lead to new insights into the long-time properties of such lossy systems.

Another line of research in this area stems from the desire to calculate the optical conductivity spectrum of the charge ordered steady states we observed in the Hubbard model in chapters 3 and 4. This spectrum is typically used as a fingerprint for superconductivity in solid-state matter experiments [7, 14, 15, 16, 17, 18, 19] and would allow us to make a more direct connection between our results and the phenomena of emergent superconductivity in photo-excited compounds.

Lastly, but by no means least, in chapter 3 we showed how the condition $\langle O^+ O^- \rangle \propto \mathcal{O}(L^2)$ (where O is either η or S and L is the number of lattice sites) is necessary for observing the heating-induced formation of a steady state with uniform off-diagonal long-range order in the thermodynamic limit of the Hubbard model. Following a seminal paper by E. Lieb [20] it is known that such a condition is satisfied by the ground state of *any* unbalanced bi-partite Hubbard lattice[4]. The mechanism of heating-induced order therefore ensures the emergence of macroscopic order upon driving the ground state of the Hubbard model on a whole class of lattices. This remarkable result is the subject of Ref [21] and provides a general understanding of how strong driving can expose macroscopic order that has been suppressed in equilibrium.

[4]Unbalanced in the sense that the number of sites in the two sublattices are not equal.

References

[1] T. Byrnes, K. Wen, and Y. Yamamoto, "Macroscopic quantum computation using Bose-Einstein condensates," *Phys. Rev. A*, vol. 85, p. 040306, 2012.

[2] S. N. Andrianov and S. A. Moiseev, "Magnon qubit and quantum computing on magnon Bose-Einstein condensates," *Phys. Rev. A*, vol. 90, p. 042303, 2014.

[3] L. DiCarlo, J. M. Chow, J. M. Gambetta, L. S. Bishop, B. R. Johnson, D. I. Schuster, J. Majer, A. Blais, L. Frunzio, S. M. Girvin, and R. J. Schoelkopf, "Demonstration of two-qubit algorithms with a superconducting quantum processor," *Nature*, vol. 460, pp. 240–244, 2009.

[4] S. Wildermuth, S. Hofferberth, I. Lesanovsky, S. Groth, P. Krüger, J. Schmiedmayer, and I. Bar-Joseph, "Sensing electric and magnetic fields with Bose-Einstein condensates," *Appl. Phys. Lett.*, vol. 88, p. 264103, 2006.

[5] S. S. Mirkhalaf, D. Benedicto Orenes, M. W. Mitchell, and E. Witkowska, "Criticality-enhanced quantum sensing in ferromagnetic Bose-Einstein condensates: Role of readout measurement and detection noise," *Phys. Rev. A*, vol. 103, p. 023317, 2021.

[6] J. Clarke and A. Braginski, *The SQUID Handbook: Applications of SQUIDs and SQUID Systems*. Wiley, New Jersey, 2006.

[7] M. Buzzi, D. Nicoletti, M. Fechner, N. Tancogne-Dejean, M. A. Sentef, A. Georges, T. Biesner, E. Uykur, M. Dressel, A. Henderson, T. Siegrist, J. A. Schlueter, K. Miyagawa, K. Kanoda, M.-S. Nam, A. Ardavan, J. Coulthard, J. Tindall, F. Schlawin, D. Jaksch, and A. Cavalleri, "Photomolecular high-temperature superconductivity," *Phys. Rev. X*, vol. 10, p. 031028, 2020.

[8] B. Buca, C. Booker, and D. Jaksch, "Algebraic theory of quantum synchronization and limit cycles under dissipation," *arXiv Preprint: quant-ph/2103.01808*, 2021.

[9] F. Iemini, A. Russomanno, J. Keeling, M. Schirò, M. Dalmonte, and R. Fazio, "Boundary time crystals," *Phys. Rev. Lett.*, vol. 121, p. 035301, 2018.

[10] G. Piccitto, M. Wauters, F. Nori, and N. Shammah, "Symmetries and conserved quantities of boundary time crystals in generalized spin models," *arXiv Preprint: quant-ph/2101.05710*, 2021.

[11] C. Honerkamp and W. Hofstetter, "Ultracold fermions and the SU(n) Hubbard model," *Phys. Rev. Lett.*, vol. 92, p. 170403, Apr 2004.

[12] S. Dutta and N. R. Cooper, "Long-range coherence and multiple steady states in a lossy qubit array," *Phys. Rev. Lett.*, vol. 125, p. 240404, 2020.

[13] S. Dutta and N. R. Cooper, "Out-of-equilibrium steady states of a locally driven lossy qubit array," *Phys. Rev. Research*, vol. 3, p. L012016, 2021.

[14] M. Mitrano, A. Cantaluppi, D. Nicoletti, S. Kaiser, A. Perucchi, S. Lupi, P. Di Pietro, D. Pontiroli, M. Riccò, S. Clark, D. Jaksch, and A. Cavalleri, "Possible light-induced superconductivity in K_3C_{60} at high temperature," *Nature*, vol. 530, pp. 461–464, 2016.

[15] D. Fausti, R. I. Tobey, N. Dean, S. Kaiser, A. Dienst, M. C. Hoffmann, S. Pyon, T. Takayama, H. Takagi, and A. Cavalleri, "Light-induced superconductivity in a stripe-ordered cuprate," *Science*, vol. 331, pp. 189–191, 2011.

[16] W. Hu, S. Kaiser, D. Nicoletti, C. R. Hunt, I. Gierz, M. C. Hoffmann, M. Le Tacon, T. Loew, B. Keimer, and A. Cavalleri, "Optically enhanced coherent transport in $YBa_2Cu_3O_{6.5}$ by ultrafast redistribution of interlayer coupling," *Nat. Mat.*, vol. 13, pp. 705–711, 2014.

[17] D. Nicoletti, E. Casandruc, Y. Laplace, V. Khanna, C. R. Hunt, S. Kaiser, S. S. Dhesi, G. D. Gu, J. P. Hill, and A. Cavalleri, "Optically induced superconductivity in striped

$La_{2-x}Ba_xCuO_4$ by polarization-selective excitation in the near infrared," *Phys. Rev. B*, vol. 90, p. 100503, 2014.

[18] M. Budden, T. Gebert, M. Buzzi, G. Jotzu, E. Wang, T. Matsuyama, G. Meier, Y. Laplace, D. Pontiroli, M. Riccò, F. Schlawin, D. Jaksch, and A. Cavalleri, "Evidence for metastable photo-induced superconductivity in K_3C_{60}," *Nat. Phys.*, 2021.

[19] K. A. Cremin, J. Zhang, C. C. Homes, G. D. Gu, Z. Sun, M. M. Fogler, A. J. Millis, D. N. Basov, and R. D. Averitt, "Photoenhanced metastable c-axis electrodynamics in stripe-ordered cuprate $La_{1.885}Ba_{0.115}CuO_4$," *Proc. Natl. Acad. Sci.*, vol. 116, pp. 19875–19879, 2019.

[20] E. H. Lieb, "Two theorems on the Hubbard model," *Phys. Rev. Lett.*, vol. 62, pp. 1201–1204, 1989.

[21] J. Tindall, F. Schlawin, M. Sentef, and D. Jaksch, "Lieb's theorem and maximum entropy condensates," *arXiv Preprint: cond-mat.str-el/2103.04687*, 2021.